The Effect of Grain Size Distribution and Bimodal Sea States on Coarse Beach Sediment Dynamics

Thesis

OPEN UNIVERSITY: EARTH AND ENVIRONMENTAL SCIENCES AFFILIATED
RESEARCH CENTRE: HR WALLINGFORD LIMITED

The effect of grain size distribution and bimodal sea-states on coarse beach sediment dynamics

Thesis submitted in partial fulfilment of the requirements for the degree of Doctor of Philosophy

Andrea Polidoro

December 2018

Abstract

In this work we investigated the effect of gravel beach profile response under wave spectra characterised by swell and wind wave periods in various combinations. This was done by running an extensive series of 2D physical model tests. It was found that even a small percentage of wave energy within the low frequency range triggers a significant landward displacement of the beach crest. Based on this 2D physical model study, a new parametric model, Shingle-B, was derived and an online tool was developed and made available.

This research also presents a study on the effect of the grain size distribution, i.e. permeability, on the beach profile response. It was investigated, using a permeameter, how a stationary porous flow is influenced by the grain size distribution. The results clearly show that the D_{15} parameter dominates the flow/resistance behaviour for all the tested samples and the other parameters (D_{50} or D_{85}) have only second order effects on the flow/resistance relationship.

Additionally, in order to investigate how the grain size distribution influences both the wave-induced pore pressure and beach profile evolution, a 2D physical model study was carried out using ten different gravel beaches. Observations made during this study, in which more complex phenomena were involved, proved that the pore pressure attenuation was mainly influenced by the grading width parameter D_{85}/D_{15}. Measurements on the internal wave set-up recorded during these experiments showed that the internal wave set-up was strongly influenced by both the incident wave conditions and the sediment characteristic D_{50}.

Post-storm beach profiles, with similar grading parameters (e.g., $D_{50,}$ D_{15} and D_{85}/ D_{15}), were then compared. These comparisons demonstrated that the crest moves upwards and shoreward as D_{50} and D_{15} decrease. In particular the crest elevation increases with increasing internal wave set-up.

Acknowledgements

Firstly my sincere thanks goes to HR Wallingford which provided me with the opportunity to carry out this research, giving me access to the laboratory and research facilities. Without its generous support, it would not have been possible to conduct this research.

I would like to express my sincere gratitude to my advisors Dr. Tim Pullen and Dr. Dave Simmonds for the continuous support of my Ph.D. study and related research, for their patience, motivation, and knowledge. Their guidance helped me throughout this research and the writing of this thesis. I am thankful to Dr. Keith Powell, the director of this study and also a gravel beaches expert, for his crucial remarks and suggestions that shaped my final dissertation. I am also grateful to Prof. William Allsop for his insightful comments and for sharing with me his tremendous experience in physical modelling.

Besides my advisors, I would like to thank Dr. Giovanni Cuomo, for his insightful comments and encouragement, but also for the hard questions which incentivized me to widen my research from various perspectives.

A very special thanks to Dr. Belen Blanco for her invaluable advice and feedback on my research and for always being so supportive of my work.

I would also like to show my gratitude to Dr. Travis Mason and Dr. Andy Bradbury for sharing their knowledge, passion and inspiration on gravel beaches during the course of this research. Without their support part of this research would not have been possible.

My deep appreciation goes out to Jack Eade, and Bryant and Mary Duncan. Their excellent work during data collection has made an invaluable contribution towards my PhD. I am also grateful to them for their friendship and the warmth they extended to me during this research.

I would also like to thank the experts who were involved in the validation survey for this research project: Dr. Dornbusch Uwe, Peter Ferguson, Jonathan Clarke, Andrew Pearce and Dave Picksley. Without their passionate participation and input, the validation survey could not have been successfully conducted.

I also wish to acknowledge support provided by the HR Wallingford Froude Modelling Hall staff. In particular Paul Tong, who spent many hours sieving tons of material.

Last, but not least, I would like to dedicate this thesis to my family and friends, for their love, patience, and understanding—they allowed me to spend most of the time on this thesis. For the past nine months, they kept on reminding me: “by perseverance the snail reached the ark”!

Contents

List of Tables

List of Figures

List of Symbols

a	= Forchheimer coefficient describing energy losses due to viscous dissipation	[s/m]
b	= Forchheimer coefficient describing energy losses due to inertial dissipation	[s^2/m^2]
D	= characteristic grain size	[m]
D_{50}	= median grain size	[m]
$D_{x\%}$	= grain size that exceeds by size x% of the sediment distribution	[m]
$D_{15\%}$	= grain size diameters that exceed the 15% value of the sieve curve	[m]
$D_{85\%}$	= grain size diameters that exceed the 85% value of the sieve curve	[m]
E	= the energy associated with the wave motion, per unit surface area	[N/m]
f	= frequency	[Hz]
g	= acceleration due to gravity (= 9.81)	[m/s²]
H	= wave height	[m]
H_s	= significant wave height based on time domain analysis	[m]
$H_{1/x}$	= average of highest 1/x th of wave heights	[m]
$H_{x\%}$	= wave height exceeded by x% of all wave heights	[m]
H_{m0}	= spectral significant wave height	[m]
$H_{m0\ toe}$	= H_{m0} determined at toe of structure	[m]
H_{0mrs}	= 1.71 H_s offshore root mean square wave height	[m]
i	= hydraulic gradient	[-]
J	= percolation slope	[-]
k	= permeability	[m^2]
K_D	= hydraulic conductivity	[m/s]
k	= angular wave number (= $2\pi/L$)	[rad/m]
L	= wave length measured in direction of wave propagation	[m]
L_{0p}	= peak wave length in deep water = $gT^2_p/2\pi$	[m]
$L_{m-1,0}$	= deep water wave length based on $T_{m-1,0}$= $gT^2_{m-1,0}/2\pi$	[m]
m_0	= zeroth order moment of the wave energy density spectrum	[m^2]
n	= porosity	[-]
P_{m0}	= significant wave-induced pore pressure height	[m]
Q_p	= peakedness parameter	[-]
R_e	= Reynolds number	[-]
$R_{2\%}$	= run-up exceeded by 2 percent of the run-up crests	[m]
R_{max}	= Highest run-up height	[m]
S	= specific surface	[m^2/kg]
S	= radiation stress	[N/m]
S(f)	= incident spectral density	[m²/Hz]
S(%)	= swell percentage component within a bimodal wave spectrum	[-]

s	= wave steepness = H/L	[-]
$s_{m-1,0}$	= wave steepness with L_0, based on $T_{m-1,0} = H_{m0}/L_0 = 2\pi H_{mo}/(gT^2_{m-1,0})$	[-]
SWL	= still water level	[m]
t	= variable of time	[s]
T	= wave period	[s]
$T_{m0,2}$	= average wave period defined by $(m_0/m_2)^{1/2}$	[s]
$T_{m-1,0}$	= average wave period defined by m_{-1}/m_0	[s]
T_p	= spectral peak wave period = $1/f_p$	[s]
$\tan\alpha$	= beach slope	[-]
w_s	= sediment fall velocity	[m/s]
V	= velocity through the voids	[m/s]
x	= cross-shore axis coordinate	[-]
α	= coefficient of the linear term in the Forchheimer equation	[-]
β	= coefficient of the non-linear term in the Forchheimer equation	[-]
Δ	= Ratio of the densities of the sediment and water (Relative density of sediment)	[-]
ε	= broadness parameter	[-]
ϕ	= phi diameter, where $\phi = -\log_2 D$	[-]
λ	= ratio of model to prototype parameter (length scale factor)	[-]
λ_{CD}	= drag coefficient scale factor	[-]
λ_D	= diameter scale factor	[-]
λ_Δ	= density scale factor	[-]
η	= wave induced set-up	[m]
ρ_w	= density of water, assumed = 1000 for fresh water and 1025 for salt water	[kg/m^3]
ρ_s	= density of sediment	[kg/m^3]
τ	= bed shear stress, where	[kg/ms^2]
ν	= kinematic viscosity of water, set at 10^{-6} in this thesis	[m^2/s]
ν	= narrowness parameter	[-]
ξ_o	= breaker parameter based on s (= $\tan\alpha/s^{1/2}$)	[-]
θ	=Shields parameter	[-]

1. Introduction

1.1. Introduction

Gravel beaches are a particular type of beach in which the sediments are solely composed of gravel sediment (2mm to 64mm, according to the Wentworth scale, Folk scheme, BGS, 1987) as reported in Lopez de San Roman Blanco (2001). It is also common to find coarse grained beaches which include both gravel and mixed (sand and gravel) sediments.

These beaches are common in mid to high latitude coasts (Carter and Orford, 1993; Horn and Walton, 2007; Hayes *et al.*, 2009) but also present on the shores of many parts of the world. Gravel beaches assume particular importance, as defence systems, along stretches of the heavily populated south coast of England where they are known as shingle beaches (Nicholls, 1990; Moses and Williams, 2008). Approximately one-third of the beaches in England and Wales are classified as coarse grained, especially along the south coast of England (Blanco, 2001). Literature on beach processes contains fewer studies of gravel beaches than the study of sandy beaches (Buscombe and Masselink, 2006), possibly because sand beaches are located in parts of the world where their economic value (properties and recreational areas) are relatively greater.

Coarse grained beaches are also known to be an efficient form of natural sea defence capable of dissipating up to 90% of incident wave energy (Powell 1990). A major advantage of a coarse-grained beach is its ability to absorb wave energy efficiently over a short distance as a result of the large infiltration flow allowed in the beach. This advantage quickly disappears as the permeability is reduced. It is therefore important that the coastal engineer is aware of the potential for changes in beach profile response when the permeability, i.e., beach grain size distribution, is modified.

Sediment size and permeability are considered very important factors affecting the response of gravel beaches under wave action. Many studies have stressed the importance of infiltration on sediment transport, especially on coarse beaches (Buscombe and Masselink, *2006*; Austin and Masselink, *2005*; Horn and Li, 2006; Pedrozo-Acuña *et al.*, *2006, 2007*; Williams *et al, 2012*). Additionally, knowledge of pore pressures and related wave attenuation inside the gravel material is an important factor governing beach responses such as: wave run-up; wave overtopping; wave reflection and transmission. A better understanding of the flow through gravel materials and the interaction between incident waves and groundwater as function of the grain size distribution is therefore essential to allow robust prediction of beach evolution. This interaction, acknowledged as

a key factor in controlling the morphodynamics of coarse-grained beaches (Bagnold 1940; Duncan 1964; Nelson and Miller 1974; Packwood 1983; Turner and Nielsen 1997; Masselink and Li 2001, Horn *et al. 2007*), is still not fully understood.

Gravel beaches are an important form of natural coastal defence, protecting significant urban settlements as well as agricultural, recreational and environmental land areas against flooding and erosion (Van Wellen *et al.*, 2000; Powell, 1990). Extreme storm surges and subsequent coastal erosion/breaching and flooding have the potential to result in severe direct and indirect consequences. The direct consequences might, for instance, be associated with damage to property, infrastructure and public safety. Interruption of production processes represents an example of indirect economic damages that can be accounted for in flood risk assessments. Their functions as coastal defenses and natural habitats therefore compel coastal engineers to understand the processes occurring across the gravel beachface (Buscombe and Masselink, 2006).

An example of the effect of the storm events on gravel beach response took place during the winter of 2013/14 along the Atlantic coast of Europe. This unprecedented sequence of very energetic wave conditions occurred over a 3-month period. Measured offshore wave data from the southwest of England showed that the significant wave height during the largest recorded storm exceeded 9 m with a peak wave period of 23 s (Masselink, 2016). These energetic wave climates, characterized by both long-period ocean swell and short-period local seas (bimodal sea state), caused extensive physical and socio-economic (flooding, damage to infrastructure) impacts throughout the west coast of Europe (Ireland, UK, France, Spain and Portugal). Total economic damage for England and Wales during the winter period was estimated to be between £1bn and £1.5bn, including the damage due to fluvial and groundwater flooding (DEFRA, 2016).

All of these sea-states were characterised by having a double-peaked wave spectra, highlighting the potential importance of complex wave conditions that combine wind and swell waves. Subsequent to these storm events, a connection between wave spectrum shape and beach response was observed. It had been highlighted that little is known about the effect of bimodal sea conditions on sea defences or beaches (Bradbury, 1998; Coates and Bona, 1997; Bradbury *et al.*, 2007) and swell is rarely considered explicitly in the design or assessment of shoreline management operations.

As will be described in more detail in Chapter 7, the use of the existing prediction models for gravel beach profiles (Powell, 1990) known as SHINGLE, and the process-based XBeach-G (McCall *et al.*, 2014) are not appropriate for bimodal wave conditions as they have been developed and calibrated to mimic the interaction of shingle beaches with unimodal sea-states, neglecting the possibility of having complex wave conditions that combine wind sea and swell, forming a bimodal spectrum. There is, therefore, an urgent need to better understand the effect of the interaction between wind and swell waves on beach profile response and to develop our understanding of the prediction of beach response under bimodal storm conditions.

From an engineering point of view, there is an urgent requirement to improve the prediction of the beach profile response under:

- Different grain size distributions
- Bimodality of the sea-states

1.2. Objectives of the research

The objective of this research is to improve the current understanding of gravel beach dynamic response by:

- Improved understanding of the key hydrodynamic processes within gravel materials
- Improved understanding of the effect of grain size distribution on beach profile response
- Improved understanding of gravel beach profile response under bimodal sea-states

In order to achieve the research objectives, extensive physical model studies and data analysis were carried out.

Following this introductory chapter, there are an additional seven chapters. The eighth and final chapter contains the conclusions and recommendations. The remaining six chapters contain the main body of this work. They are described briefly in the following sections, each of which is indicated by the relevant chapter title.

1.2.1. Understanding gravel beach dynamics

In Chapter 2 we shall define the characteristic of gravel beaches and the importance of permeability for their behaviour. A brief description of the main hydrodynamic processes in the swash zone that influence cross-shore sediment transport will be given. A selection of available

methods to predict gravel beach response to wave actions will be reviewed, and these have been chosen to allow later comparison to be made.

1.2.2. Flow through gravel material

The wave interaction with the beach comprises a multitude of process, such as: wave breaking; wave reflection; wave run-up and overtopping. These are influenced by the wave-induced porous flow inside the beach, therefore knowledge of the hydrodynamic pore pressures associated with the porous flow is very relevant for a beach profile response. As most of the existing formulae of porous flow through coarse granular material are based on stationary flow, some of the research on stationary flow will be discussed briefly in Chapter 3, together with a brief review of the current state of knowledge on permeability.

1.2.3. Wave characteristics and bimodal sea-states

An introduction to gravity waves and the main characteristics of wind and swell waves are described in Chapter 4. A description of the wave spectrum parameters will be given to facilitate the discussions that follow. The final part of this Chapter will examine the characteristics of a bimodal sea-state and its effect of beach profile response.

1.2.4. Verification of the Forchheimer coefficients for coarse grained materials

One of the main characteristics of gravel beaches is their high permeability, which allows most of the energy from the incident waves to be dissipated through percolation within the beach, as opposed to a sand beach which over the duration of a wave period, is effectively impermeable to percolation. Chapter 5, therefore, will describe how porous flow is influenced by the grain size distribution. A description of the design and execution of the experimental programme will be given in the first part of this chapter, while analysis and results will be discussed in the second part of this chapter.

1.2.5. Effect of grain size distribution on gravel beach response

As briefly indicated above, the distribution of grain sizes in gravel beach sediments, directly influences their permeability. The first part of Chapter 6, will therefore, describe a new 2D physical model study carried out to improve our understanding of wave-induced pore pressure within gravel material, for a range of sediment sizes. The second part deals with the influence of grain size distribution on beach profile dynamics.

1.2.6. Beach response to bimodal sea-states

Chapter 7, as its title suggests, will examine the response of gravel beaches under wave spectra, characterised by swell and wind wave periods in various combinations. This new work is divided into two parts. The first part deals with the results of a 2D physical model study, this demonstrates a significant step forward in understanding the key cross shore processes involved and their interaction. The second part deals with the new parametric model, Shingle-B, where the relationship between beach profile parameters and bimodal wave variables will be described, which will lead onto the conclusions for this study.

2. Understanding gravel beach dynamics

2.1. Introduction to gravel beaches

Gravel beaches are an important form of natural coastal defence, protecting significant urban settlements as well as agricultural, recreational and environmental land areas against flooding and erosion (Van Wellen *et al.*, 2000; Powell, 1990). Their function as coastal defenses and natural habitats therefore compel coastal engineers to understand the processes occurring across the gravel beachface (Buscombe and Masselink, 2006).

Shoreline managers are increasingly using beach recharge as a method of improving beaches for coastal defence purposes. Therefore interest in these environments and their dynamic behaviour in response to wave climate and water level variation has increased in recent years (Bradbury, 2000; William et al, 2012). A challenge that a manager or engineer may face is that the recharge material is different from the natural beach sediment and often more widely graded. As a consequence, the permeability will be affected and unexpected erosion can occur. It is therefore important that the coastal engineer is aware of the potential for changes in beach profile response under different grain size distributions. Sediment size and porosity are considered very important factors affecting the response of gravel beaches under wave action. Many studies have stressed the importance of infiltration for sediment transport in the swash region and especially on coarse beaches (Buscombe and Masselink, 2006; Austin and Masselink, 2005; Horn and Li, 2006; Pedrozo-Acuña *et al.*, 2006, 2007; William et al, 2012). Additionally, knowledge of pore pressures and related wave attenuation inside the porous media is an important factor governing beach responses such as wave run-up, wave overtopping, reflection and transmission. A better understanding of the flow through gravel materials and the interaction between waves with the groundwater table within the beach is therefore essential to allow robust prediction of beach evolution, especially in the swash zone. This interaction, acknowledged as a key factor in controlling the morphodynamics of gravel beaches (Bagnold 1940; Duncan 1964; Nelson and Miller 1974; Packwood 1983; Turner and Nielsen 1997; Masselink and Li 2001, Horn *et al.* 2007), it is still not fully understood. During this research a physical model study (using a permeameter) was therefore carried out to investigate the effect of grain size distribution on the flow/resistance relationship under stationary flow regimes. This study will be discussed in Chapter 5. Furthermore, a 2D physical model study, described in Chapter 6, was carried out to investigate the effect of the grain size distribution and pore pressure attenuation on the beach profile response.

A review on the formation and characteristics of gravel beaches, with particular emphasis on the shingle beaches in the south of England is discussed in the first part of this chapter. In the second part, the hydrodynamic processes influencing the gravel beach responses are presented, together with the models currently used to predict the response of gravel beaches.

2.2. Definition and characterisation of gravel beaches

Beaches consisting of gravel or shingle (2 to 64 mm) are generally known as coarse beaches or shingle beaches (Carter and Orford, 1993; Van Wellen *et al.*, 2000; Orford *et al.*,2002) (see Figure 2.1) and can be found in many, formerly glaciated, mid / high-latitude parts of the world (England, Iceland, Canada, Russia, etc.). Gravel beaches are also found along unconsolidated cliff-type coasts eroded by wave attack, like the Mediterranean coasts of Italy, Greece, Spain (Ortega-Sánchez et al, 2017).

Gravel beach coastlines were formed as a result of the last ice age, which ended about 10,000 years ago. As the ice sheets melted, the sea level rose rapidly (about 120m between 20,000 and 6000 years ago) (CIRIA 2010). Due to this phenomenon, a large amount of sediment was carried by rivers to the sea during this period, eventually forming the pre-cursor to our present coastlines (CIRIA 2010). Many of our beaches today are composed of the remnants of these sediments, composed predominantly of sand and gravel. These sources of beach material have subsequently been supplemented by coastal erosion of soft cliffs and the reduced but continuing supply of sediments from rivers (Lee and Clark, 2002). Material has also been derived from offshore banks left behind by relatively rapid rises of sea level during ice ages.

The material sizes on any particular gravel beach will normally comprise a wide range of grain sizes, with the sediments spatially differentiated in terms of both size and shape (Bluck, 1967; Orford, 1975). Sediment distributions may vary across the beach profile, along the shore and with depth below the beachface, as well as with time (Orford, 1975).

In 1993, HR Wallingford carried out a study on the sediment distributions for the beaches along the south coast of England. During this study, the grading sediment sizes for several beaches were analysed and the results are reported in HR Wallingford Report SR350. These showed that the south coast of England can be considered to have an average median sediment size of D_{50} = 15.5mm (std. dev. = 6.0mm). A summary of the grading and median sediment size of material on a number of UK shingle beaches is reported in Table 2.1. This tells us that even though gravel beaches have a similar value of D_{50}, they can be characterised by having both a

narrow and a wide range of sediment sizes. An indicator of the uniformity in mass of the sediment distribution is the ratio of D_{85}/D_{15} (grading width or gradation ratio). Narrow or single-sized gradation has the $D_{85}/D_{15} < 1.5$, while wide gradation is denoted by $1.5 < D_{85}/D_{15} < 2.5$ and very wide by $2.5 < D_{85}/D_{15} < 5.0$. Figure 2.1 shows an example of two gravel beaches with a narrow (left) and wide grading curve (right).

Another characteristic of these beaches is their high permeability, as opposed to a sand beach, which increases the potential for infiltration during the uprush and exfiltration during the backwash (Masselink and Li, 2001). The average value of the hydraulic conductivity (or coefficient of permeability) of sand is about 0.0001 m/s and may rise to 0.01 m/s on coarse sand while permeability on gravel varies from 0.001 m/s to 1.0 m/s (Bear, 1972; Foote *et al.*, 2002). The porosity, defined as the ratio of the volume of air/water and the volume of the mixture, ranges, for gravel beaches, typically between 0.25 to 0.4 (Domenico and Schwartz, 1997). The importance of permeability on the beach performance is further discussed in Section 2.3.

Table 2.1: Natural shingle beach sediment characteristics, Powell (1993)

Site	D_{10} (mm)	D_{50} (mm)	D_{100} (mm)	D_{85}/D_{15}
Seaford	6.1	13.7	38.0	2.7
Whitstable	7.6	12.6	50.0	2.4
Chesil (Portland)	23.8	30.0	-	-
Chesil (Westexington)	8.5	10.0	13.0	1.3
Littlehampton	7.3	13.0	42.0	2.3
Hayling Island	7.0	16.0	64.0	4.0
Hurst Spit	6.0	20.0	63.0	4.3
Pevensey Bay	6.6	14.3	-	3.1
Southwold	6.1	14.0	50.0	4.4
Sidmouth	7.0	22.2	90.0	5.8
Hythe	2.8	5.2	23.2	3.1
Pensarn (N. Wales)	6.9	15.0	50.0	4.1

Source: HR Wallingford Report SR 350

Figure 2.1: Narrow (left) and wide (right) graded gravel materials having the ratio D_{85}/D_{15} equal to 1.3 and 3.1 respectively

A gravel beach can be seen as a sum of different zones where the interaction of hydrodynamic processes and beach characteristics influence the final response of the beach. These zones are schematised in Figure 2.2. The surf zone is the zone of wave action extending from the water line out to the most seaward point of the zone where waves start breaking (breaker zone). The breaking process is gradual and generates a surf zone in which the wave height decreases progressively as waves approach the shore. In the surf zone the sediments will be subject to a

complex set of forces which are produced due to bed friction and the impact of the breaker, which generate significant turbulence and sediment sorting. As will be shown in Chapter 6 and Chapter 7, the surf zone is a very dynamic zone and its profile response is very closely linked to changes in the incident wave energy.

The dominant modes of sediment transport on gravel beaches are assumed to be mainly bed load and sheet flow transport. Gravel transport mainly takes place in the swash zone, which is the zone intermittently wet and dry (see Figure 2.2). The swash zone is the most dynamic part of the nearshore zone for the gravel beaches (Elfrink and Baldock ,2002; Butt and Russell, 2000; Austin and Masselink, 2005). It is a particularly complex zone of where waves, tides, sediments and groundwater flow (infiltration/exfiltration) all play an important role. A detailed discussion on the morphodynamic processes in the swash zone, and the effect of infiltration/exfiltration on the beach profile response, which also influence the beach slope, is given in Section 2.3. These beaches have generally steeper slopes, with overall slopes typically ranging between 1 in 5 and 1 in 20 (Carter and Orford, 1984).

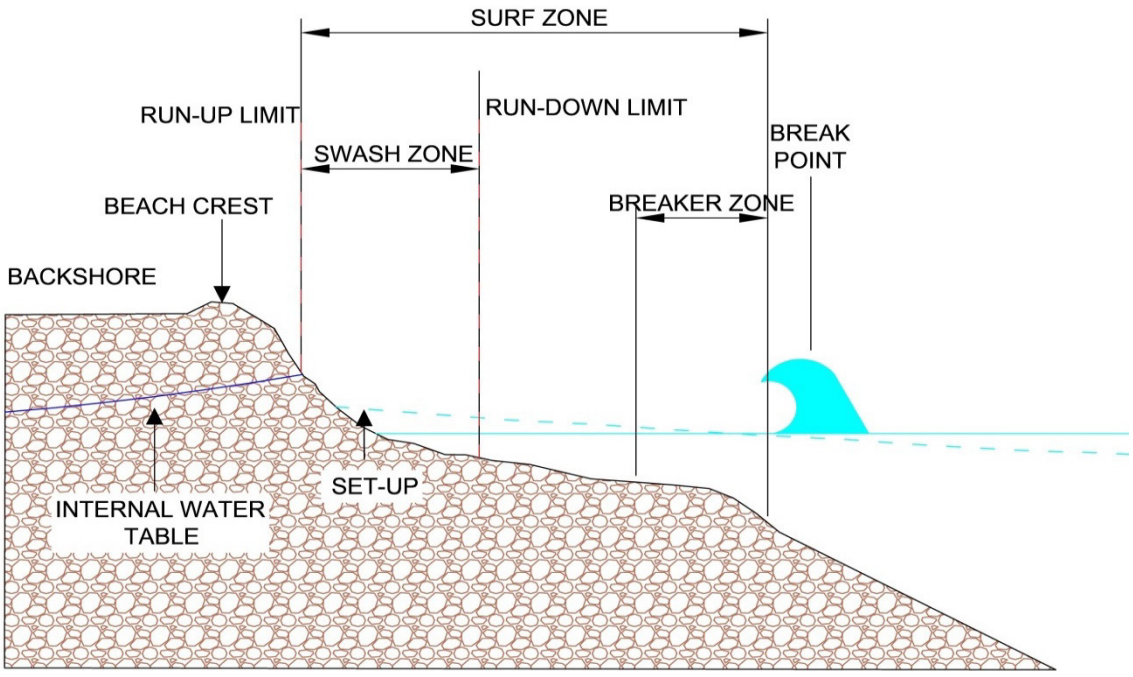

Figure 2.2: General beach profile. Adapted from “Beach Management manual” (2010)

Sediment properties such as grain size, shape and specific fall velocity control the rate of sediment transport and the direction in which sediment travels, either in bedload or suspended transport by waves or currents. Despite the effect of the grain shape on transport, it is generally neglected because of the uncertainties involved in assigning a value to a chosen shape parameter. A natural grain population is often characterised by diverse minerals and grain sizes which both influence the

grain shape. A population of grains is therefore inevitably heterogeneous with regard to grain shape. These charateristics make it difficult to define a representative shape for the population as a whole. As a consequence of this, the grain shape parameter is out of the scope of the present study and therefore not considered further here.

Jennings and Schulmeister (2002) defined three types of gravel beaches:

- 'pure' gravel beaches comprised of gravel-size material (D_{50} = 2–64 mm) across the entire intertidal region ;
- 'composite' gravel beaches comprised of a pure gravel upper beach fronted by a sandy low tide terrace; and
- 'mixed' gravel beaches comprised ofa mixture of sand and gravel sediment.

Both "composite" and "mixed" may have a noticeable break of slope between the gravel and sand sections, as shown at Highcliffe beach in Figure 2.3, where the red line shows the location of changing slope. The beaches on which this study concentrates are those composed of gravel material with no inclusion of sand, i.e. "pure gravel".

Figure 2.3: Highcliffe beach, the red line shows the location of changing slope due to the difference in sediment sizes

2.3. Morphodynamic processes in the swash zone

The swash zone is defined as the region of the beach that is alternately wet and dry due to wave motion and can be seen as the transition between sea and land (see Figure 2.2). The wave motion in the swash zone is one of the main drivers for cross-shore sediment transport and is characterised by strong and unsteady flows, high turbulence levels, large sediment transport rates and rapid morphological change. It represents the most dynamic region of the nearshore (Puleo *et al*., 2000; Kikkert, 2013; Pintado-Pati *et al*., 2015). There is a lot that is still unknown about the hydrodynamic and morphodynamic processes taking place in the swash zone. It is difficult and complex to carry out accurate experiments in the swash zone due to the small water depths and the highly dynamic characteristics of the swash zone. Additionally, most measurement equipment is either designed for wet or for dry conditions, while the swash zone contains both (Masselink and Hughes, 1998). A lot of research has been conducted in recent years, with Elfrink & Baldock (2002), Masselink & Puleo (2006) and Almeida *et al* (2013) reporting field experiments in the swash zone. This section provides an overview of the hydrodynamic processes in the swash zone that influence cross-shore sediment transport.

2.3.1. Swash cycle

When waves approach the shore, a cyclic pattern of wave run-up and run-down is induced. The run-up and run-down of flow due to a single wave is referred to as the swash cycle. A swash cycle consists of two different phases: 1) wave run-up, also referred to as uprush; and, 2) wave run-down, also referred to as backwash. During uprush, the flow velocity will decrease (due to bottom friction and gravity) until it reaches zero. When the water reaches its maximum run-up elevation it will start moving back. Following this point the velocity increases again, but now is directed offshore. The duration of backwash is typically longer than the uprush (Hughes et al., 1997).

This difference in uprush and backwash during one swash cycle is referred to as swash asymmetry. In contrast to the backwash, the uprush acceleration is short and strong and the velocities will generally be higher and the duration shorter. Another aspect to consider during the swash cycle is the groundwater flow. Water infiltrates the (dry) beach during uprush and will exfiltrate during backwash, therefore part of the water transported upslope by the uprush is still within the bed during backwash. The effect of infiltration/exfiltration is discussed in the following sections.

Another interesting phenomenon, which happens often, is known as swash-swash interaction. This happens when a wave reaches the coast and travels up a beach, but is not able to complete a full swash cycle before the next wave arrives. This generally occurs when the swash duration is larger than the incident wave period. In this case, the second wave will catch up and absorb the first wave (when the first wave is still in the uprush phase) or both waves will collide (when the first wave is in the backwash phase) (Erikson *et al*., 2005). There is very little discussion in the literature about the effect of swash-swash interactions on sediment transport in the swash zone. Erikson *et al*. (2005) concluded that this phenomenon enhances the turbulence in the swash motion and that it has a large influence on the maximum run-up length and the swash duration. Blenkinsopp *et al*. (2011) concluded that swash-swash interaction induces larger transport rates, either onshore or offshore. This phenomenon was observed during the experiments carried out for the present study and is discussed further in Chapter 7.

2.3.2. Swash motion

There are generally two approaches to describing swash motions on natural beaches (Baldock et al., 1997; Masselink and Puleo, 2006): (1) swash flows resulting from the collapse of high-frequency bores (f > 0.05Hz) on the beachface; and, (2) swash flows characterised by standing, low-frequency (f < 0.05 Hz) motions (Butt et al., 2005).

Physical processes in the swash zone are known to control erosion and accretion at the shoreline (Puleo et al. 2000; Jamal *et al*., 2012). This is exacerbated for coarse grained beaches, where the surf zone is much narrower and closer to the shoreline than on sandy beaches. Swash motions on gravel beaches are particularly influenced by the form of wave breaking (Pedrozo-Acuña, 2005; Jamal *et al*., 2012). Plunging is normally the dominant mode of wave breaking on steeper beaches, and under this type of breaking the velocity on the wave crest is much higher than the wave trough. The phenomenon of sharp wave crests and flat wave troughs is referred to as wave skewness. Since the velocity differs, more sediment is mobilized under the crest, and thus, a net onshore transport. Wave skewness could also cause net offshore transport due to a phase lag between the mobilisation and the transport of sediment. In that case, sediment is mobilized by the higher crest velocities and transported by the trough velocities (Grasso *et al*., 2011). Whether a phase-lag between mobilisation and transport exists, depends on the sheet-flow layer, the wave period and the sediment settling velocity (Dohmen-Janssen et al., 2002).

Another phenomenon often clearly visible near the shoreline is the presence of bore or broken waves. Breaking creates energetic bores which collapse in proximity to the shoreline and subsequently travel up the beach triggering the swash oscillations (Baldock and Holmes, 1997). This mechanism generates a shoreward asymmetry in the velocity profile which pushes turbulent flow shoreward. Turbulence is the highest frequency motion in the swash zone, and generally plays a relevant role for sediment transport by stirring up the sediment and bringing it into suspension. Puleo and Butt (2006) and Masselink and Puleo (2006) concluded that the turbulence existing during uprush is dominated by the wave bore, while turbulence during backwash is dominated by bed turbulence and the growing boundary layer. Moreover, the turbulence that persists into the swash intensifies the up-rush, rather than the backwash (Hughes et al. 1997). The effects of such asymmetry in the cross shore velocity upon the resulting sediment transport in the swash zone, is further enhanced by the volume of water that infiltrates into the porous surface during the run-up. The effect of infiltration/exfiltration to sediment transport is discussed in the following sections.

2.3.3. Sediment transport in swash zone

Sediment transport in the swash zone is of particular importance to the overall sediment budget, as swash and backwash processes influence whether sediment is deposited inshore, or returned offshore (Horn, 1994; Masselink, 2006). A quantitative understanding of sediment transport in the swash zone is needed as an important part of the littoral sediment transport occurs in the swash zone. Sediment concentrations are often high in the swash zone, and may typically be several orders of magnitude higher than in the inner-surf zone (Osborne and Rooker, 1999; Beach and Sternberg, 1991).

Saltation, bedload and sheet flow dominate the nearshore transport of gravel beaches. Saltation refers to the transport of sediment particles in a series of irregular jumps and bounces along the bed. Bedload sediment transport is caused primarily by fluid shear stresses initiating sediment particle motion and moving the particles along the bottom. The sheet-flow regime occurs when the fluid flow driven by the waves applies a sufficiently large shear stress on the bottom layer to enable the motion of a thick and dense layer of sediments. Due to the unsteady characteristics of swash flow, and the small water depths, it is expected that bed load transport (or sheet flow) is the dominant type of transport in the swash zone (Buscombe and Masselink, 2006). Horn and Mason (1994) analysed the ratio between bed and suspended load transport in the swash zone for a

number of field experiments, and found that bed load generally dominates in the swash zone. Similarly, in the uprush suspended load transport was found to be dominant only occasionally, while bed load transport generally dominates the backwash.

Also the work carried out by Masselink (2006) showed a clear difference between the relative importance of bedload and suspended load in the swash and backwash, and the importance of bedload, particularly for backwash. The results of this work suggested that bedload is the dominant mode of transport in the backwash, while its importance in the swash varies from beach to beach. Hughes (1992) considered the form of the backwash to be important and observed two types of backwash. In one type, the entire swash lens decreased in depth at a similar rate, thus maintaining the wedge shape that the lens reached at the time of maximum uprush throughout most of the backwash. In this case, which may correspond to saturated conditions, sediment is assumed to remain in suspension in the backwash. In the second type of backwash observed by Hughes (1992), the depth at the seaward end of the swash lens decreased at a faster rate than the landward end, and the swash depth became uniformly shallow over much of its length. This type of backwash lens contained a mixture of sediment and water, in which the top several centimetres of the bed became mobile, with no clear fluid layer overlying. In this case, bedload transport would dominate and may represent unsaturated conditions (Elfrink and Baldock, 2002; Masselink, 2006; Pintado *et al*., 2015).

2.3.4. Effect of in/exfiltration in the swash zone

The material property that most controls the degree of infiltration, is the permeability or hydraulic conductivity of the beach material (Masselink and Li 2001). Infiltration and exfiltration of water through the beach surface are expected to vary during run-up and backwash, depending on groundwater levels, the permeability of the beach material and whether the beach sediment is saturated or unsaturated (Elfrink and Baldock, 2002; Pintado *et al*., 2015).

The effects of infiltration and exfiltration on sediment transport in the swash zone can be summarised as: (1) reduction of backwash volume and duration; (2) increase and decrease of the effective weight of sediment particles; and, (3) increase and decrease of the shear force on the sediment particles (Elfrink and Baldock, 2002; Pintado *et al*., 2015). The flow velocity during the run-down is slightly reduced by the reduction in volume and duration of the backwash. However, this effect is expected to be of minor importance on sandy beaches as the vertical flux through the

beachface is small compared to the horizontal flux in the swash zone. On shingle and permeable beaches, this effect may become important.

Seepage is another associated mechanism, and this can alter the effective weight of sediment (Nielsen, 1992) and also affects bed shear stress (Puleo and Holland, 2001; Pedrozo-Acuña *et al*., 2007) by thinning (infiltration) or thickening (exfiltration) the bottom boundary layer of the swash flow. Infiltration increases the effective weight of the sediment, and therefore less sediment will be in suspension, but may also increase the bed shear stress, thereby promoting sediment transport. Conversely, during exfiltration, the opposite occurs and the sediment mobility increases. Nielsen (1997), Turner and Masselink (1998) and Butt et al. (2001) included these two processes and the boundary layer alteration into a modified version of the Shields parameter, by considering the net effect on sediment transport of these (opposing) mechanisms across saturated beds in the swash zone.

A recent investigation of the hydrodynamics of large-scale, bore-driven swash, on steep permeable beaches was carried out by Kikkert *et al*.(2013). This work showed that the gravel beach is much more permeable than sandy beaches and therefore the wetting front, which forms when water infiltrates into the beach, moves much faster on impermeable beaches. During a swash cycle almost 35% and 50% of the surface water infiltrated into the coarse sand and gravel beaches, respectively. Infiltration rates were highest immediately after bore arrival on the beach, then gradually decreased to become very close to zero in the backwash. As expected, due to the water loss, the maximum run-up for the permeable beach is lower than for an impermeable beach and the same wave / water level conditions. In addition, since air below the wetting front can escape more easily, the pore-air pressure builds up at a much smaller rate, and the wetting front reaches the groundwater level very soon after the bore arrival. From this moment the beach becomes saturated and further infiltration into the beach is significantly reduced (Steenhauer et al., 2011).

Masselink and Li (2001) showed that infiltration enhances the swash cycle asymmetry by reducing the backwash velocity and increasing the backwash duration. The increased swash asymmetry enhances onshore sediment transport and this results in berm formation, and relatively steep beach gradients. However, they also found this effect only occurs when the infiltration volume (Vi) is more than two percent of the swash uprush volume (Vu). The infiltration volume can be related to the grain size (larger grains result in larger pores, therefore more infiltration). The threshold condition for increased swash asymmetry (Vi > 2% Vu) can therefore be translated into a critical grain size of D_{50} = 1.5 mm (Masselink and Li, 2001). This threshold value, indicates that the swash

asymmetry effect of infiltration only takes place on gravel beaches with a D_{50} > 1.5mm and not on sandy beaches where grain sizes are usually smaller than 1mm.

In order to protect beaches from storm wave action, in the UK it is common practice to recharge beaches using mixed sand-gravel sediment (DEFRA, 2007). A study carried out by DEFRA (2007) investigated the influence of permeability on the performance of recharged beaches and the formation of cliffing. Both physical model (Trim, 2003) and field measurements (Pevensey Bay, Kingsdown, Eastoke Hayling Island and Tankerton Bay) showed that the performance of a recharged mixed sand-gravel beach was closely related to the hydraulic performance of the beach. It was observed that the sand fraction, in the order of 30 to 40% (variation in permeability), influenced the overall performance of mixed beaches. It was also observed that a connection existed between cliffing formation and the minimum values of the hydraulic conductivity of the sediment matrix.

In summary, it can be stated that the effect of infiltration and exfiltration on the effective sediment weight promotes offshore transport, while the modification in thickness of the boundary layer and the swash flow asymmetry enhance a net onshore transport. From the literature, it is not entirely clear which process is dominant, although some suggestions have been made.

2.3.5. Effect of groundwater table on beach profile response

The elevation and profile of the beach water table are characterised by the properties of the beach material, such as its particle size range, particle shape, permeability of the beach material, and by the hydraulic conditions such as wave height, wave period and tidal range (Gourlay, 1992). Although the tidal response of the water table is quite important (rising steeply with a flooding tide, and falling more slowly during the ebb), this is beyond the scope of the present study and is not considered in this thesis, where only the effects of the waves are investigated.

Water table dynamics have been of interest for coastal managers due to the problems associated with salt water intrusion to the aquifer, wastewater disposal from coastal developments and coastal flooding problems (Duncan, 1964; McLachlan, 1989; Kang and Nielsen, 1996; Maselink and Turner, 2012). Several studies observed the influence of the groundwater table within the beach on the infiltration/exfiltration rate, swash-backwash dynamics, sediment transport and further wave interactions (Bagnold 1940; Duncan 1964; Nelson and Miller, 1974; Packwood, 1983; Turner and Nielsen, 1997; Lara *et al.*, 2006, Maselink and Turner, 2012).

Erosion and accretion of the beachface as a result of variations of the beach water table have been analysed by many researchers (e.g., Bagnold, 1940; Shepard and LaFond, 1940; Emery and Foster, 1948; Duncan, 1964, Buscombe and Masselink, 2006; Horn and Li, 2006; Horn *et al.*, 2007 and Maselink and Turner, 2012). It is generally accepted that a low water table fosters both infiltration and onshore sediment transport, whilst a high water table elevation facilitates exfiltration and offshore sediment transport (Grant, 1946, 1948; Nelson and Miller, 1974; Maselink and Turner, 2012).

A less obvious, but potentially significant process, is the effect of the interactions between the particle size range, the beach groundwater table, swash motion on sediment transport processes on the upper beach (Turner and Masselink, 1998) and, therefore, beach stability. These interactions are strongly controlled by the permeability of the beach and the elevation of the beach groundwater table relative to the sea level.

As a result of these studies, analytical and numerical models have been developed to predict beach water table fluctuations, however, most of them investigated the groundwater elevation in response to tides (Nielsen, 1990; Turner 1995; Li *et al.*, 1996, 1997; Baird *et al.*, 1996, 1997, 1998; Raubenheimer *et al.*, 1998, 1999), under predicting the water table elevations under conditions when wave effects are important (Horn, 2002). Few numerical models included the effect of wave action through wave run-up infiltration (Li *et al.*, 1997; Li and Barry, 2000; Nielsen *et al.* 1988), however, because gravel beach research in the laboratory is rare, none of the models which include wave effects have yet been tested against field or laboratory data. The notable exception being the GWK (Blanco, 2002) and BARDEX experiments (William *et al.*, 2012). The GWK measurements included not only the wave field and resultant equilibrium profile development, but also detailed measurements of pore water pressures under the swash face. The behaviour of the groundwater was analysed, concluding that the water table at the gravel and mixed beaches responds to individual waves in a different manner; the response in the mixed beach being cumulative in time. New formulae for the setup at the shoreline and the over-height of the water table were proposed for coarse grained beaches, as well as for the propagation speed through the sediment.

One of the objective of the BARDEX experiments was to investigate the role of back barrier lagoon levels on the dynamic groundwater profile through the barrier and to assess whether varying groundwater levels induced differing morphological response at the beachface. Specific research included: the effects of lagoon and seaward water levels on the beach groundwater profile; and, the

effect of changes in beach groundwater profile on erosion and accretion processes. Test results carried out with sea levels equal to the lagoon elevation showed the groundwater mounding due to the action of waves at the land-sea boundary was primarily a function of the vertical run-up excursion, rather than the hydraulic characteristics of the aquifer (i.e. hydraulic conductivity). Moreover, the primary effect of raising/lowering the back-barrier lagoon level was to decrease/increase the observed groundwater mounding. As the above experiments were carried out in large wave flumes, it was not possible/practical to investigate the effect of the grain size distribution on the groundwater elevation under incident wave conditions. This was investigated during the present research and is discussed in Chapter 6.

As previously discussed, the present research focuses attention on wave-driven rather than tidal effects on the groundwater elevation. The role of the waves in modifying groundwater elevation in the coastal zone can be observed, according to Turner *et al.*(1997), in two ways: the first is due to set-up at the shoreline, which results in a raising of the mean water surface at the shoreline. The second, is due to the wave run-up of waves across the beach-face, which further elevates the potential zone of seawater inflow. Run-up of waves is super-imposed on the already elevated mean water level induced by wave set-up as schematised in Figure 2.4.

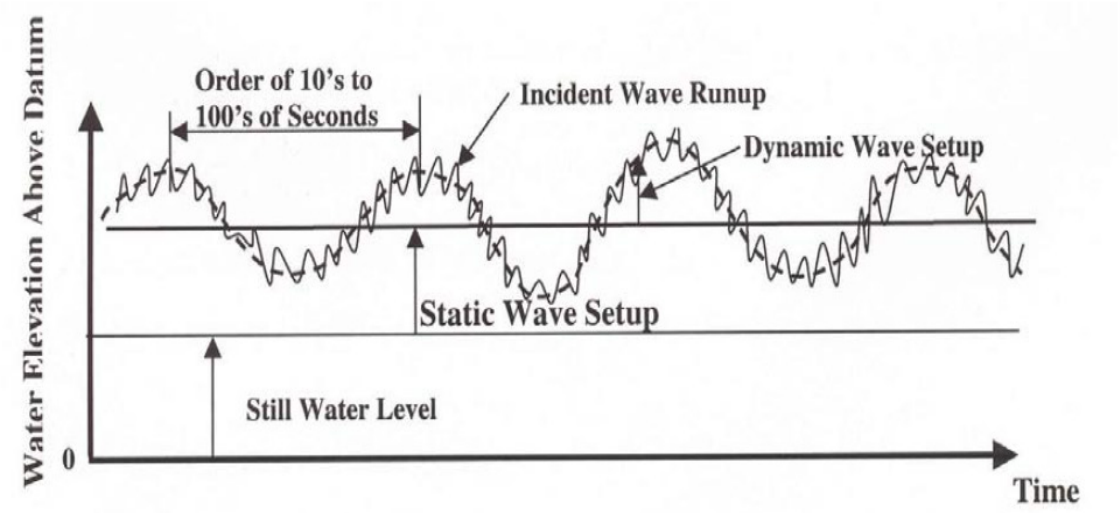

Figure 2.4: Definition of wave set-up (*Guidelines and Specifications for Flood Hazard Mapping Partners, January 2005*)

Following the recognition of wave set-up as a key contributor to flooding and erosion hazards, a series of studies were carried out to provide empirical equations of wave set-up (Fairchild 1958; Savage 1957; Saville 1961). Some of the most utilised formulae of wave set-up are presented

below, where they all include offshore wave height (which governs the energy available to produce set-up), and some of them also incorporate the beach slope.

Bowen *et al.* (1968) proposed a simple linear model of set-up at the shoreline as a function of wave height for impermeable, smooth and constant slopes:

$$\eta_{max} = \eta_{min} + \frac{3}{8}\gamma H_b \tag{2.1}$$

where η_{min} is the maximum set-down immediately prior to breaking, γ the wave height to water depth ratio at breaking, and, H_b is the breaking wave height.

According to linear wave theory, waves usually break at a depth approximately 1.2 times their height, which can account for a set-up at the shoreline approximately 25% of the wave height at breaking.

Fredsoe and Deigaard (1992) suggest:

$$\eta_{max} = \frac{3}{8}\gamma H_b = 0.2\, H_b \tag{2.2}$$

Guza and Thornton (1981) proposed :

$$\eta_{mean} = 0.17 H_{0s} \tag{2.3}$$

where η_{mean} is the time averaged mean set-up at the shoreline and H_{0s} is the significant wave height in deep water.

Following an extensive investigation, Hanslow and Nielsen (1993) suggested the following empirical relationship for the set-up at the shoreline:

$$\eta_{max} = 0.048 \sqrt{L_0 H_{0rms}} \tag{2.4}$$

where L_0 is the offshore wave length and H_{0mrs} (1.71 H_s) is the offshore root mean square (rms) wave height. This means that the set-up on natural beaches will raise the mean water level at the beachface by approximately 40% of the H_{orms} wave.

For the case in which no tide is present, Nielsen (1999) combined the results of Kang and Nielsen (1994) and Kang (1996) for sandy beaches and suggested the following expression for the maximum water table wave set-up:

$$\eta_{max} = 0.44 \sqrt{L_0 H_{0rms}}\, tan\alpha \tag{2.5}$$

where $\tan\alpha$ is the local beachface slope.

Turner and Masselink (2012) observed, during the BARDEX experiments, that for the beachface composed of gravels (D_{50} =11mm; D_{10} =5.4mm and D_{90} =16.9mm), the maximum groundwater elevation is generally in line with the results obtained by Nielsen (1999) for sandy beaches. Other studies also recognized the role of the beach morphology by incorporating the beach-face slope into the predictor. Cross-shore variations in wave setup have been described by Bowen (1968) by using:

$$\frac{d\eta}{dx} = \frac{tan\ \alpha}{(1 + \frac{8}{3}c^2)} \tag{2.6}$$

where η is the setup inside the wave break point, x the cross-shore coordinate, tanα the beach slope, and c=0.55= h / H assumes that the height (H) of a broken wave, or bore, remains an approximately constant proportion of the water depth (h).

Goda (1985) proposed the following expression:

$$\eta = \frac{0.01\ H_{s,0}}{\sqrt{\frac{H_{s,0}}{L_0}(1 + \frac{h}{H_{s,0}})}} \tag{2.7}$$

where h is the water depth at any location in the surf zone and H_{s0} is the significant offshore wave height.

Raubenheimer *et al.* (2001) found setup to be related to wave height and the average surf zone beach slope:

$$\frac{\eta}{H_{0,s}} = 0.19 + \frac{0.003}{tan\alpha v} \tag{2.8}$$

where $tan\alpha v$ is the average surf zone beach slope

All of these equations, however, were developed on sandy beaches with relatively flat slopes. Set-up at the shoreline on coarse-grained beaches were measured by Powell (1990) in laboratory experiments, concluding that generally the degree of wave set-up is between 10-30% of the significant wave height, with a pronounced wave steepness dependency, and proposing the following relationship:

$$\frac{\eta}{H_{0,s}} = 0.31 - 3.5\ \frac{H_{0,s}}{L_m} \tag{2.9}$$

where $\eta/H_{0,s}$ is the dimensionless set-up at the shoreline.

Blanco (2001) following the results from the GWK proposed the expressions for the maximum water table wave set-up:

$$\eta_{max} = c\sqrt{L_0 H_{m0}}\, tan\alpha \tag{2.10}$$

where tanα is the local beachface slope and c is a coefficient function of the beach material (c = 0.45 for sand; c = 0.5 for mixed beaches and c = 0.05 for gravel)

Turner and Masselink (2012) also found, during the BARDEX experiments on gravel beaches, that the mean water table elevation within the beachface was of the order of 25% of the incident wave height. During the present study, however, the mean water table elevation within the beachface was of the order of 10-20% of the incident wave height depending on the beach grain size, as described in Chapter 6.

All the above studies clearly suggest that the groundwater table (also referred hereafter as internal wave set-up) is influenced by the incident wave condition (H_s, T_p). However, even though, it would be expected to have a correlation between internal wave set-up and beach permeability, the formulae available in the literature do not explicitly consider it. During this research a 2D physical model study was carried out to investigate the effect of the grain size distribution on both the internal wave set-up and wave-induced pore pressure decay. The results and analysis from this this study are discussed in Chapter 6.

2.3.6. Wave breaking

When waves approach the coast, the majority of the wave energy is dissipated across the surf zone by wave breaking. A portion of that energy is transformed into wave run-up in the swash zone, which is the subject of the next section. Firstly, this section briefly discusses the phenomenon of wave breaking as part of our discussion of the swash zone.

As a wave propagates from relatively deep to shallow water, its wave height tends to increase while its wavelength reduces, this leads to a steepening of its profile that becomes increasingly asymmetric and unstable causing the wave to break. Wave breaking is an important process which allows energy to be released and transformed into nearshore circulation and sediment transport.

There are four main types of wave breaking: spilling; plunging; collapsing; and, surging (Figure 2.5). The breaker type depends on the wave height and period of the wave, and the

characteristics of the beach slope. This can be described by the breaker parameter, surf similarity or Iribarren number, defined as:

$$\xi_{m-1,0} = \frac{tan\alpha}{\sqrt{H_{m0} L_{m-1,0}}} \quad (2.11)$$

where H_{m0} is the spectral wave height, $L_{m-1,0}$ being the deep water wave length and $\tan\alpha$ is the slope of the beach.

A spilling breaker ($\xi_{m\,1,0} < 0.2$) can be characterized by white water tumbling down from the wave crest to the front face of the wave (white-capping). The beach slope is gentle and the waves will generally be of higher steepness (say, s > 0.05).

Plunging breakers ($0.2 < \xi_{m\,1,0} < 2\text{-}3$) are breakers where the wave crest forms an overturning jet. This breaker type is common on beaches with steeper slopes.

Collapsing breakers ($\xi_{m\,1,0} \pm 2\text{-}3$) are breakers where the lower part of the wave crest overturns, and is an intermediate case between spilling and plunging breakers.

Surging breakers ($\xi_{m\,1,0} > 2\text{-}3$) occur where the surface remains smooth during breaking. They appear when waves encounter a very steep slope and cannot transform before the surge reaches the crest.

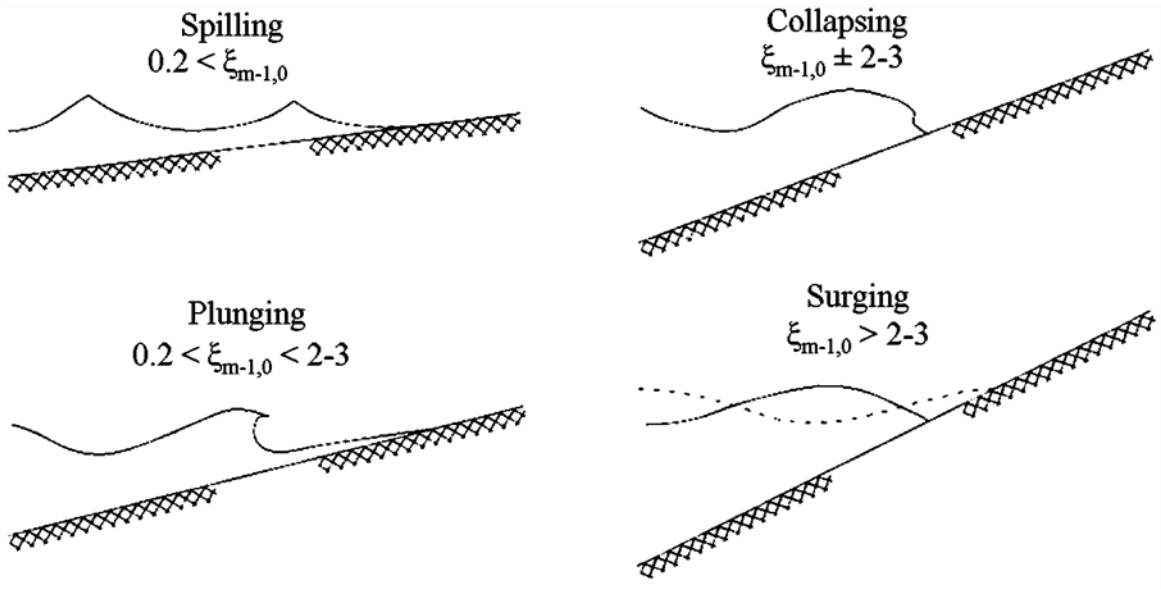

Figure 2.5: Type of breaking on a slope (EurOtop, Pullen *et al*. 2007)

It has been shown theoretically, and in the laboratory, that wave breaking characteristics can also be described by the surf-scaling parameter (ε_b) (Guza and Inman, 1975):

$$\varepsilon_b = \frac{a\omega^2}{g\ tan^2\beta} \quad (2.12)$$

where α is the wave amplitude at breaking, ω is the wave radian frequency ($\omega = 2\pi L$, where L is wave length), g is acceleration due to gravity, and $tan\beta$ the beach gradient.

For waves to be completely reflected with negligible dissipation, ε_b must be less than 1. However, Guza and Bowen (1975) found that low dissipation, and strong reflection and resonance, will occur if ε_b < 2.0-2.5. Under these conditions, breakers will be of the surging type, and the height of the runup relative to incident wave height will be maximized (for any given beach face permeability), and setup of the mean water level will be minimal. Since long, lower steepness, waves and steep beach slopes result in low ε_b values, pronounced reflectivity is most likely to characterize beaches composed of coarse material and experiencing long period low-amplitude swell (Wright, 1979; Masselink, 2006).

As ε_b increases, either due to increasing wave steepness or to decreasing bed gradients, reflectivity decreases and viscous dissipation of wave energy increases. Guza and Inman (1975) demonstrated that when ε_b > 2.5, waves cease to surge up the beach and begin to plunge, causing a substantial increase in eddy viscosity. This leads to the dissipation of much of the wave energy before the waves reach the beach face. Further increases in ε_b cause the surf zone to increase in width, resulting in more complete dissipation as the broken waves assume the form of dissipative bores, which decrease progressively in amplitude as they approach the shore. Studies of breaking waves (Galvin, 1972) indicate that when ε_b > 33 breakers change to the highly dissipative spilling type. Under dissipative conditions, radiation-stress (excess momentum flux) gradients develop across the entire surf zone (Longuet-Higgins and Stewart, 1962, 1964; Bowen et al., 1968; Bowen and Inman, 1969). These gradients are responsible for a setup of mean water level landward of the break point and play a major role in driving the response of gravel beaches to wave action.

2.3.7. Wave run-up on gravel beaches

Presently, our understanding of wave run-up on shingle beaches is poor. Approaches to calculate run-up usually rely on formulae developed for the structure types described in the Overtopping Manual (EurOtop, 2007) or other literature on structures and beaches (e.g. Hughes, 2005; Stockdon et al., 2006; van der Meer and Janssen, 1994). Some of the available formulae are briefly described below.

Van der Meer & Janssen's method describes wave run-up on dikes and similar sloping structures, revetments and seawalls. Various effects can be incorporated in the formulation, and if the allowance for friction / permeability is considered to be negligible, then the 2% exceedance wave run-up elevation ($R_{u2\%}$) is given by:

$$\frac{R_{u2\%}}{H_{m0}} = 1.65\,\xi_{m-1,0} \tag{2.13}$$

where H_{m0} is the spectral significant wave height and $\zeta_{m-1,0}$ is the Iribarren or surf similarity parameter based on the mean spectral wave period.

Hughes (2005) provides a new formula for the estimation of irregular wave run-up on rough, impermeable slopes based on the wave momentum flux parameter (PMF), where PMF is defined as

$$P_{MF} = \frac{M_F}{\rho g h^2} \tag{2.14}$$

The concept of the PMF relates the properties of the wave condition and water level to the structural response of the wave loading (Hughes, 2003). Hence the wave run-up is related to the PMF and we can write;

$$\frac{R_{u\,2\%}}{h} = 4.4(\tan\alpha)^{0.7}\left(\frac{M_F}{\rho g h^2}\right)^{\frac{1}{2}} \tag{2.15}$$

where H_{m0} is defined at the toe and h is the depth at the toe.

Powell (1990) investigated 2D physical model tests exploring the behaviour of shingle beaches under normally incident random waves and developed the following formulation for wave run-up:

$$\frac{R_{u\,2\%}}{H_{s0}} = \frac{hc}{H_{s0}}\left[-\frac{\ln(0.02)}{4.2}\right]^{0.455} \tag{2.16}$$

where:

$$\frac{hc}{H_{s0}} = 2.86 - 62.69\left(\frac{H_{s0}}{L_{0m}}\right) + 443.29\left(\frac{H_{s0}}{L_{0m}}\right)^2 \tag{2.17}$$

and H_{s0} is the offshore wave height, L_{0m} is the offshore wave length based on the mean period and h_c is the crest level of the beach. It therefore couples $R_{u2\%}$ to the maximum built-up ridge of the beach h_c (i.e. the storm beach profile) and so h_c can be used as a proxy for $R_{u2\%}$.

Stockdon (2006) suggested that the elevation of extreme run-up peaks, given by the 2% exceedance value, $R_{2\%}$, be dependent on the sum of two dynamically different processes; the time averaged set-up (second term in the equation below) and the wave run-up as follows:

$$R_{u\,2\%} = 1.1(0.35\,\beta\,(H_{m0}L_{0p}))^{\frac{1}{2}} + \frac{\left[H_{m0}L_{0p}(0.563\beta^2 + 0.004\right]^{\frac{1}{2}}}{2} \quad (2.18)$$

where H_{m0} is the offshore spectral wave height, L_{op} is the offshore wave length and β is the foreshore slope.

Polidoro *et al*.(2013) used field measurements on gravel beaches to develop an improved run-up formula, specific to the beaches along the southeast coast of England where mixed sand and gravel beaches are dominant and a bimodal wave climate prevails. This equation includes the effect of wave set-up and the shape of the wave spectrum. Polidoro *et al*.(2013) compared the predicted run-up using the above formulae with the data collected at Worthing. In general, the equations analysed showed good agreement for low levels of wave run-up, and under prediction for higher values of run-up. The suggested formula (Polidoro *et al*., 2013), was empirically developed using the extensive Worthing data set, and it was used for other beaches to assess its validity. Moreover, the validation of the method was further done by comparing the prediction with the measured results from 2D physical model experiments.

Polidoro *et al's*. (2013) run-up formula is:

$$\mathrm{R_{u2\%}} = 1.04\ \mathrm{H_{m0}}\left(\frac{\mathrm{T_{m-1,0}}}{\mathrm{T_{m0,2}}}\right)^{0.5} \xi_{\mathrm{m-1,0}}{}^{0.5}\ \mathrm{Exp}\ (-\mathrm{Q_P})^{0.5} + \left(0.095\mathrm{H_{m0}}{}^{0.5}\ \mathrm{L_{m-1,0}}{}^{0.5}\right) \quad (2.19)$$

where H_{m0} is defined offshore at the buoy (h≈12m), $T_{m-1,0}$ is the spectral wave period, $T_{m0,2}$ is the mean wave period, Qp the peakedness parameter (discussed in more details in Section 4.1.6), $\zeta_{m-1,0}$ is the surf similarity parameter and $L_{m-1,0}$ is the wave length measured at the buoy.

More recently, Poate *et al* (2016) developed a new wave run-up equation from the XBeach-G data and validated using the field data.

$$R_{u\,2\%} = 0.21\ D_{50}^{-0.15}\ tan\beta^{0.5} H_s T_{m-1,0} H_s \quad (2.20)$$

where D_{50} is the mean size diameter of the beach grading curve, $T_{m-1,0}$ is the spectral wave period, H_s is the significant wave height and tanβ is the beach slope.

2.4. Existing predictive methods for shingle beach response

2.4.1. Introduction to the current prediction models

Presently our understanding of shingle beach morphodynamic response to wave attack is limited and based upon relatively few studies (Powell, 1990; Blanco, 2002; Bradbury et al, 2008; Williams et al 2012, Pedrozo-Acuna *et al.*, 2007). The approaches in use for predicting shingle beach response, crest erosion and potential breaching rely on both parametric and process-based models (Powell, 1990; Bradbury et al, 2008; Obhrai, 2008; Blanco, 2002; Buscombe *et al.* 2008; Van Rijn *et al.* 2003, 2007; Pedrozo-Acuña *et al*., 2006; Jamal *et al.* 2012; McCall *et al.*, 2014).

Parametric models generally ignore the underlying physical processes and try to relate directly the development of the beach profile to the incident wave condition and beach material characteristics. A process-based model is the mathematical / numerical representation of the dominant physical processes and their interactions which satisfactorily capture the behaviour of a system. Despite the fact that these models allow for a more realistic representation of the relevant physical processes, they suffer from the issues of computational burden (despite the increasing availability of High Performance Computing), data requirements and the stability of the numerical methods used and underlying issues related to the complexity of the process interactions. Currently, the most often used models for predicting gravel beach profile response to wave forcing are those of Powell (1990) known as SHINGLE and the process-based XBeach-G (Jamal *et al.*, 2012; McCall *et al.*, 2014).

XBeach-G is a process-based storm impact model for gravel coasts that is an extension to the existing process-based, time-dependent nearshore model XBeach (Roelvink *et al.*, 2009). A non-hydrostatic extension to the XBeach model (Smit *et al.*, 2010), similar to the SWASH model (Smit *et al.*, 2013; Zijlema *et al.*, 2011) was applied that allows XBeach to solve intra-wave flow and surface elevation variations due to short waves in intermediate and shallow water depths. To account correctly for upper swash infiltration losses and exfiltration effects on lower swash hydrodynamics on gravel beaches, XBeach-G computes groundwater dynamics and the exchange between groundwater and surface water using the XBeach groundwater model. Gravel sediment transport processes have been included in XBeach-G to simulate the morphodynamics of gravel beaches during storms. These transport processes are currently under further development and validation (McCall *et al.*, 2014).

In addition to SHINGLE and XBeach-G, a profile model CROSMOR developed by the University of Utrecht (Van Rijn 2006, Van Rijn et al. 2003, 2007) is also used to predict gravel beach profile response. The CROSMOR profile model (Van Rijn, 2006, 2007) is a probabilistic wave-by-wave model which simulates the propagation, transformation (shoaling) and breaking of individual waves along a cross-shore profile, which is assumed to be uniform in the longshore direction. Statistical parameters are computed from the results of the individual waves allowing them to shoal until an empirical breaking criterion is satisfied. Wave height decay, due to bottom friction and breaking, is modelled by using an energy dissipation method, with wave-induced set-up / down and cross-shore currents also modelled. The sediment transport rate of the model is determined for each wave (or wave class), based on the computed wave height, depth-averaged cross-shore and longshore velocities, orbital velocities, friction factors and sediment parameters. The net (averaged over the wave period) total sediment transport is obtained as the sum of the net bed load and net suspended load transport rates. The net total sediment transport is obtained as the sum of the net bed load and net suspended load transport rates.

As the present research is focused on an experimental studies, attention mainly focusses on the parametric models which are commonly used in practical coastal engineering applications due to their limited computational requirement and ease of use. Among the many available, this research focused on the use of those prediction tools that can be used straightforwardly by coastal managers and other practitioners: the SHINGLE model (Powell, 1990), which is used extensively in the UK as the standard parametric model to predict cross-shore profile change on gravel beaches (DEFRA, 2008) and XBeach-G, which provides a very simple GUI (Graphical User Interface) for the user.

2.4.2. The SHINGLE model (Powell, 1990)

The beach profile prediction model SHINGLE was developed at HR Wallingford as a coastal management tool (Powell, 1990). It is a parametric model which allows the user to predict changes to gravel beach profiles based on input conditions of sea-state, water level, existing profile, sediment size and the underlying stratum. The profile shape and its location against an initial datum can be predicted and confidence limits for the predictions determined.

The data used to derive the basic algorithms for SHINGLE were gathered during a physical model testing programme carried out in a wave flume at HR Wallingford. The results have been validated against field data at several UK locations (HR Report SR 219). A total of 181 detailed flume tests

were undertaken at a scale of 1:17. A range of particle sizes and gradings from typical UK shingle beaches were represented by crushed anthracite, which provide the most satisfactory reproduction of natural beach permeability, sediment mobility threshold and onshore-offshore transport characteristics (Powell, 1990). Test conditions included 29 different wave conditions (based on JONSWAP spectra), and all tests commenced with a standard beachface slope of 1:7.

The parameters measured by the flume study were: wave height (H_s); wave period (T_m); number of waves (N); beach material size (D_{50}); beach material grading (D_{85}/D_{15}); and effective thickness of beach material (D_B, which is the effective thickness of beach material measured relative to the initial slope). The maximum and minimum values for the input parameters used during Powell's experiments are summarised in Table 2.2. Other factors of interest such as: water level (*SWL*); initial beach profile, wave spectrum shape; and, angle of wave attack were derived from other test results.

Table 2.2: Maximum and minimum input parameter values during Powell 1990 experiments

	D_{50} (mm)	D_{85}/D_{15}	H_s (m)	T_m (s)
Min	10	2.19	0.8	4.5
Max	30	2.6	3.0	8.5

The test results showed that the influence of wave height is most significant in the upper beach zone where an increase in wave height causes an increase in surf zone width (i.e. a flattening of the upper beach profile). The effect of wave period variation is apparent in the vertical dimensions of the profile; thus an increase in wave period will increase the crest elevation and lower the profile toe (Powell, 1990). Variations in the steep initial beach slopes typical of shingle beaches are considered to have little effect on the ultimate beach profile, though they may affect the mode and duration of formation.

The prediction model divides the profile into three curves between the following limits as shown in Figure 2.6:

- Beach crest (*Pc, hc*) and still water level (*SWL*);
- SWL and the top edge of the profile step (*Pt, ht*);
- The top edge of the profile step and the lower limit of profile deformation (*Pb, hb*).

where *Pc* and *hc* are the horizontal and the vertical distance of the crest position from the shoreline (0,0) respectively; *Pt* and *ht* are the horizontal and the vertical distance of the breaker position from the shoreline (0,0) respectively; *Pb* and *hb* are the horizontal and the vertical distance of the lower

limit of the profile deformation from the shoreline (0,0), respectively. These curves are characterised by a series of profile descriptors defining the position and elevation of each transition point, for more details on the expression of these parameters see Powell (1990).

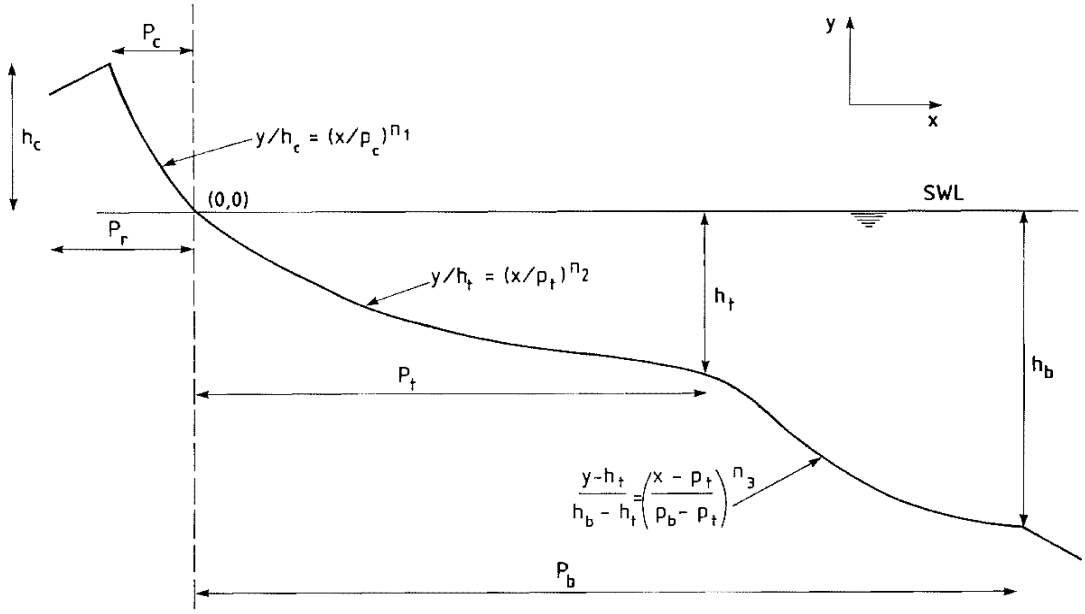

Figure 2.6: Schematised beach profile. (Powell, 1990)

The position of a predicted profile, relative to an initial profile, assumes that beach material moves only in the onshore-offshore direction and that differential longshore transport is zero. The areas under the two curves are compared relative to a common datum and the predicted curve is shifted along the SWL axis until the areas equate to provide the location of the predicted profile.

The validity of the lightweight modelling approach for a mobile physical model study has been called into question from different authors (Kamphuis ,1985; 1991; Hughes, 1993; Loveless and Grant, 1995). Loveless and Grant (1995) suggested two approaches to modelling the sediment transport on gravel beaches: 1) reproducing correctly the threshold for sediment motion (orbital velocity or shear stress) and the rate of percolation of water within the beach; 2) reproducing correctly the threshold and the ratio of the percolation forces on the sediment to its submerged weight. The latter can be expressed as the ratio i/(1-n)(s-1), where *i* is the percolation slope, *n* is the porosity and *s* is the sediment specific gravity. If *i* and *n* remain the same, but *s* (model) equals 1.3, then a scale effect error of 6 would result (if the prototype sediment had a specific gravity s = 2.65). Hence lightweight sediments will grossly over predict scour at the toe of coastal structures. If, however, a lightweight sediment is not used it is not possible to model the rate of percolation into the beach correctly for a sediment which satisfies similarity of the threshold of

motion condition. Loveless and Grant (1995) found that a sediment having a specific gravity of about 2.0 would give scale effect errors not exceeding 3.0 for both percolation rate and percolation force. Results from Loveless and Grant (1995) using both approach 1 (anthracite) and 2 (sand) produced different results under the same wave conditions, although they were difficult to compare as initial beach slope and water depth at the toe were different. They went on to suggest that the angle of repose (angularity of grains) and porosity (percolation rate) of the model sediments should be varied in order to achieve suitable results. This method, however, is quite difficult to achieve in practice (Whitehouse, 1998).

The alternative approach is based upon a technique originally developed by Yalin (1963), in which lightweight sediments with distorted geometry are used to represent the gravel material in physical models. The theoretical technique of Yalin (1963) was used and outlined by Powell (1990) to scale the gravel material in his study. As Powell (1990) employed lightweight material during his study, concerns were expressed with regards to the accuracy of the predictions of the rate of evolution of the dynamic equilibrium profile of the beach, wave run-up and also the evolution of the key beach descriptors, such as: the crest; the step; and, the base of the profile.

The use of anthracite in reproducing correctly the behaviour of a prototype gravel beach was confirmed by the comparisons between the measured test profiles from the Großen Wellen Kanal (GWK) (Blanco et al , 2006) with the profile predicted by SHINGLE (Powell, 1990). The good agreement between predicted and measured profiles, Figure 2.7, generally indicated that the methodology previously adopted by Powell (1990) for small-scale testing of shingle beaches (use of anthracite) correctly describes the cross-shore profile response under normally incident wave conditions (Bradbury, 2002). A weakness in Powell's model and in other beach shape models, that is of particular concern to the current research reported here, is that they are derived from experimental observations obtained from tests employing simple unimodal wave spectra, neglecting the possibility to have the complex wave conditions that combine wind sea and swell, forming a bimodal spectrum. As indicated above, a detailed discussion of this topic will be the subject of Chapter 7.

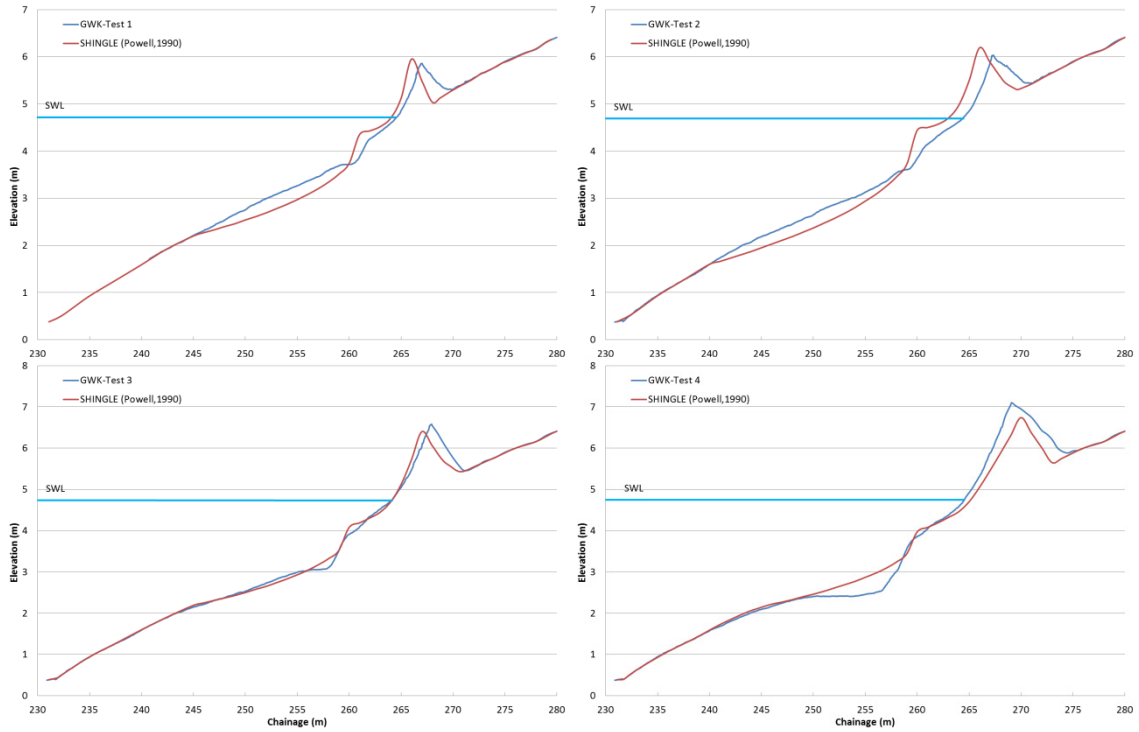

Figure 2.7: Comparison SHINGLE model prediction with GWK profile results, (Blanco, 2002)

2.4.3. XBeach-G

Jamal et al (2012) had previously shown how the X-Beach code could be adapted to predict erosion and accretion on coarse grained beaches against the GWK data. A non-hydrostatic extension to the XBeach model (Smit *et al.*, 2010), similar to the SWASH model (Smit *et al.*, 2013; Zijlema *et al.*, 2011) was applied, that allows XBeach to solve intra-wave flow and surface elevation variations due to short waves in intermediate and shallow water depths.

To account correctly for upper swash infiltration losses and exfiltration effects on lower swash hydrodynamics on gravel beaches, XBeach-G computes groundwater dynamics and the exchange between groundwater and surface water using the XBeach groundwater model. Again, interaction between swash flows and the beach groundwater table are considered particularly important on gravel beaches due to the relatively large hydraulic conductivity of the sediment. Finally, gravel sediment transport processes have been included in XBeach-G to simulate the morphodynamics of gravel beaches during storms. These transport processes are currently under further development and validation.

2.5. Discussion

In recent decades, the UK has gradually moved towards soft engineering schemes based on replenishment and maintenance of natural beaches in order to maintain an adequate level of

defence (Powell, 1993; DEFRA, 2016). To optimise the benefits of these investments and improve the level of management, the nourished beach has to be designed and managed carefully. Design parameters that need to be assessed include the size grading of the imported gravel and the profile of the resulting beach. Recharge material is likely to be more widely graded than the natural beach sediment, as a consequence the permeability of the recharged beach will be less than the natural beach, this can result in severe and unexpected erosion (Powell, 1993).

As previously described in Section 2.3, one of the key controlling factors of the beach profile is the permeability. Many researchers (Puleo *et al*., 2000; Buscombe and Masselink, 2006; Austin and Masselink, 2005; Horn and Li, 2006; Williams *et al.* 2012, Kikkert, 2013; Pintado-Pati *et al*., 2015) proved the importance of permeability on coarse-grained beaches and Mason and Coates (2001) identified permeability as the main parameter of a mixed beach, which influences sediment transport processes and swash zone hydrodynamics. Beachface gradient in relation to sediment transport and beach profile evolution has been studied by considering:

- sediment characteristics, sediment grain size and sorting (Bagnold, 1940; Bascom, 1951; Wiegel, 1964; Turner, 1995; Wilson *et al.*, 2008);
- swash infiltration/exfiltration and its effects on cross-shore sediment transport (Grant, 1948; Kemp, 1975; Quick, 1991; Turner, 1995; Hughes *et al.*, 1997; Masselink and Hughes, 1998; Turner and Masselink, 1998; Butt and Russell, 1999; Hughes and Turner, 1999; Puleo *et al.*, 2000; Butt *et al.*, 2001; Masselink and Li, 2001; Baldock and Hughes, 2006; Masselink and Puleo, 2006; Kikkert, 2013; and, Pintado-Pati *et al*., 2015);
- influence of the beach groundwater flow in the swash zone (Hegge and Masselink, 1991; Turner, 1993; Kang and Nielsen, 1996; Turner, 1998; Nielsen, 1999; Li *et al.*, 2002; Horn, 2006; Kikkert, 2013; and, Pintado-Pati *et al*., 2015).

Most researchers of coastal groundwater dynamics have focused attention on groundwater in sandy beaches (Kang and Nielsen, 1996; Turner *et al.*, 1997; Nielsen and Voisey, 1998; Nielsen, 1999), focusing their measurement on the beach water tables in response to low frequency tidal forcing. Only a few studies, such as Turner and Nielsen (1997), Horn *et al.* (1998) and Turner and Masselink (1998), Blanco (2002) and recently Turner and Masselink (2012), Kikkert, (2013); Pintado-Pati *et al*. (2015), have measured higher frequency fluctuations due to waves.

When studying the beach profile response of gravel beaches under wave action, knowledge of pore pressures and the related wave attenuation inside the porous media as function of sediment size distribution is important since the pore pressures can affect the response of wave run-up, wave overtopping, reflection and transmission. This interaction, acknowledged as a key factor in controlling the morphodynamics of coarse-grained beaches (Bagnold 1940; Duncan 1964; Nelson and Miller 1974; Packwood 1983; Turner and Nielsen 1997; Masselink and Li 2001, Horn 2007), is still not fully understood.

Most of the studies (Packwood 1983; Turner and Masselink 1998; Masselink and Li 2001, Pedrozo-Acuña *et al*., 2006; Jamal *et al.* 2012) on the effects of infiltration/exfiltration in the swash zone were performed using numerical simulations (Horn, 2002 and 2006), whereas controlled laboratory experiments on gravel beaches are much rarer. In the last 15 years, only two large wave flume studies were carried out (Blanco, 2002 and Williams *et al.*, 2012). Results from the Großen Wellen Kanal (GWK) improved our understanding on mixed gravel beach performance (Blanco, 2002). More recently, the study carried out at the Delta Flume in the Netherlands during the BARDEX experiments investigated the behaviour of gravel beaches where the groundwater table was intentionally modified by increasing or lowering the lagoon behind it (Williams *et al.*, 2012).

Although these studies have significantly contributed to improving our understanding of gravel beaches, the large size of the wave flumes used during these studies made it impracticable to investigate the effect of different grain sizes and grading curves on the groundwater elevation and the resulting beach profile. The interaction between wave action, beach groundwater level and influence of beach grading (grain size distribution) for gravel beaches is currently not well described by empirical models. During the present research these interactions have been addressed and are discussed in Chapter 6.

As described above, equations available in the literature for describing the flow through porous media were mainly developed using fine material, and the effect of the entire grain size distribution on both the hydraulic processes and on the beach profile response is not considered. However, since grain size distribution controls the nature of the interconnections between pores, the entire grain size distribution, rather than a single point on the grain size distribution curve, needs to be considered to reliably estimate the permeability of granular soils (Freeze and Cherry, 1979). Further examination of the effects of the grain size distribution curve on both the hydrodynamic processes and on the cross shore transport mechanisms on gravel beaches is therefore required.

The key research question addressed here is how a different shape of grading curve will affect the wave dissipation within the beach, the beach groundwater table elevation and the resulting cross-shore beach profile. To answer these questions two main studies will be described in Chapter 5 and Chapter 6:

- The first study describes permeameter experiments performed to improve our understanding of fluid flow through coarse granular media for a wide range of sediment sizes.
- The second study describes the influence of grading curves and sediment sizes on the profile response of gravel beaches.

3. Flow through gravel material

3.1. Introduction

The wave interaction with the beach comprises multiple processes, such as: wave breaking; wave reflection; wave run-up; and, wave overtopping. These are influenced by the wave-induced porous flow inside the beach, and so therefore knowledge of the hydrodynamic pore pressures associated with the porous flow is very relevant for a beach profile response (Blanco, 2002). It is very difficult, however, to estimate the magnitude of the pore pressure accurately, due to the lack of analytical and measured data (Horn, 2002; Horn 2006).

As previously described in Section 2.3, some of the most important parameters in a beach groundwater system are the elevation of the beach water table, pore water pressures and the hydraulic conductivity (Horn, 2002). The fluctuation of the beach water table, and the induced wave pressure decay within the beach, depends on both hydrodynamic conditions (tidal elevation, wave condition, wave run-up) and on the characteristics of the beach sediment (hydraulic conductivity, i.e., sediment size, sediment shape, sediment size sorting, and porosity) (Gourlay, 1992).

Reliable assessment of the overall stability/behaviour of a gravel beach subject to wave action can be achieved only if the flow regime at and within the beach can be defined (Horn, 2002; Horn, 2006). It is often accepted (Horn, 2006, Baird *et al.*, 1998; Raubenheimer *et al.*, 1999) that the groundwater flow through gravel material can be described by using the Forchheimer approximation, which assumes that the horizontal flow is dominant and neglects the vertical flow (Horn, 2002; Horn, 2006).

As most of the existing formulae for porous flow through coarse granular material are based on stationary flow, some of the research on stationary flow will be discussed briefly in the following section. Firstly, a brief description of permeability is given to facilitate the discussions that follow.

3.2. Permeability – previous investigations

Permeability (also referred to as intrinsic or specific permeability), denoted by k (L^2), is the measure of the ability of a porous media to transmit fluids and is a function solely of the characteristics of the porous medium and not the fluid which passes through it (Bear, 1972).

The hydraulic conductivity K_D (m/s), is a measure of the ease with which a fluid flows through a porous media. It is a function of both the sediment properties and the fluid flowing through it. It depends on both the characteristics of the medium and the fluid properties (Bear, 1972).

From the analytic derivations of Darcy's law the hydraulic conductivity (K_D) can be expressed as:

$$K_D = \frac{k\,\rho\,g}{\mu} \tag{3.1}$$

where ρ is the density of the fluid (kg/m^3) and μ is the dynamic viscosity (kg/m s)

The value of K_D for different types of soil are typically within the ranges shown in Table 3.1 (Craig, 2004):

Table 3.1: Coefficient of hydraulic conductivity (m/s)

Clean Gravels	Clean sands and sand-gravel mixtures	Very fine sands, silts and clay	Unfissured clays
$1 \sim 10^{-1}$	$10^{-1} \sim 10^{-4}$	$10^{-4} \sim 10^{-7}$	$10^{-7} \sim 10^{-10}$

Source: R. F. Craig (2004) "Soil Mechanics"

As previously mentioned, the permeability of the porous medium is dependent on the granular matrix, including particle size, shape, orientation and surface roughness. These properties are difficult to obtain in laboratory or prototype measurements (Smith, 1991), therefore researchers concentrated their efforts on relating permeability to a representative grain size or porosity, the latter as a descriptor of the permeability (Smith, 1991; Scheidegger, 1961). Several empirical equations for estimating permeability or hydraulic conductivity have been proposed in the past, and some of these are discussed briefly now.

A formula suggested by Krumbein and Monk (1943) where permeability, k (in units of Darcies where 1 Darcy = 9.87x10^{13} m^2), is given by:

$$k = 760D^2 e^{-1.31\sigma} \tag{3.2}$$

where D is the geometric mean grain diameter (mm), and σ is the sediment sorting (in phi (ϕ) units, 1 ϕ = -log$_2$D).

For loose, clean, filter sand, Hazen (1930) proposed an empirical relationship for hydraulic conductivity in the form:

$$K = cD_{10}^2 \tag{3.3}$$

where K is in cm/s, c is a constant that varies from 1.0 to 1.5 and D_{10} is the effective size in mm. The advantage of Hazen's formula is that D_{10} can be quickly and easily determined to compute permeability. This helps evaluate the variability of permeability at a given site in a quick and cost effective manner, however, a major limitation of Hazen's formula is that it is more valid for clean sands with D_{10} ranging from 0.1 to 3.0 mm (Holtz *et al.*, 2011).

Another formula of the form given previously was proposed by Harleman (1963), stated as:

$$k = (6.54 \times 10^{-4})\, D_{10}^2 \tag{3.4}$$

where k is the permeability in cm^2 and D_{10} is again the effective grain size in cm.

Kozeny (1927) using the steady-state Navier-Stokes equations (neglecting inertial terms) with Darcy's law and describes the permeability as:

$$k = \frac{cn^3}{S^2} \tag{3.5}$$

where c is a factor to take into account the shape and tortuosity of channels (approximately 0.5 for circular capillaries, 0.562 for square capillaries, and 0.597 for equilateral triangles), and S is the specific surface area of the solid (m^2/kg). The equation is known as the *Kozeny equation* and has been modified in many ways by different researchers to obtain better fits to experimental results.

A common modification to Kozeny's equation is that proposed by Carmen (1937), resulting in the *Kozeny-Carmen equation*,

$$k = \frac{n^3}{5\, S^2 (1-n)^2} \tag{3.6}$$

where S, is a specific surface (m^2/kg) and the empirical factor of 1/5 replaces Kozeny's term c= 0.5 to give a better fit to the data.

It is also possible to define some mean particle sizes as d_m= 6/S (Bear, 1972). The Kozeny - Carmen equation, becomes:

$$k = \frac{n^3}{(1-n)^2} \frac{{d_m}^2}{180} \tag{3.7}$$

where k is the permeability, ρ_w the fluid density, μ the fluid viscosity, g is the acceleration due to gravity, and d is a representative grain size (Bear, 1972). This equation is not appropriate for soils with effective particle size D_{10} > 3 mm or for clayey soils (Carrier, 2003).

Kenney and Lau (1984) conducted laboratory tests on granular soils in which the particle sizes in various specimens ranged from 0.074 to 25.4 mm. The uniformity coefficients, C_U (D_{60}/D_{10}) of these specimens ranged from 1.04 to 12. Results showed that for laminar flow conditions the permeability can be expressed as follows:

$$k = (0.05\ to\ 1)D_5 \tag{3.8}$$

where k is in mm^2 and D_5 is the diameter (mm) through which 5% of soil passes. They concluded that for the range of materials used the permeability properties are primarily dependent on the size of particles in the fines fraction, and are essentially independent of the shape of the gradation curve.

There still exists some lack of prediction of permeability from *a priori* knowledge of physical and geometrical parameters. The concept of the permeability of a porous medium has yet to be well defined. It is dependent upon, and sensitive to, many parameters that are difficult to control even in a laboratory environment. To this day, the permeability coefficient must still be determined indirectly in laboratory permeameter tests, for no reliable general predictive formulae have been produced.

3.3. Flow through porous media

The porous media is normally schematised and treated as one continuum which exerts forces on the fluid due to drag, friction, and acceleration (Bear, 1972). Researchers have aimed to describe the form of this resistance and investigations into porous media flow have provided a better understanding of the phenomenon involved during this process. Most of the work on porous media flow was based on empirical studies (e.g. Darcy, 1856). Such investigations have identified the parameters relevant to the physical phenomenon and have provided useful relationships between them. Analytical studies have also derived such empirical relationships from the equations of motion and continuity (with appropriate simplifications and approximations), thereby isolating the effects of, and the relative importance of, individual terms. In order to better understand the nature of the present investigation, a review of the previous theoretical and empirical results is described here.

The classical equation describing the correlation between hydraulic gradient and flow velocity through porous media was proposed by Darcy in 1856. Darcy's law can be written as follows:

$$\frac{Q}{A} = V = K_D \frac{\Delta H}{L} = K_D I \tag{3.9}$$

where Q=volume of water flowing per unit time (m^3/s), A = cross-sectional area of soil corresponding to the flow Q (m), V = discharge velocity (m/s), L = the length of the sample (m), ΔH =head difference (m) and ΔH/L = I = gradient (-). The factor of proportionality K_D (m/s) is the hydraulic conductivity, it is independent of either velocity or gradient, being a material constant and it represents a measure of the ability to flow through porous media.

As previously described, when waves interact with a beach, a part of the wave energy is reflected back to the sea, part of the energy is dissipated within the surf zone, and the remaining part is transmitted through the beach. The porous flow inside the beach may be both laminar and turbulent. In the case of relatively large velocities and relatively large accelerations, the porous flow through coarse material will differ from Darcy flow (Bear, 1972; Burcharth and Christensen, 1991).

Laminar flows occur over a range of Reynolds number ($Re = UD_{50}/\nu$) ~ 1-10 (Bear, 1972). For higher values of Re, inertia effects start to play a significant role and linear law is not valid any more. In 1901 Forchheimer suggested an equation to describe hydraulic resistance as a gradient

(I) in terms of the superficial velocity (V) over the laminar to turbulent transition regime. To account for inertia terms, Forchheimer proposed a quadratic correction term:

$$I = aV + bV^2 \tag{3.10}$$

The Forchheimer regime is the regime in which the flow is initially steady laminar but as it progresses the inertial effects become very important. The Forchheimer regime corresponds to a Reynolds number ranging between 10 – 1000 (Schneebeli, 1955; Dudgeon, 1966; Wright 1968, Bear, 1972). The Reynolds number ranges for various flow regimes are given in Table 3.2, (Dybbs and Edwards, 1984) for Plexiglas spheres.

The general interpretation of the Forchheimer equation is that the linear term constitutes the contribution from the laminar flow, therefore the factor *"a"* depends on the viscosity. The non-linear term, factor *"b"* represents the fully turbulent flow contribution.

Table 3.2: Reynolds number ranges for various flow regimes through plexiglass spheres

Darcy Flow	Forchheimer Flow	Transitional Flow	Turbulent Flow
Re<1	1≤Re≤150	150≤Re≤300	Re≥300

Source: Dybbs and Edwards (1984)

The flow resistance for non-laminar conditions is normally described with the Forchhimer equation where the unknown resistance coefficients (*a* and *b*) are determined from physical experiments. Attempts have been made to determine generalised formulations for the resistance coefficients *"a"* and *"b"* in terms of various material descriptions. Many empirical and semi-empirical formulation of these two coefficients were derived from physical modelling studies (Ergun, 1952; Engelund, 1953; Den Adel, 1987; Shih, 1990; Burcharth and Christensen, 1991; Van Gent, 1993). In order to provide a general overview some of these experimental results are summarised below.

Ergun (1952) performed experiments with porous gas (hydrogen, methane and nitrogen) flow in the Forchheimer regime. Crushed porous material was packed with different porosities, ranging between 0.44 and 0.53. The following expressions for the *a* and *b* coefficients were proposed:

$$\mathrm{a} = \alpha_{\mathrm{ERG}} \frac{(1-\mathrm{n})^2}{\mathrm{n}^3} \frac{\nu}{\mathrm{gD}^2} \tag{3.11}$$

$$\mathrm{b} = \beta_{\mathrm{ERG}} \frac{1-\mathrm{n}}{\mathrm{n}^3} \frac{1}{\mathrm{gD}} \tag{3.12}$$

where the value of the two coefficients α_{ERG} and β_{ERG} must be determined empirically, *n* is the porosity, *D* is the characteristic grain size, ν is the kinematic viscosity and *g* is the acceleration due to gravity.

Engelund (1953) carried out experiments on coarse flinty and calcareous sand of fairly uniform grain-size ranging between 1.4 mm and 2.6mm, proposing the following alternative expressions:

$$a = \alpha_{ENG} \frac{(1-n)^3}{n^2} \frac{\nu}{gD_{EQ}^2} \tag{3.13}$$

$$b = \beta_{ENG} \frac{1-n}{n^3} \frac{1}{gD_{EQ}} \tag{3.14}$$

Engelund (1953) pointed out that the values of α_{Eng} and β_{Eng} (see Table 3.3) were based only on a very few experiments. Sizes of materials tested were much less than 5mm. As a result, the measurements were taken in a flow condition corresponding to a much smaller Reynolds number than would be observed in rubble structures.

Similar relationships for *a* and *b* were proposed by Den Adel (1987), who ran experiments on single size samples of uniform grain size ranging between 6 mm and 24 mm. The porosity of the samples ranged between 0.38 and 0.40. Shih (1990) proposed a new expression for the Forchheimer coefficients *a* and *b*, based on steady flow permeameter test results for single size and wide grade samples of crushed limestones (2.67 t/m^3). The porosities of the samples used by Shih (1990) were not specified. Burcharth and Christensen (1991) tested eight samples of gravel and crushed rock density 2.5 - 2.7 t/m^3. The stone size ranged between 10mm and 40mm. The tests results showed a dependency between the characteristic diameter and the width of the grading, although no relationship was formulated.

Van Gent (1993) carried out a study of flow through coarse granular material in a U-tube tunnel. Tests with stationary flow and tests with oscillatory flow were performed. Five samples with rocks (D_{50} = 20, 30, 48, 60mm) and one with spheres (D_{50} = 46mm) were tested. Porosity values ranged between 0.39 and 0.45, the grading widths were narrow and kept at the similar value of D_{n85}/D_{n15} ~ 1.2.

Most of the formulae used to describe the flow through porous media were originally developed for stationary flow, and as the samples tested by various authors were constructed differently, a comparison is rather difficult. A range of expressions for *a*, *b* together with the suggested values of α and β for each research programme is reported in Table 3.3. Due to the different ranges of the

diameter, porosity, *Re* and testing configuration used in these studies, the values of α and β vary significantly for the different studies, as can be seen in Table 3.3. For instance Van Gent (1993) proposed the following Forchheimer coefficients values of α = 554 and β = 0.91, while Den Adel (1987), using materials having same range of porosity, proposed the following Forchheimer coefficients values of α = 170 and β = 2.2.

Table 3.3: Some of the existing formulae for stationary porous flow

Source	D_{50} (mm)	Re (-)	Porosity (n)	a (s/m)	b (s^2/m^2)	Values of α and β
Ergun (1952)	-	1-1300	0.44 - 0.53	$\alpha_{ERG}\frac{(1-n)^2}{n^3}\frac{\nu}{gD^2}$	$\beta_{ERG}\frac{1-n}{n^3}\frac{1}{gD}$	α_{ERG}=150 β_{ERG}=1.75
Engelund (1953)	1.4 - 2.6	-	0.395	$\alpha_{ENG}\frac{(1-n)^3}{n^2}\frac{\nu}{gD_{EQ}^2}$	$\beta_{ENG}\frac{1-n}{n^3}\frac{1}{gD_{EQ}}$	α_{ENG}=1500 β_{ENG}=3.6
Koenders (1985)	-	-		$\alpha_{K}\frac{(1-n)^2}{n^3}\frac{\nu}{gD_{15}^2}$	$\beta_{K}\frac{1}{n^5}\frac{1}{gD_{15}}$	α_{K}=290 (250-330) β_{K}=1.4
Den Adel (1987)	6 - 24	-	0.37 - 0.4	$\alpha_{DA}\frac{(1-n)^2}{n^3}\frac{\nu}{gD_{15}^2}$	$\beta_{DA}\frac{1}{n^2}\frac{1}{gD_{15}}$	α_{DA}=160 (75-350) α_{DA}=2.2 (0.9-5.3).

Source	D_{50} (mm)	Re (-)	Porosity (n)	a (s/m)	b (s^2/m^2)	Values of α and β
Shih (1990)	2 - 60	50-6000	Na	$\alpha_S \frac{(1-n)^3}{n^2} \frac{\nu}{gD_{15}^2}$	$\beta_S \frac{1-n}{n^3} \frac{1}{gD_{15}}$	$\alpha_S = 1684 + 3.12\ 10^{-3} (\frac{g}{\nu^2})^{\frac{2}{3}} d_{15}^2$ $\beta_S = 1.72 + 1.57 \exp[-5.10\ 10^{-3} (\frac{g}{\nu^2})^{1/3} d_{15}]$ For wide graded samples, the d_{15} values is replaced by D*. $D^* = D_{15} (\frac{D_{15}}{D_{50}})^{-1.11} (\frac{D_{50}}{D_{85}})^{0.52}$
Burcharth & Christensen (1991)	10-37	-	0.46 - 0.47	$\alpha_{BC} \frac{(1-n)^3}{n^2} \frac{\nu}{gD_{15}^2}$	$\beta_{BC} \frac{1-n}{n^3} \frac{1}{gD_{15}}$	-
Van Gent (1993)	20 - 60	-	0.39 – 0.44	$\alpha_{VG} \frac{(1-n)^2}{n^3} \frac{\nu}{gD^2}$	$\beta_{VG} \frac{1-n}{n^3} \frac{1}{gD}$	$\alpha_{VG, D15}$=554 $\beta_{VG, D15}$= 0.91

n is porosity, D is particle size, D_{eq}: equivalent sphere diameter defined as $D_{eq}=(6M_{50}/\pi\rho_a)^{1/3}$, M_{50} is the average mass of a rock grading, ρ_a is the rock density

During the recent BARDEX study, (Williams, 2012; Turner and Masselink, 2012) it was observed that for a hydraulic gradient of the beach water table less than i = 0.025, in the absence of waves, the hydraulic conductivity (K_D) is independent of the Reynolds number, supporting Darcy's assumption. For an hydraulic gradient of the beach water table exceeding 0.025 however Darcy's assumption is no longer valid as turbulent flow results in an increase in turbulent kinetic energy (Turner and Masselink, 2012).

The Forchheimer equation (Equation (3.10) is valid for stationary flow. For non-stationary flow, an additional external force must be required to accelerate the mass of water (Dean and Dalrymple, 1984; den Adel, 1987). Polubarinova Kochina (1962) added an additional term (time-dependent term) as shown below:

$$I = aV + bV^2 + c\,\frac{du}{dt} \tag{3.15}$$

where c (acceleration coefficient) is a dimensional coefficient (s^2/m). Van Gent (1991) proved that this equation can be derived analytically from the Navier-Stokes equations. Van Gent (1991) and Gu and Wang (1991) derived an expression for the coefficient c :

$$c = \frac{1 + \gamma\,\frac{(1-n)}{n}}{n\,g} \tag{3.16}$$

where γ is a non-dimensional coefficient taking into account the added mass (amount of momentum required to accelerate the volume of water (Van Gent (1993)).

Gu and Wang (1991) suggested that while the magnitude of the turbulent resistance relative to the laminar resistance is linear with the Reynolds number, the magnitude of turbulent resistance relative to the inertial resistance is linear with the Keulegan-Carpenter number (*KC*). The *KC* number is defined as *UT/D* where *T* is the wave/oscillation period, U the amplitude of the flow velocity oscillation and D is the diameter. Gu and Wang (1991) also suggested that the ratio of *Re/KC* for a gravel material is of the order of 10^4. Smith, (1991) assumed that one force dominates over another if the ratio is greater than 10.

3.4. Discussion

In Chapter 2 a definition and characterisation of gravel beaches was given. We have discussed the importance of these beaches as coastal defenses, and we have introduced the models currently used to predict the response of gravel beaches. A brief overview on the main hydrodynamic processes, which influence the beach profile responses, was given in Section 2.3. From this discussion it was evident that the effect of permeability and sediment size are key factors in controlling the beach response.

In Chapter 2 it was emphasised that a reliable assessment of the overall stability/behaviour of a gravel beach subject to wave action can be achieved only if the flow regime at and within the beach can be defined (Horn, 2002; Horn, 2006). Therefore, the Forchheimer equation was presented in Chapter 3 as one of the main equations that can be used to describe the groundwater flow through gravel material (Horn, 2002; Horn, 2006). As most of the existing formulae of porous flow through coarse granular material are based on stationary flow, some of the research on stationary flow was discussed in Section 3.3.

To complete this overview on gravel beach performance, we need to introduce their dynamic behaviour in response to different wave climates. An introduction to ocean waves and their characteristics is therefore required to facilitate the discussions that follow. An explanation as to how sea states can be described is discussed in the first part of Chapter 4, and this will be followed by an examination of the interaction between wind and swell waves on beach dynamic response.

4. Wave characteristics and bimodal sea-states

4.1. Introduction

Gravel beaches functioning as coastal defences and natural habitats compel coastal engineers to understand the processes occurring across the gravel beachface (Buscombe and Masselink, 2006). The beach behaviour is coupled with the incident wave conditions, hence the need for coastal engineers to study the approaching wave climate in order to have a reliable prediction of the beach response.

The first part of this Chapter gives a brief introduction to ocean waves and examines in more detail the characteristics of gravity waves. An explanation as to how a sea state can be described by a wave spectrum is also given to facilitate the discussions that follow. The second part of this Chapter examines the characteristics of a bimodal sea-state and its effect on beach profile response.

4.1.1. Introduction to gravity waves: wind and swell

Ocean waves can be classified in several ways, the most commonly used classification is based on the wave period or the associated wavelength (Toffoli *et a*l, 2017). The shortest-period waves, and the first to be observed on the ocean surface when wind starts blowing are the capillary waves. These are characterised by a fine structure of small ripples with a wavelength of less than 1.5cm and period less than 0.1s. The dynamics of capillary waves is dominated primarily by surface tension. As waves keep growing under the influence of wind, the initially small ripples evolve into longer waves. For wavelengths of approximately 1.7cm (or wave period of about 0.33 s), gravity becomes the predominant effect and capillary action can be neglected (Lamb, 1994). At this stage wave groups and wave phases propagate at the same speed. Above this threshold, gravity effects dominate the wave dynamics and surface tension only plays a secondary role. The resulting oscillations are normally classified as an ultra-gravity wave. As the wave period becomes larger than 1s, surface tension becomes negligible and gravity remains the sole restoring mechanism. Under these circumstances, waves are classified as gravity waves (periods ranging from a minimum of about 1s up to maximum of approximately 30s).

Under the direct effect of the local wind, a large number of wave components with different wave periods, directions and phases are generated. The resulting wave field is an interaction of all these components, which generates an irregular pattern, normally known as wind sea. When waves propagate over a depth that is much deeper than the wavelength, longer waves travel faster than shorter ones, dispersing from one another (Holthuijsen, 2007). As a consequence, long waves rapidly move outside the generating area and become known as swells. Swells have a typical wavelength that is greater than 260 m (i.e., a period generally larger than 13 s) up to a maximum of around 900 m (period of 25 s, Hanafin et al., 2012). As their height is normally small, dissipation is less intense if compared with wind sea.

Nonlinear interactions between wave components transform part of the energy associated to wind-generated gravity waves into subharmonics with periods ranging from about 20 to 30 s up to a maximum of approximately 5 min (Herbers, Elgar, and Guza, 1995). These long oscillations, which are driven primarily by swell (Tucker, 1950), are bound to the generating wave trains and are normally known as infra-gravity waves. Infra-gravity waves may, however, affect sediment transport and other coastal processes and activities, including port operations and moorings due to induced harbour oscillations, but these will not be discussed further as part of the present research.

4.1.2. Introduction to short term wave analysis and representation

Sea-states have often been characterised by using a few statistical parameters, such as the zero-crossing significant wave height H_s (or $H_{1/3}$) and the corresponding zero-crossing significant wave period T_s (or $T_{1/3}$) (Hogben and Lamb 1967). This representative wave parameters are calculated by means of the upward zero crossing (up-crossing) analysis which first identifies and then ranks in descending order the single waves within a sea-state; H_s and T_s are then calculated as the average of the highest 1/3 of the wave height and their associated period, respectively. Similarly, the mean wave height (H_m) and associated period (T_m) are the means of all the wave heights and periods identified in a sea state.

As well as statistically, sea-states can also be characterised by means of the distribution of their energy within the frequency domain, leading to a spectral characterisation of the sea state. This is achieved by assuming that a sea-state is the result of the superimposition of an infinite number of

periodic waves having different amplitude, frequencies and directions (Goda, 2010). An example of an irregular wave time-history, obtained by superimposing sinusoidal waves of different amplitudes and frequencies is shown in Figure 4.1. Vice-versa an irregular wave time-history (Figure 4.1) can be decomposed into a number of component waves; this is a transformation from time-domain to the frequency-domain. The process of identifying the amplitude, frequency and phase of each single component wave is called spectral analysis in the time-frequency domain and leads to a different representation of the sea state, that is: the wave spectra. The Fourier transform is a mathematical algorithm that allows the determination of the wave spectra and is widely used in different contexts to derive a spectral representation of a time-history; this method has been successfully applied to the analysis of sea-states to the point that these are often described by means of their spectral parameters, as discussed in the following section.

The wave energy spectral density or simply the wave spectrum may be obtained directly from a continuous time series of the surface $\eta(t)$ with the aid of the Fourier analysis.

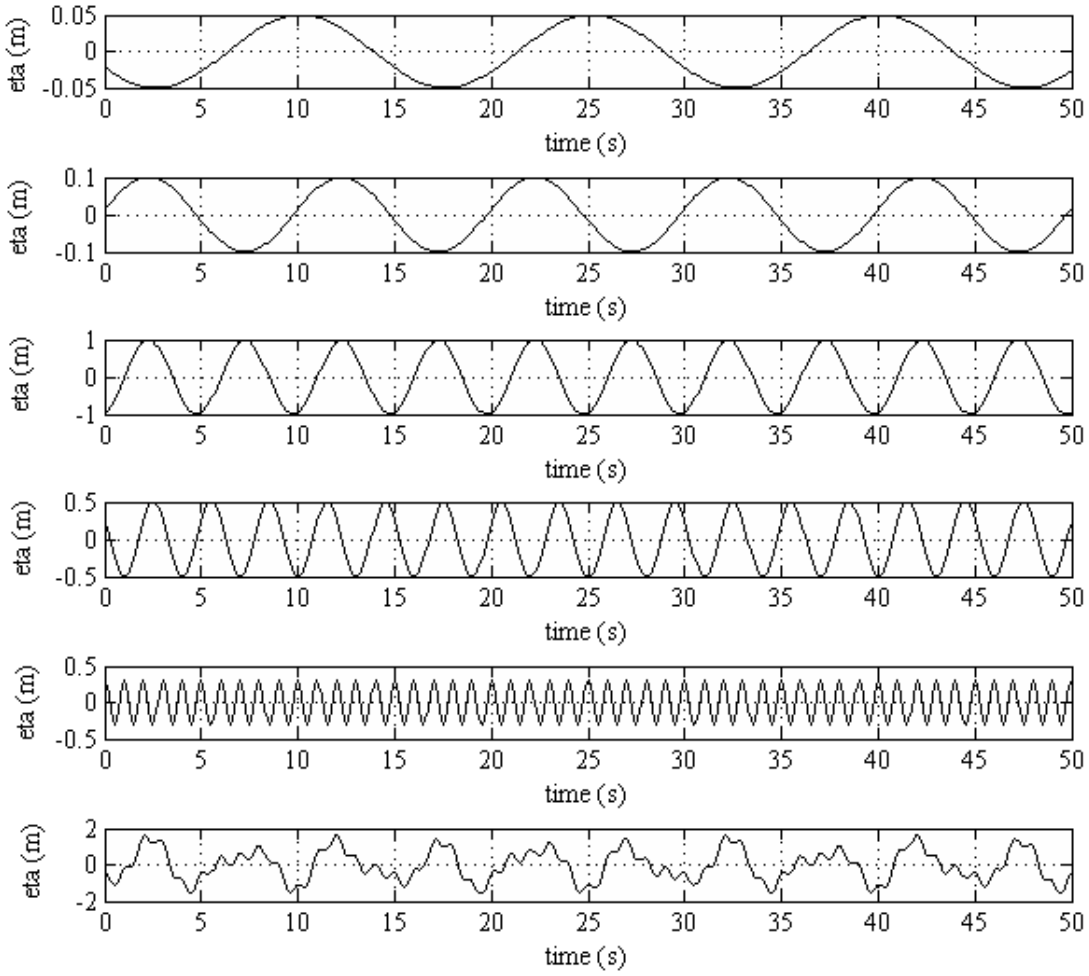

Figure 4.1: Irregular waves by superposition of sinusoidal waves.

4.1.3. Spectral shape and spectra shape parameters

The time history of the free surface elevation (measured above the still water level) can be written as:

$$\eta = \eta\,(x, y, t) = \sum_{n=1}^{\infty} a_n \cos\,(k_n x * \cos\theta_n * k_n y \sin\theta_n - 2\pi f_n t + \varepsilon_n) \qquad (4.1)$$

where η = elevation of the water surface above the mean water level, *a* = wave amplitude, *k* = 2π/L = wavenumber and *L*= wave length, θ = angle between the x-axis and the direction of wave propagation, f = wave frequency and ε = phase angle. This equation describes a random sea state with a stochastic variation of wave height and wavelength spatially and temporally.

At a fixed point the surface elevation variation can be expressed as:

$$\eta = \eta\,(t) = \sum_{n=1}^{\infty} a_n \cos\,(2\pi f_n t + \varepsilon_n) \tag{4.2}$$

This equation suggests that the summation of the squares of wave amplitudes over an interval from *f* to *f+df* is finite and unique (Goda, 2010). The value of the sum is denoted by S(f) and is given by:

$$S(f)\,df = \sum_{f}^{f+df} \frac{1}{2} a_n^2 \tag{4.3}$$

The function of *S(f)* is called the frequency spectrum and represents the distribution of the density of the wave energy in the frequency domain, as shown in Figure 4.2.

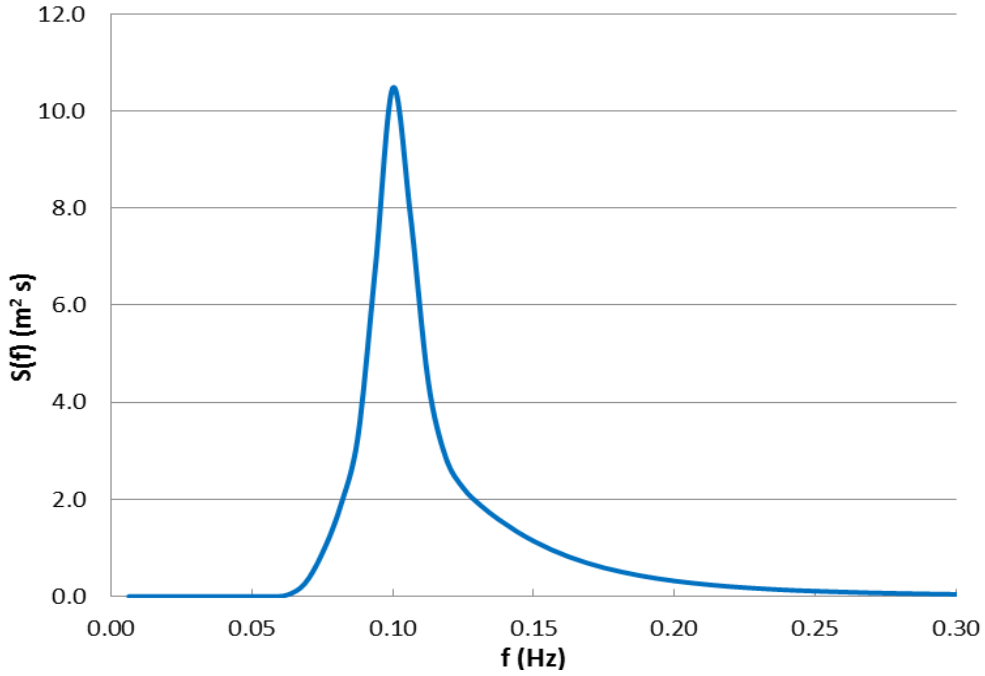

Figure 4.2: Example spectrum of sea-state

The characteristics of ocean / nearshore wave spectra have been described by many authors (Moskowitz, 1964; Hasselmann *et al.*, 1973; Guedes Soares, 1984; Kerbiriou, 2007; Ochi and Hubble, 1976; Torsethaugen and Haver, 2004; Goda, 1976; Bretschneider,1959). The theoretical function most widely used to represent a sea state in the form of energy spectrum is the two-parameter spectrum developed by Bretschneider (1959). Successively Goda (1976), based on Bretschneider (1959), modified the equation using the coefficients suggested by Mitsuyasu (Goda, 1976) to represent a spectrum of fully developed wind waves.

In 1964 Pierson and Moskowitz derived a formula to include the wind velocity as the principal parameter, it was derived to predict fully developed waves in the ocean. In 1972 Nagai, based on the Pierson - Moskowitz spectrum, applied an adjustment to the relation of the significant wave height and total wave energy proposing a new formula for the frequency spectrum of wind waves. Both Pierson – Moskowitz and Nagai spectra are appropriate for fully developed seas over long fetches and long durations, Wind waves rapidly developed over reduced fetches and shorter duration than Pierson - Moskowitz, typically have narrower spectra than these (Goda 2010). Hasselmann *et al.* (1973) proposed a spectral description developed during the joint wave observation program for the North Sea (JONSWAP). The JONSWAP spectrum (reduced fetches and shorter duration than Pierson – Moskowitz) incorporates the wind speed to allow hindcasting, but it can also be written in terms of wave height and period (Goda, 2010). Where H_s is the mean height of the highest one-third of observed waves within a recorded time-series and T_p is the spectral peak period, which is the reciprocal of peak frequency, in seconds. The peak frequency is the frequency of the total wave spectrum at which the wave energy is at a maximum.

$$S(f) = \beta_j H_{1/3}^2 T_p^{-4} f^{-5} exp\left[-1.25\left(T_p f\right)^{-4}\right] \gamma^{exp\left[-\left(T_p f-1\right)^2/2\sigma^2\right]} \quad (4.4)$$

where:

$$\beta_j = \frac{0.0624}{0.230 + 0.0336\gamma - 0.185(1.9+\gamma)^{-1}}[1.094 - 0.01915 \ln \gamma] \quad (4.5)$$

$$T_p \cong T_{\frac{1}{3}}/[1 - 0.132(\gamma + 0.2)^{-0.559}] \quad (4.6)$$

$$\sigma = \begin{cases} \sigma_a : f \leq f_p \\ \sigma_b : f \geq f_p \end{cases} where\ \sigma_a \sim 0.07\ ;\ \sigma_b \sim 0.09 \quad (4.7)$$

The JONSWAP spectrum is characterised by γ, the peak enhancement factor, which ranges between 1 and 7 (mean of 3.3 determined for the North Sea). This parameter describes the sharpness of the spectral peak, and for γ = 1 the JONSWAP spectrum reduces to the Pierson - Moskowitz spectrum.

The wave spectrum of wind waves transforms when the wave propagates over a long distance from the generating area (Pierson, Neumann and James, 1955). The spectrum of swell is therefore transformed from that of wind waves due to its propagation over long distances and

effects of dispersion. The dispersive phase of wave evolution begins when waves exit from the storm area or wind intensity diminishes. The sea that arises in the area of generation, disperses as it moves away from the area. That is the mixture of frequencies separate by virtue of their frequency dependant speed of travel, with lower frequencies travelling faster. This creates narrow banded swell as the waves propagate over longer distances. A distant observer will see a peaked wave spectra whose peak frequency slowly shifts with time to higher frequency as the slower, shorter waves follow on from the longer (Hasselmann, 1985; Goda, 2010). The swell waves have a spectra confined in a narrow frequency range and thus have a peak much sharper than that of wind waves (Goda, 2010). Analysis of swell waves generated off New Zealand showed that the swell spectra peaks were equivalent to the JONSWAP spectra with $\gamma = 8 \sim 9$ (Goda, 1983).

As shown from field measurements with directional buoys, the spectral representation of the sea-states may be different from those of standard form (Guedes Soares,1984;Kerbiriou,2007, Bradbury and Mason, 2006; Saulnier, 2011). In particular, when swell waves coexist with wind waves, a secondary peak (bimodal spectrum) is present at the low frequency. One of the first models proposed to describe double-peaked spectra was proposed by Strekalov and Massel (1972) who have suggested that it would be obtained by one high frequency spectrum describing the wind driven component and a Gaussian shaped model describing the swell system. Ochi and Hubble (1976), have proposed another form by combining a JONSWAP and a Pierson-Moskowitz spectrum describing the two individual wave systems. Guedes Soares (1984) proposed a model that represents both sea components by JONSWAP spectra of different peak frequencies. While the choice of the model for the wind sea component is obvious, the choice to model the swell component was made because the JONSWAP model is able to fit very peaked spectra as would be appropriate for the narrow swell spectral component as shown by Goda (1985). The bimodal spectrum is composed into two parts; each one has three parameters, which are: the significant wave height; the modal frequency; and, the peak enhancement factor. When the wave height and period of wind and swell waves are known *a priori*, the resultant bimodal spectrum can be estimated by linearly superimposing the wind and swell spectra (Goda, 2010) as shown in Figure 4.3. This figure shows the linear superposition of the wind wave spectrum ($\gamma = 3.3$, $H_{m0} = 2.7$m and $T_p = 7$s) with the swell wave spectrum ($\gamma = 1.5$, $H_{m0} = 1.2$m and $T_p = 18$s).

During this study it was decided to model the bimodal spectra using a standard JONSWAP spectrum with a peak enhancement factor of γ = 3.3 for the wind component to match standard practice. For the swell component a JONSWAP spectrum with enhancement factor of γ = 1.5 was selected. Even though swell waves tend to have a narrow and peaked spectrum, this was necessary to allow a suitable description of the distribution of the swell energy in the frequency domain, which would have otherwise been less accurately resolved within the low frequency band. Spreading the swell energy over a broader range of frequencies also meant that wave components were less energetic and therefore less inclined to spread their energy via non-linear interaction. This ensured that the spectra kept reasonably stable over the swell frequency range while propagating along the flume.

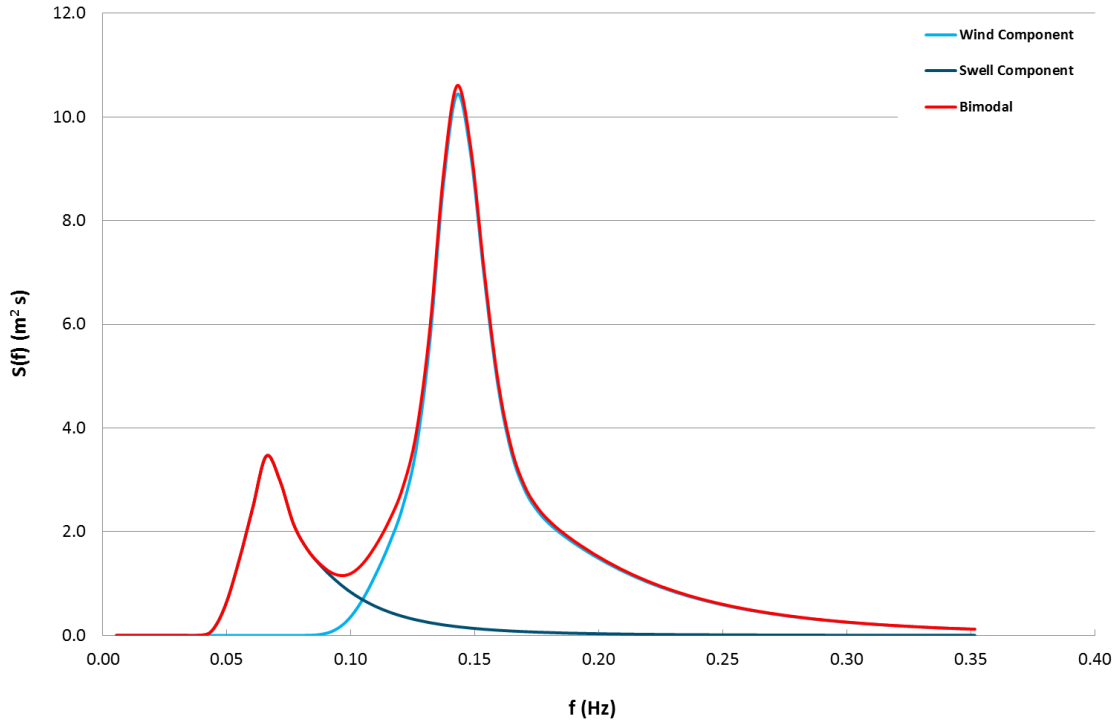

Figure 4.3: Wind and swell wave components combined to make a bimodal spectrum

The distribution of the spectral energy may be more important, for the beach profile response, than the wave period or the wave height (Coates and Bona, 1997), and conventional methods of analysis will generally only use these basic parameters (Hawkes and Coates, 1998). To enable a more detailed method that allows for the distribution of energy in the wave record, a fuller description of the shape factors of the spectra is required, (Bradbury et. al.; 2007).

The parameters derived from the spectral energy density are defined in terms of the spectral moments, which are all found using the following equation.

$$m_n = \int_0^\infty f^n S(f) df \tag{4.8}$$

where n (= -1, 0, 1, 2 and 4) is the exponent of the frequency and m_n is the spectral moment for n.

The area under the wave spectrum, the wave height, and the period spectral parameters are then calculated as follows: wave height $H_{m0} = 4(m_0)^{1/2}$; mean spectral wave period $T_{m0,2} = (m_0/m_2)^{1/2}$; and spectral significant wave period $T_{m\,-1,0} = m_{-1}/m_0$; where m_0, m_2 and m_{-1} are derived from Equation (4.8) and are the moments of order 0, 2 and -1, respectively.

The spectral significant wave period ($T_{m\,-1,0}$) is not much affected by the high frequency of the spectrum, therefore, when the wind waves interact with the swell waves, and the spectral peak of the wind waves overcome that of swell, $T_{m\,-1,0}$ experiences a small variation. The spectra peak period T_p, conversely, moves from the swell period to the wind wave period at a certain stage of wave development (Goda, 2010).

In addition to the wave periods and wave height, there are three important shape parameters that can be used to describe the spectral shape. These will change with the generic sea type, wind, swell, bimodal etc., and also with the degree of energy for each of those types. Analysis of the spectra, and calculation of the shape parameters, can therefore indicate the type of sea state in more detail than the simpler wave height and period parameters. For the present discussion in the following section, the narrowness (ν), broadness (ε) and peakedness (Q_p) parameters will be compared with the peak enhancement factor (γ) to show how each varies for typical seas.

4.1.4. Narrowness parameter

The first of the shape parameters is the narrowness parameter defined by Longuet-Higgins (1983), which is used to measure the distribution of the frequency components in a sea and is used to validate the assumption of a narrow spectrum:

$$\nu = \sqrt{\left(\frac{m_2 m_0}{m_1^2} - 1\right)} \tag{4.9}$$

Because of the presence of the 2nd-order moment, this parameter is sensitive to the high-frequency bands of the spectrum. For a spectrum with a narrow bandwidth, ν will tend to zero, however, generally for the Pierson-Moskowitz spectrum (γ = 1.0) ν=0.33 and for the JONSWAP spectrum (γ = 3.3) ν=0.30. This means that there is very little difference in this value for the two spectral shapes, and that in general the variation in range is also somewhat narrow, suggesting no dependency between the narrowness parameter and the peak enhancement factors (γ)

4.1.5. Broadness parameter

The spectral width parameter (broadness) was introduced by Cartwright and Longuet-Higgins (1956) in order to describe whether the wave energy was concentrated within a narrow frequency band $\varepsilon \approx 0$ or a broad-banded $\varepsilon > 0$. This, as with the narrowness parameter, is sensitive to the high frequency components of a sea due to their use of the higher order moments. This parameter is a measure of the standard deviation of the width of a wave energy spectrum (Chakrabarti, 1987). It ranges from 0 to 1, and it is expressed as:

$$\varepsilon = \sqrt{1 - \frac{m_2^2}{m_0 m_4}} \tag{4.10}$$

The broadness will peak around γ = 2.0 and decreases as γ increases. As with the narrowness parameter, its range is also limited across the range for γ. Generally for the Pierson-Moskowitz spectrum ν=0.60 and for a peak enhancement factor of γ = 7.0, ν = 0.58.

4.1.6. Peakedness parameter

Goda (1976) created the peakedness parameter, Q_p, which characterises how grouped the successive wave heights are, and he observed from field measurements that the wave groupness is more pronounced as the wave spectrum becomes narrow. The peakedness parameter, Q_p is defined as follows:

$$Q_p = \frac{2}{{m_o}^2} \int_0^\infty fS(f)^2 \, df \tag{4.11}$$

The peakedness parameter (Q_p) can be seen in Figure 4.4, where it has been plotted for a range of peak enhancement factors (γ) for the same total m_0 value. Q_p is more sensitive to the difference between a very sharply peaked spectrum (γ=7) and a Pierson-Moskowitz type spectrum (γ=1).

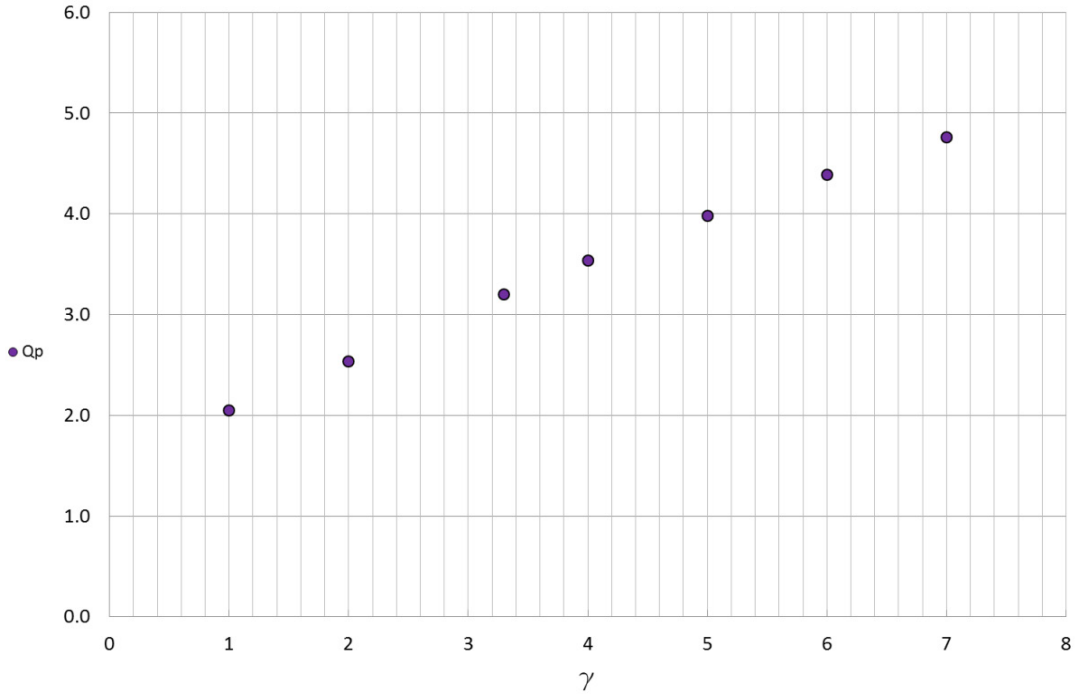

Figure 4.4: Relationship between the peakedness parameter (Q_p) and factor shape (γ)

It has been shown that the broadness and narrowness parameters, discussed above, do not show a wide variation for changes to the shape of the spectra. It is even less clear how differences would be discernible for irregularly shaped spectra, given that there will inherently be noise within the data that is likely to be of the same magnitude as the variations in the two parameters. Polidoro *et al.* (2013) proposed that Q_p was a suitable parameter for identifying the potential

variation with spectral shape in the formula to predict wave run-up on gravel beaches. However, as discussed in more detail in Chapter 7, during the analysis carried out to investigate which wave parameter influenced the beach profile response, the spectral shape parameters (ν, ε, Q_p) did not have an important role.

4.2. Bimodal sea forcing of gravel beaches in the UK

4.2.1. Bimodal seas importance / prevalence around the UK

The impact of wind waves on the coast in terms of wave overtopping, wave run-up and beach erosion, etc., are relatively well understood for many simple configurations (van der Meer, 1988; Powell, 1990; EurOtop 2007). Conversely, swell waves, having longer periods than wind waves (Goda, 2010), are not generally considered in coastal structures design. However, it is possible that extreme swell wave conditions (or a combination of wind-sea and swell) represent a worst case sea-state for some aspects of beach design (Bradbury, 2006). Indeed, recent work carried out by Thompson *et al.* (2017) has noted that bimodal sea-states lead to greater overtopping and that the formulae available in literature underestimate wave overtopping under bimodal wave conditions.

Around England, it is not uncommon to have Atlantic swell waves penetrating into the English Channel (up to about Beachy Head) leading often to wave conditions with a broad, bimodal (combination of wind and swell wave components) or multi-modal spectrum (Bradbury *et al.,* 2007). Along the south coast of England a significant presence of bimodal sea-states is recorded within the regional wave climate. Typical sites affected by the bimodal conditions are: Milford-on-Sea, Hayling Island, Rustington, Boscombe, Chesil, West Bay and Penzance (Bradbury *et al.*, 2007).

An example of the effect of the bimodal sea-states on coastlines was observed during the winters of 2006 and 2014, where several sites along the south coast of England were subjected to significant damage due to flooding and the associated damage. A programme of nearshore wave measurement, wave hindcasting and measurement of beach response to extreme storm events in the English Channel, observed that bimodal (double-peaked) wave conditions produced more damage to the beaches than suggested by empirical models based on statistical wave parameters (Bradbury *et al.*, 2002; 2004; 2007). In particular, the beach responses related to the measured

wave data during these events suggested that the unexpected beach behaviour and breaching phenomena were linked to the spectral characteristics of the storm events (Bradbury, 2007). Interestingly these sea-states were characterised as moderate rather than storm wave conditions, and their wave spectra indicated significant energy components at low frequency (Mason et al, 2008). Subsequent to these storm events, a correlation between bimodal wave spectra, beach response and breaching events was identified.

A 2D physical model study carried out by Hawkes *et al.* (1998), confirmed the critical impact of long period energy influencing the beach response, however, during that study a predictive method was not developed. Hawkes *et al.* (1998) states that, following the results of the study, the existing method of predicting beach response could be inadequate when bimodal conditions are present.

Similar conclusions were confirmed by Bradbury *et al.* (2007) who observed that bimodal conditions significantly affect the beach profile performance, influencing the impact of wave run-up, erosion and over-washing. He also emphasised the need to consider bimodal wave conditions as a design variable for some areas of the English Channel coast, where new design methodologies are required to consider the impacts of bimodal conditions on the design of coastal defences.

Unfortunately, still little is known about the effect of bimodal sea conditions on performance of sea defences or beaches (Bradbury, 1998; Coates and Bona, 1997; Bradbury, *et al.,* 2007) and swell is rarely considered explicitly in the design or assessment of shoreline management operations. Indeed, as will be demonstrated in Chapter 7, the use of the existing prediction models for gravel beach profiles (Powell, 1990) known as SHINGLE, and the process-based XBeach-G (McCall *et al.*, 2014) are not appropriate for bimodal conditions. Jamal et al (2012) had previously shown how the X Beach code could be adapted to predict erosion and accretion on coarse grained beaches against the GWK data, however bimodal wave conditions were not investigated. Therefore, there is an urgent need to better understand the effect of the interaction between wind and swell waves on beach dynamics. Chapter 7 goes on to describe the development of a predictive capability for beach profile response under bimodal storm conditions.

4.2.2. Gravel beach dynamics & bimodal forcing – the argument for new techniques

The presence of bimodal (double-peaked) wave spectra has been observed along several coasts of the globe, e.g., Atlantic and Pacific Oceans (Garcia-Gabin, 2015), the west coast of New Zealand (Ewans, 2006), the Gulf of Mexico and Southern California (Mackay, 2016). In particular, along the south coast of England, Atlantic swell waves penetrate into the English Channel leading often to wave conditions with a broad, bimodal or multi-modal (having several maxima) spectrum (Bradbury *et al.* 2007). The swell propagates up the English Channel reaching the coastline east of the Isle of Wight, and occasionally, it can extend the full length of the English Channel (Mason *et al* 2008). Analysis of wave spectra from the National Network of Regional Coastal Monitoring Programmes' coastal wave network has identified that bimodal sea conditions occur on a regular basis (Mason *et al* 2008). Typically, the highest presence of bimodal seas is associated with sites exposed directly to Atlantic swell e.g. Porthleven in Cornwall. The occurrence of bimodal seas is seasonal, being more common during the winter months (December, January, and February) and less common in the summer (June, July and August) as shown in Figure 4.5, where an average seasonal percentage of bimodal wave conditions recorded during the period from July 2003 to April 2018 is reported.

The effect of long period waves on gravel beaches in the South coast of England was already observed in the past. A typical example is Hurst Spit, which during its life, was breached several times, and the spit was in particular breached several times between 1983-84. The most severe damage, however, occurred on 16 and 17 December 1989, when south-westerly storms combined with a surge in excess of 1 m flattened an 800 m length of Hurst Spit (Wright, D, 1998), as shown in Figure 4.6. Analysis of beach profile field data indicated that damage to the Spit occurs most frequently in severe wave conditions associated with storm surges and swell wave conditions (Bradbury, 1998).

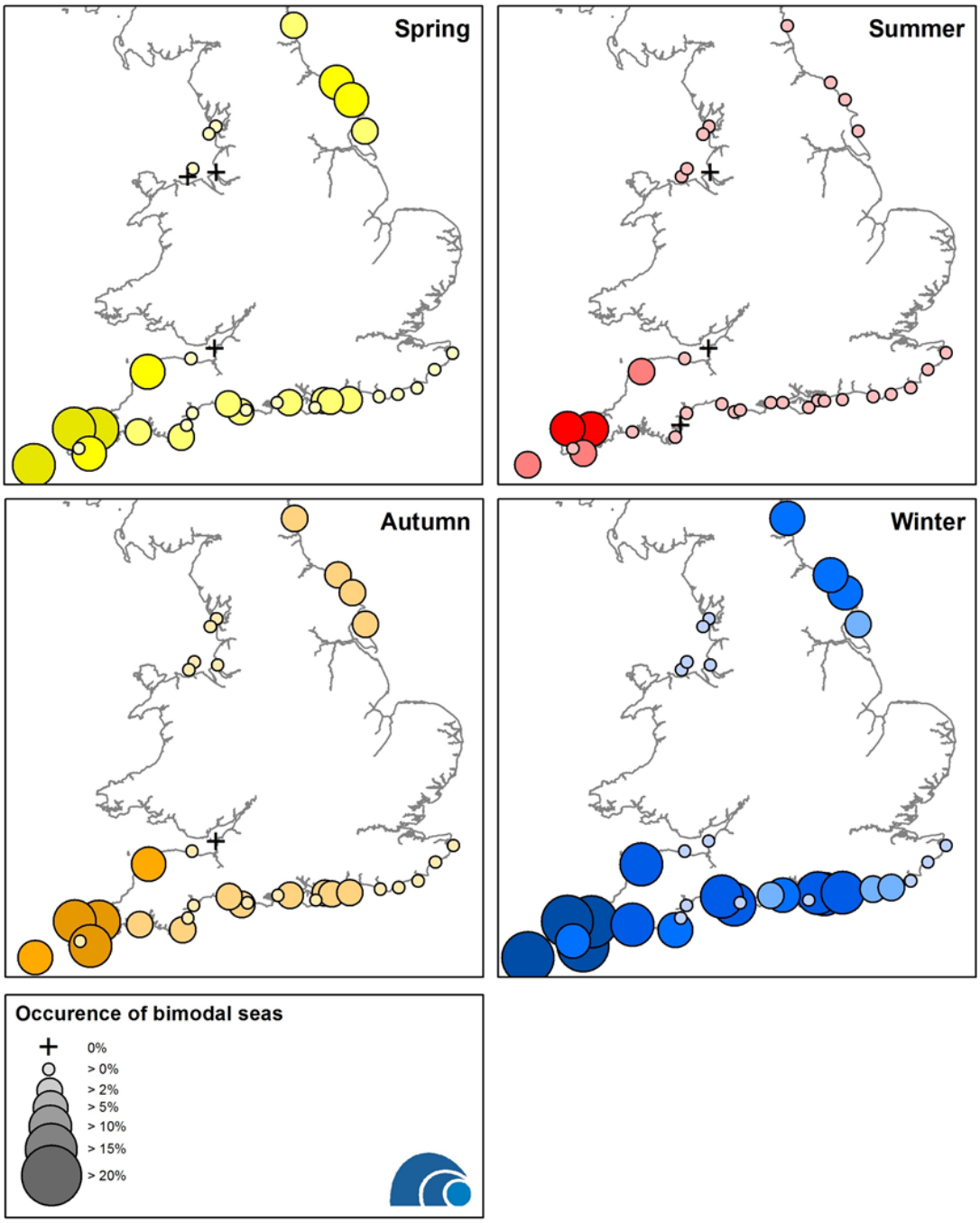

Figure 4.5: Seasonal occurrence of bimodal seas (Extracted from Channel Coastal Observatory study, 2018)

More recently, during the winter of 2013 – 2014, the south coast of England was exposed to an unusual and prolonged combination of severe storms. Many sites in central southern England experienced between 5 and 7 storms during this winter period (October 2013 to February 2014). A number of storms exceeded the extreme wave conditions of 1 in 10 year, or 1 in 50 year return

periods as shown in Figure 4.7, where the geographical occurrence/location of recorded return period exceedance between October 2013 and February 2014 is shown. Analysis of a 60-year hind-cast wave model record (validated by offshore wave buoy measurements) by Masselink *et al.* (2016) suggests that the 2013/2014 winter was the most energetic since 1948. The storm sequences during the winter of 2013 to 2014 along the south coast of England had a considerable impact on many of the beaches. During these storms, Hurst Spit was subjected to an unpredicted breaching (see Figure 4.8), and in many other parts of the south coast of England, flooding and overwash events were observed.

Figure 4.6: Hurst Spit, breached in 1989, copyright: New Forest District Council

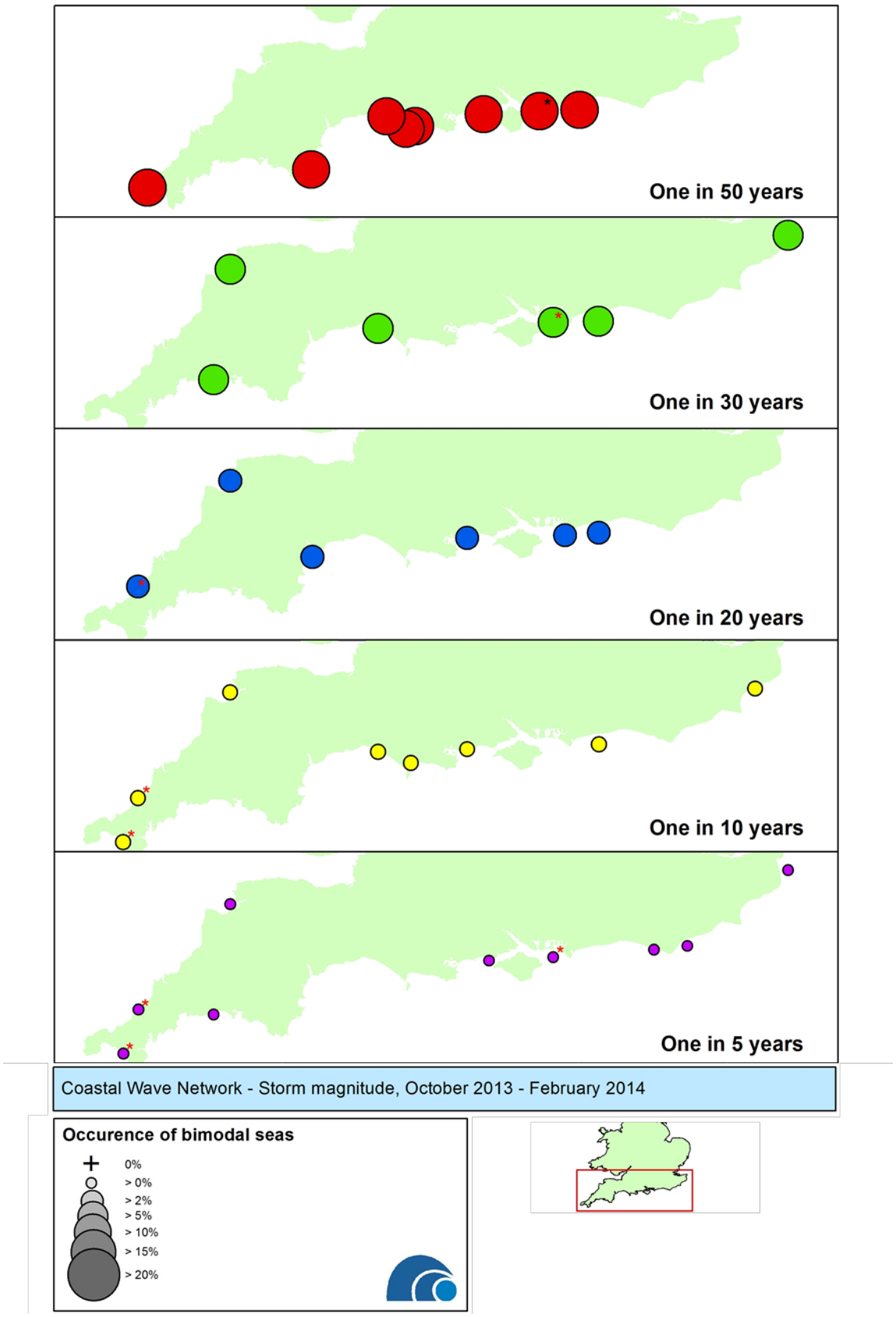

Figure 4.7: Distribution of storms exceeding the 1 in 5, 1 in 10, 1 in 20, 1 in 30 and 1 in 50 years return period between October 2013 and February 2014

Interestingly, a sequence of unexpected (not forecasted) coastal flooding events was also observed in the past at Seaton, Cornwall, in October 2006 and at Hayling Island on 03 November 2005. All these instances were recorded during periods of moderate rather than storm wind wave conditions, but were notable for the underlying presence of long period swell waves (Mason *et al.,* 2008). Figure 4.9 shows Seaton during one of these unpredicted flooding events in October 2006. As can be seen the flood-gate had remained open during the flooding event, highlighting that the wind-wave forecast alone was unable to predict the potential for flooding.

Figure 4.8: Hurst Spit, breached in 2014, (courtesy Peter Ferguson copyright: New Forest District Council)

Figure 4.9: Seaton beach, Cornwall, 2006, the flood gate remains open during the flooding event (copyright: Environment Agency)

For the present study, in order to investigate the occurrence of the swell percentage on the total wave energy spectrum, the bimodal half-hourly spectra recorded at Chesil, Milford, Rustington and Hayling Island, from January 2005 to September 2015, were analysed. The spectra were obtained from the National Network of Regional Coastal Monitoring Programmes, and the results are shown in Figure 4.10, where it can be seen that for a bimodal wave spectrum, the swell component percentage ranges between 10% to 70%. Most of the bimodal wave spectra present a swell component between 10% and 20% with a peak of 70%, but cases of swell between 30% and 50% are common. Most of the wave spectra recorded during the storms of 2013-2014 show a swell percentage between 20% and 40%. As discussed in more detail in Chapter 7, the 2D physical model wave conditions tested during this research consisted of swell percentages ranging between 10% to 40%, as these represent the vast majority of all the sea-states analysed.

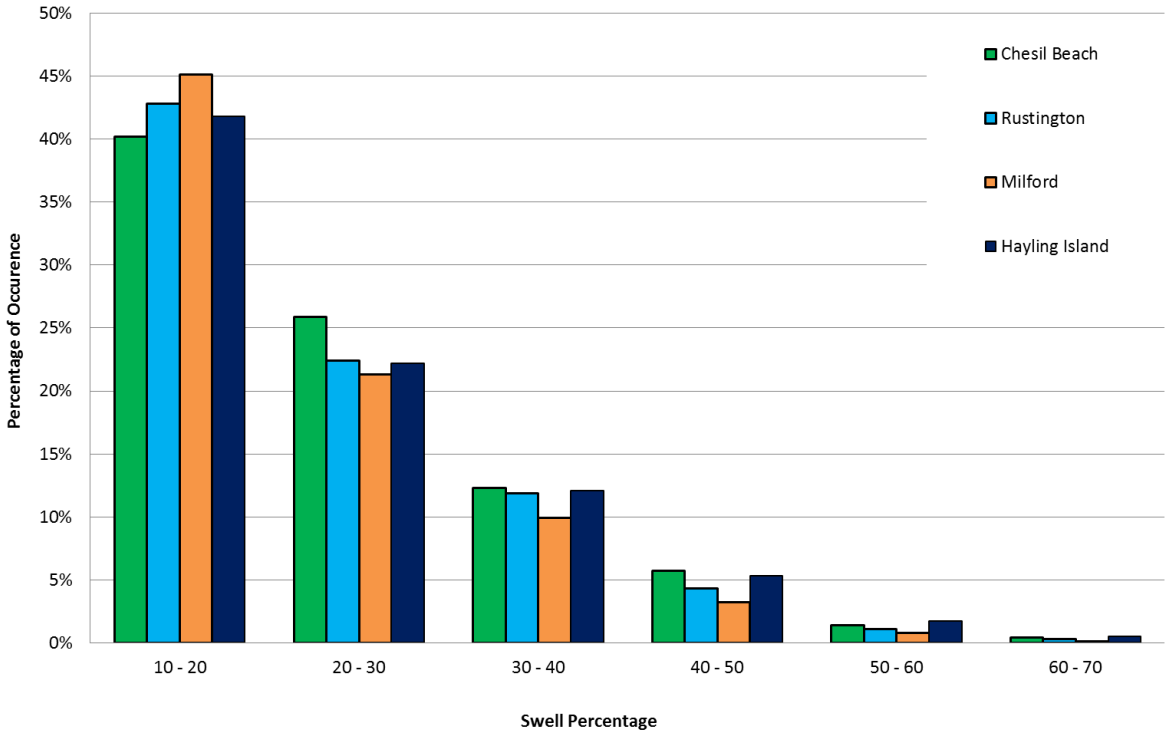

Figure 4.10: Swell percentage occurrence for the bimodal wave spectra recorded during the period from 2005 to 2015

4.3. Discussion

As discussed in this Chapter, the south coast of the UK is identified as a location where significant swell wave components are present within the regional wave climate. During the winters of 2006 and 2014, several sites along the south coast of the UK experienced significant damage where flood events were recorded. These sea-states were characterised by having a double-peaked wave spectra, observing a connection between wave spectrum shape and beach response. Little is known about the effect of bimodal sea conditions on sea defences or beaches (Bradbury, 1998; Bradbury, 2007, Coates and Bona, 1997) and swell is rarely considered explicitly in the design or assessment of shoreline management operations.

As will be described in more detail in Chapter 7, the use of the existing models to predict gravel beach profiles (Powell, 1990; McCall *et al.*, 2014) are not appropriate for conditions with long period swell, bimodal wave conditions, or conditions where overwash may occur (Bradbury *et al.*, 2011., Van Rijn and Sutherland, 2011). There was therefore a need to develop a test programme to examine the response of gravel beach profiles to bimodal wave spectra, characterised by swell

and wind wave periods in various combinations. A physical model study of gravel beaches and the development of the parametric model to predict gravel beach profile response under bimodal sea-states is described in Chapter 7, and is one of the main objectives of this research.

The first impression when visiting a beach is that the terrain may be identified as a porous medium characterised by its seemingly uniform medium-sized material. Yet the grain sizes on a beach are extremely variable, and a close examination of the beach surface shows that fine and medium particles are present together with coarse sand, gravel and pebbles. This will then often be categorised according to an averaged grain-size, which subsequently ignores the natural variability and responses of the sediments. Moreover, as discussed in Section 2.3, the effect of the variability in existing grain sizes can be clearly observed from different beach slopes/profiles on adjacent beaches with slightly different sediment content under otherwise similar wave conditions (Calliari, 1994 and Birkemeier *et al.*, 1985, DEFRA, 2007). As already described in Section 1.2, one of the main objectives of this research is to improve the understanding of how different grain size distributions affect the beach response both in terms of groundwater elevation and in terms of beach crest erosion. Before studying the effect of the sediment size distribution on the groundwater table under wave motion, it is, however, necessary to have a better understanding of how the water that flows through gravel material is influenced by the sediment size distribution under a more simplistic set of water flow regimes. In particular, which of the typical characteristic grain size parameters (D_{50}, D_{15}, D_{85}/D_{15}) has the greater influence on the flow/resistance relationship within a porous medium. To address this question, a permeameter study was carried out using samples with a wide range of sizes and gradings under a wide range of stationary flow rates. The test design, results and analysis of the permeameter study are discussed in the next chapter.

5. Verification of the Forchheimer coefficients for coarse grained materials

5.1. Introduction to porous flow

Gravel beaches are used to protect coastal areas from wave action by absorbing most of the energy from the incident waves (Powell, 1990; Horn, 2006). As discussed in Chapter 2, the wave interaction with the structure comprises a multitude of processes, such as: wave run-up, wave overtopping, wave reflection and wave transmission. These are influenced by the incident wave conditions, the properties of the material and the wave-induced porous flow inside the structure (Van Gent, 1992; Burcharth, 1991; Horn, 2006). These processes, particularly transmission, dissipation and reflection, are related to the wave-induced porous flow within the structure. Therefore, knowledge of the porous flow and pore pressure attenuation is relevant to beach design.

The porous media is normally schematised and treated as one continuum which exerts forces on the fluid due to drag, friction and acceleration (Bear, 1972). The flow resistance is normally described with the Forchheimer equation, where the unknown resistance coefficients were determined from physical experiments (Horn, 2006, Baird *et al.*, 1998; Raubenheimer *et al.*, 1999; Van Gent, 1992; Burcharth, 1991). For these studies the values of the coefficients in the Forchheimer equations were based on only a limited number of tests and most of the formulae for the Forchheimer coefficients presented in the literature are based on experimental results. As the samples tested by various authors were constructed differently, a comparison is rather difficult. Moreover, due to the different ranges of the diameter, porosity, Reynolds number and testing configurations used in the previous studies, there is a wide variation in the published coefficients. Some of this research on stationary flow is discussed in Chapter 3.

Most research into the Forchheimer equation has focused on the effect of sediment size described, e.g., by D_{50} or D_{15}, rather than the shape of the sediment grading curve. Whilst such simple parameterisations can be very effective within the expectations of experimental and observational accuracies for some behaviours/physical processes, it is felt here that there is sufficient justification to consider sensitivities related to the form of the grading curves themselves. Indeed the spectrum of poorly and well sorted sedimentary environments that exist in natural coastal environments is

well reported (McLean and Kirk, 1969; Powell, 1993; Holmes et al, 1996). This could affect the stability and equilibrium shape of such structures, with implications for performance.

It is suggested here that through controlled sample preparation and experimentation, the effect of grading curves on the Forchheimer coefficient values can be discerned and will be significant. This would lead to better understanding of how to model flow in coarse grained porous media, relevant to beach management and the modelling of coastal engineering structures. In this work a new dataset used to explore the effect of grading curve characteristics on the Forchheimer parameters for gravel sediments is reported. A review of current understanding of porous flow in terms of Forchheimer theory was discussed in Chapter 3. A description of the design and execution of the experimental programme is reported in the first part of this chapter. Discussion of the results presented in this Section are focused on the following grain size diameters: D_{15}, D_{50} and D_{85}. Other grain size diameters, such as D_{10} and D_{60}, were also considered at the beginning of the study, however D_{15}, D_{50} and D_{85} were found to have a much larger effect on the flow/resistance relationship than D_{10} and D_{60}. Therefore the following analysis and results will be discussed in terms of D_{15}, D_{50} and D_{85} only. Analysis and conclusions are discussed in the second part of this chapter.

5.2. Forchheimer coefficients

The classical assumption for the description of flow in porous media is that, at the microscopic scale, a creeping flow (type of fluid flow where advective inertial forces are small compared with viscus forces) takes place. This at the macroscopic scale, is equivalent to a linear relationship between the flow rate and the piezometric head. This is expressed by the well-known Darcy's law. As the flow velocity increases, the inertial effects start dominating the flow, in these conditions where the inertial effects are not negligible, the relationship between the flow velocity and the driving pressure gradient is no longer linear. This condition is typical of Reynolds number, Re >10 ($R_e = qD/\nu$, with D [L] the porous medium particle diameter and ν [L^2T^{-1}] the kinematic viscosity of the fluid). To account for the non-linear behaviour between the hydraulic resistance, expressed as the hydraulic gradient (*I*), and the superficial velocity (*V*) (total flow rate divided by the cross sectional area), Forchheimer suggested the following expression (Bear, 1972):

$$I = aV + bV^2 \tag{5.1}$$

where *a* and *b* are the coefficients describing energy losses due to viscous and inertial dissipation mechanisms. The coefficient *a* of the linear term in the Forchheimer equation is a function of the properties of both the porous medium and the fluid characteristics. It represents energy losses due to viscous forces (viscous friction) at the fluid–particle interface. Coefficient *b* depends on the properties of the porous medium only, and it is related to inertial forces, which are less affected by the viscous forces. The purpose of this study is to investigate the influence of sediment size distribution on the Forchheimer parameters *a* and *b*. The following expressions for the *a* and *b* coefficients were proposed:

$$\mathrm{a} = \alpha \frac{(1-\mathrm{n})^2}{\mathrm{n}^3} \frac{\nu}{\mathrm{gD}^2} \tag{5.2}$$

$$b = \beta \frac{1-\mathrm{n}}{\mathrm{n}^3} \frac{1}{\mathrm{gD}} \tag{5.3}$$

where the value of the two coefficients α and β must be determined empirically, *n* is the porosity, *D* is the characteristic grain size, ν is the kinematic viscosity and g is the acceleration due to gravity.

Turbulent flows are unsteady by definition, but a turbulent flow can be statistically stationary (Pope, 2000). The random velocity field is statistically stationary if all statistics are invariant if shifted in time, i.e., all statistical properties are constant in time. During the present study, both the recorded velocities and the recorded hydraulic gradients were constant in time. Therefore the flow conditions used during the experiments have been considered as statistical stationary.

The Forchheimer regime (shown in Figure 5.1), can be considered as a transition regime, between laminar and turbulent, in which initially the flow is steady laminar but as it progresses the inertial effects becomes very important. As discussed in Chapter 3, the range of validity of the Forchheimer model is strongly dependent on the characteristic of the porous matrix, however the Forchheimer regime can be representative for flow regimes where the Reynolds number ranges approximately between 10 and 1000 (Bear, 1972). The coefficient *a* [TL^{-1}] of the linear term in the Forchheimer equation depends on the properties of both the porous medium and the fluid. It represents energy losses due to viscous forces (viscous friction) at the fluid–solid interface.

Coefficient *b* [T^2L^{-2}] depends on the properties of the porous medium only. It is related to inertial forces, which are not related to viscous forces.

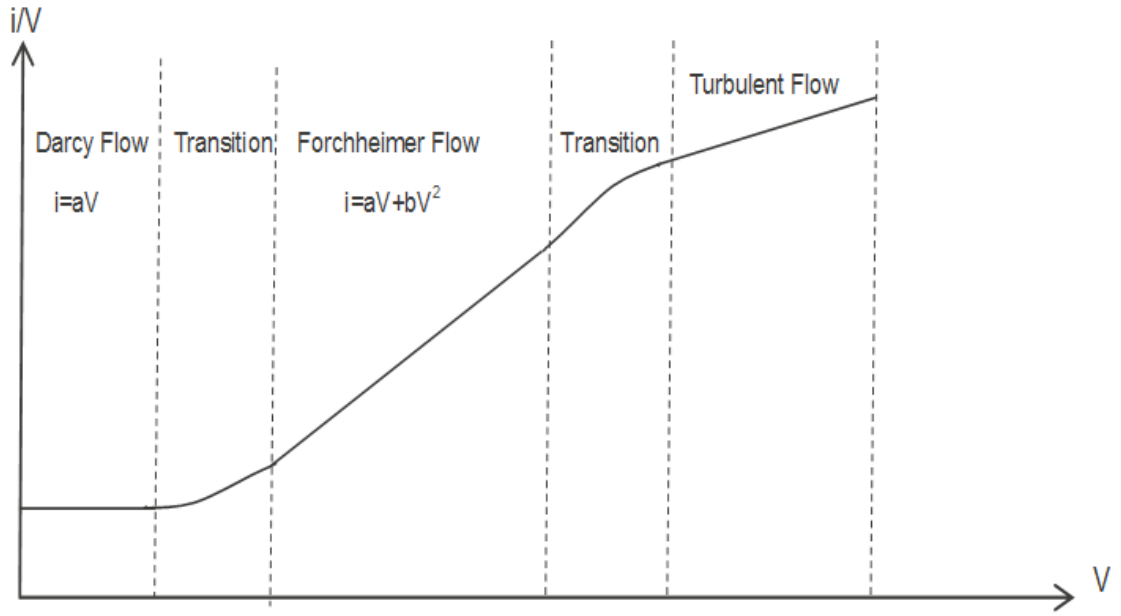

Figure 5.1: Flow regimes suggested by Burcharth & Christensen (1991)

Attempts have been made to determine generalised formulations for the resistance coefficients *"a"* and *"b"* in terms of various material descriptions. Many empirical and semi-empirical formulae for these two coefficients were derived from physical modelling studies. These Forchheimer linear and non-linear resistance parameters are expressed in terms of more fundamental empirical coefficients α and β. As reported in Chapter 3, there are a variety of such formulae, the majority of which are summarised in Table 3.3 (Section 3.3). These expressions show differences in not only the form of the relationships assumed for expressing *a* and *b* in terms of empirical α and β coefficients, but also the values of the empirical α and β coefficients themselves. It should be noted that most of the formulae were originally developed for stationary flow.

5.3. Permeameter tests

5.3.1. Permeameter design

The permeameter used during this study was cylindrical in shape with overall height and internal diameter equal to 1.45m and 0.6m respectively, as shown in Figure 5.2 and schematised in Figure 5.3. In order to avoid wall effects, Dudgeon (1967) suggested that the diameter of the permeameter should be at least ten times the diameter of the largest material to be tested. For these tests, the limiting grain diameter is 60mm. The permeameter was designed with a bottom water entry, and this allowed the majority of air entrained in the voids between particles to be eliminated by running water through the system for a few minutes before commencement of the test. Water was pumped through the permeameter, initially through a 0.3m baffled inlet section, and allowed to flow freely over the upper rim, as shown in Figure 5.2 and Figure 5.4. On this inlet the flow rate was measured by an electromagnetic flow meter. A general layout of the permeameter system is schematised in Figure 5.5. The discharge water from the permeameter was allowed to drain back freely into the reservoir, within which the pump intake was located, thus providing continuous water cycling. Rigid perforated steel plates were placed to contain the sample at the top and bottom of the permeameter (see Figure 5.4).

In order to measure the hydraulic gradient through the sample, water pressures were measured at two levels, 0.5m apart, inside the permeameter. At each level, the measurement arrangement consisted of a pair of tapping tubes. These tubes were made of suitable stiff PVC tubes 9mm in diameter. The open ends of these two tapping tubes were connected outside the permeameter via a looped PVC tube. The pressure head loss was measured using both a piezometer and pressure sensors connected to the two sets of PVC tubes.

Figure 5.2: Permeameter operation during flushing procedure in Froude Hall, HR Wallingford

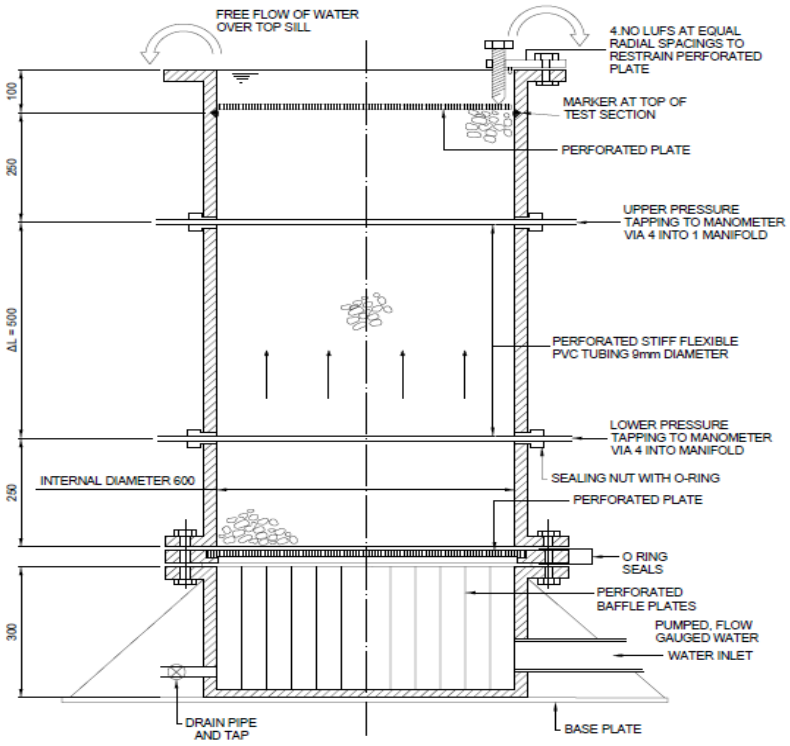

Figure 5.3: Schematised section permeameter

Figure 5.4: Upper plate of the permeameter (above), base of the permeameter (below)

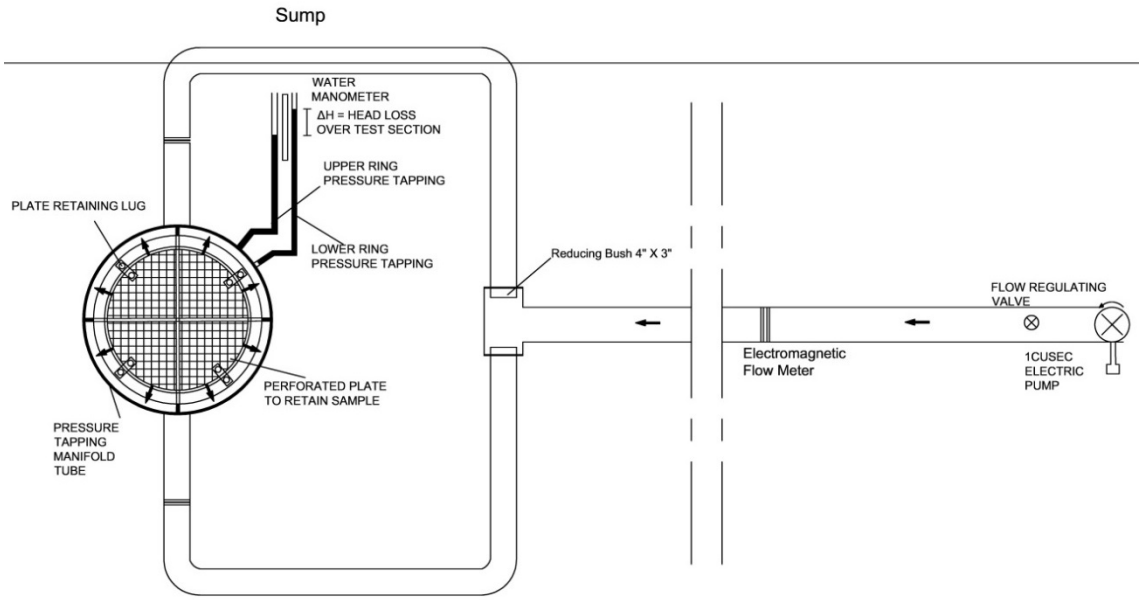

Figure 5.5: Permeameter, general layout

5.3.2. Experimental procedure

The material selected during the tests was limestone with density approximately 2.7 t/m^3. In order to ensure that the designed grading curve was obtained, the materials were sieved in sub-divisions and then mixed in the correct proportions. The sample was then washed to eliminate fine material which could affect the porosity during testing. The wide grading curves were produced by mixing the single size classes in different proportions, covering a wide range of D_{85}/ D_{15}. Both narrow and wide theoretical grading curves are reported in Table 5.1 and Table 5.2. The tested grading curves were designed to have a similar value for at least one of the characteristic size diameters (D_{50}, D_{15}, D_{85}/ D_{15}). This allowed, during the analysis, to identify which of the characteristic size diameters have more influence on the flow/resistance relationship. In Table 5.3, the characteristic size diameters which are similar for the different grading curves are reported. The actual sieved samples (red line) are plotted in Figure 5.6 and Figure 5.7 for narrow and wide grading curves, respectively. Before testing, the porosity of the samples was measured. The measured porosities were compared with the predicted values based on the grading curves (see CUR, 2010) and the results show a good similarity between predicted and measured porosities, ranging between $0.37 \leq n \leq 0.45$.

The samples placed in the permeameter were tested under 15 - 18 constant flow rates, incrementally increased from ~ 0.2 to ~ 26 l/sec. For each flow rate the pressure measurement readings were taken once the system stabilised. The system was considered stable when three consecutive readings (occurring at intervals of 2min each) of both pressure sensor measurements and piezometric levels were the same. For each sample, tests were repeated twice to both account for differences in packing and to ensure consistency of data and repeatability of testing procedure, but also to quantify system uncertainties.

Samples, in small quantities (approximately 25kg), were carefully loaded into the permeameter. The weight of each loaded-box was recorded so that the total quantity placed in the permeameter could be determined. The loading was carried on until the top of the sample was approximately 100 mm from the top of the permeameter. After the level surface was achieved, the covering lid was clamped in position, the volume of the sample in the permeameter was therefore fixed between the upper and lower perforated plates. Before starting a new series of tests, water was

pumped through the sample for 10 minutes at the highest discharge to allow natural settlement to take place and to remove the majority of air entrained in voids between particles. Photos of the different tested materials are shown below in Figure 5.8 and Figure 5.9, where the inner dimensions of the container are 410mm x 580mm. Figure 5.8 shows the different narrow grading curves plotted in Figure 5.6, sorted in ascending order in terms of D_{50}. As can be seen, although they have different size materials, they are all characterised by a very homogenous grain size distribution. This can be observed, for example, for the grading curve A, in Figure 5.8 where almost all the rocks presented in the box have a similar diameter size of 14mm. This homogeneity in the size distribution is expressed in terms of grading curve in Figure 5.6, where the characteristic size diameters D_{15}, D_{50} and D_{85} are all close to 14mm.

Conversely, Figure 5.9 which illustrates the grading curves plotted in Figure 5.7, shows very wide grain size distributions, in particular "Material G" (Figure 5.9), which has the highest value of D_{85}/D_{15}. This means, as can also be seen in Figure 5.9 and in Table 5.2, that a significant range of sediment sizes (D_{15} = 6mm and D_{85} = 27mm) are present within the sample. This variety in the size distribution for the material G is expressed in terms of grading curve in Figure 5.9, where the characteristic size diameters D_{15} and D_{85} are very different from the mean value D_{50}. Additionally, comparing Figure 5.8 (material A) with Figure 5.9 (material G), it can be seen that the samples look quite different, however they have a similar D_{50} (see also Table 5.3). Therefore it is expected that this difference in the grain size distribution will have an influence on the flow/resistance relationship, despite a similar D_{50}.

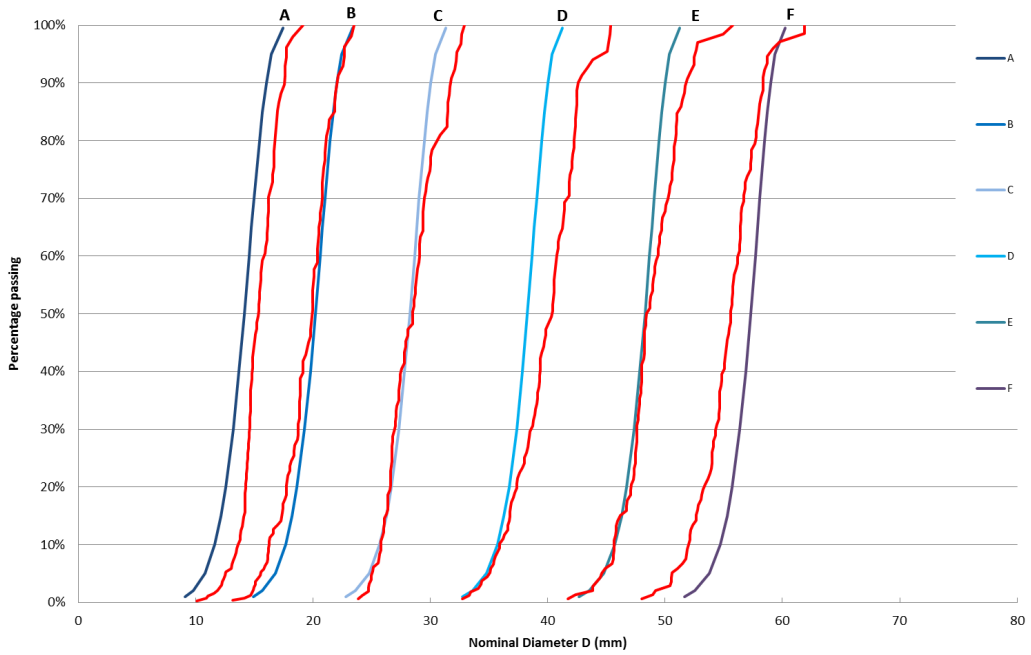

Figure 5.6: Specified and measured (red-line) sample grading curves: narrow grading

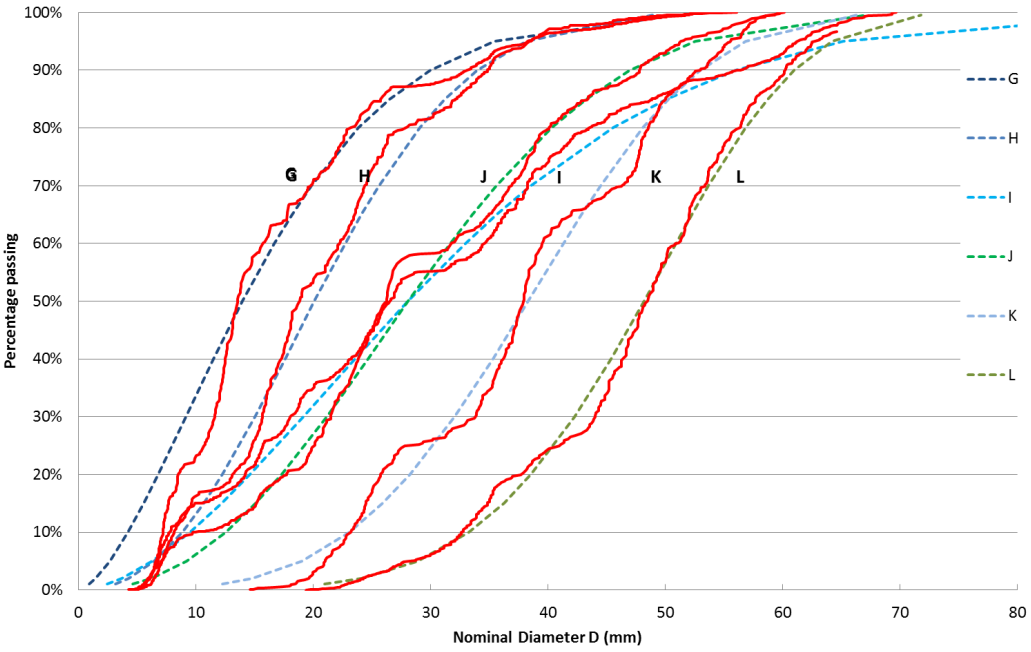

Figure 5.7: Specified and measured (red-line) sample grading curves: wide grading.

Table 5.1: Single size classes parameters

Test Name	D_{50} (mm)	D_{15} (mm)	D_{85} (mm)	D_{85}/D_{15}
A	14	12	16	1.3
B	20	18	22	1.2
C	28	26	30	1.1
D	38	36	40	1.1
E	48	46	50	1.1
F	57	55	59	1.1

Table 5.2: Wide grading curves parameters

Test Name	D_{50} (mm)	D_{15} (mm)	D_{85} (mm)	D_{85}/D_{15}
G	14	6	27	4.8
H	20	11	31	2.9
I	28	12	50	4.1
J	28	15	43	2.9
K	38	26	50	1.9
L	48	36	59	1.6

Table 5.3: Similarities, in terms of particle sizes, between single and wide graded samples

Samples	Similarities
A, G	D_{50}
B, H	D_{50}
C, I, J	D_{50}
D, K	D_{50}
E, L	D_{50}
A, J	D_{15}
C, K	D_{15}
D, L	D_{15}
C, H	D_{85}
L, F	D_{85}
I, K	D_{85}
H, J	D_{85}/ D_{15}
G, I	~ D_{85}/ D_{15}

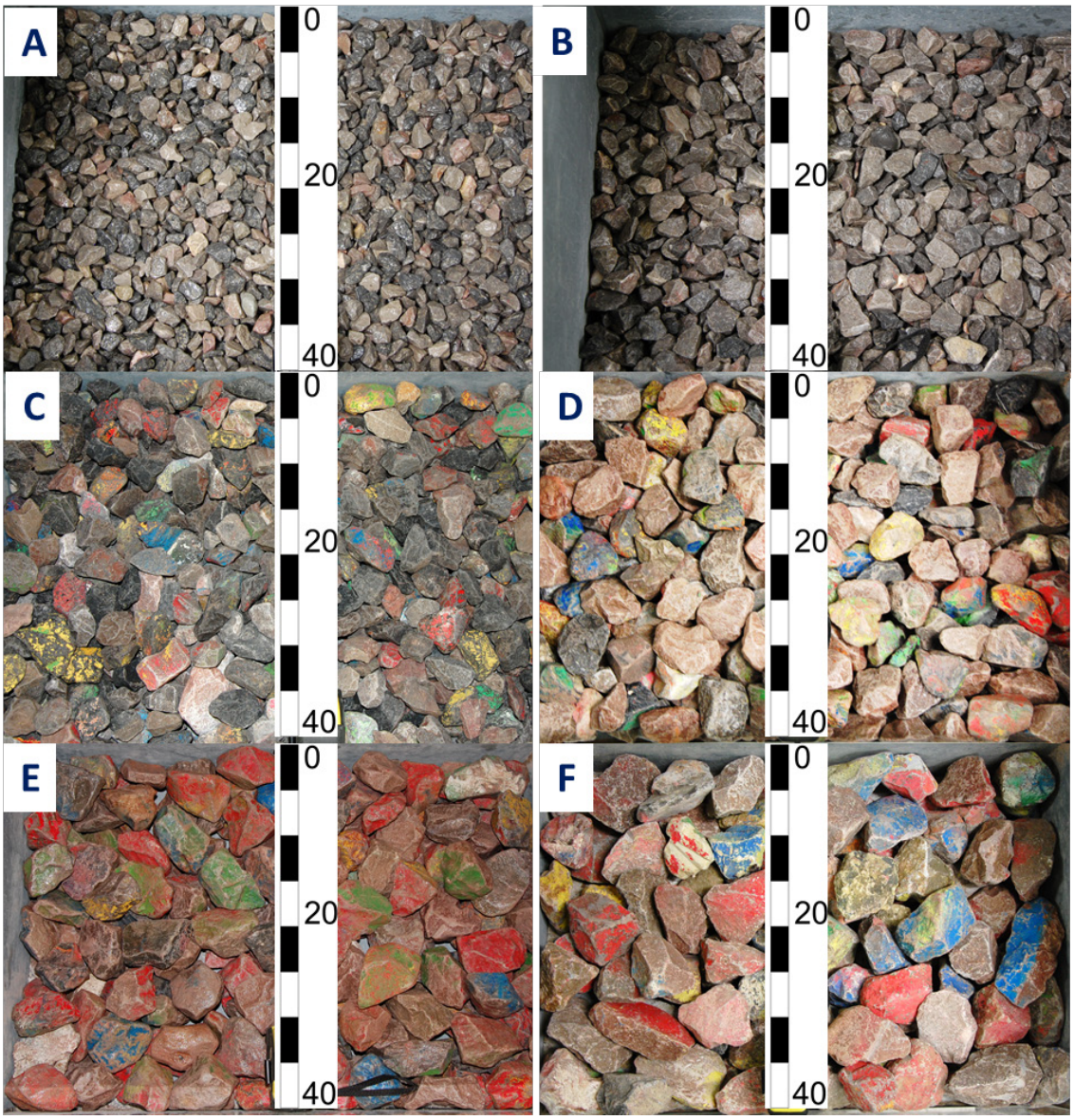

Figure 5.8: Narrow grading curves plotted in Figure 5.6, sorted in ascending order in terms of D_{50}

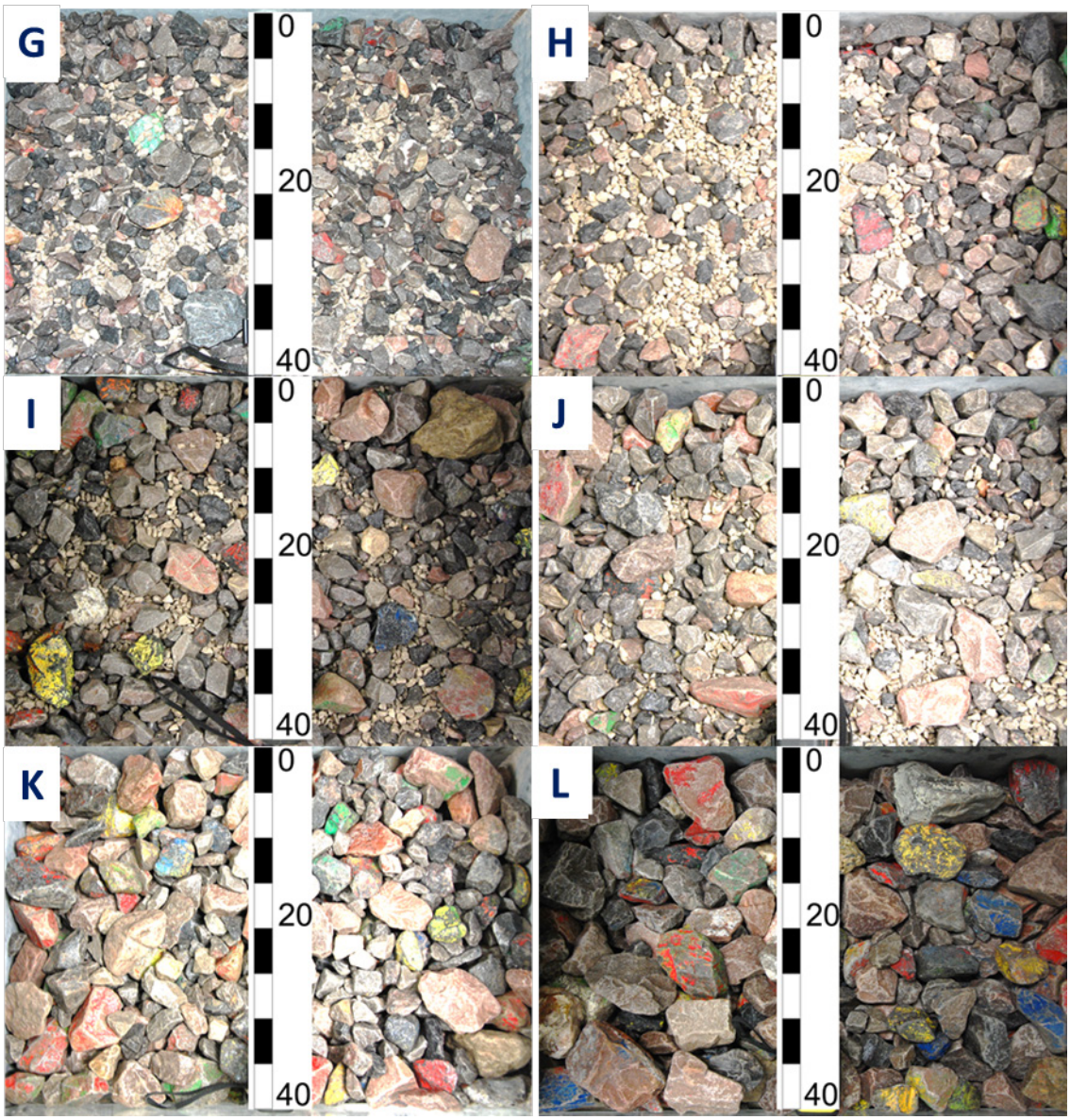

Figure 5.9: Wide grading curves plotted in Figure 5.7, sorted in ascending order in terms of D_{50}

5.4. Test Results

5.4.1. Introduction

As previously mentioned, this study aimed to provide a better understanding of the permeability properties of gravel materials, particularly the effect of sediment size and grading curve on the Forchheimer coefficient values. A discussion on the whole variation in approach and results for previous research has been summarised in Chapter 3. The discrepancies between previous results may be influenced by the different configurations in which the different samples were tested. During this present research tests were all carried out by constantly using the approach discussed in Section 5.3.2.

The Forchheimer coefficients *a* and *b* were derived by using the measured pressure gradient and the measured superficial velocity and applying a linear regression analysis. During the tests it was therefore assumed that the flow/resistance relationship was described in terms of the Forchheimer equation (Equation (5.1)). This equation can also be rewritten as $i/V=a+bV$ and assuming that the coefficients *a* and *b* are constant for each sample, these are given by the linear regression of i/V vs V. The values of i are the measured hydraulic gradients and V is the superficial velocity (the volumetric flow rate divided by the column cross-section area).

5.4.2. Results

Six different narrow grading curves, shown in Figure 5.8, were tested. As might be expected from physical principles *a priori*, and within the range studied, the values of *a* and *b* show increasing hydraulic resistance with decreasing porosity and particle size. In the plot of i/V against V (see Figure 5.10 and Figure 5.11) the intercept and slope regression represent respectively the coefficients *a* and *b*. Results plotted in Figure 5.10 and Figure 5.11 show good agreement with theory / linear relationship, evidenced by R^2 values close to 1.0. Although under conditions of less turbulent flow, when the term *av* in the Forchheimer equation has greater influence on the total resistance force, a more complex form for the coefficients for *a* and *b* emerges. As suggested by Burcharth and Christensen (1991), the Forchheimer equation does not model the behaviour of the flow through porous media within this range accurately. The plot of i/V against V for narrow grading curves (see Figure 5.10) does not have the linear form suggested by the Forchheimer

equation, but has a form close to the extreme portion of the graph, representing laminar flow as shown in Figure 5.1. It may be noted that this effect will only significantly influence the total resistance force at very low flow velocities (less than 0.01m/s), a condition of less concern in this study.

The corresponding experimental observations of steady flow for samples with wide grading curves, (samples G-M), are shown in Figure 5.11. Here the test results are also consistent with expectations, with *a* and *b* (intercept and slope regression) show increasing hydraulic resistance with decreasing porosity. This phenomenon is illustrated in the plot by having a very steep line for the sample G and a more mild slope line for the sample M (more permeable). For more severe turbulent flow conditions (when the term bv^2 in the Forchheimer equation dominates the total hydraulic resistance) the value of *b* increases as expected. The Forchheimer coefficients *a* and *b* together with the range of Reynolds numbers and porosities are also summarised in Table 5.4. The Reynolds number was derived as follows:

$$Re = \frac{VD_{50}}{\nu} \tag{5.4}$$

where *V* is the superficial velocity (m/s) (total flow rate divided by the cross sectional area), D_{50} is the mean size diameter of the gravel sample and ν is the kinematic viscosity of water. As discussed in Chapter 3, the Forchheimer regime corresponds to a Reynolds number ranging between 10 – 1000 (Bear, 1972), while higher values are relative to a turbulent regime. Values of Reynolds number shown in Table 5.4 suggest that tests were carried out at both Forchheimer and turbulent regimes.

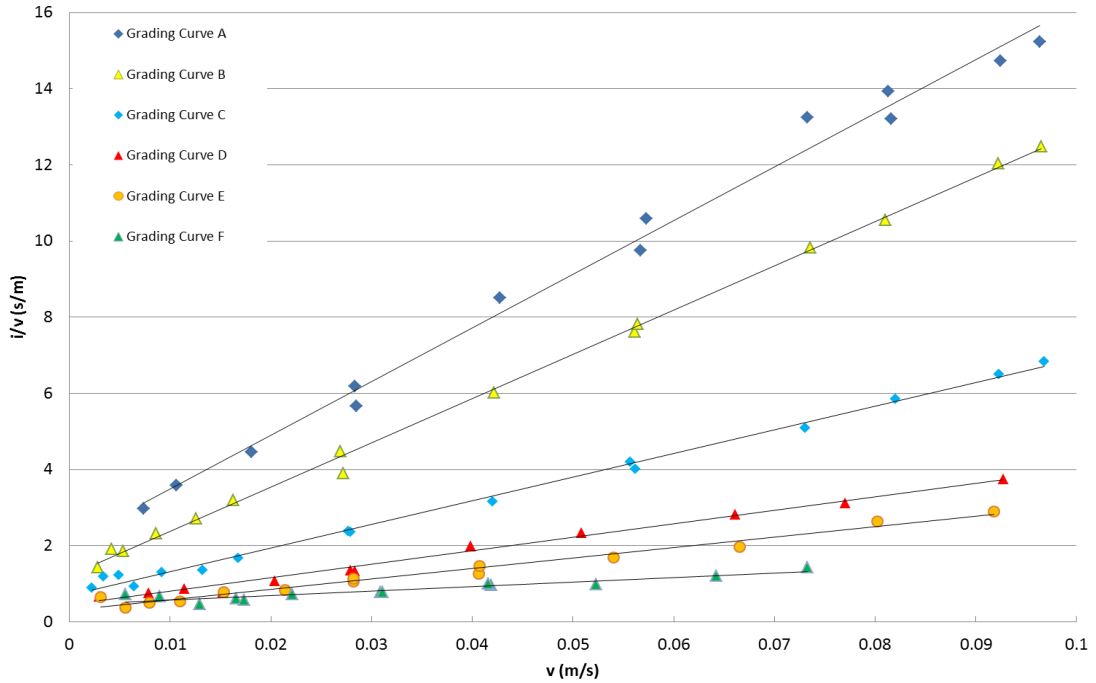

Figure 5.10: Linear regression used to determine Forchheimer parameters for samples A-F: narrow graded samples.

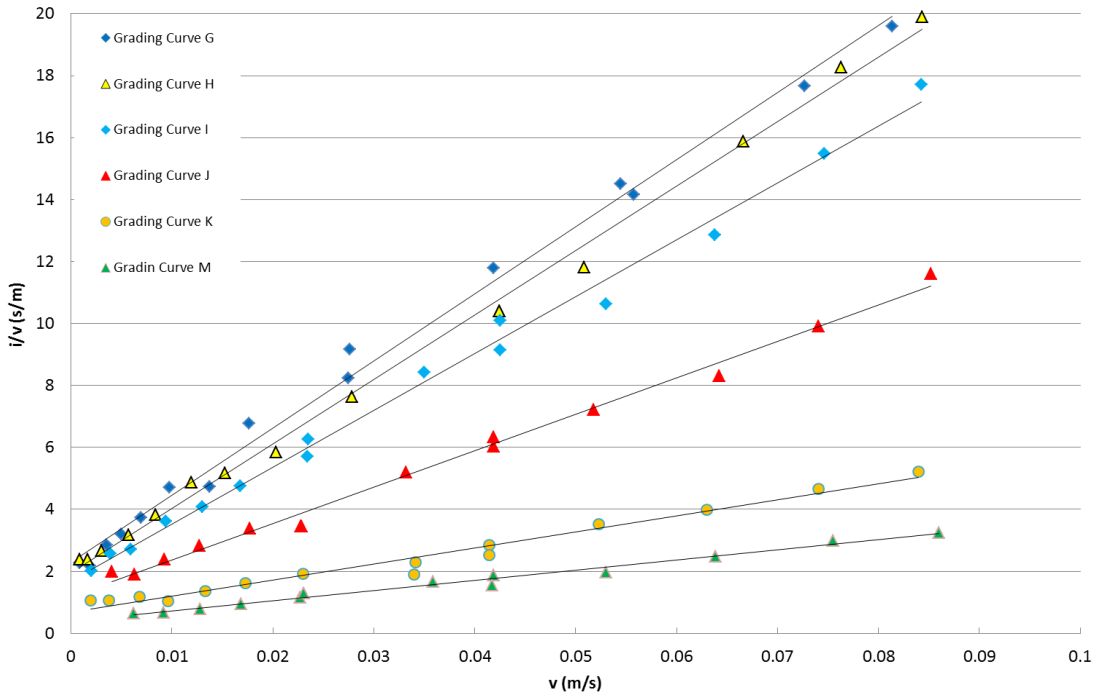

Figure 5.11: Linear regression used to determine Forchheimer parameters for samples G-M: wide graded samples.

Table 5.4: Forchheimer equation coefficients for steady flow tests

Grading Curve	D_{15}(mm)	D_{50}(mm)	D_{eq}(mm)	D_{85}/D_{15}	n (-)	Re (-)	a (s/m)	b (s^2/m^2)
A	14	15	16.8	1.21	0.37	100-1300	2.1	141
B	17	20	21.8	1.26	0.37	140-2000	1.2	116
C	26	29	31.1	1.20	0.40	14.6-2420	0.7	62
D	37	40	44.1	1.15	0.42	28.5-3286	0.5	35
E	46	48	52.8	1.10	0.42	31-3898	0.3	27
F	53	56	60.7	1.10	0.45	45-4142	0.5	12
G	8	14	-	3.62	0.38	11-1003	2.3	217
H	10	19	-	3.35	0.39	14-1397	2.0	208
I	10	27	-	4.94	0.40	19-1735	1.7	183
J	15	26	-	2.85	0.38	21-1966	1.2	117
K	24	38	-	2.04	0.42	32-2795	0.7	52
L	35	48	-	1.65	0.44	40-3656	0.4	33

Note: D_{eq} is defined as $D_{eq}=(6M_{50}/\pi\rho_a)^{1/3}$ where M_{50} is the average mass of a rock grading,

5.4.3. Uncertainty regression analysis

The spread of the actual points either side of the regression line (*y* on *x*) can be expressed in terms of the regression residuals, $y_i - \hat{y}_i$, where *y* is a generic value and $\hat{y}_i$ is the mean value of the sample. The greater these residuals the greater the uncertainty in where the true regression line actually lies. The uncertainty in the regression is therefore calculated in terms of these residuals. The following expression represents the standard error of the regression, $\sigma_{y/x}$:

$$\sigma_{y/x} = \sqrt{\frac{\sum(y_i - \hat{y}_i)^2}{N-2}} \tag{5.5}$$

where *N* is the sample size.

The slope of the regression line is obviously important, as it determines the sensitivity of the head loss function. The uncertainty in the slope is expressed as the standard error (or deviation) of the slope, σ_b, and is calculated in terms of the standard error of the regression as:

$$\sigma_b = \frac{\sigma_{y/x}}{\sqrt{\sum(x_i - \bar{x})^2}} \tag{5.6}$$

where x_i is a generic value and $\dot{x}$ is the mean value.

The uncertainty in the intercept is also calculated in terms of the standard error of the regression as follows:

$$\sigma_a = \sigma_{y/x} \sqrt{\frac{\sum x_i^2}{n \sum (x_i - \bar{x})^2}} \quad (5.7)$$

The standard errors together with the corresponding confidence intervals (95%) for the intercept and slope regression (coefficients *a* and *b*) are reported in Table 5.5. As shown in Table 5.5, the confidence interval for the coefficient *a* is slightly higher for the grading curve A. This could be triggered by the fact that grading curve A was the first material to be tested and it was run using insufficient flow rates within the laminar regime. The coefficient value *a* for grading curve A was therefore excluded during the later analysis.

Table 5.5: Errors in the regression analysis

Grading Curve	a (s/m)	b (s^2/m^2)	$\sigma_{regression}$	$\sigma_{slope, b}$	$\sigma_{intercept, a}$	Conf. int. a_{95}	Conf. int. b_{95}
A	2.1	141	0.43	3.92	0.24	± 0.52	± 8.63
B	1.2	116	0.17	1.35	0.07	± 0.15	± 2.91
C	0.7	62	0.14	1.11	0.06	± 0.12	± 2.39
D	0.5	35	0.11	1.05	0.05	± 0.10	± 2.29
E	0.3	27	0.12	1.16	0.05	± 0.11	± 2.52
F	0.5	12	0.10	1.33	0.05	± 0.11	± 2.93
G	2.3	217	0.45	4.46	0.17	± 0.37	± 9.64
H	2.0	208	0.35	3.31	0.14	± 0.29	± 7.15
I	1.7	183	0.40	4.00	0.17	± 0.36	± 8.64
J	1.2	117	0.28	2.96	0.13	± 0.28	± 6.44
K	0.7	52	0.22	2.29	0.10	± 0.21	± 4.94
L	0.4	33	0.11	1.20	0.05	± 0.12	± 2.65

5.5. Analysis of results

5.5.1. Effect of the grading size on the flow resistance

In order to analyse the effect of both the particle size, and the sediment distribution on the flow resistance, the samples with similar grading parameters (e.g., $D_{50,}$ D_{15} and D_{85}/ D_{15}) reported in Table 5.3 were compared. A comparison between narrow and wide grading curves having similar D_{50} and D_{15} is plotted in Figure 5.12 to Figure 5.15.

Figure 5.12 compares gradings with similar D_{50} and similar D_{15}. This plot shows that the samples with similar D_{15} have closer behaviour, in these instances, than samples with similar D_{50}. As previously discussed, the samples A and G have similar D_{50}, however as shown in Figure 5.8, and Figure 5.9, they look very different. Sample A is a narrow grading curve with an homogenous grain size distribution, conversely sample G is a wide grading curve with a very wide grain size distribution. It is likely that the finest particles of this sample (sample G) will fill up the gaps created by the bigger rocks reducing the permeability of the sample and therefore affecting the flow/resistance relationship. This phenomenon can be observed in the plot of i/V against V (Figure 5.12), where, as expected there is an increase in the hydraulic resistance with decreasing porosity (sample G steeper than sample A). Differently, when comparing samples A and J they also look very different (Figure 5.8 and Figure 5.9), although in the plot in Figure 5.12 they show a similar flow/resistance relationship. This is because, even though they have a different D_{50} and D_{85} they have a similar D_{15}.

Figure 5.13, Figure 5.14 and Figure 5.15 demonstrates this trend further. Pairs of samples B & J and I & H (Figure 5.13), D & L (Figure 5.14) and C – K (Figure 5.15) have similar D_{15} which seems to dictate the behaviour more strongly than the D_{50}, regardless of whether the samples are narrow or wide graded. A further confirmation that the characteristic diameter D_{50} has a less significant influence in the flow resistance is observed in Figure 5.16, where both narrow and wide grading curves having similar D_{50}, were plotted. Although these grading curves (C, I and J, Figure 5.16) have similar D_{50}, a significant difference of the hydraulic gradient can be observed.

The results obtained for both narrow and well sorted particle distributions showed that D_{15} is the representative size that influences the ease with which a fluid flows through a porous media. This

has an important implication to model and predict porous flow and sediment transport processes in granular beaches. Future studies need to start considering the grain size D_{15}, together with the widely used D_{50}, as a critical size parameter to understand the interaction between waves with the groundwater flow within the beach. This will improve predictions of beach evolution, especially in the swash zone.

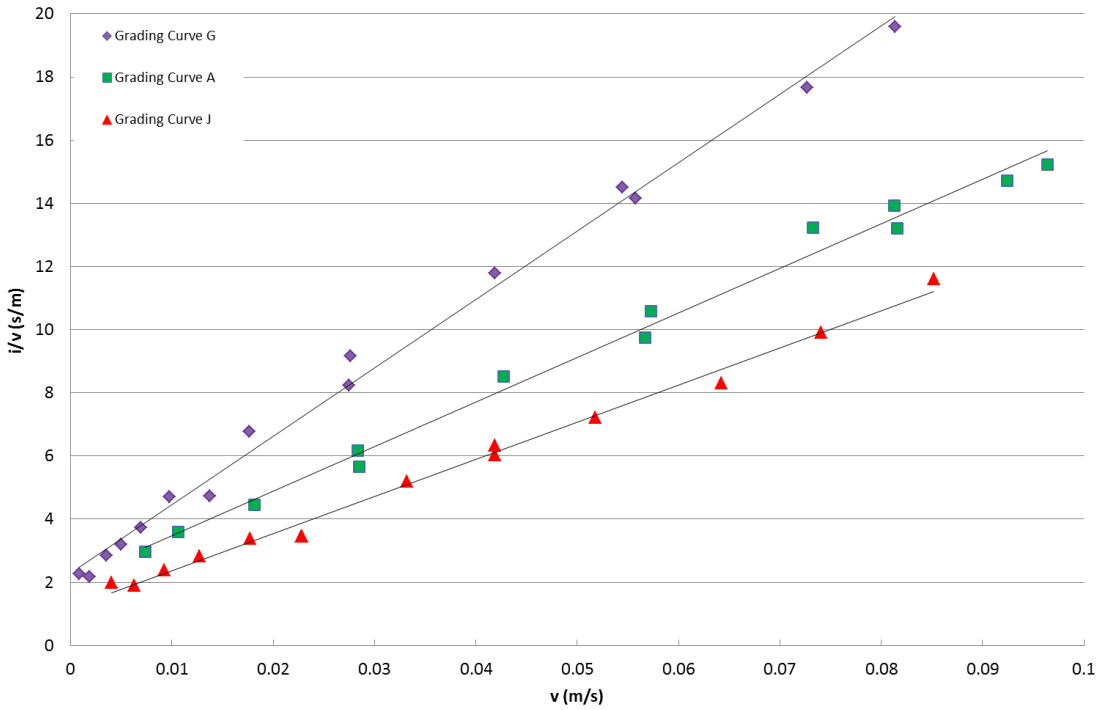

Figure 5.12: Demonstrating the importance of D_{15} vs D_{50} : Samples A and J have similar D_{15} ; A and G have same D_{50}

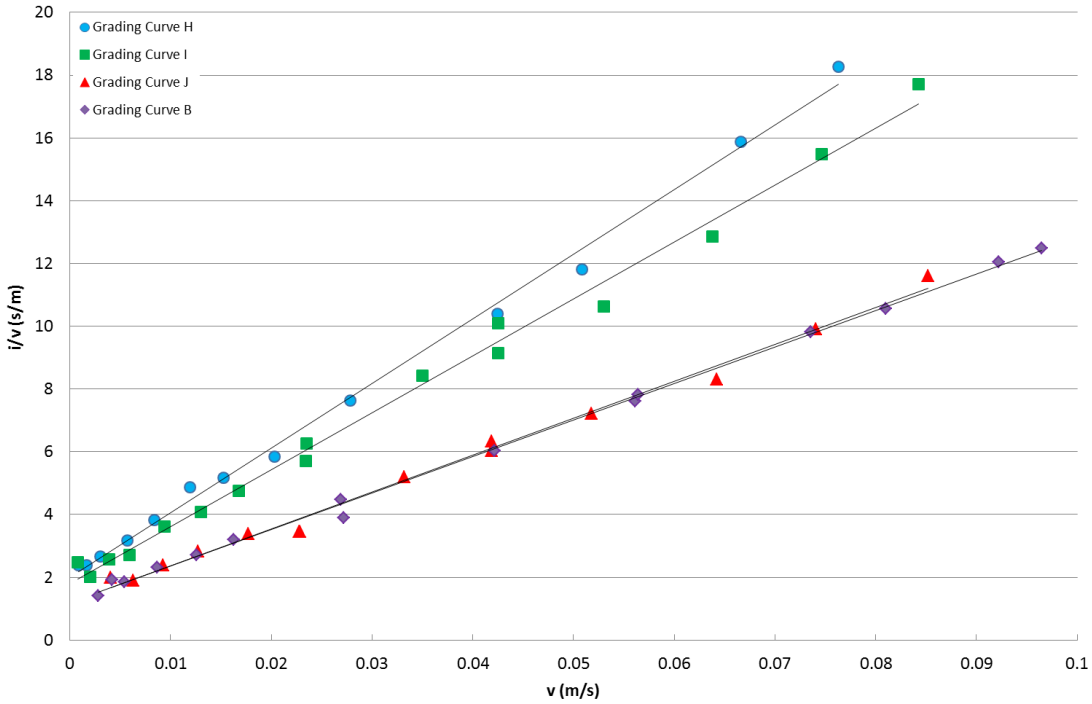

Figure 5.13: Demonstrating the importance of D_{15} vs D_{50}. Samples B - J and I - H have similar D_{15}, while B - H and I - J have same D_{50}.

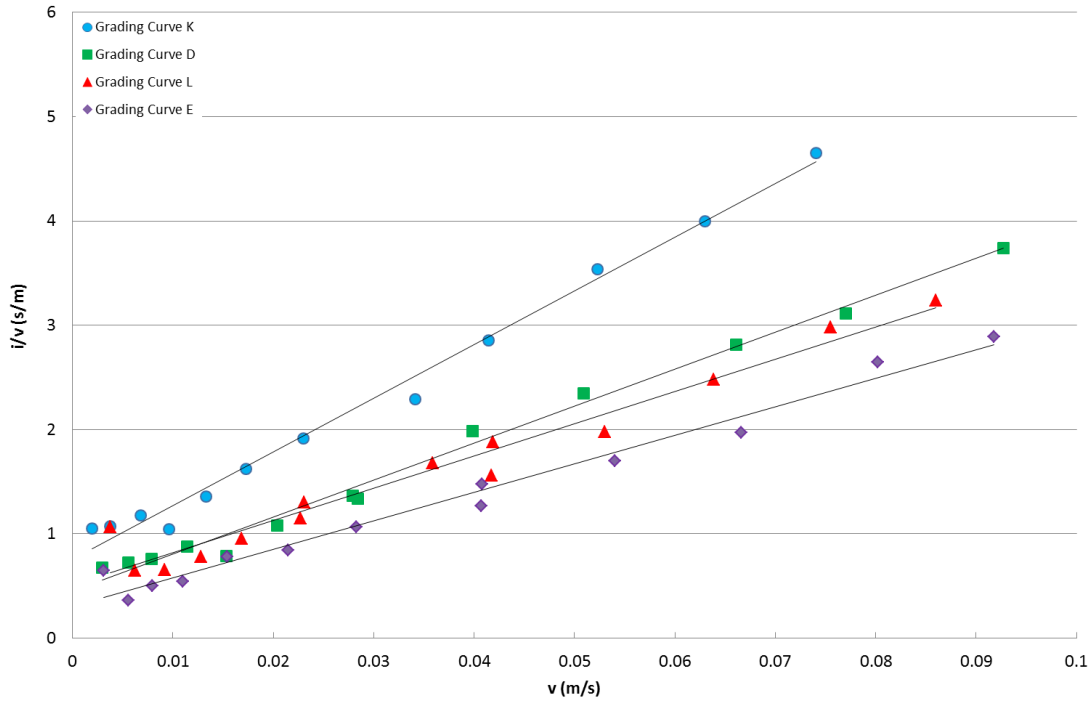

Figure 5.14: Demonstrating the importance of D_{15} vs D_{50}. Samples D - L have similar D_{15} while E - L and D-K have same D_{50}.

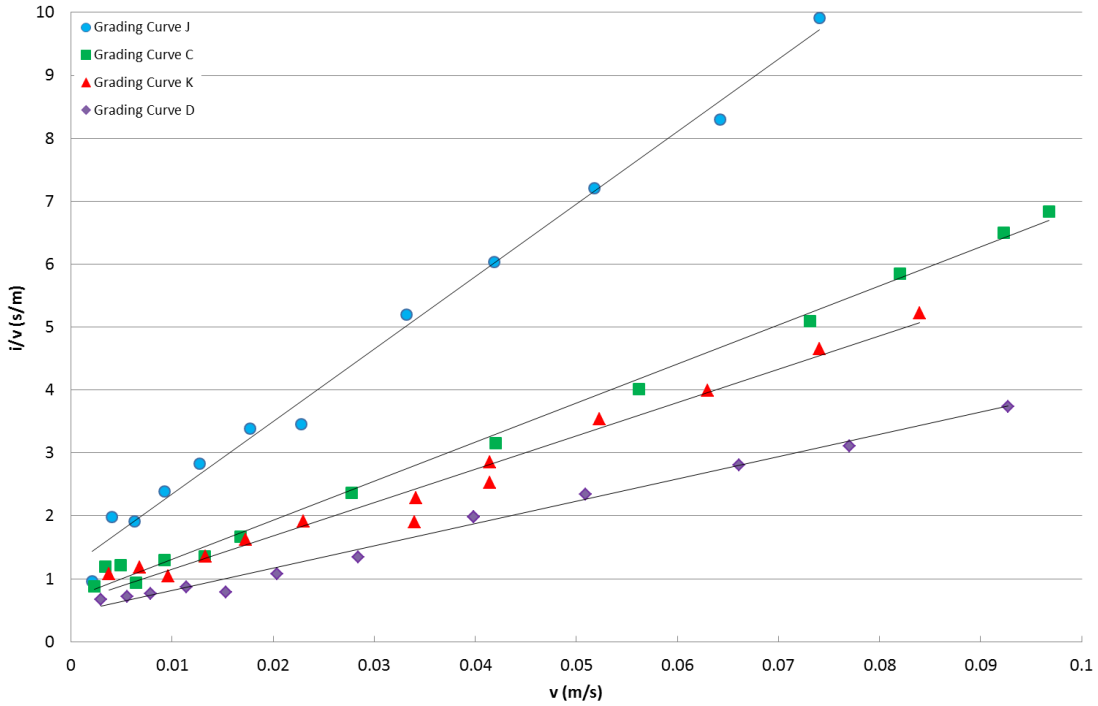

Figure 5.15: Demonstrating the importance of D_{15} vs D_{50}. Samples C - K have similar D_{15} while C - J and D-K have same D_{50}.

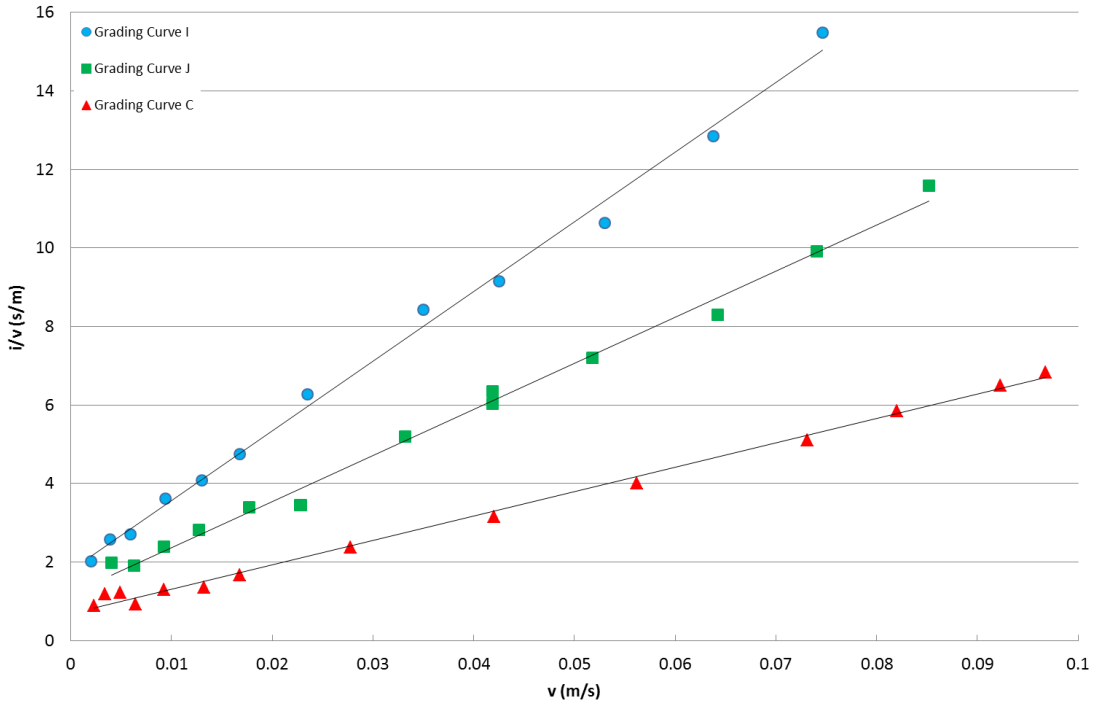

Figure 5.16: Effect of D_{50}, sample narrow grading curve C (D_{50} = 29mm) and sample wide grading curves I (D_{50} = 27mm) and J (D_{50} = 26mm)

Another parameter, which is used to describe the grading of sediment samples, is the classification D_{85}/ D_{15}. Grading curves with similar D_{85}/ D_{15} are shown together in Figure 5.17 and Figure 5.18. Once again these plots show that a similar behaviour of the hydraulic head losses was obtained only when the grading curves had a similar D_{15} (Figure 5.17). Figure 5.17 compares samples with similar D_{85}/ D_{15} and similar D_{15}, while Figure 5.18 compares samples with similar D_{85}/ D_{15} and different D_{15}. Once again samples G & H with similar D_{15} have closer behaviour, suggesting that it is D_{15} that dictates the behaviour more strongly than D_{85}/ D_{15}, regardless of whether the samples are narrow or wide graded.

Those results, therefore, suggested that the particle size D_{15} can be considered as the key sediment parameter with regard to flow/resistance for both narrow and wide grading curves. This could be explained because the D_{15} of a granular material is related to the size of its voids. Indeed, Silveira (1975), based on theoretical and experimental work, suggests a relationship between the size of voids and the characteristic diameter D_{15}. The expression suggest by Silveira (1975) is: pore size = $D_{15}/5$. Based on the results discussed above, the grading parameter D_{15} was therefore used as the characteristic diameter for the remaining analysis of the present study.

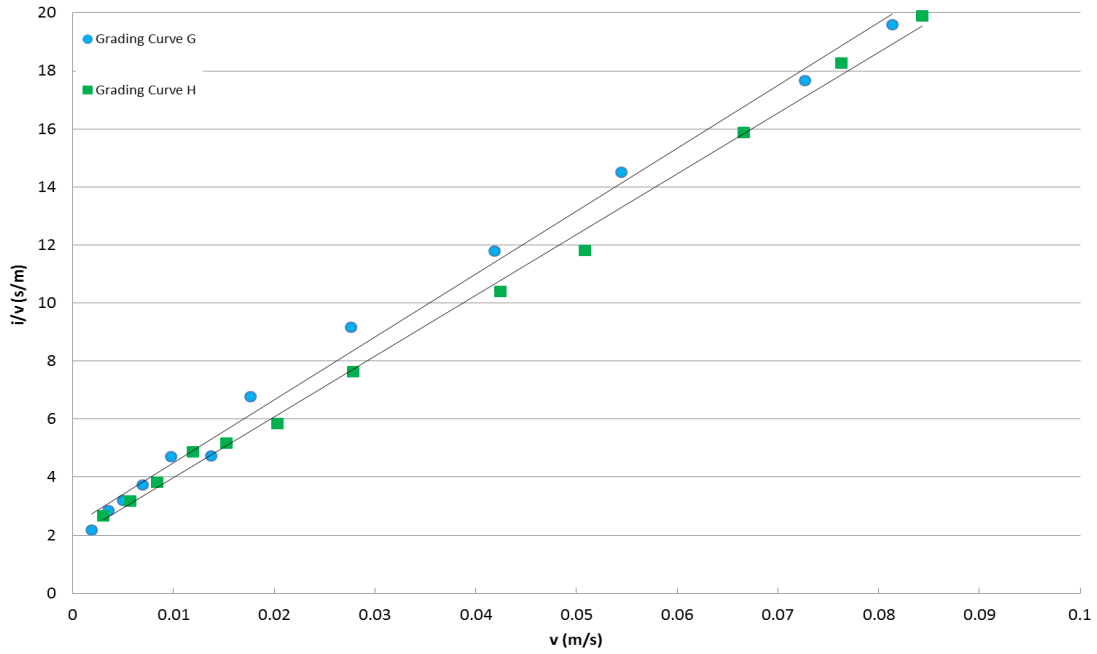

Figure 5.17: Effect of D_{85}/D_{15} . Samples G and H have similar D_{85}/D_{15} =3.4, although they also have similar D_{15} = 10mm.

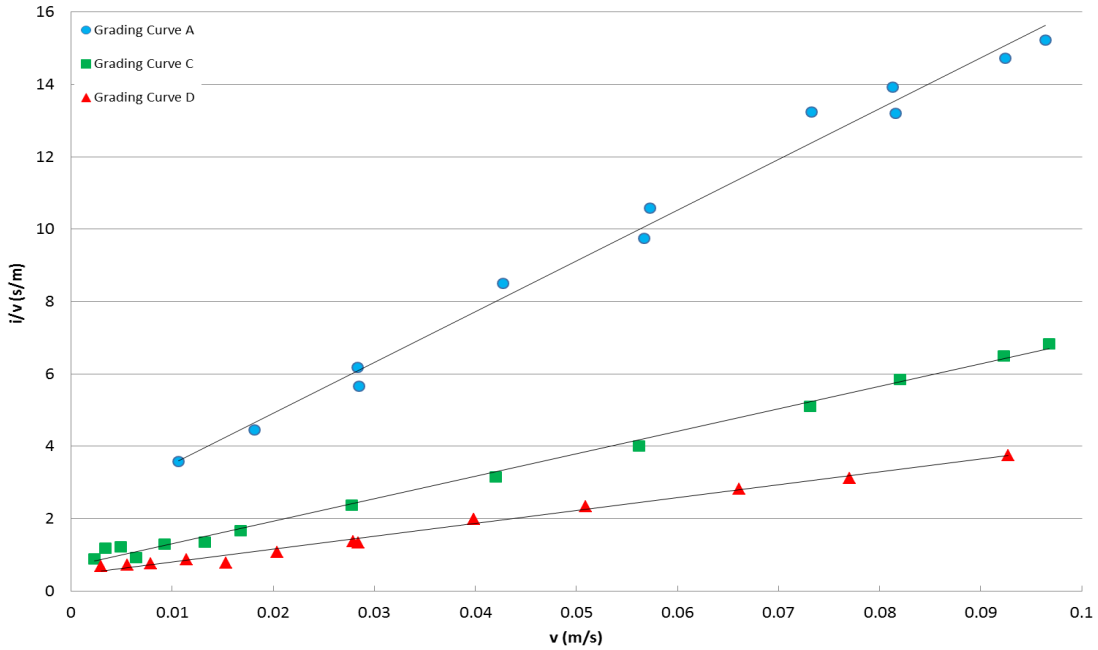

Figure 5.18: Effect of D_{85}/D_{15} . Samples grading curves A, C and D with similar D_{85}/D_{15} = 1.2 although different D_{15}.

5.5.2. Comparison of test results with existing formulae in literature

In the literature, two main expressions are used to describe the laminar Forchheimer parameter *a*. One was proposed by Ergun (1952) and the second one was proposed by Engelund (1953). The existing formulae for the Forchheimer parameters were summarised in Chapter 3. As previously discussed, for flow regimes where the inertial effects in the pore scale are not negligible, the flow/resistance relationship is described by the Forchheimer equation (Equation (5.1)).

The values of the parameters *a* and *b* and the related coefficients α and β, extracted during this study are summarised in Table 5.6. The Forchheimer parameters were calculated using two characteristic particle sizes, D_{15} and D_{50}. The results of these tests indicate, as expected, that the coefficient α and β are not constant for all samples, as reported in Table 5.6.

Table 5.6: Results stationary flow tests

Grading Curve	D_{15} (mm)	D_{50} (mm)	D_{85}/D_{15}	Re_{min}	Re_{max}	a_{meas}	b_{meas}	α_{15}	β_{15}	α_{50}	β_{50}
A	14	15	1.2	100	1300	2.1	141	470	1.6	559	1.8
B	17	20	1.3	140	2000	1.2	116	400	1.6	531	1.8
C	26	29	1.2	15	2420	0.7	62	718	1.7	850	1.8
D	37	40	1.2	29	3286	0.5	35	1152	1.6	1389	1.8
E	46	48	1.1	31	3898	0.3	27	1278	1.6	1403	1.7
F	53	56	1.1	45	4142	0.5	12	3403	1.0	3788	1.1
G	8	14	3.4	11	1003	2.3	217	172	1.5	532	2.6
H	10	19	3.3	14	1397	2.0	208	242	1.9	919	3.6
I	10	27	4.9	19	1735	1.7	183	254	1.9	1819	5.0
J	15	26	2.8	21	1966	1.2	117	359	1.6	1066	2.8
K	25	38	2.0	32	2795	0.7	52	788	1.6	1879	2.5
M	35	48	1.7	40	3656	0.4	33	1134	1.7	2193	2.4

A comparison between the measured and theoretical expressions of the laminar coefficients, *a*, suggested by Ergun (1952), Engelund (1953), Koenders (1985), Den Adel (1987), Shih (1990) and Van Gent (1993) is shown in Figure 5.19. For each theoretical expression, the laminar coefficient α, proposed by the originator of the expression was used (see Table 3.3). Use of the theoretical expressions significantly underestimates the observed values for the coefficient, *a*, for smaller D_{15}, but provides better agreement for bigger D_{15}. The Engelund (1952) and Den Adel (1987) expressions also underestimate *a* at large D_{15}.

A more conclusive comparison between the measured and predicted turbulent coefficient *b*, is presented in Figure 5.20. This shows that Den Adel (1987) and Ergun's (1952) expression matches the entire dataset well, whilst Engelund (1953) overestimates the measured values by 40% and Van Gent's similar expression (1993) underestimates the measured values by 30%. This discrepancy could be due to the differences in the testing configuration used by the equivalent studies carried out to extract the values of the theoretical coefficients β (see Table 3.3).

Additionally, in Figure 5.21 and Figure 5.22, the measured values of *a* and *b*, for both narrow (red triangle) and wide (blue triangle) graded samples were compared with the formulae suggested by Shih (1990). For wide graded samples, Shih suggested D_{15} be replaced with D_* (see Table 3.3). The trend in the data is well matched across the data sets, save for the smallest diameter sediment

mixture for the wide graded samples. The Shih formulae seems to predict both the *a* and *b* values correctly for the narrow grading materials, while a bigger scatter is observed for the wide grading curves. It is evident that the suggested improvement for wide grade samples in Shih's updated formulae does not match the values measured during this study.

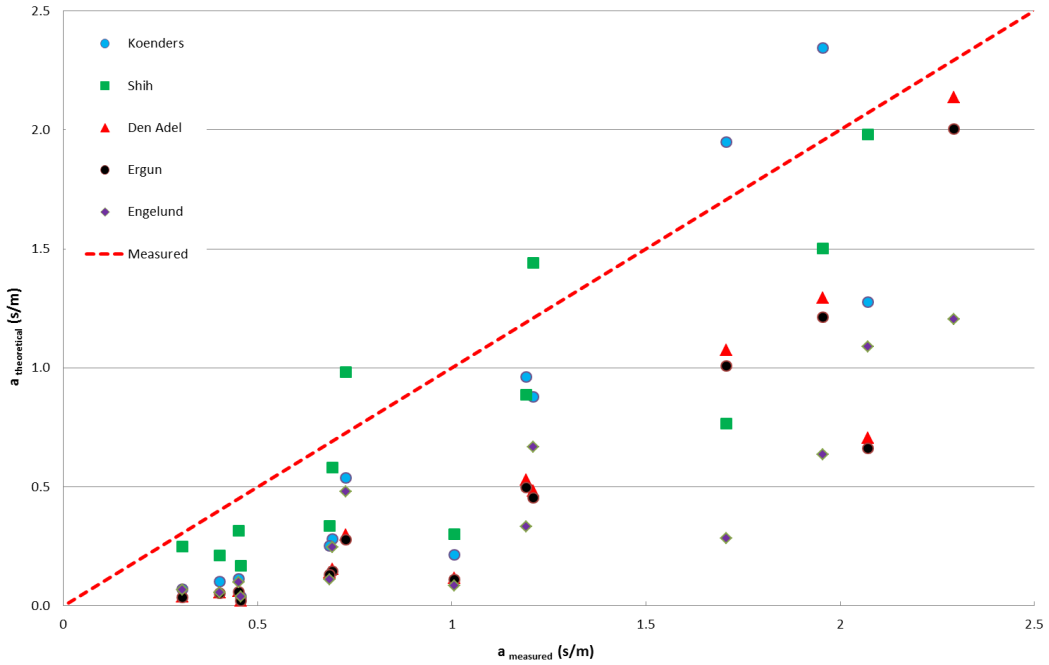

Figure 5.19: Evaluation of measured Forchheimer coefficient *a* against previous formulae

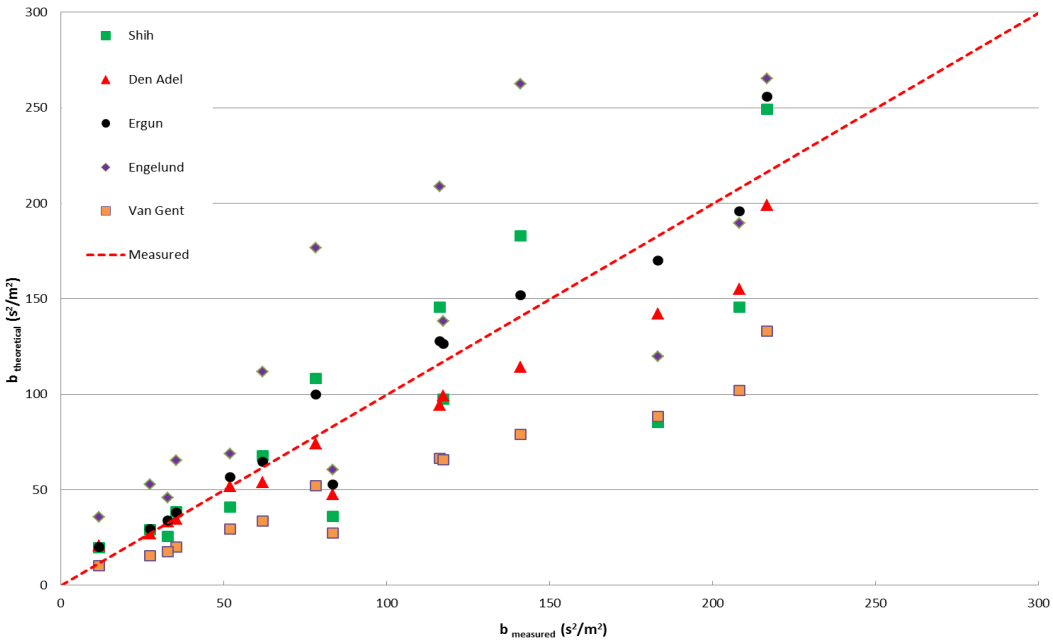

Figure 5.20: Evaluation of measured Forchheimer coefficient *b* against previous formulae

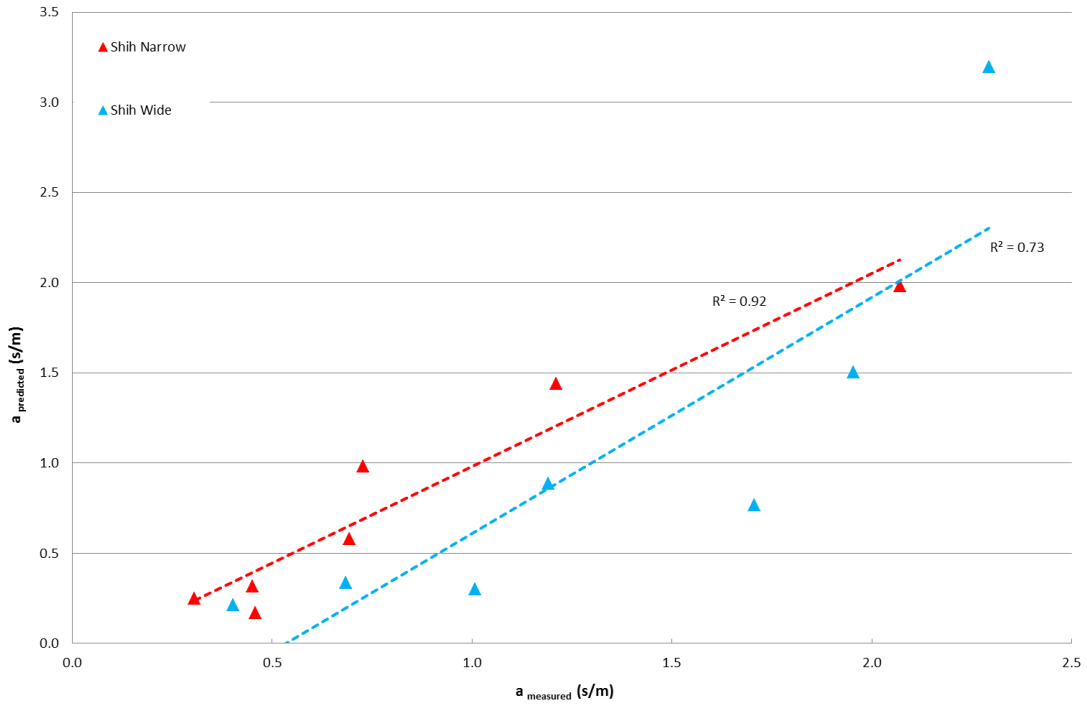

Figure 5.21: Evaluation of empirical Forchheimer *a* coefficients against Shih's (1990) formulae for narrow and wide graded sediments

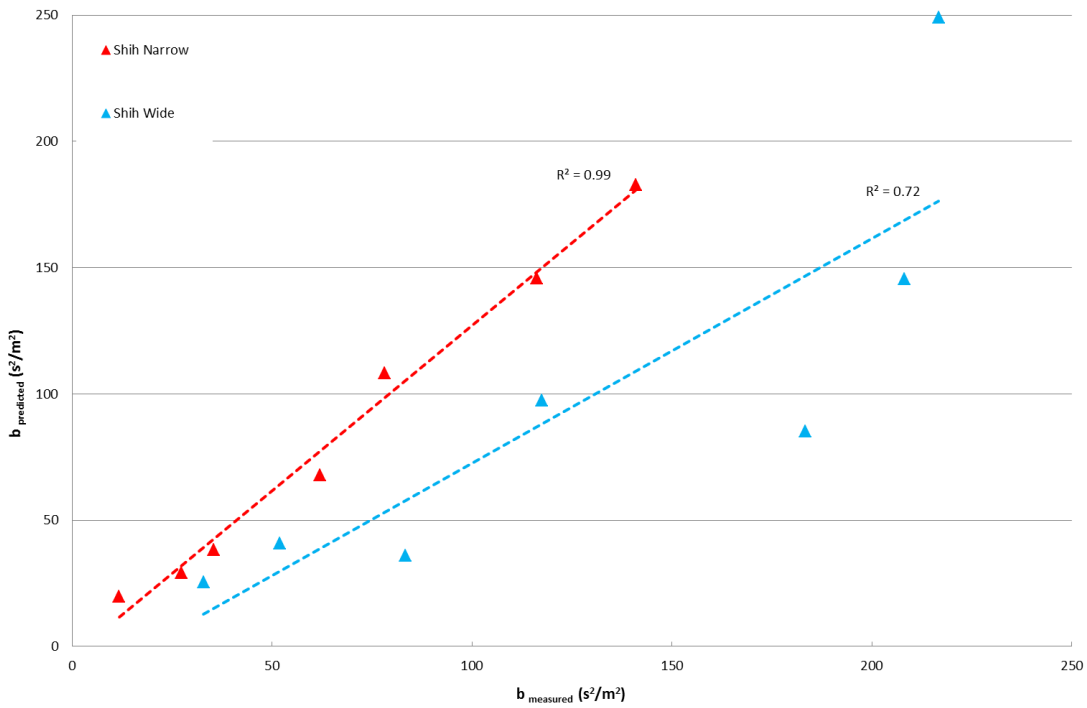

Figure 5.22: As Figure 5.21 for Forchheimer *b* coefficient.

5.5.3. A new suggested formulation for the Forchheimer coefficients

The above results show that none of the experimental formulae reported in the literature, derived from a consideration of the Forchheimer approach, are universally satisfactory for the data presented here, especially for turbulent flow conditions. This is likely attributable to the differences and uniqueness of this dataset and each previous investigation. In particular, there is a considerably wide range of flow conditions and sediment grading characteristics in this current study.

Given this latter point, a new assessment of the coefficient, *a*, which includes the effect of both narrow and wide grading curves is presented. This is derived through regression of the empirically derived laminar flow terms *a* against the porosity term ($(1\text{-}n)^2/n^3$) from this new data set. As previously demonstrated, D_{15} is considered the characteristic diameter influencing the permeability and therefore the flow resistance within the gravel sample. Figure 5.23 indicates a strong linear relationship between these parameters, which is in agreement with those relationships proposed in other studies (Ergun, 1952; Den Adel, 1987 ; Shih, 1990; Van Gent, 1993). Similarly the data set is used to estimate the coefficient β, in the Forchheimer equation from regression of the measured Forchheimer coefficients *b,* versus the porosity term $(1\text{-}n)/n^3D_{15}$, in Figure 5.24. Again, a satisfactorily strong linear relationship is obtained.

Linear regression of the data presented in Figure 5.23 and Figure 5.24, allows the following new expressions for characterising the Forchheimer coefficients *a* and *b*:

$$a = 152 \left(\frac{\nu}{D_{15}^2 g}\right)\frac{(1-n)^2}{n^3} + 0.53 \ \ (s/m) \tag{5.8}$$

$$b = 1.65 \ \frac{(1-n)}{n^3}\ \frac{1}{gD_{15}} \ \ (s^2/m^2) \tag{5.9}$$

where D_{15} is the characteristic sediment diameter (m), ν is the kinematic viscosity of fluid (m^2/s), n is the porosity of the sample and g is gravitational acceleration (m/s^2).

These expressions are mainly functions of D_{15} and implicitly account for the effect of grading size and sediment distribution. These formulations are valid within the following range of porosity $0.37 \leq n \leq 0.45$. A comparison between predicted (Equation (5.8) and (5.9)) and measured

Forchheimer coefficients *a* and *b* is plotted in Figure 5.25 and Figure 5.26. For a good fit, the points should be close to the fitted line (red dotted line); as expected, a good agreement is observed.

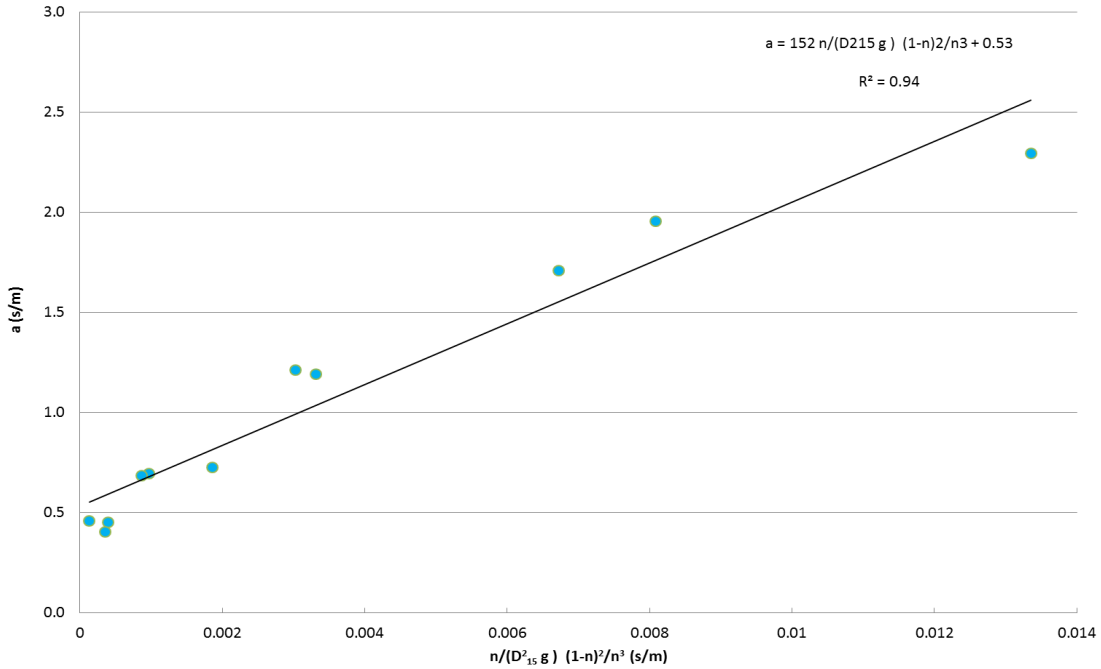

Figure 5.23: Linear regression statistics, comparison between measured Forchheimer coefficient *a* vs size material and porosity factor

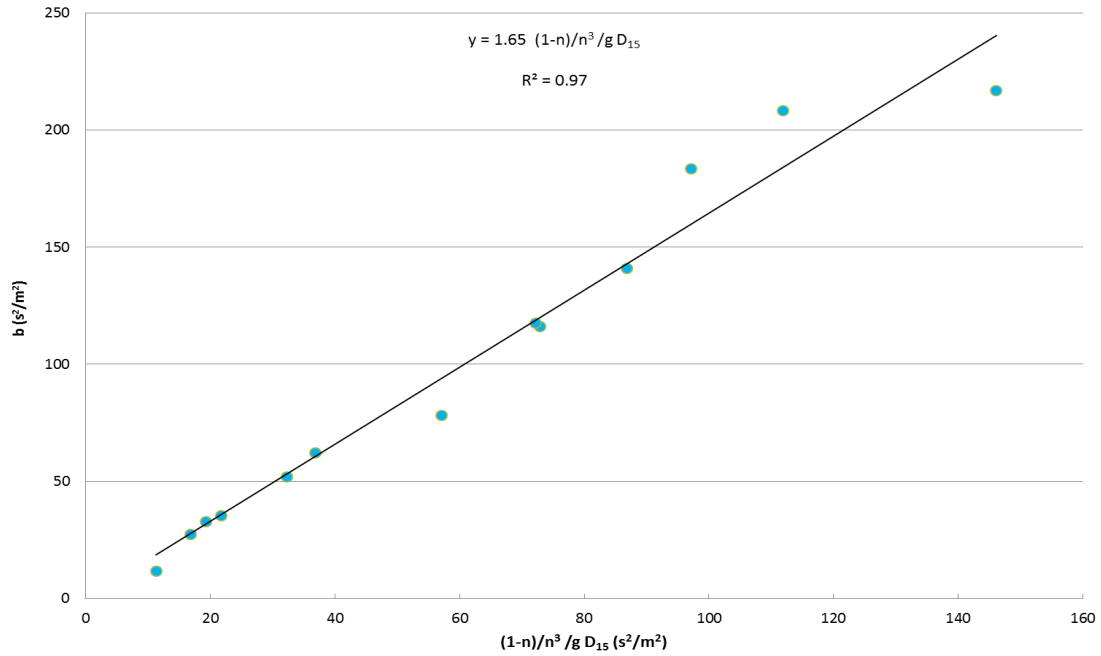

Figure 5.24: Linear regression statistics, comparison between measured Forchheimer coefficient *b* vs size material and porosity factor

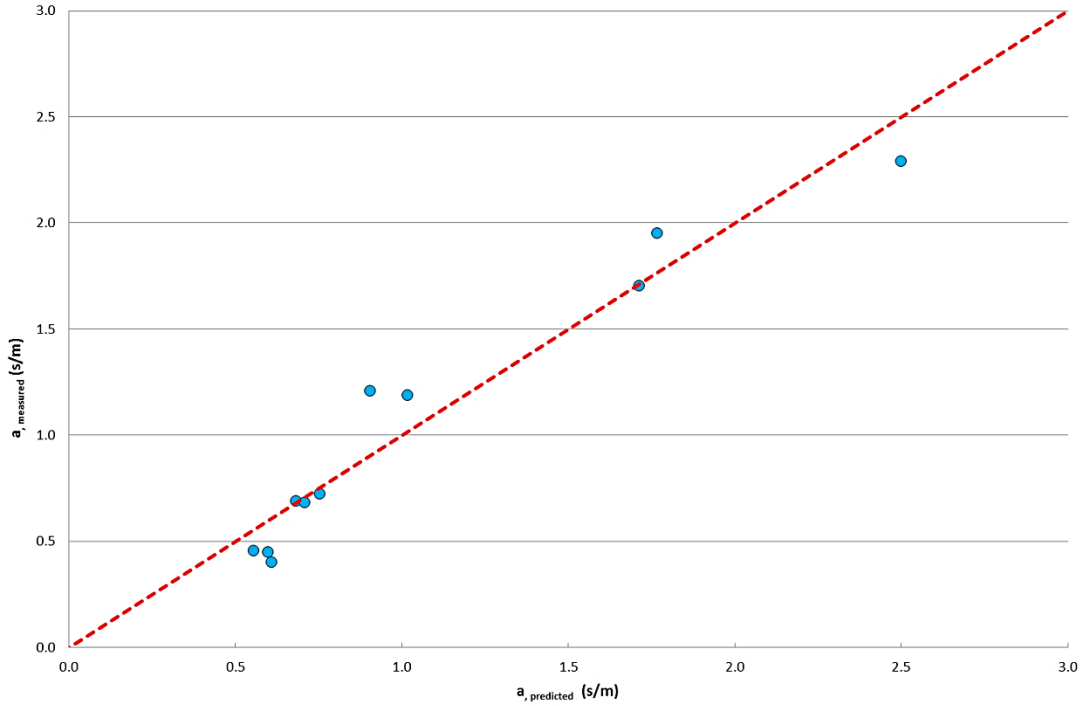

Figure 5.25: Comparison between measured and predicted Forchheimer coefficient *a*

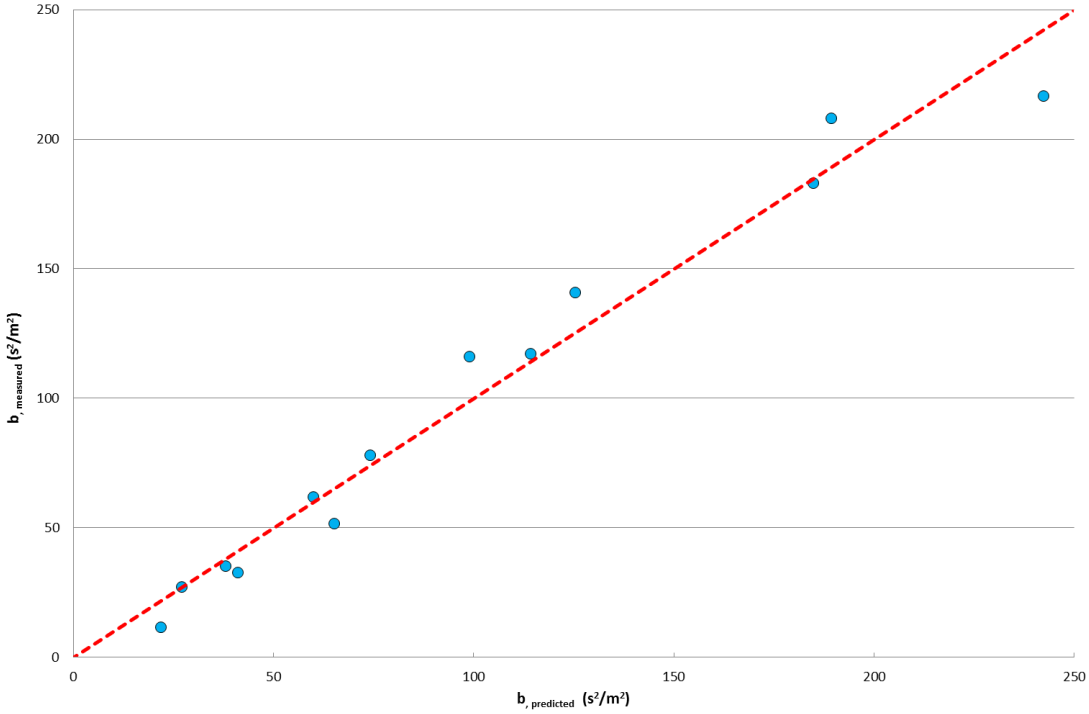

Figure 5.26: Comparison between measured and predicted Forchheimer coefficient *b*

5.6. Discussion

In physical hydraulic modelling of coastal defences, various researchers have considered the importance of the permeability of rubble core material and the effects of permeability on the beach morphological response, especially on the swash zone where the effect of infiltration/exfiltration and groundwater fluctuations may be important for sediment mobility (Burcharth & Christensen, 1991; Horn and Li, 2006; Austin and Masselink, 2006; Masselink and Turner, 2012 and Pintado-Pati *et al*., 2015).

The lack of convergence on the characterisations of porous flow formulae produced between all these studies (Bear, 1972; Burcharth and Christensen, 1991; Van Gent, 1993) indicates that permeability is a complex feature of these materials. As already discussed in Chapter 3, permeability relies on the interaction between the size distribution and particularities of the measurement of shapes and contact structure between the constituent sediment particles.

Darcy's law, which states that a fluid flow rate is directly proportional to the pressure gradient, is shown to be accurate only at low flow velocities. At higher flow rates, Darcy's law is usually replaced by the Forchheimer equation, which includes a term that is quadratic in the flow rate. It is often accepted (Baird *et al.*, 1998; Raubenheimer *et al.*, 1999, Horn, 2006) that the flow through gravel material can be described by using the Forchheimer approximation, which assumes the horizontal flow as the dominant one and neglects the vertical flow. In beaches that are underlain by relatively impermeable material, it is likely that Forchheimer theory provides an adequate description of groundwater flow, and field studies such as those of Baird *et al*. (1998) and Raubenheimer *et al.* (1998) support this assumption.

As previously discussed the Forchheimer equation is characterised by its coefficients (*a* and *b*) with their values based on experimental results. As discussed in Chapter 3, discrepancies between experimental methodologies, scales and sediment sample construction make inter-comparison between these studies rather difficult. Indeed many of these studies (Ergun 1952; Engelund, 1953; Den Adel; 1987), were performed using limited sediment size ranges and without considering the effect of the grading curve on the flow regime.

Numerous analytical solutions and numerical methods are available for the simulation of Darcy flows. Similar tools are also available for the simulation of non-linear inertial flows. Their use, however, requires knowledge of the phenomenological coefficients *a* and *b* of the Forchheimer equation. Thus, in this work, a new programme of tests was designed in order to investigate both the influence of grading of the sediment samples and the dependence of the Forchheimer coefficient values on the flow regimes. The study used a large permeameter under stationary flow conditions with a wide range of both single and mixed size classes of limestone with density equal to 2.7 t/m^3. Groups of samples with comparable D_{50}, D_{15} and D_{85}/D_{15} were tested. The results clearly suggested that the D_{15} parameter dominates the flow/resistance behaviour for all the samples. This is probably due to the relationship between the D_{15} and the opening size of the voids within the sample. The other parameters: D_{50} or D_{85}, have only second order effects on the flow/resistance relationship.

Consequently, it has been shown how new formulae for the Forchheimer coefficients *a* and *b* were conceived in terms of the D_{15} parameter. These show a good characterisation of the experimental data collected for this work. These equations can be applied for a different number of coastal applications, including physical and numerical model studies, used to reproduce the behaviour of the groundwater flow and the percolation throughout porous media characterised by different grain size distributions As the new equations were derived under stationary flow conditions, they are not valid for non-stationary flow, in which an additional external force is required to accelerate the mass of water (Dean and Dalrymple, 1984; den Adel, 1987), as discussed in Section 3.2.

The following Chapter 6 and 7 will show the importance of the flow percolation within the gravel beach and how this phenomenon influences the groundwater elevation and consequently the beach profile response. The effect of the groundwater elevation and wave-induced pore pressure to the beach performance will be discussed in more detail in Chapter 6. These phenomena, groundwater elevation and wave-induced pore pressure within the beach, are influenced by the beach permeability, i.e., grain size distribution (see Chapter 3). The effective porosity and the grain size are considered as fundamental granulometric parameters which express an effect of the forces driving fluid movement through the saturated porous media. In the next chapter it will be shown how, under wave motion, not only D_{15} but also other characteristic grain sizes have a

primary influence on the groundwater elevation and wave-induced pore pressure. Consequently, it will be shown how gravel beaches characterised by different grain size distribution and subject to the same wave conditions, show a different beach profile response.

6. Effect of grain size distribution on gravel beach response

6.1. Introduction

The distribution of grain sizes in gravel beach sediments, directly influences their porosity as already discussed in Chapter 2. This affects the volume of water that percolates into such beaches and, in turn, their overall stability. It is well established that a direct influence between the beach profile and the beach sediment size exists (e.g. McLean and Kirk, 1969). The value of the beach slope is controlled, at least in part, by the volume of water that percolates through the beachface during the uprush phase (Puleo *et al*., 2000; Kikkert, 2013; Pintado-Pati *et al*., 2015). Coarse materials have much greater permeability than, for instance, poorly-sorted fine sand. Therefore over gravel beaches, the return backwash is relatively weaker, which creates an onshore bias in the sediment transport capacity of the broken waves which is balanced by the steeper slopes observed in comparison to those on sandy beaches. Furthermore, the beach sediment sizes also exert a primary control on sediment transport processes and swash zone hydrodynamics (Puleo *et al*., 2000; Kikkert, 2013; Pintado-Pati *et al*., 2015).

It has already been discussed how gravel beaches act as coastal defence elements. These protection systems are, however, subject to erosion due to wave action. Resilient beach nourishment therefore requires adaptive management strategies that build with nature to maintain long-term sustainability. Maintenance costs for these defence structures were estimated in 2001 at £10,300 km/yr for tidal flood defences, £32,300 km/yr for coastal flood defences and £53,700 km/yr for coast protection (DEFRA, 2001). Future climate change is likely to require a further increase in investment in order to mitigate the potential for future losses.

In order to optimise the benefits of these investments, the material has to be carefully chosen and the scheme has to be carefully designed. Parameters that need to be carefully designed include the size grading of the imported gravel and the profile of the resulting beach. For these reasons, in order to increase our confidence in how these features evolve, what the dynamic response is and how the eventual profile will be created, we need to understand how these sediment accumulations respond to waves and water levels. The aim of this chapter will be to improve our understanding of

wave-induced pore pressure within gravel material for a range of sediment sizes, and to elucidate its influence on beach profile dynamics.

6.2. Physical model design

In order to investigate the relationship between wave conditions, sediment characteristics and beach response, an extensive programme of physical model tests was conceived. The programme was carried out in a wave basin at HR Wallingford. For this study a basin was used to allow a number of different sediment sizes and grading materials to be tested simultaneously with the same wave sequences through the sub-division of the facility into three separate, one metre wide flumes (Figure 6.1). A wave generator (composed of 8 single elements) was located at the end of the three flumes, and for each flume two elements were used to reproduce the required sea-states. The red crosses, in Figure 6.1, denote the wave gauge positions which have been used to run a reflection analysis and extract the incident wave condition at the toe of the gravel beach materials. Figure 6.2 shows a cross section of the experimental flume, where the black area represents the model bathymetry (flat bathymetry). As can be seen the actual bathymetry is connected with the floor of the flume by an approach slope. This different in level between actual bathymetry and flume floor was needed to ensure enough water depth in front of the wave generator and allow wave condition to be generated without the risk of breaking. Wave-induced pore pressures were measured using an array of 8 pressure transducers shown in Figure 6.2. The pressure transducers were held in position, as shown in Figure 6.3, to prevent movement and to measure the wave-driven pressures within the gravel beaches. The high performance pressure sensors (see Figure 6.4) are ideally suited for measurements in hydraulic models. They have a welded diaphragm and body manufactured from 316 stainless steel, and the cables have an internal vent tube and strainer wire. The sensing element consists of a micro-machined silicon diaphragm with piezo-resistive strain gauges diffused into the surface. The sensing element is mounted behind a thin diaphragm to produce a rugged assembly. The combined linearity and hysteresis errors are less than 0.25% of full scale range (0-500mbar). The position of the pressure sensors array was decided by combining the prediction results of the beach profile (using the Shingle model, Powell 1990) together with the wave run-up predictions (using Polidoro *et al.* 2013). Following these prediction results, the first pressure sensor (shown in Figure 6.2) was located with an horizontal

offset of 150mm from the point of intersection of the beach slope/still water level. This allowed the pressure sensors to always be covered by the gravel material, even during the re-profile of the beach under wave action. Wave run-up predictions ensured that the pressure sensors remained submerged during wave action to prevent clipping and make spectral estimation possible. The horizontal distances between each pressure sensor was 240 mm, while the vertical distance between the two arrays was 150mm; the lower array was offset with respect to the upper one by 120mm, this was mainly due to construction practicability.

The beaches were placed at an initial slope of 1 in 7, the length of the slope was such that no overtopping could occur, a typical cross-section is shown in Figure 6.2. The flumes were 26 m long and equipped with:

- wave paddles able to generate non-repeating random sea-states to any required spectral form.
- wave gauges for monitoring the required wave conditions and wave reflection
- a 2D bed profiler to measure the beach profile
- a system of 8 pressure sensors used to monitor the wave-induced pore pressure within the beach.

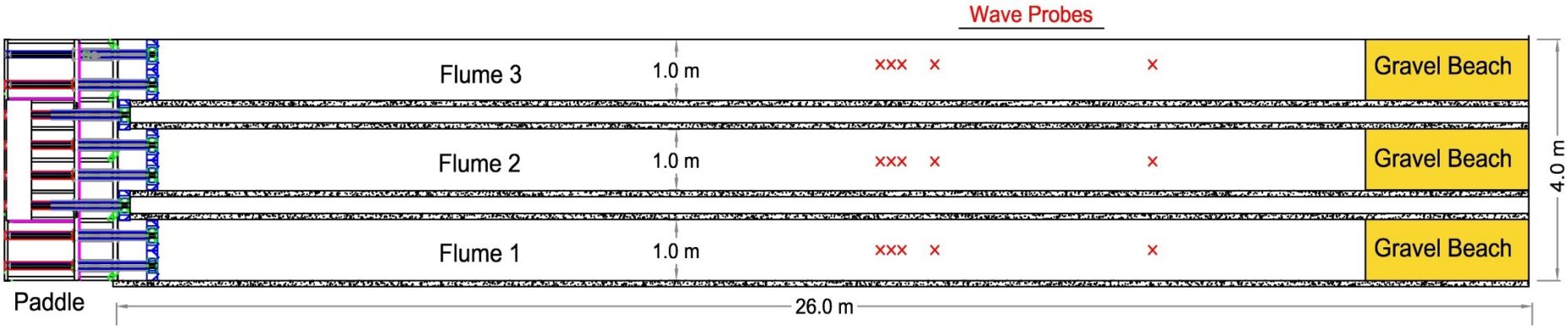

Figure 6.1: Plan view of experimental flumes in basin. Red crosses denote wave gauges

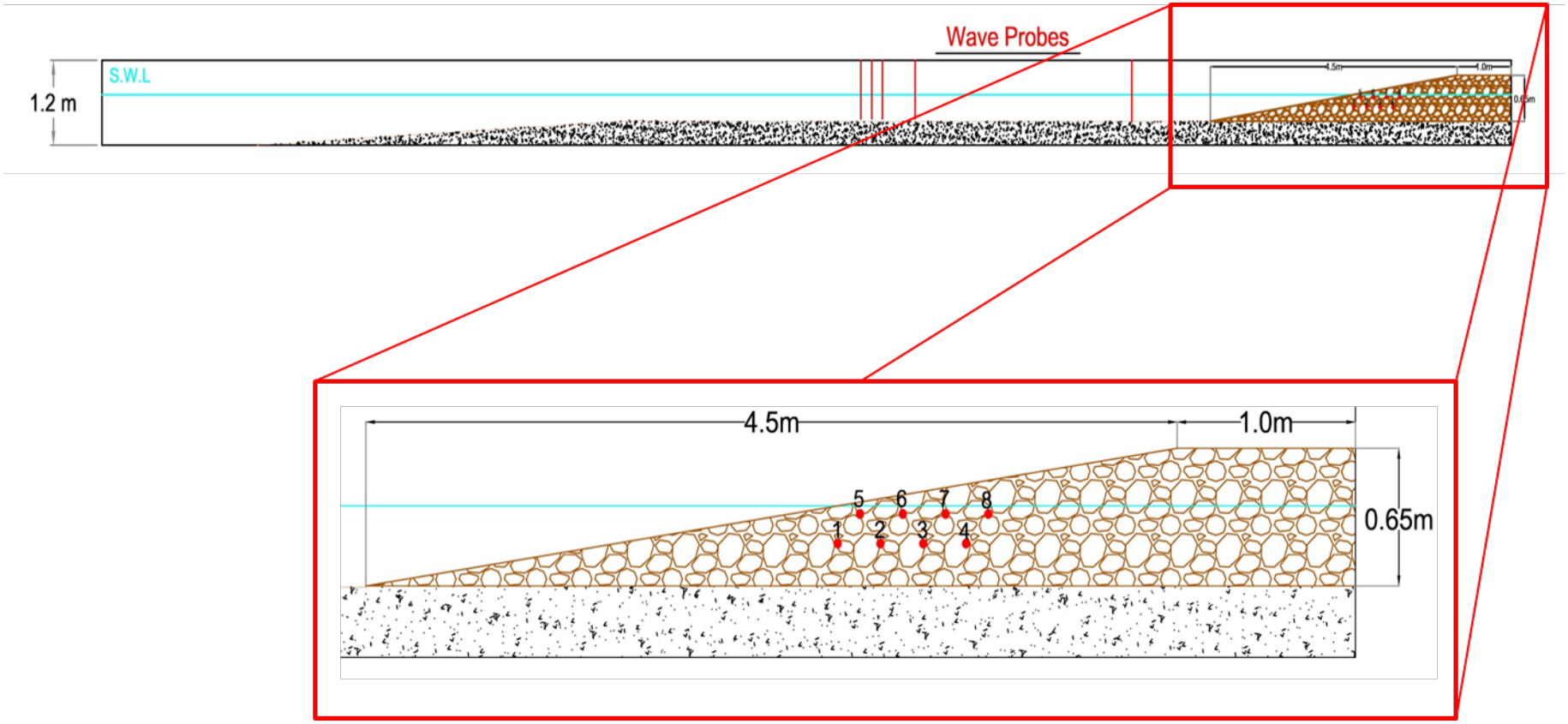

Figure 6.2: Typical tested cross section. Pressure sensors within the tested gravel beach location are represented in red-circles

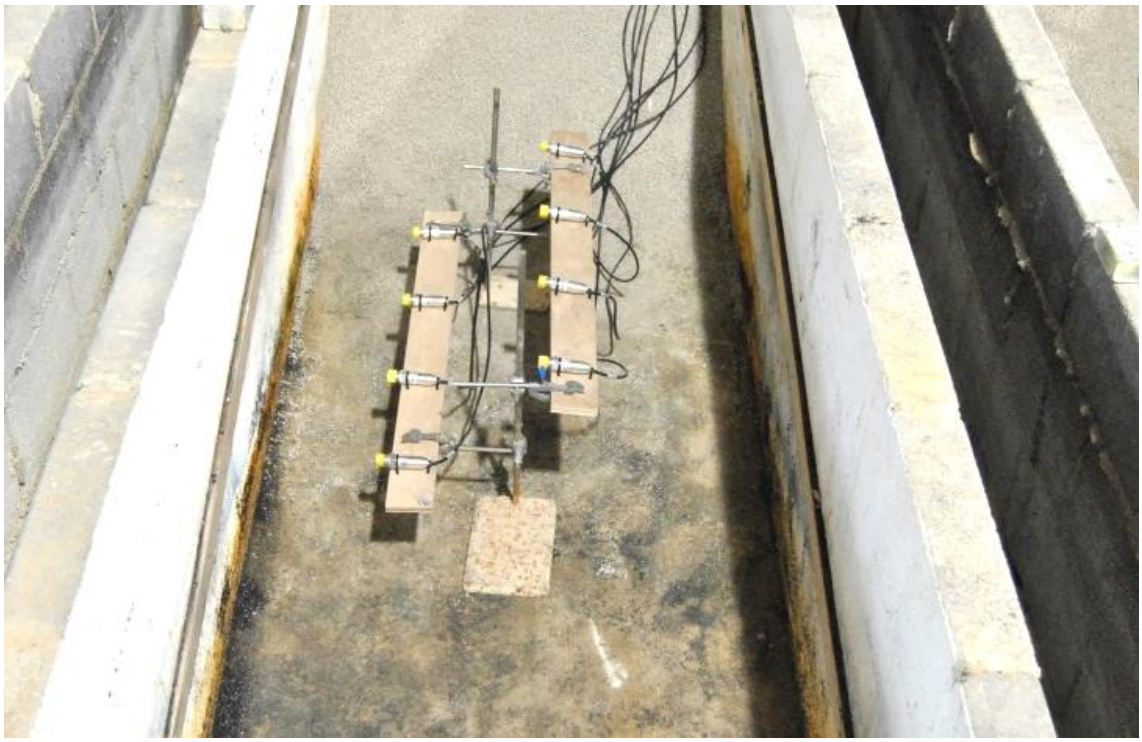

Figure 6.3: Arrangement of pressure sensor array in the central of three flumes prior to burial.

Figure 6.4: Keller high performance pressure sensor - 5m water gauge (range 0-500mbar).

6.2.1. Design of model beaches

For the beach tests, it would have been ideal to have the same grading curves designed for the permeameter tests, using the same limestone density equal to 2.7 t/m^3. However, in practise, the range of grain size used in the model was limited to those that would have been mobilised by the design sea-states, and so smaller grain sizes than the permeameter study were used. Since the aim of this test series was to assess the effect of the grain size distribution, it was decided not to apply any scale criteria (that is to use a scale factor of 1:1), as this would have further reduced the range of distributions that would have been possible to effectively simulate.

In order to ensure that the designed grading curve was obtained, the materials were sieved in sub-divisions and then assembled and mixed in the correct proportions. The sample was then washed to eliminate fine material which could alter the grading and porosity. The wide grading curve sediment mixtures were produced to cover a suitably wide variation of the D_{85}/D_{15} in line with occurrence around the UK. Both narrow and wide graded sediment size distribution curves are plotted in Figure 6.5 and summarised in Table 6.1.

At least one characteristic size diameter (D_{50}, D_{15}, D_{85}/ D_{15}) was repeated across two or more samples to identify, during the analysis, which of the parameters have more influence on the wave-induced pore pressure behaviour. In Table 6.2, the characteristic size diameters, which are similar for the different grading curves, are reported.

The sample N1 (Table 6.1) was only tested to compare the response of a fine gravel beach with a sandy beach under the same wave conditions, as discussed in Section 6.5.2. Both the sample N1 and the sandy beach were tested under the same wave conditions, which differ (less energetic) from the wave conditions used for the other gravel samples. Therefore N1 will not be included in the analysis discussed in the following sections.

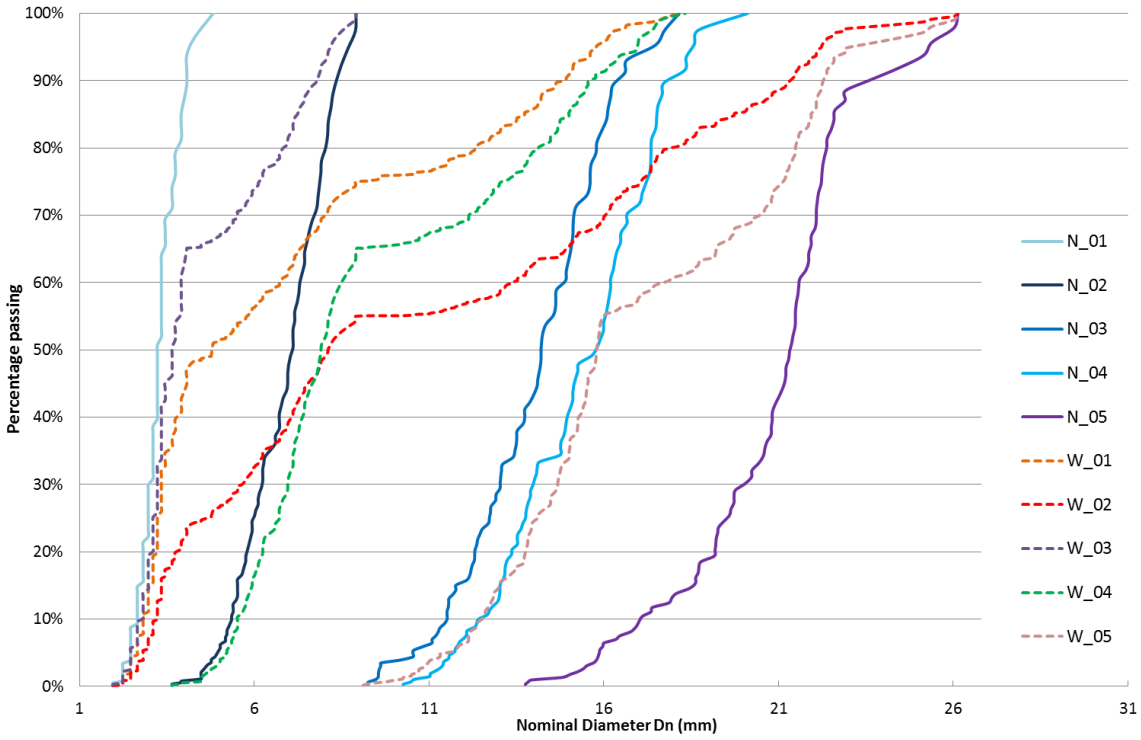

Figure 6.5: Grading curves for narrow and wide graded materials

Table 6.1: Test beach sediment characteristics for narrow graded (N) and wide (W) mixtures

Beach	D_{50} (mm)	D_{10} (mm)	D_{15} (mm)	D_{85} (mm)	D_{85}/D_{15} (-)
N_01	3	3	3	4	1.5
N_02	7	5	6	8	1.5
N_03	14	12	12	16	1.4
N_04	16	12	13	18	1.3
N_05	21	17	19	23	1.2
W_01	5	3	3	14	4.6
W_02	8	3	3	20	5.9
W_03	4	3	3	7	2.4
W_04	8	6	6	15	2.5
W_05	16	13	13	22	1.7

Table 6.2: Test sample sets for intercomparison

Samples	Similarities
N2-W2-W4	D_{50}
N4-W5	D_{50}
N2-W3	D_{85}
N3-N4-W5	D_{15}
N2-W4	D_{15}
W1-W3	D_{50}
N1-W1-W2-W3	D_{15}
N3-W4	D_{85}
W1-W4	D_{85}
N5-W5	D_{85}
N2-N3	D_{85}/D_{15}

During this study the initial beach slope was 1 in 7 (plane sloping beach) for each of the tests; the pre and post-test beach profiles were measured using a 2D bed profiler which extracted the profile elevation every 20mm along the x-axis. The bed profiler was mounted above the central section of the beach, enabling coverage of a 4m long profile across the mobile sediment. The touch-sensitive probe has a proximity switch which allows it to detect the bed with the minimum of contact pressure. The probe is stepped forward and lowered down on the bed; the encoder in the profiler then determines the bed height. This probe is particularly suitable for profiling both below and above the water surface. The bed profiler was used to monitor all tests with an accuracy of ± 1.0mm vertically and horizontally.

6.2.2. Design of wave conditions

For this study only unimodal spectral wave conditions were considered, since the main focus was to investigate the effect of the grain sizes on the beach dynamics / morphological response. This helped to reduce the number of variables and the required number of test wave conditions to nine combinations of three wave heights and wave steepness (Table 6.3) and fixed model water depth (0.4m). A JONSWAP spectrum with a peak enhancement factor γ = 3.3 was used. The wave

conditions in Table 6.3 were selected to reproduce prototype measurements of unimodal wave conditions observed along the south coast of the UK, more details on the criteria used to select the wave conditions used in the physical model study are given in Chapter 7. Surface tension is generally negligible in prototype waves and therefore if the model is not too small (wavelengths must be much greater than 20 mm, wave periods > 0.35 s, water depths > 20 mm), Weber similitude can be neglected, Le Méhauté (1976). Similarly, Hughes (1993), suggests that the viscous effects can be discounted in coastal models for a Re ≥ 10000, where the Re number is defined as follows:

$$Re = \frac{\sqrt{gH_s}D_{50}}{\nu} \tag{6.1}$$

where H_s the significant wave height (m), D_{50} the mean diameter of the beach material (m), g acceleration due to gravity (m/s^2) and ν the kinematic viscosity of water (1.0 x 10^{-6} m^2/s) (m^2/s), For the present study, with a H_s = 0.14m and D_{50} =15mm a Re = 13000, the criteria were therefore satisfied.

Experimental gravel beach profiles evolve very rapidly under wave action, reaching an equilibrium profile after 1000 waves. This is showed in Figure 6.6, where the beach profiles, tested under the same wave condition WC3 (Table 6.3), did not change significantly after 1000 waves and 3000 waves. To be conservative and consistent with the study described in Chapter 7, it was decided to run each wave condition in Table 6.3 consecutively, for 3000 waves duration and for efficiency without resetting the beach, but starting with the least severe condition and increasing up to the most severe.

The experimental observations and results are presented in the following sections and are discussed against the two main goals: firstly the wave-induced pore pressures and the related wave attenuation inside gravel materials as function of sediment size distribution are discussed; secondly the relationship between sediment sizes and beach profile response is reported.

Table 6.3: Wave conditions at constant water depth

Wave Condition	H_{m0} (m)	$T_{p,wind}$ (s)	Steepness
WC -1	0.085	1.2	0.04
WC -2	0.13	1.5	0.04
WC -3	0.14	1.6	0.04
WC -4	0.085	1.4	0.03
WC -5	0.13	1.7	0.03
WC -6	0.14	1.8	0.03
WC -7	0.085	1.6	0.02
WC -8	0.13	1.9	0.02
WC -9	0.14	2.1	0.02

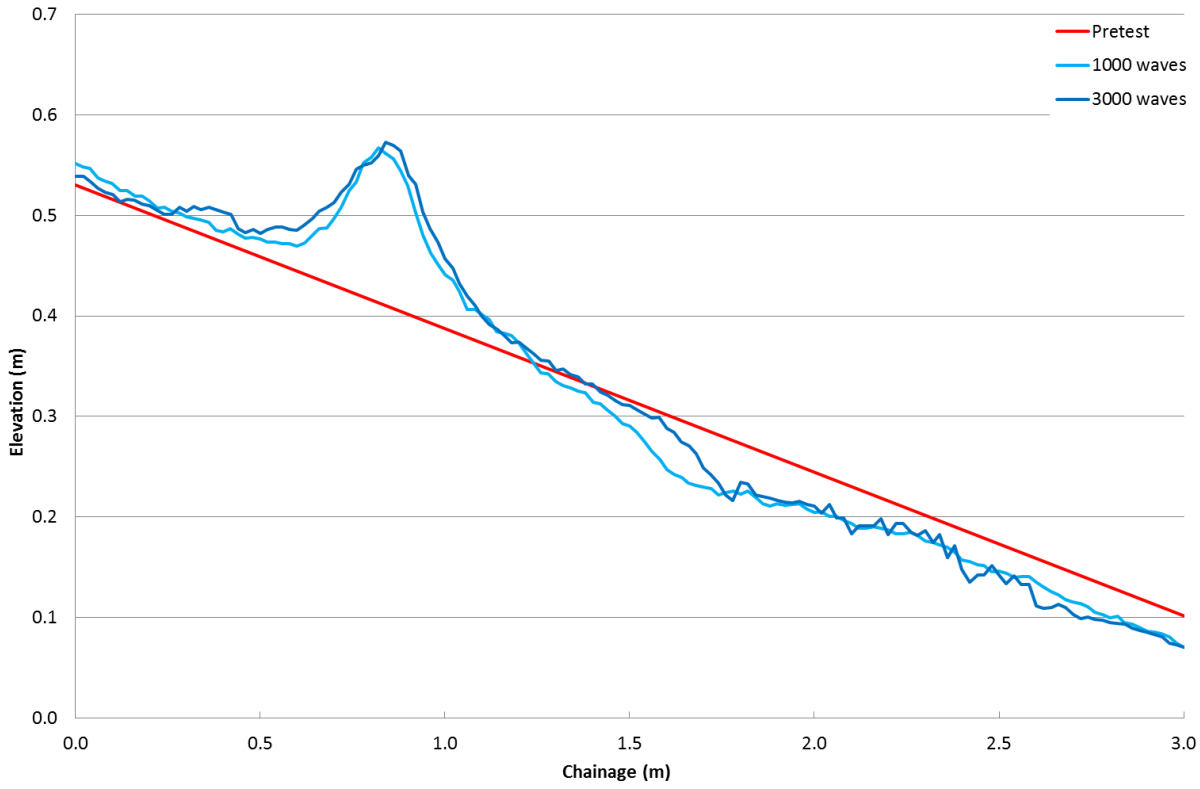

Figure 6.6: Comparison between beach profiles (N_02 gravel material) tested under the same wave condition "WC3" for a duration of 1000 and 3000 waves, indicating the beach is close to equilibrium after 1000 waves

6.3. Methodology for spectral analysis of pore water pressure signals

6.3.1. Introduction

The total excess of the pore pressure caused by the wave motion can be divided into two main parts: a high frequency, e.g., due to wave run-up, and a low frequency internal wave set-up pore pressure components. An increase in water pressure due to infiltration from the nearshore area, e.g., during wave run-up, increases the elevation of the water table. This landward propagation of the wave-induced, high-frequency, pore pressures and their effect on the water table are controlled by the properties of the porous medium - i.e., permeability (Li *et al.*, 2000, 2002). During this study the effect of the tide on the variation of the pore pressure was not investigated and only the pore pressure variation due to wave action was studied. In this section the methodology to measure and analyse the wave-induced pore pressure is described. The general intention was to measure the horizontal attenuation of the wave-induced pore pressure through a gravel beach, and additionally evaluate the beach groundwater response to wave action and its effects on the beach profile evolution.

6.3.2. Spectral analysis of pore water pressure signals

During this study the wave-induced pore pressures were quantified by using the pressure sensors located as shown in Figure 6.2. The horizontal and vertical distances between each pressure sensor were 240 mm and 150mm respectively.

Time series of the wave-induced pore pressures were recorded throughout the test duration (3000 waves). Examples of typical time histories (pressure sensors PT1-PT2, see Figure 6.2) of the wave-induced pore pressures recorded during the test, are plotted in Figure 6.7. As can be seen the pressures measured at individual transducers follow relatively consistent trends. Although, as will be discussed in more details in the following sections, pore pressures showed different values for the different pressure measurement locations and sediment size distribution.

The recorded pore pressure time series were processed with Fast Fourier Transform (FFT) (discussed in Chapter 4) to convert the recorded signal from time domain to a representation in the frequencies domain. The significant pore pressure height P_{m0} is calculated from:

$$P_{m0} = 4\sqrt{m0} \tag{6.2}$$

where m_0 is the moment of order zero:

$$m_0 = \int_{0.5f_p}^{2f_p} \mathrm{S(f)}df \tag{6.3}$$

where $f_p = 1/T_p$ is the peak frequency, S(f) is the energy density spectrum of the pressure time series.

An example of the extracted power spectra of the wave-induced pore pressures measured at different locations within the gravel beach is shown in Figure 6.8. As can be observed, the amplitude of the pressure spectra decreases in the landward direction (from PT1 to PT4). The pressure value extracted from the spectral analysis represents the power of the pressure height (in the frequency domain) at the different locations inside the beach, where the integration corresponds to the significant wave-induced pore pressure height ($P/(\rho_w g)$). This will be discussed in more details in the following section.

As previously discussed and schematised in Figure 6.9, wave-induced pore pressure results from a combination of the action of both high and low frequency waves (black line in Figure 6.9). In order to estimate the variation in pore pressure due to high frequencies (gravity) waves only, the original signal (grey solid line) was first de-trended of any significant drift, and then filetered using a band-pass filter. This allowed to derive the spectral energy corresponding only to the gravity waves (0.25Hz to 1.0Hz). The results of the analysis performed on the gravity wave-induced pore pressure are discussed in the next section.

Conversely, the elevation of the groundwater table (internal wave-setup) was computed as the difference between the initial still water level (SWL) and the mean water level reached during the test, as shown as dashed red line in Figure 6.9. Results for the internal wave set-up are discussed in Section 6.4.5. To avoid the analysis being corrupted by the initial transient behaviour of the pressure build up in the beach, the first 150s of each time history have been excluded from the analysis. A visual check on the time histories confirmed that this assumption allowed removal of any significant transient effect from the analysis.

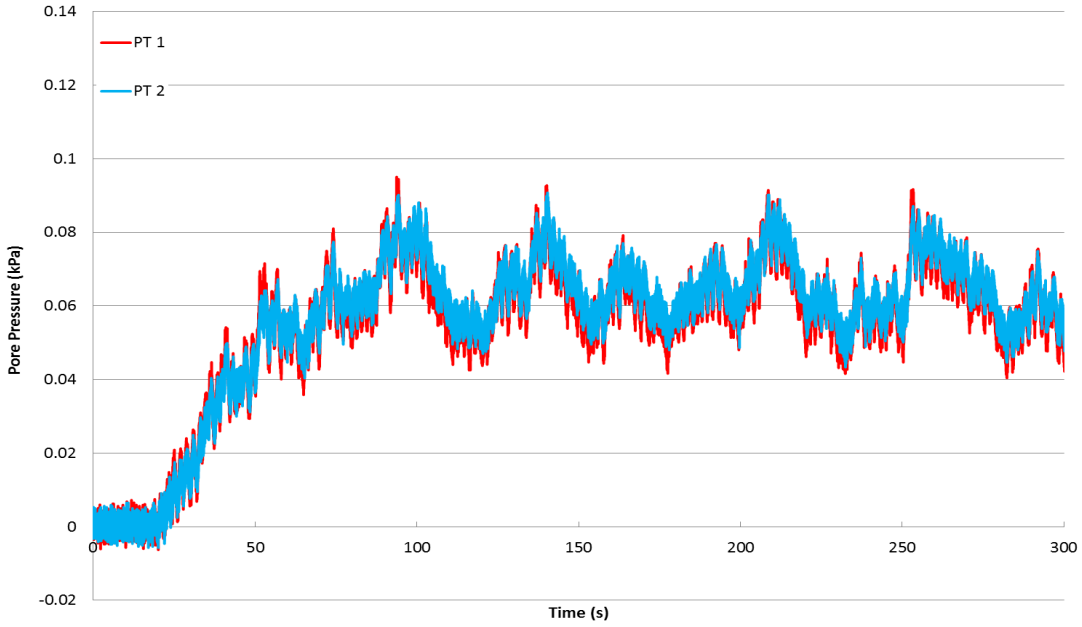

Figure 6.7: Recorded time series of wave-induced pore pressure for pressure transducers PT1 and PT2 for gravel material W3 (D_{15} =3mm and D_{50} =4mm) under wave condition H_{m0} = 0.14m and T_p = 1.6s

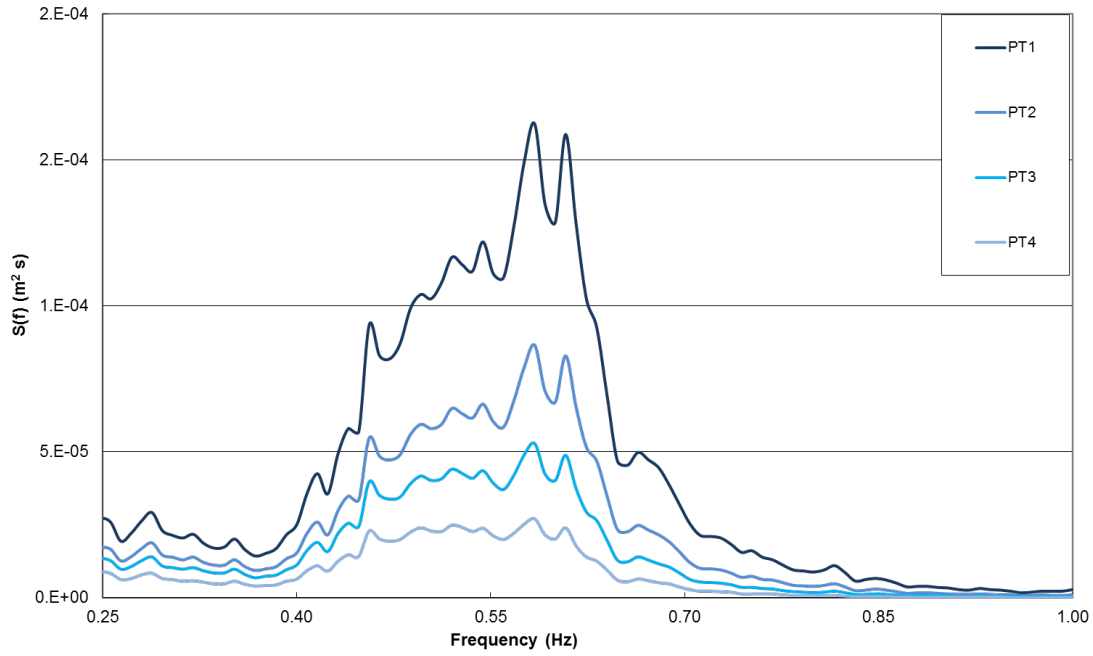

Figure 6.8: Power spectral density of water pressure variations measured simultaneously by pressure transducers PT1–PT4 for gravel material W3 (D_{15} =3mm and D_{50} =4mm) under wave condition H_{m0} = 0.14m and T_p = 1.6s.

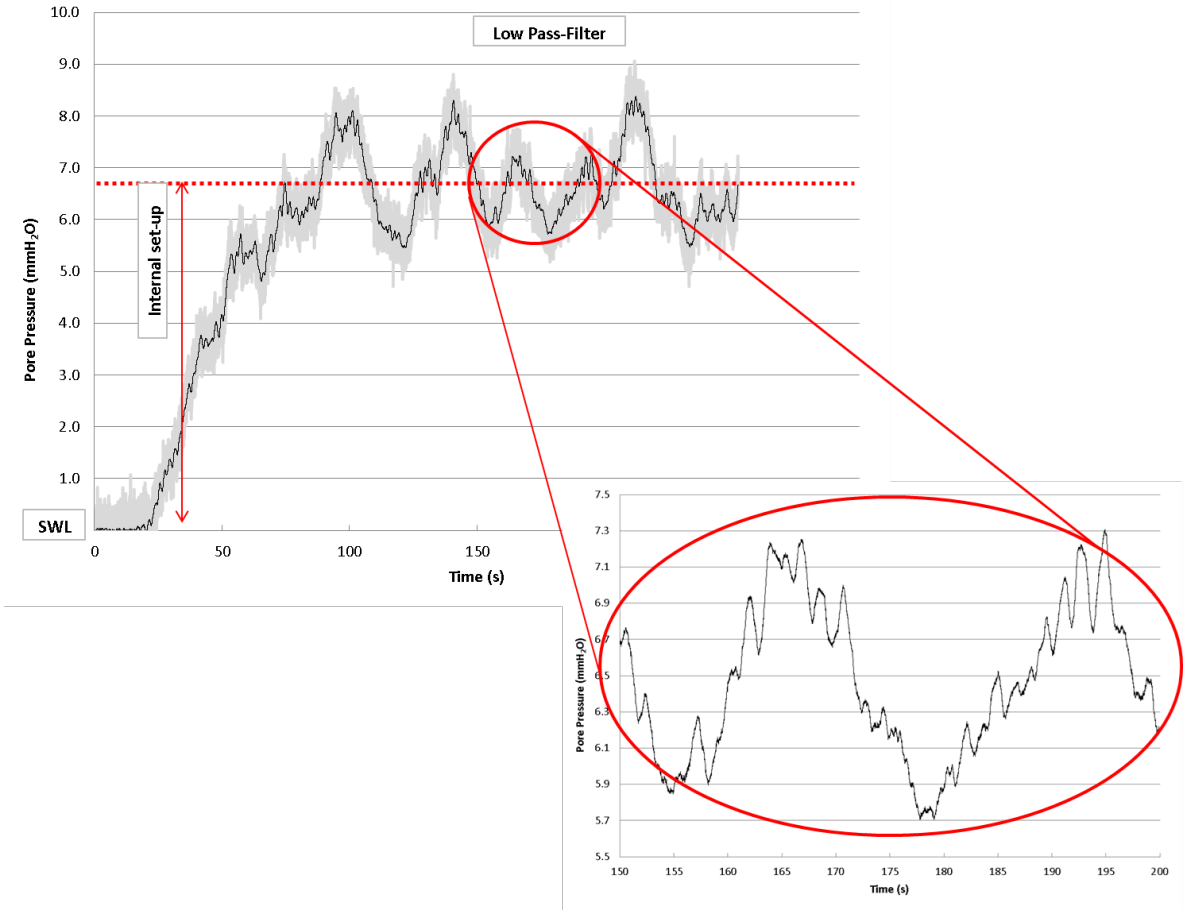

Figure 6.9: Schematisation showing the internal wave set-up (red dotted line), with respect to SWL. In the red circle the fluctuation of the wave-induced pore pressure due to gravity and infragravity waves (black line) is visible. This plot was derived for gravel material W3 (D_{15} =3mm and D_{50} =4mm) under wave condition H_{m0} = 0.14m and T_p = 1.6s.

6.4. Physical model results: wave-induced pore pressure

6.4.1. Introduction

The gravel materials, corresponding to the grading curves plotted in Figure 6.5, were tested under the wave conditions summarised in Table 6.3. Approximately 100 tests were run. It is not possible to present all this information within this section, therefore the most significant results will be presented here to illustrate trends.

As discussed in Chapter 2, only a few research studies have measured wave–induced pore pressure within gravel beaches (Blanco, 2002, Horn and Li, 2006). Additional studies where wave -induced pore pressure was measured are related to rubble mound breakwaters (Hall; 1991,

1994) and are based on small and large physical model experiments (Buerger *et al.*, 1988; Oumeraci and Partenscky, 1990; and Muttray *et al.*,1992, 1995). Very few field measurements are available and these were all conducted at the breakwater at Zeebrugge (Troch *et al.*, 1996, 1998), where the prototype data were analysed and reported by Troch *et al.* (2002). During these studies, all the researchers agreed on the exponential decrease of the pore pressure oscillations in the direction of wave propagation (Hall, 1991; Muttray *et al.*, 1995). Additionally, it was observed that the wave-induced pore pressure and the wave set-up increase with increasing wave height and wave period (Oumeraci and Partenscky, 1990; Hall, 1991) and decrease with increasing permeability of the core material (Hall, 1991). Moreover, the damping rate of the wave induced-pore pressure, increases with wave steepness (Buerger *et al.*, 1988; Troch *et al.*, 1996) and decreases landward (Oumeraci and Partenscky, 1990; Troch *et al.*, 1996). Following all the above observations, Oumeraci and Partenscky (1990) proposed the following expression for the damping of pore pressure oscillations (Burcharth *et al.*, 1999; Troch *et al.*, 2002) within the breakwater core material:

$$P(x) = \mathrm{P_0}\exp(-\delta(z)\frac{2\pi}{L'}\,x) \tag{6.4}$$

where: *P(x)* is the pore pressure height (i.e. the height of wave-induced pressure fluctuations), P_0 ($P_0/\rho g = 0.5\ H_{m0}$) is the pore pressure oscillations at position x =0 (interface underlayer-core), δ is the dimensionless damping coefficient and *L'* is the wavelength inside the structure.

During the present research, in order to quantify the pore-pressure decay within the beaches, the values of the significant wave-induced pore pressures were extracted using the spectral analysis described in the previous section. Figure 6.10 shows a plot of eight typical pore pressures spectral densities, together with the incident wave spectrum. The dotted and solid lines represent, the pore pressures measured by the first (top row) and second pressure-sensors, respectively. The graph is plotted in a semi-logarithmic scale. The blue solid line represents the incident wave spectrum, measured at the toe of the beach. The pressures measured at individual transducers followed a consistent trend within well identified frequency bands (0.25 to 1.0 Hz). Differences in pressure amplitude, due to the horizontal position of the sensors, were observed; as expected the magnitude of the spectra decreases with increasing landward position. During this study it was also observed

that the effect of the material size distribution influenced the pore pressure attenuation inside the beach.

As can be observed when comparing the dotted and solid lines in Figure 6.10, the spectra measured by the sensors on the first array almost overlap with those corresponding to the time histories recorded by the sensors of the second array. This agrees with what was found by other authors (Oumeraci and Partenscky, 1990; Troch, 2000, 2002), i.e., that the pore pressure is independent of depth. However during this study, since only two rows of pressure sensors were used, and the observed variation of pressure with depth was small, this is not sufficient to confirm the independence of the pore pressure from the depth.

The following sections will describe how the wave conditions and in particular how the grain size and grain size distributions affect the wave-induce pore pressure values within the gravel beach.

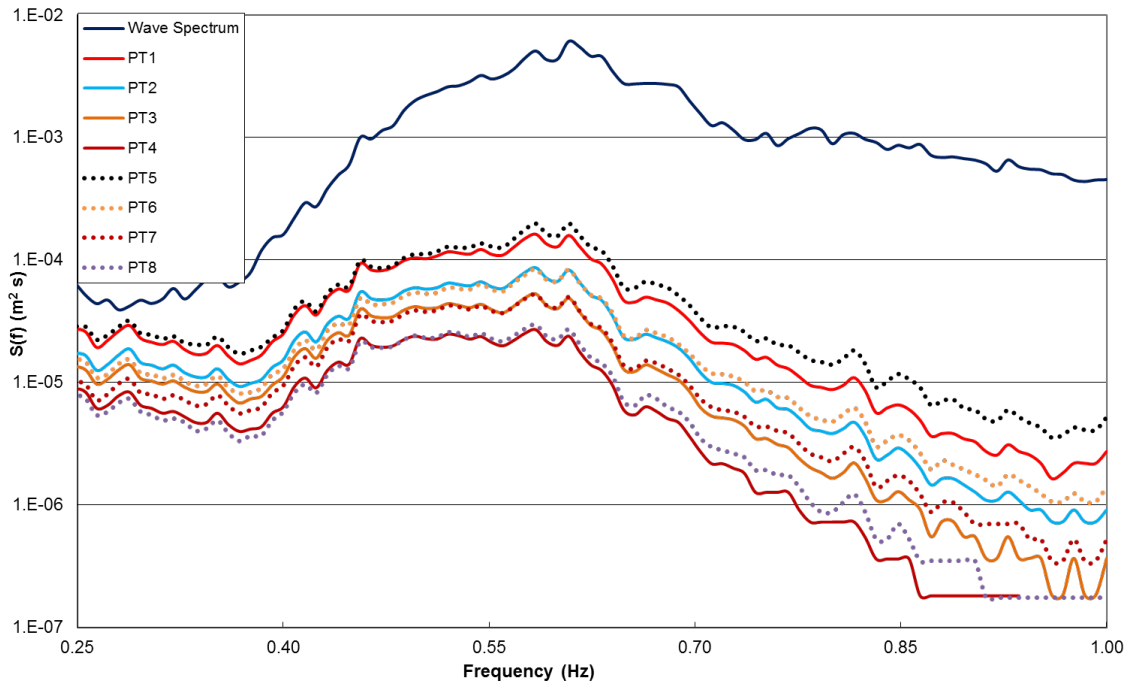

Figure 6.10: Power spectral density of both incident wave height at the beach toe and water pressure variations measured simultaneously by pressure sensors PT1–PT8 for gravel material N5 (D_{15} =19mm and D_{50} =21mm) under wave condition H_{m0} = 0.14m and T_p = 1.6s

6.4.2. Dependence between wave conditions and max pore pressure

As expected, the significant pore pressure height P_{m0} (Equation (6.2)) measured in correspondence with the most seaward pressure sensors (pressure sensors 1 and 5 in Figure 6.2) always showed the maximum recorded values. During this study these maximum values have been indicated as $P_{0,max}$. A relationship between the maximum value of the wave-induced pore pressure head ($P_{0,max}$) and the incident wave heights is shown in Figure 6.11. This plot shows, for the gravel beach material N5 (see Figure 6.5), the linear relationship between the maximum values of the wave-induced pore pressure head ($P_{0,max}$) and the incident wave heights for three different wave steepnesses (s). As expected, the maximum pore pressure increases with increasing incident significant wave height.

Similarly, the maximum pore pressure increases with increasing wave length, which can be observed in Figure 6.12. This shows a linear relationship between the maximum values of the wave-induced pore pressure head ($P_{0,max}$) and the incident wave length (L_{m-10}) is plotted for the materials N5 (D_{10} = 17mm and D_{50} = 21mm), N4 (D_{10} = 12mm and D_{50} = 16mm) and W1 (D_{10} = 3mm and D_{50} = 5mm). The plot is for all the tested wave conditions, and shows that the wave induced pore pressures increase with wave period and that the variation of the fitting slope is due to the different grain size distributions; as described in the next section. This relationship between pore pressures and wave conditions was consistently observed throughout this study for all the differently graded model sediments. This is expected since for the same grain size distribution, that is for the same flow resistance, either larger wave height or longer wave period are capable of transmitting a greater infiltrating volume of water within the beach material, as shown in Figure 6.11 and Figure 6.12.

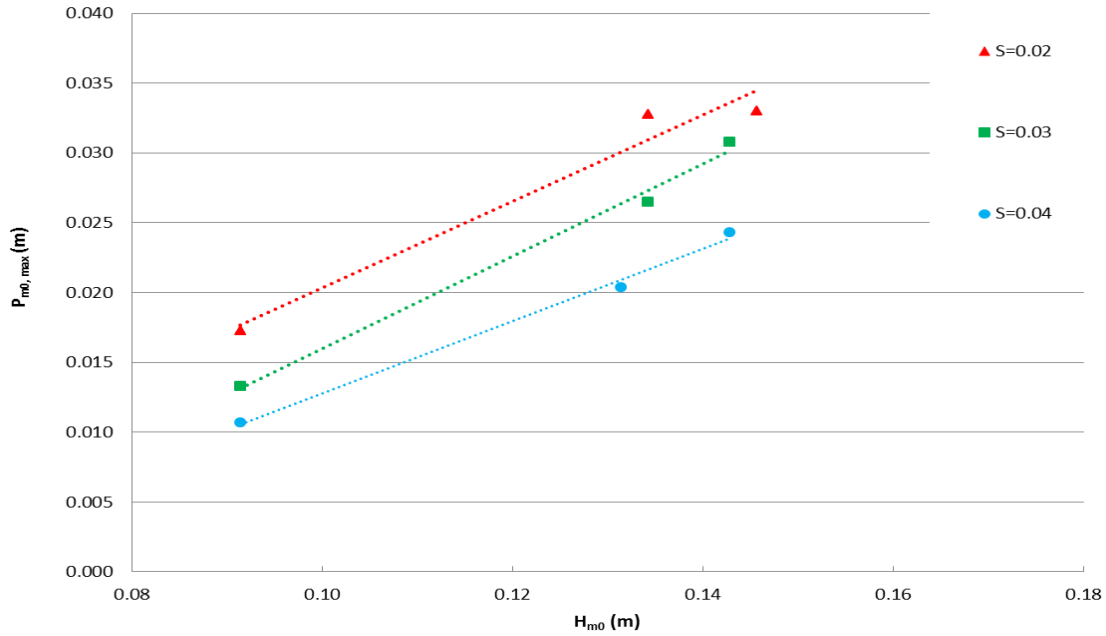

Figure 6.11: Beach Material N5 (D_{15} = 19mm and D_{50} =21 mm), maximum wave-induced pore pressure head as function of the wave height for the three different wave steepness (s).

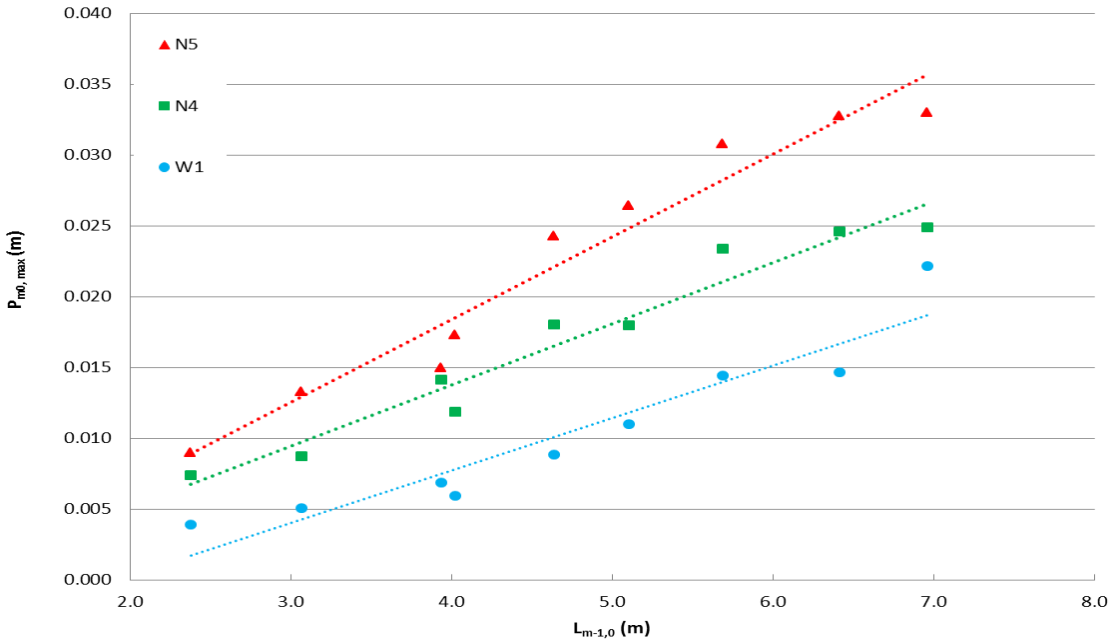

Figure 6.12: Beach Material N5 (D_{15} = 19mm and D_{50} = 21mm), N4 (D_{15} = 13mm and D_{50} = 16mm) and W1 (D_{15} = 3mm and D_{50} = 5mm), maximum wave-induced pore pressure head as function of the wave length for the tested wave conditions

6.4.3. Effect of D_{15} and D_{85}/D_{15} on the wave-induced pore pressure value

Results from the permeameter tests, discussed in Chapter 5, have shown that the particle size D_{15} can be considered as the characteristic diameter having more influence in describing the flow/resistance relationship for both narrow and wide grading curves under stationary flow conditions. In a similar manner to what was observed during the permeameter study, the particle size D_{15} played an important role in the flow/resistance relationship also during these tests. The plot in Figure 6.13 shows the relationship between the maximum values of the wave-induced pore pressure head ($P_{0,max}$) and the characteristic diameter D_{15}, for all the gravel beach materials under the same wave conditions: WC1, WC2 and WC3 (Table 6.3). As can be seen, the maximum pore pressure increases with increasing D_{15}, i.e., with increasing permeability and thus lower porous dissipation. This phenomenon will be explained in more details in the following sections.

Whilst this effect was observed during the simpler tests performed with the permeameter, the observations made during these tests showed slightly different results. Since the present study involved more complex phenomena (e.g., wave motion, fully turbulent flow regime, rearrangement of sediments), results proved that the pore pressure attenuation was not only influenced by the D_{15} but also by other grain size parameters, as shown in Figure 6.14. This plot shows the relationship between the maximum values of the wave-induced pore pressure head ($P_{0,max}$) and the characteristic diameter D_{85}/D_{15}, for all the gravel beach materials under the same wave conditions, WC1, WC2 and WC3 (Table 6.3). This plot suggests that not only D_{15} but also the grain size distribution (D_{85}/D_{15}), plays an important role in the wave-induced pore pressure within the gravel beach.

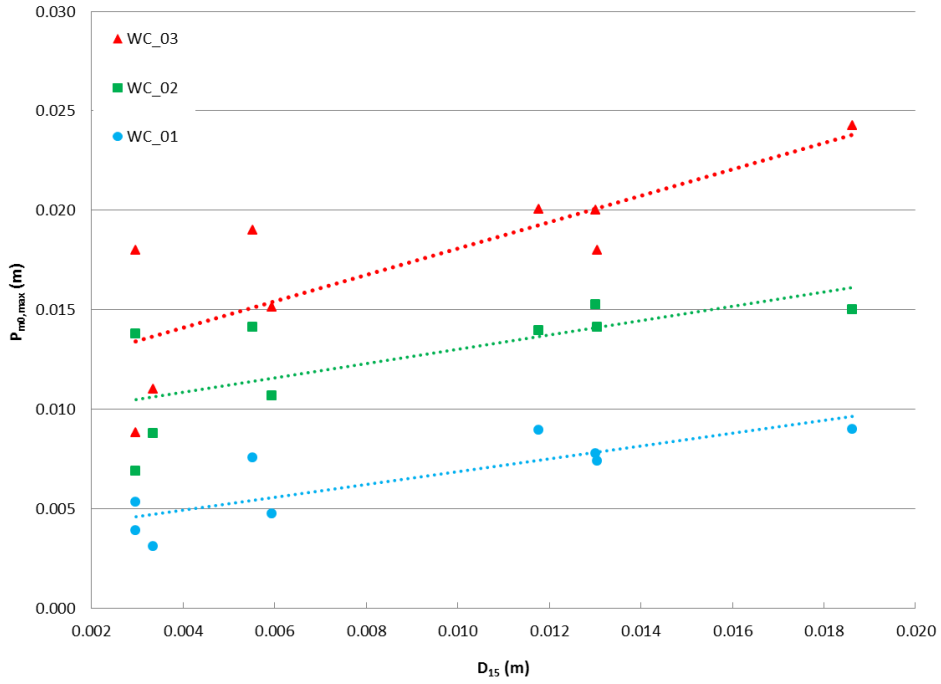

Figure 6.13: Relationship between the maximum values of the wave-induced pore pressure and the characteristic diameter D_{15} for all the gravel beach materials under the wave conditions WC1, WC2 and WC3 reported in Table 6.3.

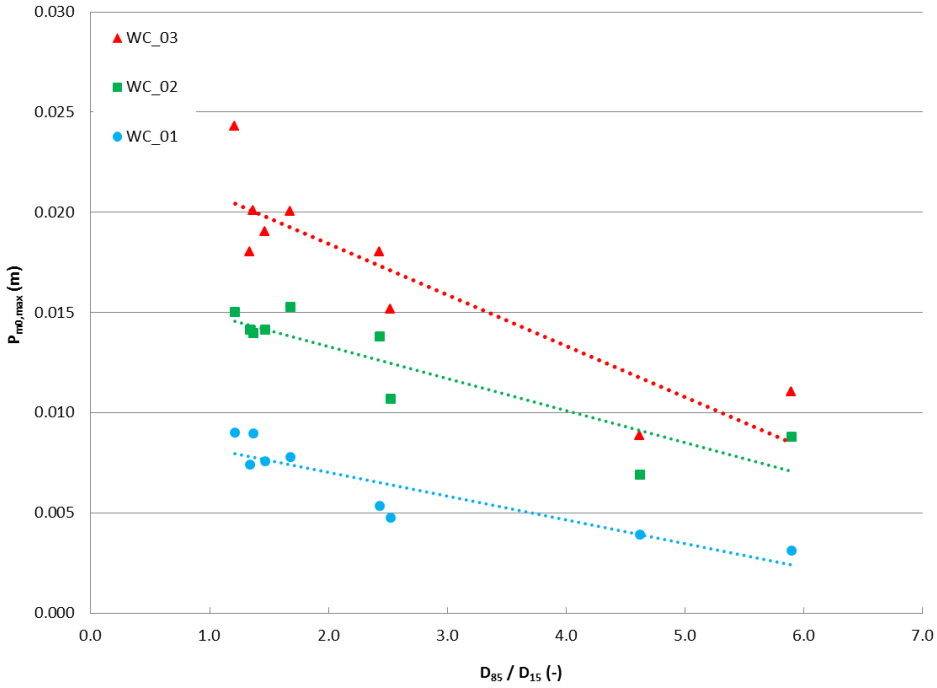

Figure 6.14: Relationship between the maximum values of the wave-induced pore pressure and the characteristic diameter D_{85}/D_{15} for all the gravel beach materials under the wave conditions WC1, WC2 and WC3 reported in Table 6.3.

6.4.4. Wave-induced pore pressure decays

The variation of the wave-induced pore pressure within the gravel beach was examined by using the measurements gathered using the horizontal array of pressure sensors. As expected, results showed that the wave-induced pore pressure, $P_{m,0}$ (m), decreases exponentially landward, and a similar trend was observed throughout all the test conditions. An example of this trend is given in Figure 6.15, showing the wave-induced pore pressure decaying for different materials under the same wave condition (WC3). The first value of the pore pressure head ($P_{0,max}$) is recorded at approximately 0.15m chainage. This is because the first pressure sensor (shown in Figure 6.2) was located with an offset of 0.15m from the point of intersection beach-slope/still water level. This allowed the pressure sensors to be always covered by the gravel material, even during the re-profile of the beach under wave action. It was important to ensure the pressure sensors remained submerged to prevent clipping and make spectral estimation possible. In Figure 6.15, each line represents a different grain size distribution. Although the trend of the pore pressure attenuation is similar for the different grading curves, differences among the values of pore pressures and their damping rates corresponding to different grading curves are clearly visible even during tests performed using the same wave condition. These results clearly suggest that the permeability, i.e., the grain size distribution, plays an important role in how the wave-induced pore pressure decays within the gravel beach. Following these observations, the effect of the grain size distribution on the pore pressure attenuation was further investigated and the results are discussed in the following section.

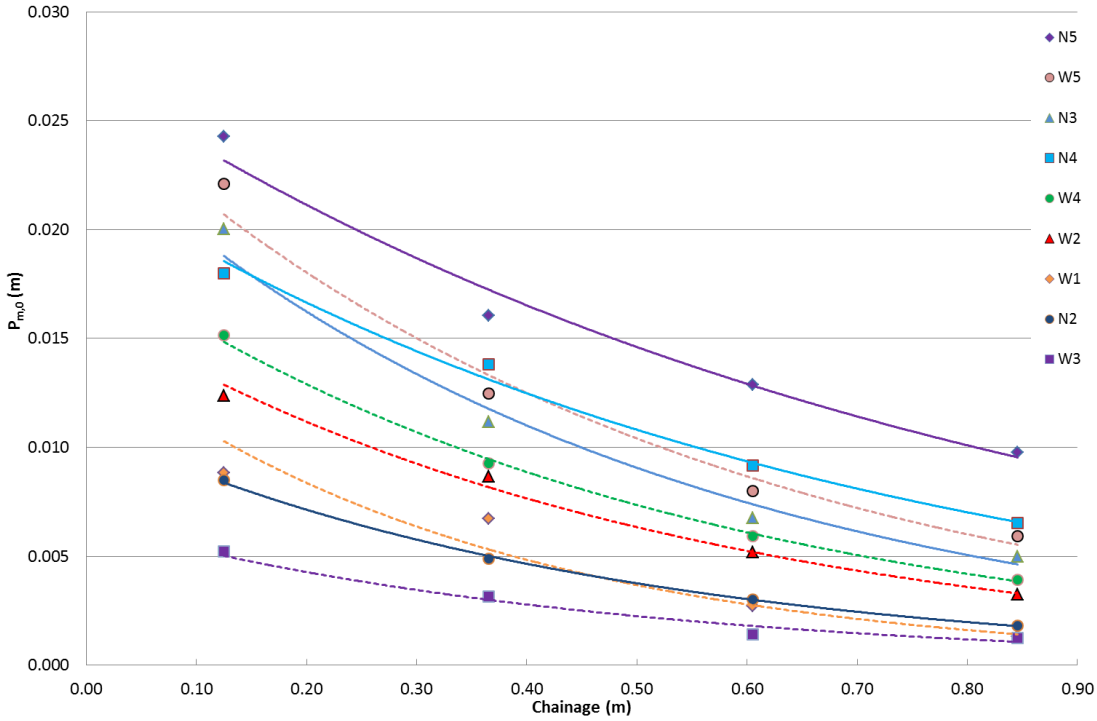

Figure 6.15: Wave-induced pore pressure decay for all the tested gravel beaches under the same wave condition (WC3). Solid lines and dotted lines represent narrow and wide grading curves, respectively

The exponential decrease of the pore pressure in the direction of wave propagation observed during testing, confirmed observations by previous researchers (Hall, 1991; Muttray *et al.*, 1995, Troch *et al.*, 1996; Horn, 2006). As indicated in Section 6.4.2, observations during physical model tests show that wave-induced pore pressures increase with increasing wave height and wave period. In Figure 6.16 the wave induced pore pressure head (P_{m0}) is plotted versus the parameter H_{m0} x/$L_{m-1,0}$ (where H_{mo} is the incident significant wave height recorded at the toe of the beach, *x* is the chainage in the landward direction and $L_{m-1,0}$ is the mean wave length). Data refers to tests performed using the same narrow grading curve (N5, see Figure 6.5) but under different wave conditions (WC-3 and WC-7) having same wave period (T_p = 1.6s) but different wave heights (WC-3: H_{m0} = 0.14m and WC-7: H_{m0} = 0.085m). As expected, wave-induced pore pressures relative to the wave condition WC-3 are higher than the wave-induced pore pressures measured during wave condition WC-7, confirming that pore pressure increases with increasing wave height, as previously shown in Figure 6.11.

Based on the above observations the following expression is proposed to interpret the variation of damping of pore pressure inside the beach, as shown in Figure 6.15. Data are presented in a non-dimensional form, aiming at generalising the observations previously made:

$$\frac{P_{m0}(x)}{H_{m0,toe}} = \mathrm{C1}\,\exp\left(-C2\,\frac{x}{L_{m-1,0}}\right) \tag{6.5}$$

where C1 and C2 are empirical coefficients, which affect both the elevation and the slope of the trends observed in Figure 6.16 and Figure 6.12. These coefficients are functions of the grain size distribution, as discussed below. It is worth emphasizing, that the wave-induced pore pressure decay was fitted by using several forms of curve (linear, polynomial, exponential and power) and the exponential form resulted to be the most consistent across the range of test parameters.

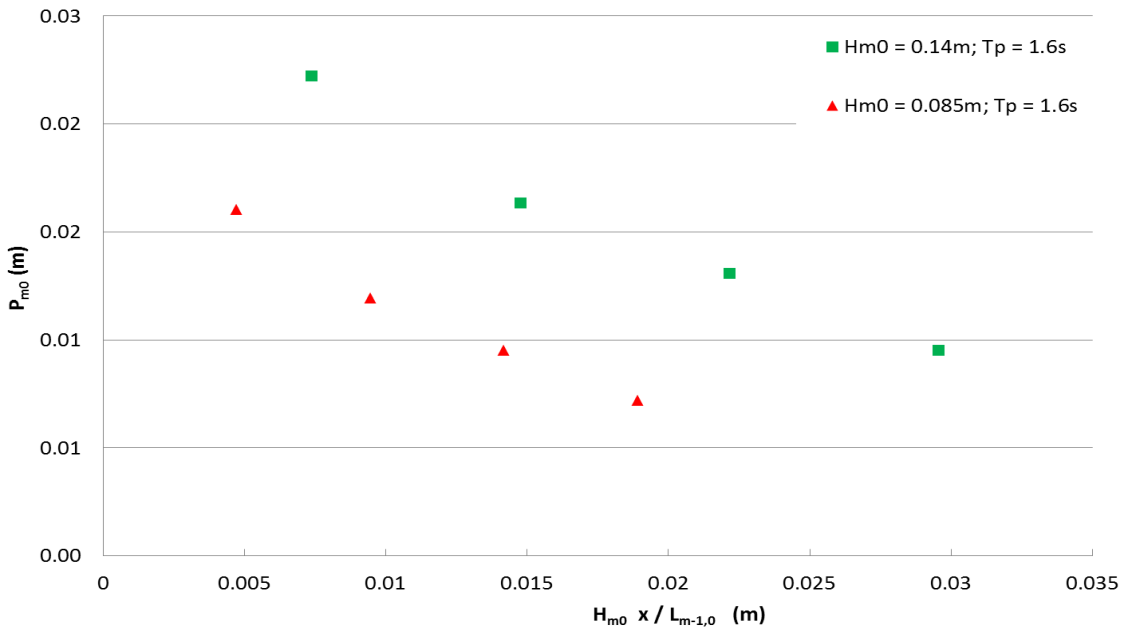

Figure 6.16: Wave-induced pore pressure recorded for the same narrow grading curve N5 (D_{10} = 17mm and D_{50} = 21mm) under wave conditions WC-3 (H_{m0} = 0.14m and T_p = 1.6s, green rectangles) and WC-7 (H_{m0} = 0.085m and T_p = 1.6s, red triangles), having same wave period but different wave height

Results from the permeameter tests described in Chapter 5, clearly suggest that the particle size D_{15} is the characteristic dimension having more influence in describing the flow/resistance relationship for both narrow and wide grading curves. To shed more light on the effect of both the

particle size and the sediment distribution on the flow resistance, we compared observations made during tests performed with similar grading parameters (e.g., $D_{50,}$ D_{15} and D_{85}/ D_{15}).

The variation of wave-induced pore pressures corresponding to the narrow grading curves N2-N3-N5 (see Figure 6.5) are compared in Figure 6.17, where the dotted lines represent the regression lines. For each regression line the relative equation is reported in the coloured rectangle, where the coefficients C1 and C2 (see Equation (6.5)) influence the elevation and the slope of the trends, respectively.

This plot shows that smaller D_{15} (N2) correspond to smaller wave-induced pore pressures and a higher damping rate, smaller and higher values of the coefficients C1 and C2, respectively. This phenomenon is particularly visible in the first part of the graph with the blue circles corresponding to N2 decaying more rapidly suggesting that smaller grain size materials result in higher wave-induced pore pressure head dissipation. Similarly, the variation of wave-induced pore pressures corresponding to the wide grading curves W1-W2-W3 having similar D_{15} (see Table 6.2), but a different D_{85}/D_{15} ratio is compared in Figure 6.18. The grading curve W1 and W2 show very similar behaviours (similar value of C1 ~ 0.09, see Equation (6.5)), while W3 (having a smaller D_{85} and therefore a smaller D_{85}/D_{15} ratio) show higher values of pore pressure and a milder damping rate (higher value of C1 = 0.11 but smaller value of C2 = 7.5 see Equation (6.5)). Comparing the behaviour of these grading curves suggests that although the characteristic diameter D_{15} has an important role in flow/resistance relationship (Figure 6.17), further insights on the pressure decay can be obtained taking into account of the effect of the D_{85}/D_{15} ratio and in particular that the overall steepness of the decay of the wave-induced non-dimensional pore pressure heads is more rapid for higher values of the D_{85}/D_{15} ratio, which is an indication of the grading width. This is further confirmed by comparing the behaviour of the grading curves N2-W4-W2 in Figure 6.19, where N2 has the smaller ratio D_{85}/D_{15}, and W2 has the smaller D_{15} and the bigger D_{85} (hence larger D_{85}/D_{15} ratio). Wave-induced non-dimensional pore pressure heads corresponding to smaller D_{85}/D_{15} ratio (N2) in Figure 6.19 are always above and more gently decaying (higher value of C1 = 0.12 but smaller value of C2 = 7.1 see Equation (6.5) than those corresponding to larger D_{85}/D_{15} ratio (W4 and W2).

The relative importance of the D_{85}/D_{15} ratio is further confirmed in Figure 6.20, in which non-dimensional pore pressure heads corresponding to grading curves having similar D_{85} (W1-W4) are plotted together. In this case, the effect of the D_{15}, which is smaller for W1 (and would therefore result in smaller pressure heads for W1), is overwhelmed by that of the D_{85}/D_{15} ratio, which is in turn larger in W1, resulting in larger pressure heads and steeper damping rate than for W4.

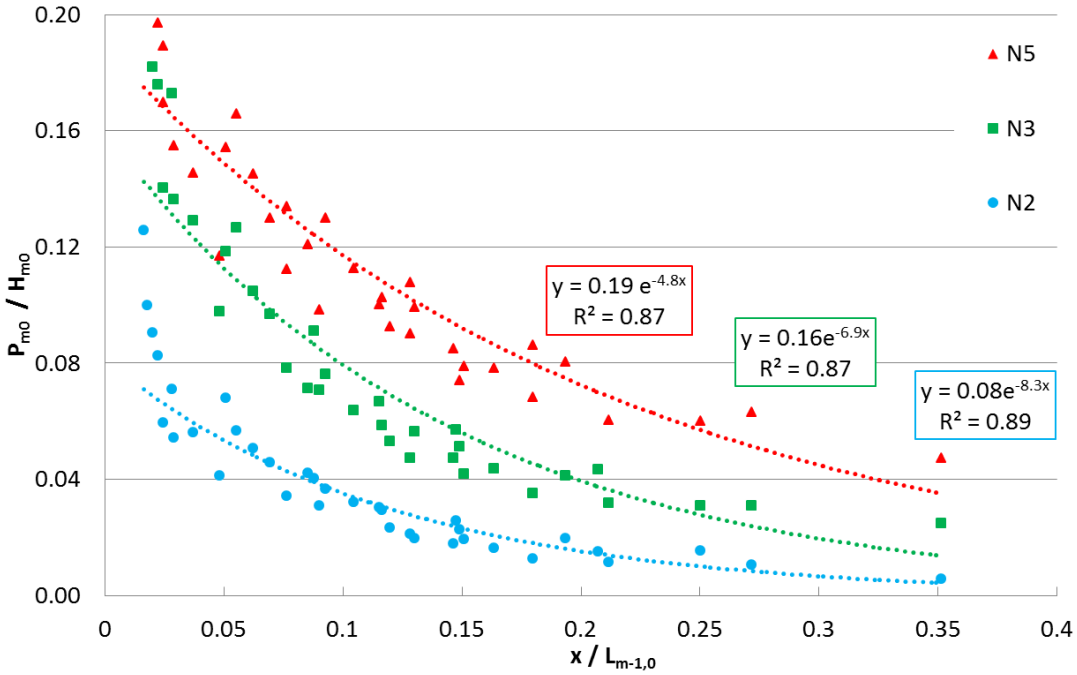

Figure 6.17: Wave-induced pore pressure decay for grading curves N2 (D_{15} = 6mm and D_{50} = 7mm), N3 (D_{15} = 12mm and D_{50} = 14mm) and N5 (D_{15} = 19mm and D_{50} = 21mm) under all tested wave conditions (see Table 6.3)

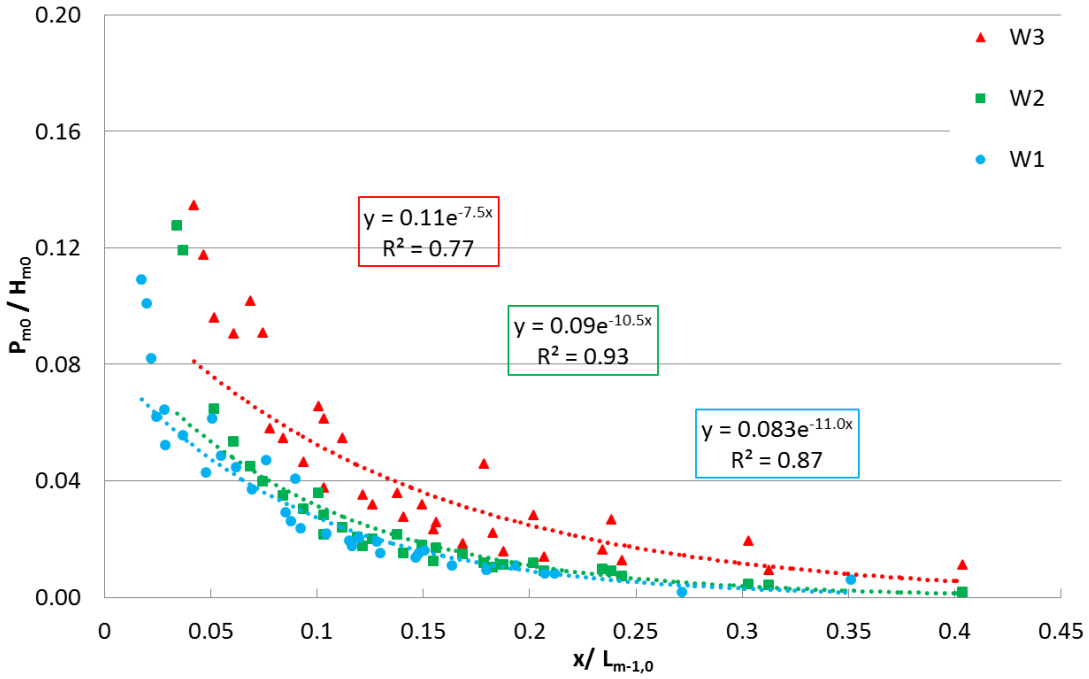

Figure 6.18: Wave-induced pore pressure decay for grading curves W1 (D_{15} = 3mm, D_{50} = 5mm and D_{85}/D_{15} = 4.6), W2 (D_{15} = 3mm, D_{50} = 8mm and D_{85}/D_{15} = 5.9) and W3 (D_{15} = 3mm, D_{50} = 4mm and D_{85}/D_{15} = 2.4), under all tested wave conditions (see Table 6.3)

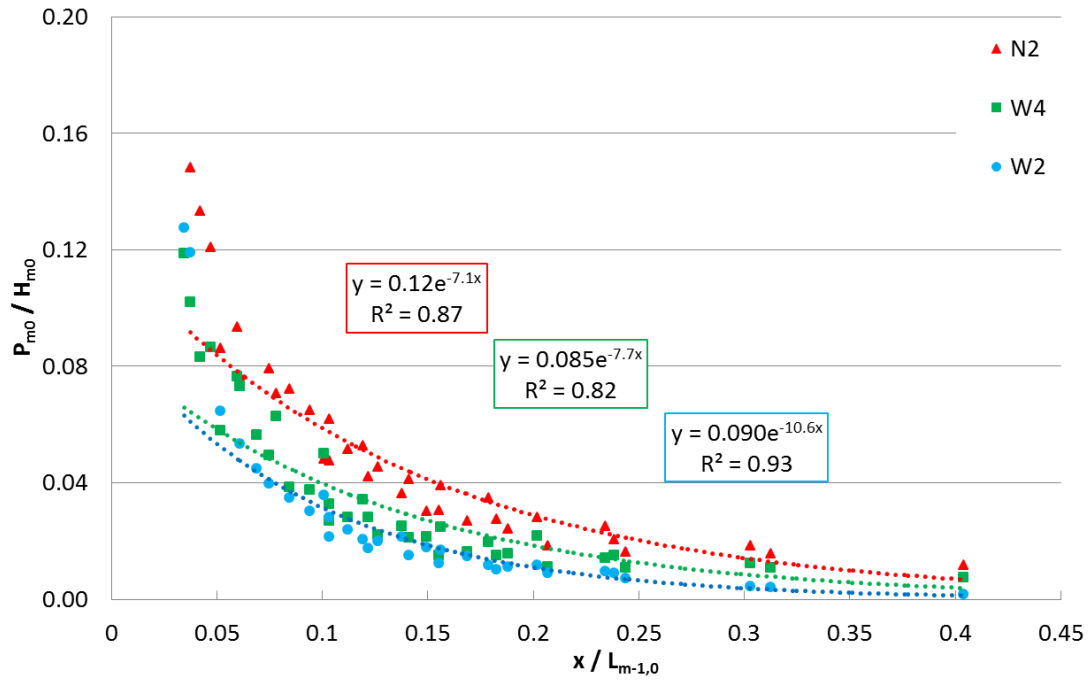

Figure 6.19: Wave-induced pore pressure decay for grading curves W4 (D_{15} = 6mm, D_{50} = 8mm and D_{85}/D_{15} = 2.5), W2 (D_{15} = 3mm, D_{50} = 8mm and D_{85}/D_{15} = 5.9) and N2 (D_{15} = 6mm, D_{50} = 7mm and D_{85}/D_{15} = 1.5) under all tested wave conditions (see Table 6.3)

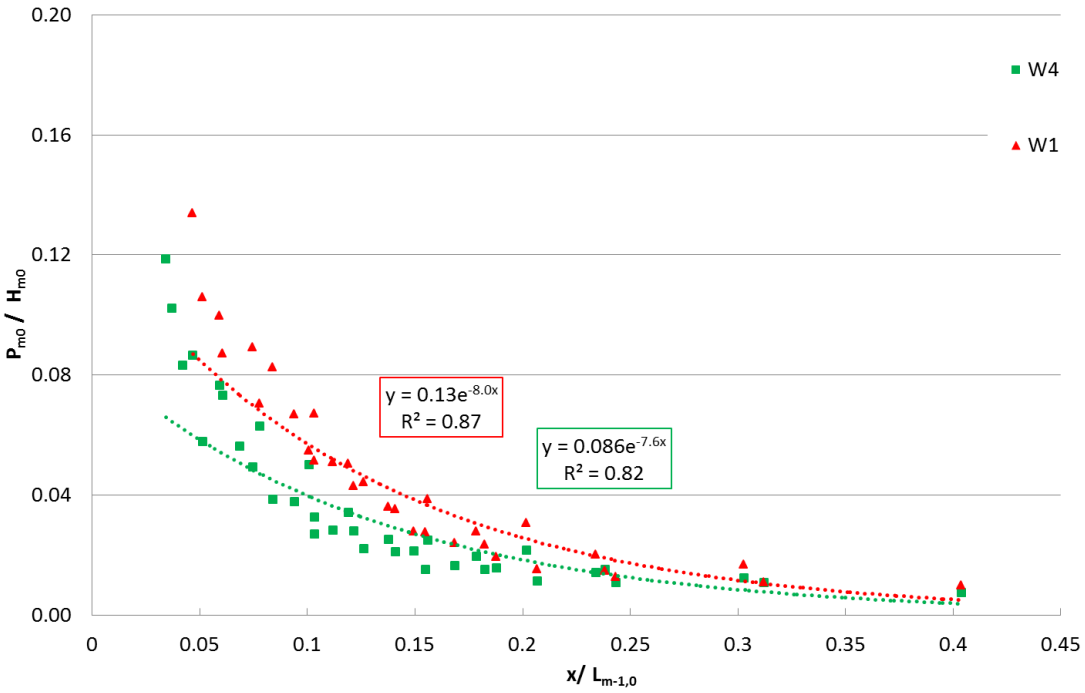

Figure 6.20: Wave-induced pore pressure decay for grading curves W1 W1 (D_{15} = 3mm, D_{85} = 14mm and D_{85}/D_{15} = 4.6) and W4 (D_{15} = 6mm, D_{85} = 15mm and D_{85}/D_{15} = 2.5)under all tested wave conditions (see Table 6.3)

Following the results discussed above, the coefficients C1 and C2 of Equation (6.5) were derived for each of the grading curves and plotted versus D_{15}/D_{85}. The linear relationships of these two coefficients with the steepness of the grading curves are plotted in Figure 6.21 and Figure 6.22 and obey equations:

$$C1 = 0.16\ \frac{D_{15}}{D_{85}} + 0.1 \tag{6.6}$$

and

$$C2 = \ 5.4\ \frac{D_{15}}{D_{85}} - 10.0 \tag{6.7}$$

Following these results, Equation (6.5) which represents the damping of wave-induced pore pressure, can be rewritten as follow:

$$\frac{P_{m0}}{H_{m0,toe}} = (0.16\ \frac{D_{15}}{D_{85}} + 0.1)\ \exp\left[\left(5.4\ \frac{D_{15}}{D_{85}} - 10.0\right)\ \frac{x}{L_{m-1,0}}\right] \tag{6.8}$$

where P_{m0} is the wave-induced pore pressure head for a given location *x* within the gravel beach; D_{15} and D_{85} are the diameters of stone that exceed the 15% and 85% value of the sieve curve, respectively; H_{m0} is the incident significant spectral wave height measured at the toe of the beach and $L_{m-1,0}$ is the wave length measured at the toe of the beach, based on the spectral period $T_{m-1,0}$. The above equation is valid for the following range:

- $3.0mm < D_{50} < 20mm$
- $1.2 < D_{85} / D_{15} < 5.9$
- $0.02 <$ s (wave steepness) < 0.04

A comparison between predicted (Equation. (6.8)) and measured wave-induced pore pressure heads along the horizontal array, for all grading curves and tested wave conditions, is given in Figure 6.23, showing very good agreement between predicted and measured values. This plot shows that for the highest values of wave-induced pore pressure heads (closer to the seaward side) the proposed equation under-predicts the measured values of approximately 20%. The flow through granular material is also influenced by the grain shape (sphericity, roundness and roughness). The grain shape affects the packing, i.e., the arrangement of grains. Variability in the grain shape can therefore prevent grains from reaching their closest possible packing arrangement, which has an impact on permeability and therefore on the flow/resistance relationship. The scatter observed in Figure 6.23, could be explained by the fact that these aspects of the granular samples were not investigated and considered in the above equations.

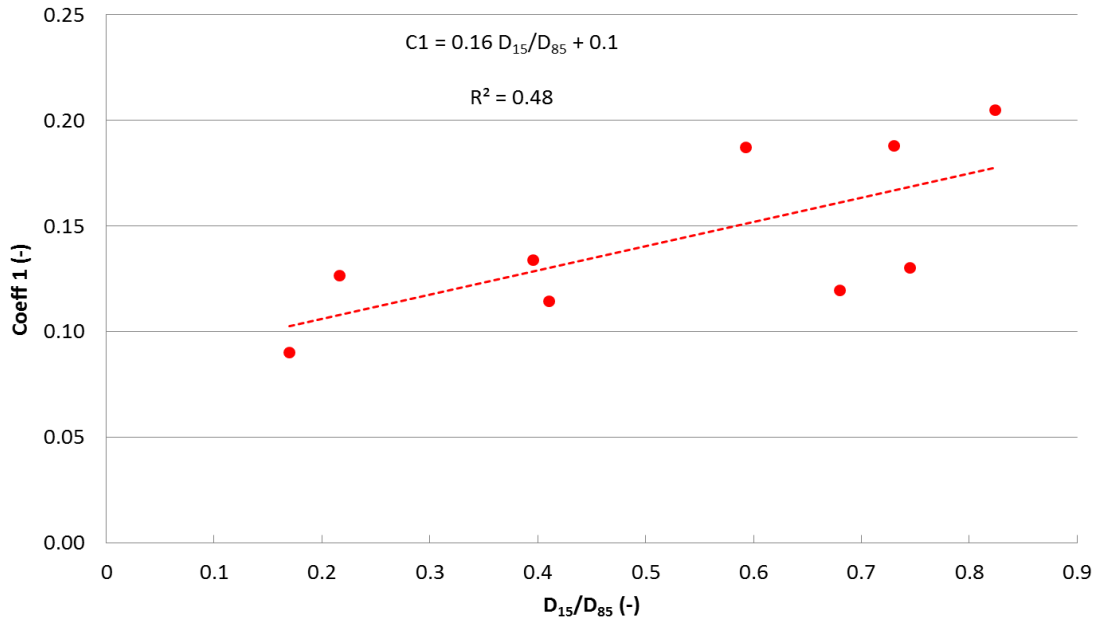

Figure 6.21: Linear relationship between the coefficient C1, Eq. (6.5), and the grain size parameter D_{15}/D_{85}.

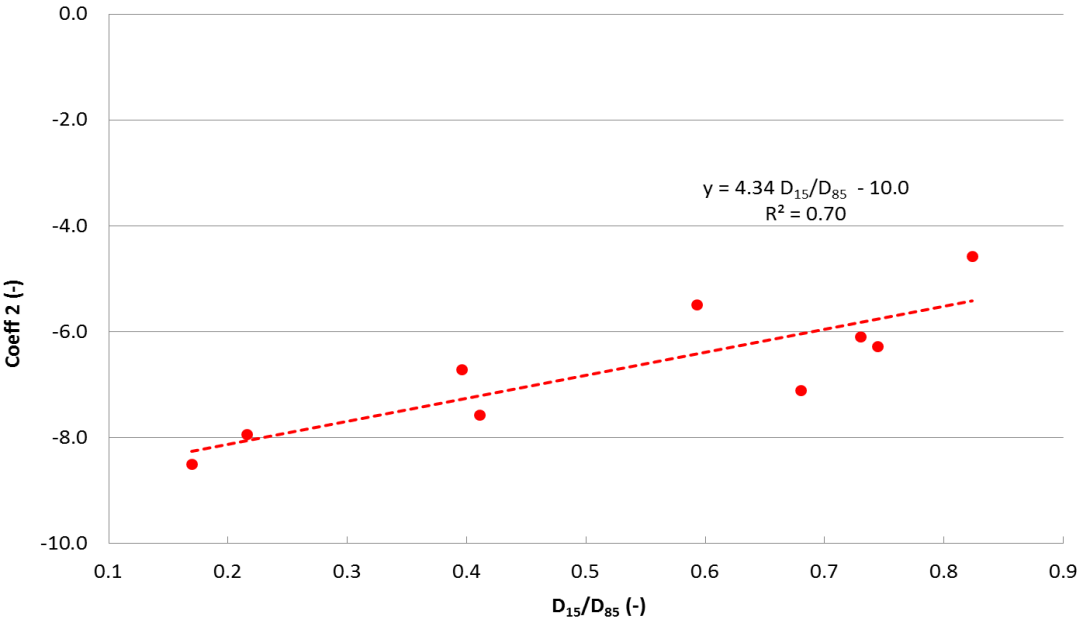

Figure 6.22: Linear relationship between the coefficient C2, Eq. (6.5), and the grain size parameter D_{85}/D_{15}.

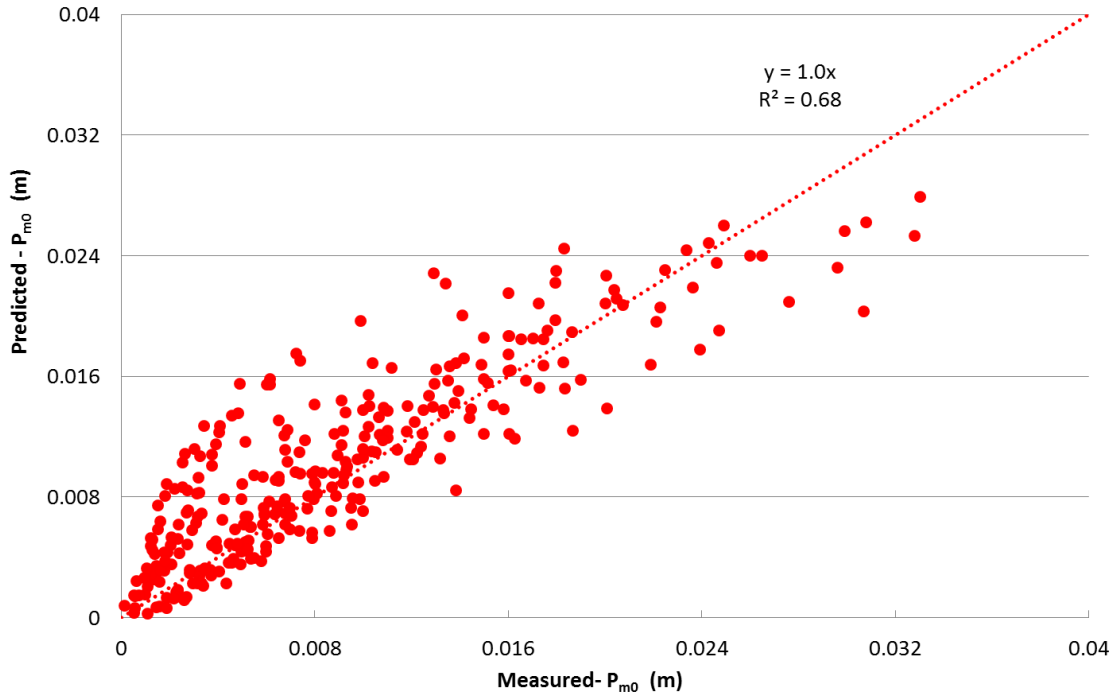

Figure 6.23: Comparison between predicted and measured wave-induced pore pressure head

6.4.5. Internal wave set-up

6.4.5.1 Introduction

The groundwater elevation in response to the sea oscillations results from the joint action of both the high-frequency and the low-frequency waves (Li *et al.*, 2002, 2004). As described in detail in Section 2.3, most of the previous investigations on modelling the interactions between wave action with beach groundwater mainly focused on tide-induced water table fluctuations (Nielsen, 1990; Baird and Horn, 1996; Li *et al.*, 1997; Guo *et al.*, 2007) and only a few studies investigated the effect of high-frequency oscillations on groundwater table elevation (e.g., Li and Barry, 2000; Kobayashi and Wurjanto, 1992).

Wave set-up and set-down are both closely linked to the breaker type and the wave height. The wave set-up that occurs on the gravel beachface can be considered as an indicator for the rate of wave energy dissipation induced by the breaking process. As schematised in Figure 6.9, the internal wave set-up is given by the change of the water level inside a porous medium under wave attack. The maximum set-up defines the dynamic shoreline position, whereas the SWL defines the

static shoreline position. As suggested by Nielsen (1997) the elevation and shape of the beach water table depends on both the hydraulic conditions and the characteristics of the beach material.

Based on laboratory experiments with regular waves on an equilibrium beach profile, Gourlay (1992) suggested that the higher the permeability the greater the volume of water flow-out from the beach between successive wave run-ups, and the lower the wave-induced beach water table elevation. However the empirical formulations presented in the literature (Section 2.3.5) show dependency only on the wave conditions and beach-face slope, and not on the beach sediment characteristics. It can be argued that the beach slope is function of the permeability of the beach, therefore the latter parameter is indirectly included in the empirical equations. Although, to the knowledge of the author, there are no equations that directly express the beach sediment size in the context of internal wave set-up.

6.4.5.2 Physical model results

The internal wave set-up was recorded for the gravel beaches with grading curves plotted in Figure 6.5 under wave conditions summarised in Table 6.3. Although the tidal response of the water table is also an important parameter affecting the internal wave set-up, this is out of the remit of the present study and therefore not considered further here. For each wave condition, the internal wave set-up was extracted as the mean water level reached during the testing (as shown graphically in Figure 6.5)

Results of these tests show that the internal wave set-up is strongly influenced by both the wave conditions and sediment characteristics. Accordingly to Gourlay (1992) the smaller the material sediment size the less the volume of water that can flow-out of the beach. Consequently, if subject to wave action for long enough, less permeable beaches are potentially able to store a higher volume of water under wave action. For this reason when the waves run up on the beachface, only a small amount of wave energy can be dissipated through percolation, triggering higher wave run-up, and consequently high levels of internal set-up.

This is confirmed in Figure 6.24 where the mean internal wave set-up (η_{int}), measured during the tested wave conditions, increases with increasing wave energy (H_{m0} and L_{m-10}). Interestingly, the latter plot shows a significant scatter in the data, suggesting that an important parameter

influencing the internal wave set-up is possibly missing. As expected, the scatter in data shown in Figure 6.24 is reduced by accounting for the effect of sediment sizes (D_{50}) as illustrated in Figure 6.25. It is important to highlight that the scatter was also reduced by accounting for the effect of sediment size D_{15}, however a better prediction was obtained by using D_{50}. The scatter observed in Figure 6.25 could be due to the fact that grain shape, which affects the packing, i.e., the arrangement of grains and therefore the flow/resistance relationship, was not directly included in the equation.

The following equation is therefore suggested to predict the mean internal wave set-up:

$$\frac{\eta_{int}}{H_{m0,toe}} = 1 \times 10^{-4} \left(\frac{L_{m-1,0}}{D_{50}}\right) + 0.03 \qquad (6.9)$$

where $H_{m0,\,toe}$ is the incident spectrum wave height measured at the toe of the beach, $L_{m-1,0}$ is the wave length measured at the toe of the beach (based on the spectral period $T_{m-1,0}$) and D_{50} is the mean size diameter of the beach grading curve.

The above equation is valid for the following range:

- 3.0mm < D_{50} < 20mm
- 1.2 < D_{85} / D_{15} < 5.9
- 0.02 < s (wave steepness) < 0.04

Measured internal wave set-up is compared to predictions using Equation (6.9) in Figure 6.26. For a good prediction, the fitted line (red dotted line) should be close to the red solid line. As can be seen, a good agreement is obtained, even though the formula appears to slightly underestimate the highest values of wave set-up.

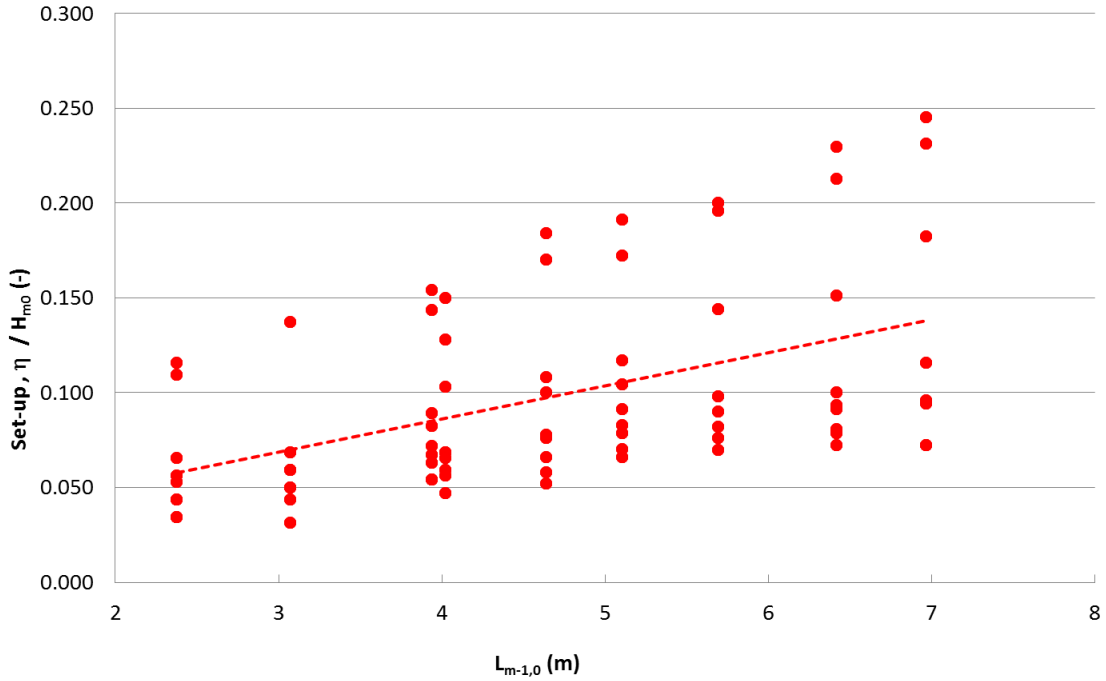

Figure 6.24: Normalised internal wave set-up as function of wave parameter ($L_{m-1,0}$)

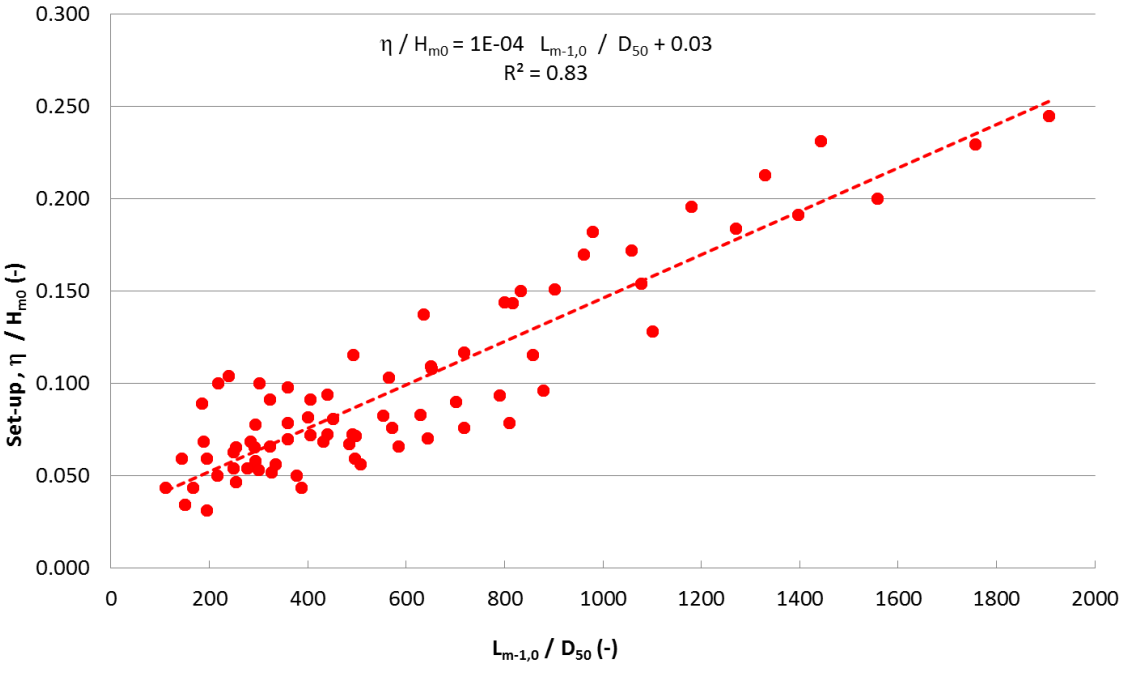

Figure 6.25: Normalised mean internal wave set-up as a function of number of grain diameters per wavelength

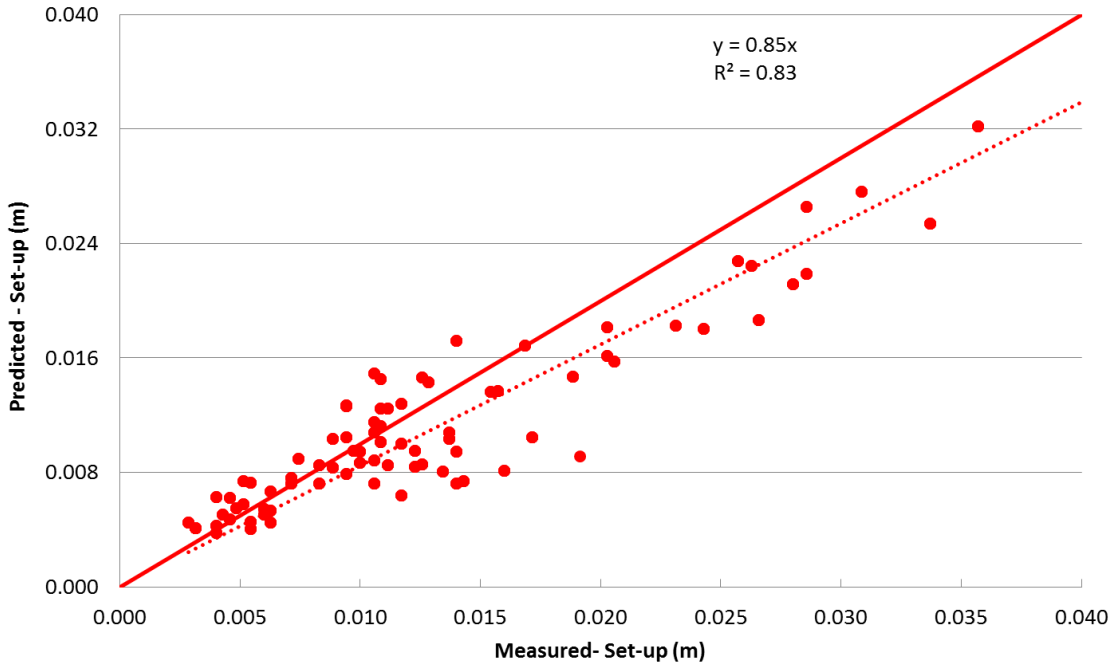

Figure 6.26: Predicted vs measured mean internal wave set-up

6.4.6. Further discussion

Following the results previously discussed, the following derivations can be made:

- For small sediment size a higher wave set-up and smaller wave-induced pore pressure is obtained

As already discussed in Section 3.2, the permeability is an indication of the ability for the water to flow through the porous medium. Therefore, gravel beaches with lower permeability will be subjected to higher levels of wave run-up and internal set-up, but also to a higher energy dissipation through the porous medium. As such, lower permeability beaches will not be able to transmit energy through the material and result in smaller wave-induced pore pressures than beaches with high permeability. This is shown in Figure 6.27, where A, B and C are the recorded pore pressure time series respectively for the wide graded material W3, W4 and W5, under the same wave condition (WC-03). The gravel material W3, characterised by a small D_{15} and D_{50}, is the less permeable and W5, characterised by a D_{15} and D_{50} four times bigger than W3, is the most permeable material. The red lines represent the internal wave set-up, and as can be seen, comparing Figure A, B and C, the gravel material W3 (less permeable) shows a higher water level

displacement, i.e., higher internal set-up. However when comparing the signal-intensity of the pore pressure, Figure D (Figure 6.27), it can be noticed that the W5 (more permeable) shows larger oscillations (amplitude). This is confirmed by the power spectral density analysis of wave induced pore pressures for the three materials, reported in Figure 6.28. The three spectra display similar shapes with well identified frequency bands, but the magnitude of the spectrum decreases with decreasing permeability. W5 (more permeable) material shows a bigger pore pressure power spectrum than W4 (less permeable).

This apparent paradox, for which less permeable materials are capable of storing larger volumes of water, resulting in higher internal set-up, is explained once the effect of time is taken into account. As also observed by Gourlay (1992), impermeable materials remain saturated throughout the wave uprush-backwash cycle, with no groundwater flow out of the beach. The internal build-up in fact takes longer to achieve its full potential in less porous beaches, as demonstrated in Figure 6.27, showing that:

- Less porous material (W3, panel A) reaches a higher internal set-up than more porous material (W5, panel C).
- More porous material fulfil their storing potential (i.e. reach their maximum internal set-up) in less time than less porous material

This is confirmed in Figure 6.29 showing how the measured time-lag for the internal set-up increases with smaller wave steepness (longer wave periods T_{m-10}). The time-lag was defined as the minimum time required for the groundwater level (starting from the still water level) to reach the mean internal wave set-up. Once again, the scatter in the data suggests that an important parameter, which influences the internal wave set-up, has not been considered. Indeed, the scatter in data shown in Figure 6.29 is reduced by accounting for the effect of sediment sizes (D_{15}) as illustrated in Figure 6.30. This relationship was also investigated by using D_{50} and D_{85}, but the best prediction was obtained by using D_{15}. This confirms that for less porous beaches more time is required for the internal set-up to build up.

The following equation is therefore suggested to predict the time needed by the groundwater elevation to reach the maximum build-up level within the beach:

$$\Delta t = -11 \left(\frac{T_{m-1,0}}{H_{m0,toe}} \right) D_{15} + 6.0 \tag{6.10}$$

where: $H_{m0,toe}$ is the incident spectrum wave height measured at the toe of the beach, $T_{m-1,0}$ is the mean spectral period and D_{15} is the diameter of stone that exceeds the 15% value of sieve curve.

The above equation is valid for the following range:

- 3.0mm < D_{50} < 20mm
- 1.2 < D_{85} / D_{15} < 5.9
- 0.02 < s (wave steepness) < 0.04

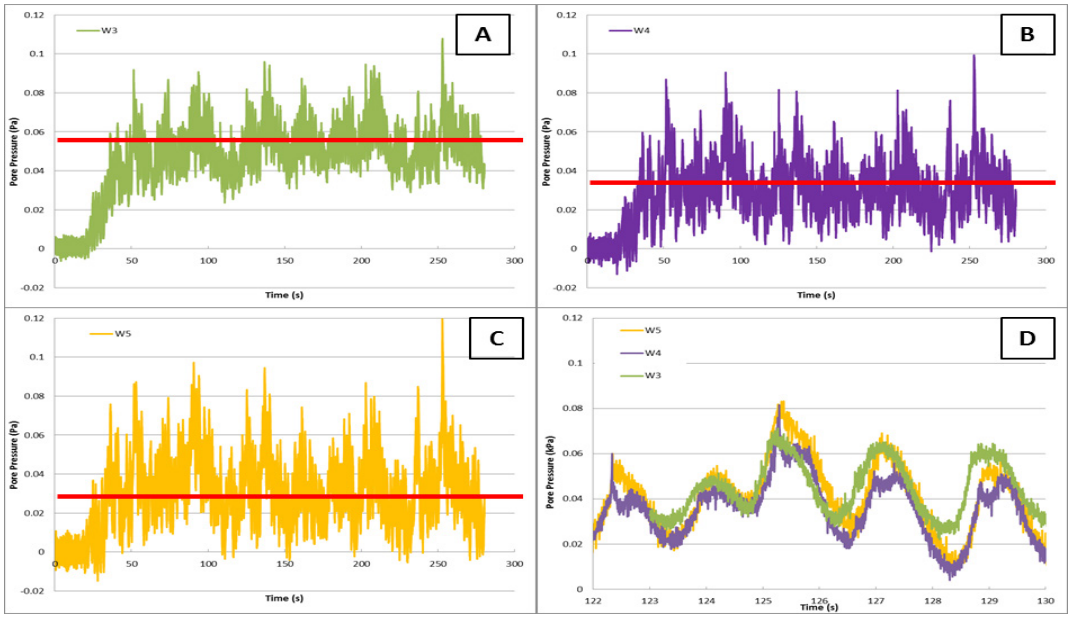

Figure 6.27: A-B-C, recorded pore pressure time series respectively for gravel material W3 (D_{15} = 3mm, D_{50} = 4mm and D_{85}/D_{15} = 2.4), W4 (D_{15} = 6mm, D_{50} = 8mm and D_{85}/D_{15} = 2.5) and W5 (D_{15} = 13mm, D_{50} = 16mm and D_{85}/D_{15} = 1.7),under the same wave condition (WC03, H_{m0} = 0.14m and T_p = 1.6s). The red lines represent the internal wave set-up. A comparison of the signal-intensity (for a random time window) of the three time series is shown in Figure D.

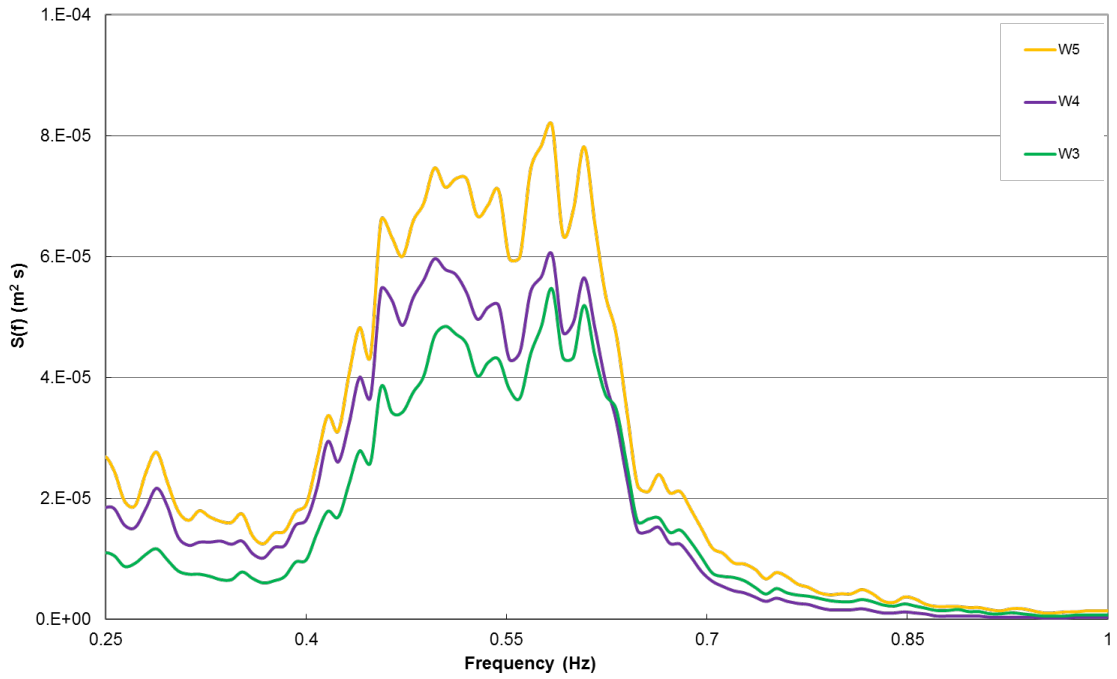

Figure 6.28: Power spectral density of wave induced pore pressure, for the first pressure sensor, for the gravel materials W3, W4 and W5, under the same wave condition (WC03).

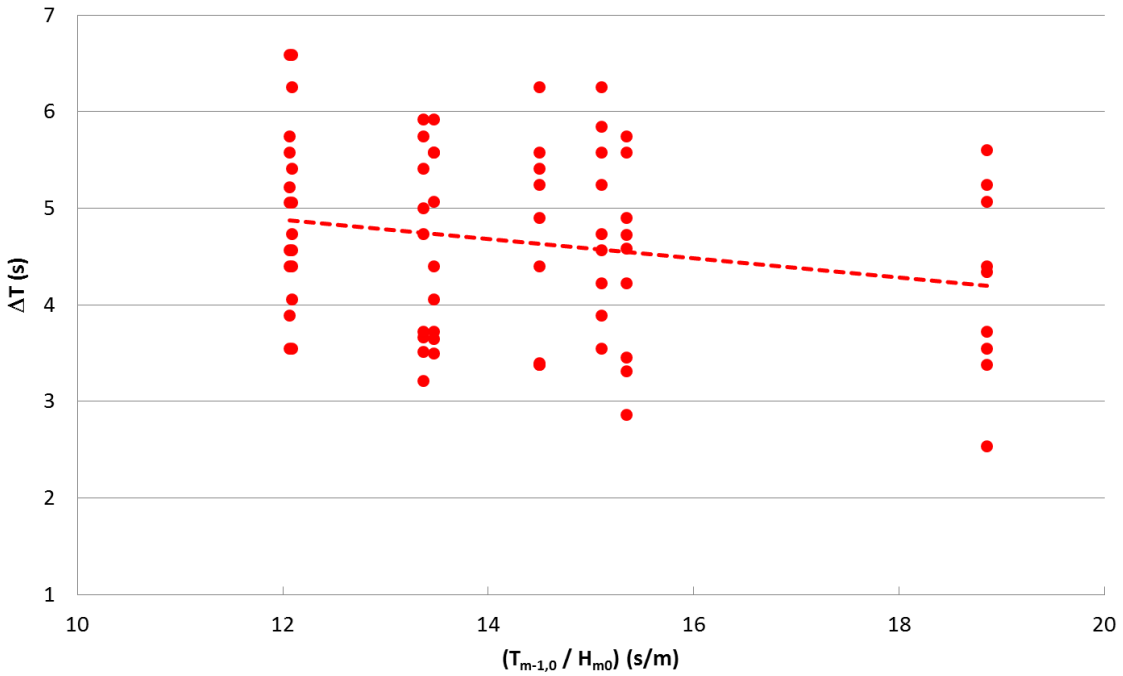

Figure 6.29: Time–lag of the internal wave set-up as function of wave parameters (H_{m0} and $T_{m-1,0}$)

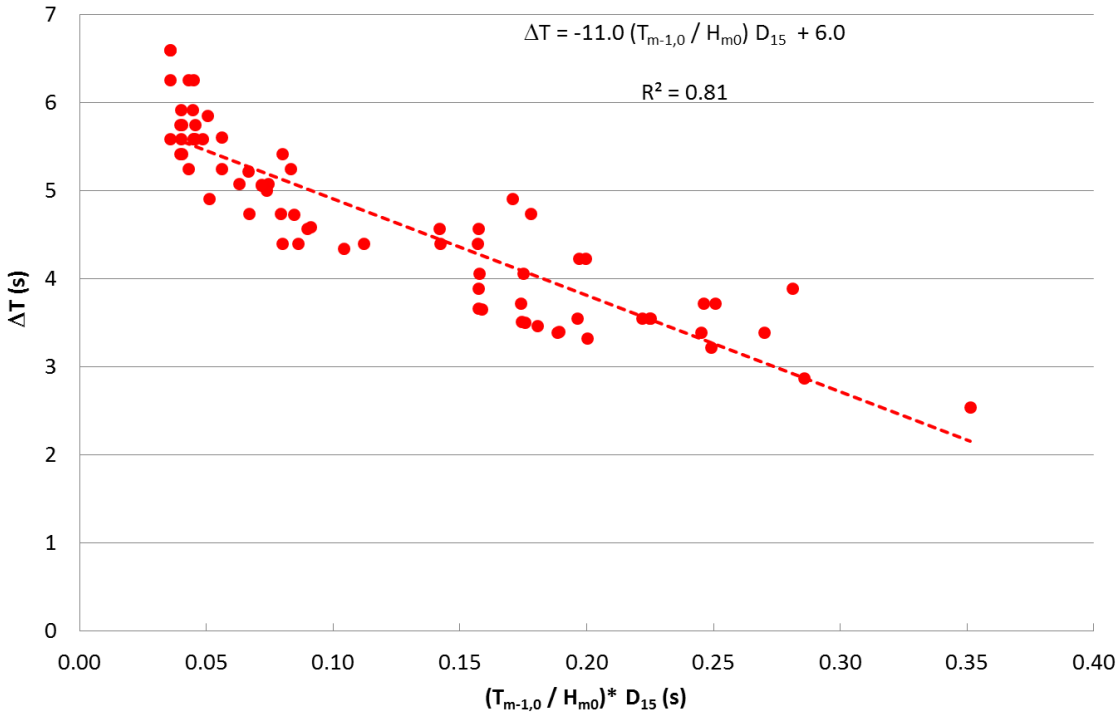

Figure 6.30: Time–lag of the internal wave set-up as function of wave parameters (H_{m0} and $T_{m-1,0}$) and sediment size characteristic D_{15}

6.5. Physical model results: effect of grain size distribution

6.5.1. Observations

During the physical model study, experiments had an initial tested beach slope of 1 in 7 (plane sloping beach) as shown in Figure 6.2. At the end of each test, the post-storm beach profile was measured using a 2D bed profiler, which extracted the profile elevation every 20mm along the x-axis, with an accuracy of ± 1.0mm vertically and horizontally, as detailed in Section 6.2.1.

Initially, in order to evaluate the repeatability of the test, the same gravel beach material (W02, D_{50} = 8mm and D_{15} = 3mm) was tested twice under the same wave condition. Before repeating the same test condition, the gravel beach was reshaped to the original plane slope of 1 in 7. Results of the comparison between the first (Test_01, H_{m0} = 0.14m and T_p = 1.4s) and repeated (Test_01_Repeated, H_{m0} = 0.14m and T_p = 1.4s) profiles are plotted in Figure 6.31, where it can be observed that the crest of the beach shows a very small horizontal and vertical displacement of 10mm and 5mm, respectively across the two tests.

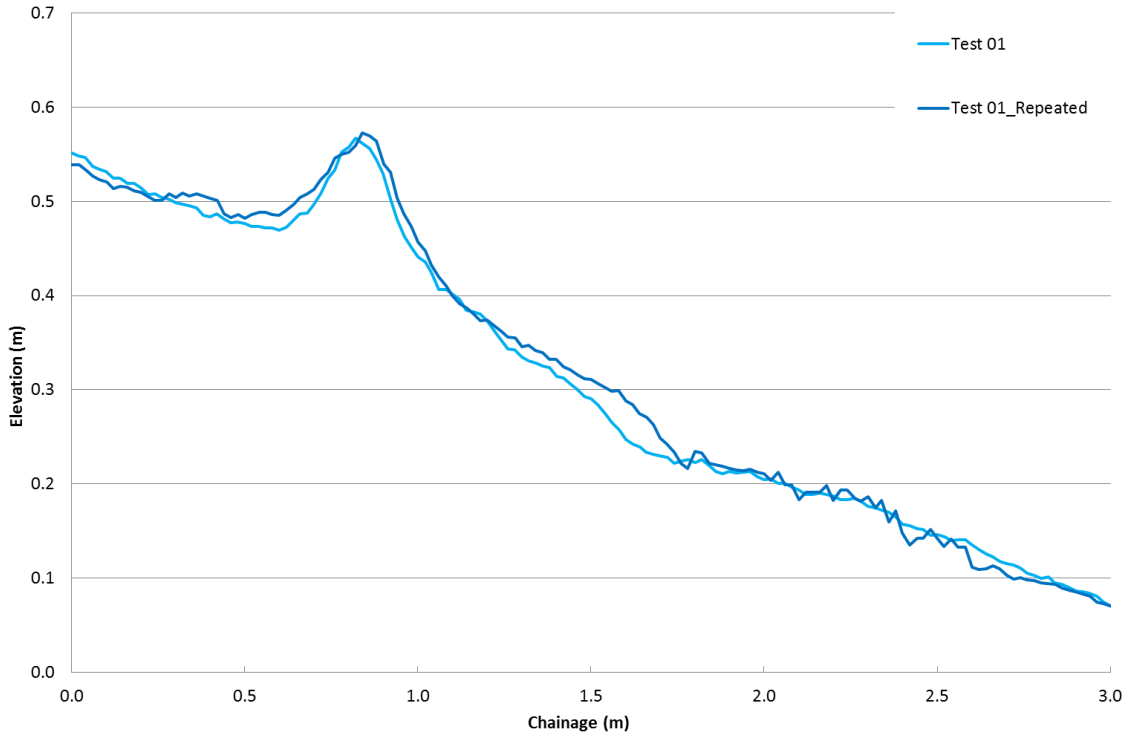

Figure 6.31: Comparison between same material (W02, D_{50} = 8mm and D_{15} = 3mm) tested twice under the same wave condition (H_{m0} = 0.14m and T_p = 1.4s). Before repeating the same test condition, the gravel beach was reshaped to the original plane slope of 1 in 7

During the tests, it was observed that beaches having smaller grain size material (D_{50}) generally exhibited larger displacements of the beach crest, as shown in Figure 6.32 and Figure 6.33, and beaches with smaller grain size distributions (D_{85}/D_{15}) (top flume) show a higher vertical displacement of the beach crest. As also expected, beaches under wave action are subject to a sorting of grain sediments, which generally results in the finer material moving down into the core of the beach leaving a coarser layer on the surface (bed armouring), as can be observed in Figure 6.34 (middle flume). In addition, the so formed coarser layer is also subjected to cross-shore sorting under wave action, which results in a variable distribution of the coarser material along the beach surface. Figure 6.34 and Figure 6.35 show typical sediment size distributions along the beach surface. The sorting of sediments is related to the wave loading on the beach, which, if strong enough, may trigger the movement of all the sediment particles within the beach material.

During these experiments it was generally observed that both beach crest and breaker-zone were characterised by the presence of coarser material following each test. Conversely, the area around the shoreline was characterised by having finer sediments, as shown in Figure 6.32 (middle flume). As discussed in the following sections, the sorting of sediments along the beach-face and the final beach profile response are functions of both grain size distribution and incident wave energy. As expected, for gravel beaches characterised by having large grain sizes, only severe wave conditions were able to trigger a profile displacement. This can be observed in Figure 6.32, where three wide gravel beaches (W03, W04 and W05) were tested under the same wave condition (WC03, H_{m0} = 0.14m and T_p = 1.6s) and the beach with the bigger grain size (W05, D_{50} = 16mm, flume at the bottom) shows a smaller crest displacement compared with the other two profiles.

Figure 6.32: Gravel beach profiles W03 (top), W04 and W05 (below) tested under the same wave condition (WC03, H_{m0} = 0.14m and T_p = 1.6s). Gravel beaches W03, W04 and W05 having D_{50} = 4mm, D_{50} = 8mm and D_{50} = 16mm, respectively

Figure 6.33: Gravel beach profiles W01 (top), W02 and N02 (below) tested under the same wave condition (WC03, H_{m0} = 0.14m and T_p = 1.6s). Gravel beaches W01, W02 and N02 having D_{50} = 5mm, D_{50} = 8mm and D_{50} = 7mm, respectively

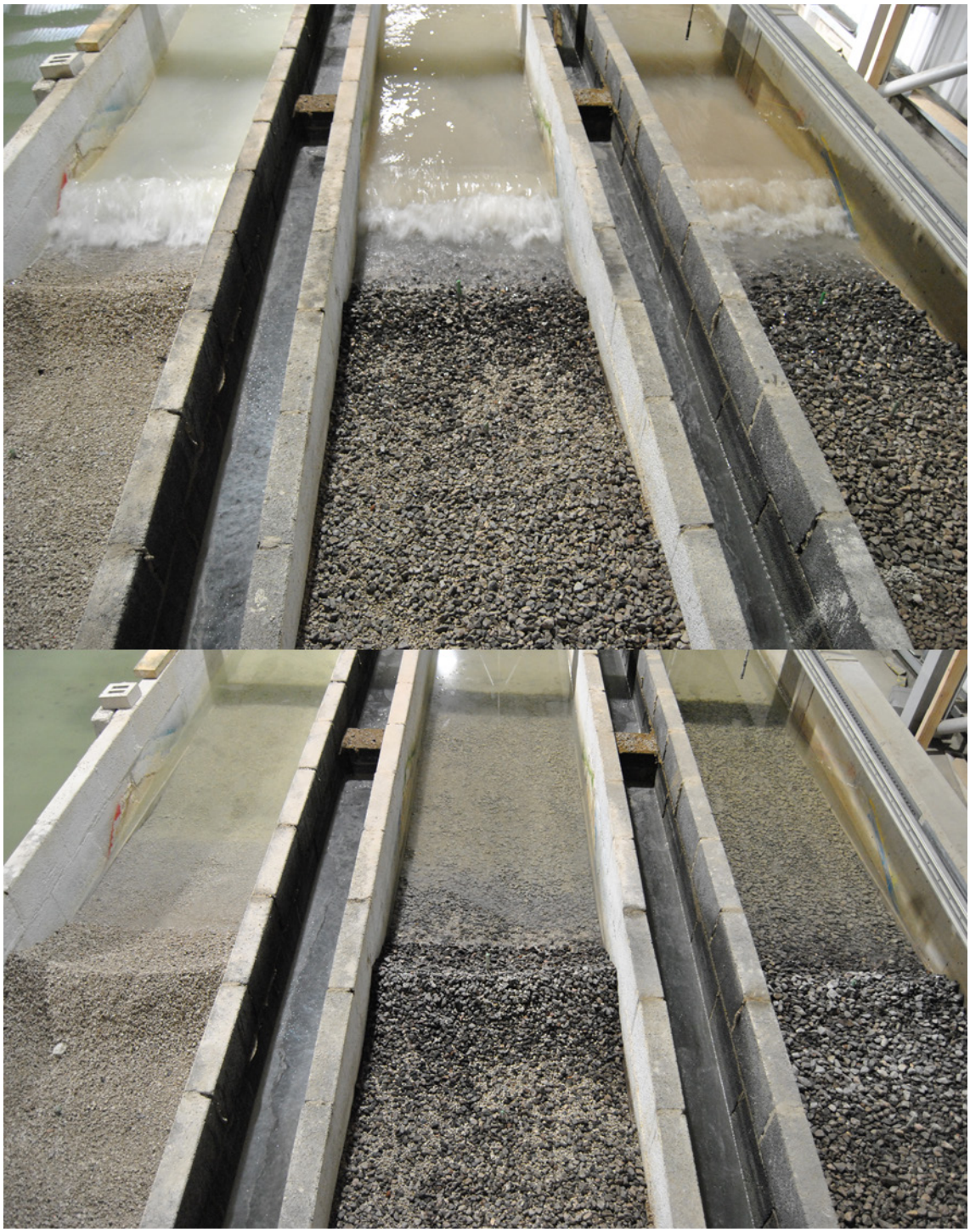

Figure 6.34: Above, gravel beach profiles W03 (left), W04 and W05 (right) tested under the same wave condition (WC03, H_{m0} = 0.14m and T_p = 1.6s). Below, gravel beach profiles W03, W04 and W05 after testing. Gravel beaches W03, W04 and W05 having D_{50} = 4mm, D_{50} = 8mm and D_{50} = 16mm, respectively

Figure 6.35: Gravel beach profiles W01, W02 and N02 tested under the same wave condition (WC03, H_{m0} =0.14m and T_p =1.6s). Gravel beaches W01, W02 and N02 having D_{50} = 5mm, D_{50} = 8mm and D_{50} = 7mm, respectively

6.5.2. Comparison between gravel and sand materials

At the beginning of this study, it was decided to run an initial test where sand material and fine gravel beaches were directly compared under the same wave conditions. As discussed in Chapter 2, permeability is a main factor controlling the beach slope. This can be observed in Figure 6.36 and Figure 6.37 where a sand beach (D_{50} = 0.1mm) and narrow gravel beach (N1, D_{50} = 3.0mm), both laid at initial slope of 1 in 7, were tested under the same wave condition (WC01, H_{m0} = 0.085m and T_p =1.2s). As expected the sand beach adopted a flatter slope, while the gravel beach shows an accretionary behaviour, as shown in Figure 6.38. This result confirmed what was expected, that is to say, the beach slope and shape is strongly dependent on the characteristics of the material chosen for the experiment (Ilic, 2005), and also suggests that, for gravel beach physical model studies, the prototype gravel material cannot be scaled or reproduced by using sand sediment particles. As already discussed in Section 2.3, the hydraulic conductivity is a main factor controlling the beach slope, in this case, as expected a more permeable material

(gravel) has a steeper slope than a less permeable material (sand). The larger permeability enabled the water to percolate into the beach more easily than in the sand model, where the downrush was more parallel to the beach. The gravel material was mainly transported onshore by the waves and much less material was moved back seaward by the downrush. Additionally, the angle of repose of the sediment is also influenced by the angularity of the particles, which is different between gravel and sand. For this reason sand sediments were not considered further during this study.

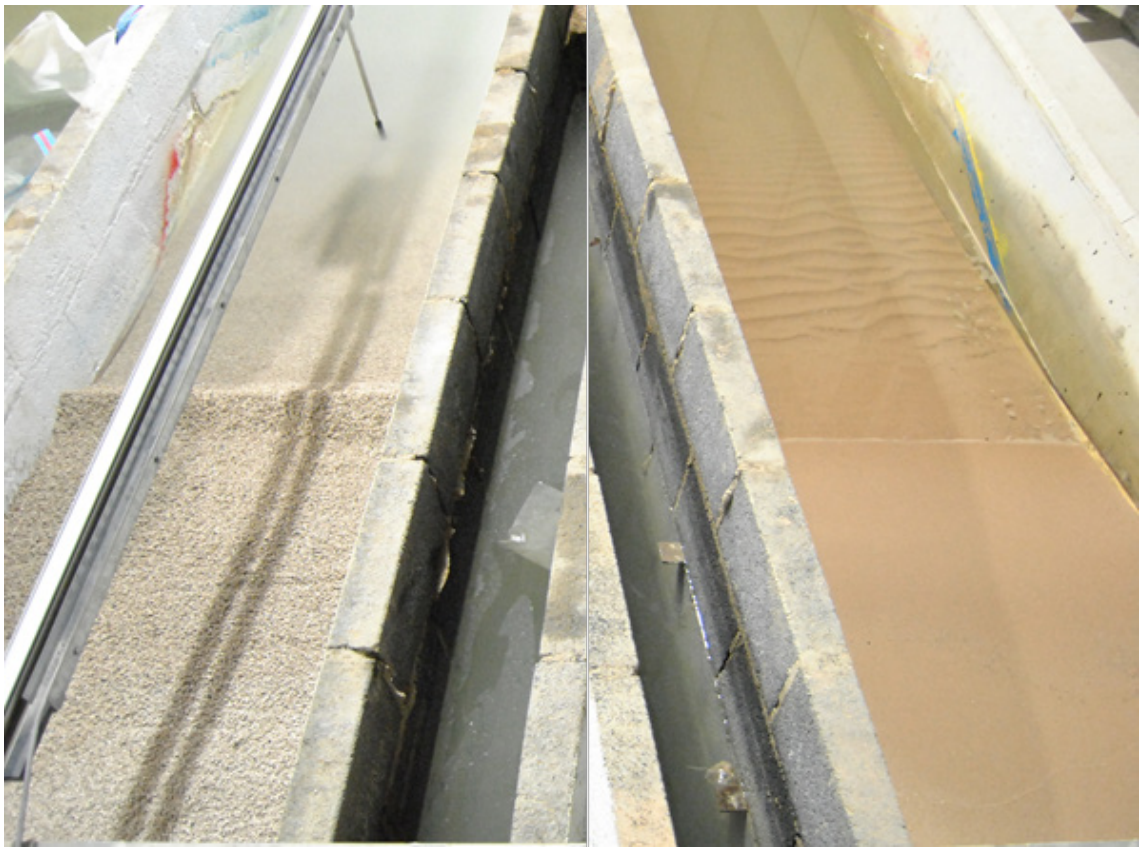

Figure 6.36: Top view of gravel beach profile N01 (left, D_{50} = 3mm, D_{15} = 3mm) and fine sand beach (right, D_{50} = 0.1mm) tested under the same wave condition (H_{m0} = 0.085m and T_p = 1.2s). As expected the sand beach (right) adopted a flatter slope, while the gravel beach (left) shows an accretionary behaviour

Figure 6.37: View from the toe of gravel beach profile N01 (right) and fine sand beach (left, D_{50} = 0.1mm) tested under the same wave condition (H_{m0} = 0.085m and T_p = 1.2s).

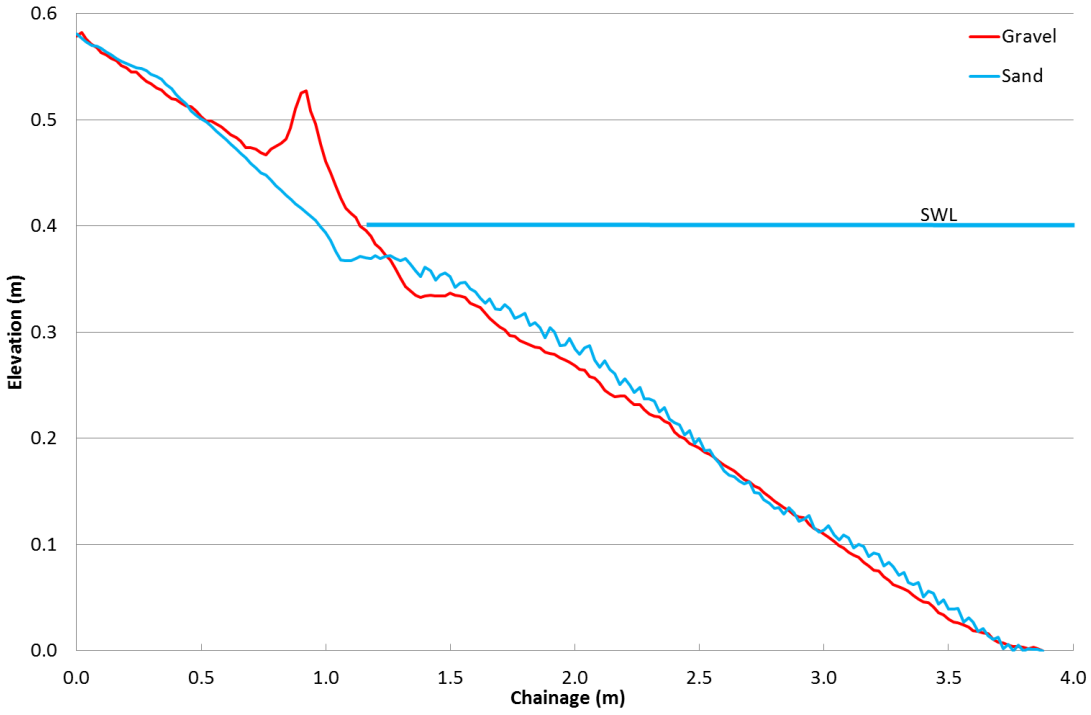

Figure 6.38: Gravel beach profile N01 and fine sand beach (D_{50} = 0.1mm) tested under the same wave condition.

6.5.3. Test results

In order to analyse the effect of both the particle size and the sediment distribution on the beach profile evolution, samples with similar grading parameters were compared (e.g., $D_{50,}$ D_{15} and D_{85}/ D_{15}) as per Table 6.2. A comparison of post-storm profiles recorded at the end of the tests performed with gravel beaches having similar D_{50} is plotted in Figure 6.39. It can be seen that both beach profiles have approximately the same crest elevation (~0.42m) but different crest positions. In particular, the beach characterised by a grading curve with a smaller D_{15} shows a larger crest displacement. Conversely, a comparison between gravel beaches having similar D_{15} is plotted in Figure 6.40 and Figure 6.41, these plots illustrate that beach profiles having the same D_{15} (N02-W04 and N3-N4) show similar crest positions but different crest elevations. In particular, the beach characterised by grading curves with smaller D_{50} show a higher crest elevation. The relative effect of the D_{50} and D_{15} on the post-storm crest elevation and position is further confirmed by comparing the post-storm profiles in Figure 6.42, confirming that the crest moves upwards and shoreward as D_{50} and D_{15} decreases. Gravel beach materials having the same ratio D_{85}/D_{15} were also compared, however no relationship with the crest elevation and position was observed. The response of the crest was mainly driven by D_{15} and D_{50}. These results can be summarised as follows:

- Materials with the same D_{50} and different D_{15} show a horizontal crest displacement
- Materials with the same D_{15} and different D_{50} show a vertical crest displacement

Following these initial observations, the next sections describe how the beach profile, and in particular the position and elevation of the crest, are not only affected by the incident wave condition but also by the grain size distribution. As described in Section 6.4, the grain size distribution influences the internal ground water elevation and pressure distribution, and therefore the evolution of the beach profile.

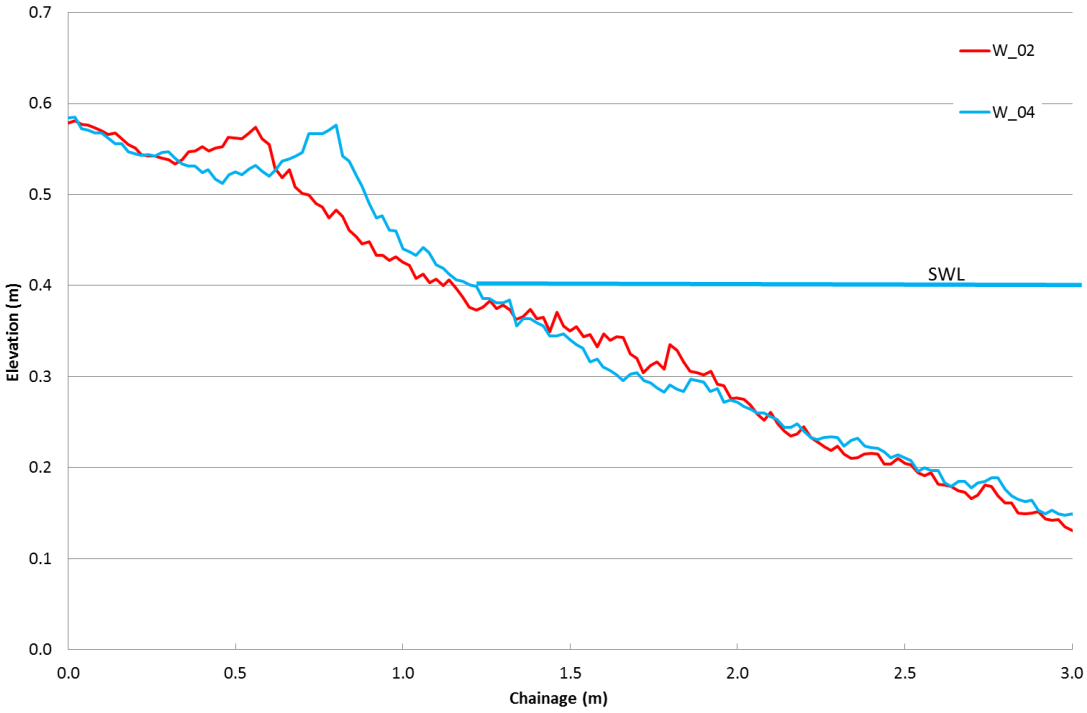

Figure 6.39: Gravel beach profiles W02 and W04 tested under the same wave condition (WC03, H_{m0} = 0.14m and T_p = 1.6s). W02 and W04 have the same D_{50} but different D_{15} (W02 < W04)

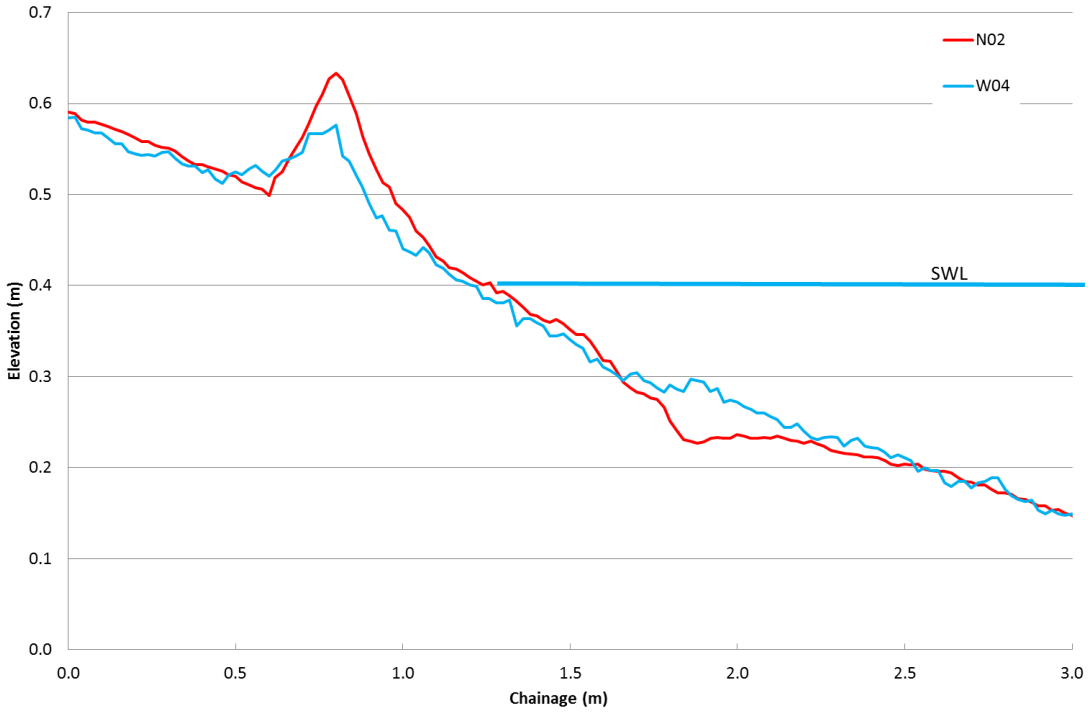

Figure 6.40: Gravel beach profiles N02 and W04 tested under the same wave condition (WC03, H_{m0} = 0.14m and T_p = 1.6s). N02 and W04 have the same D_{15} but different D_{50} (N02 < W04)

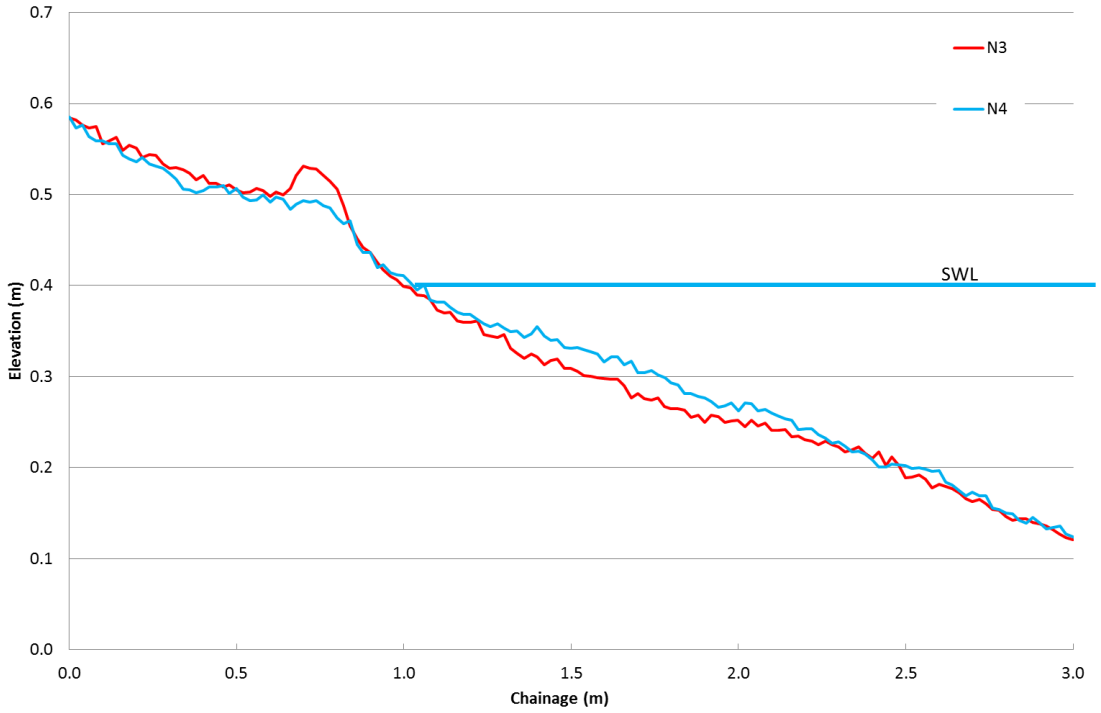

Figure 6.41: Gravel beach profiles N02 and W04 under the same wave condition (WC03, WC03, H_{m0} = 0.14m and T_p = 1.6s). N02 and W04 have same D_{15} but different D_{50} (N02 < W04)

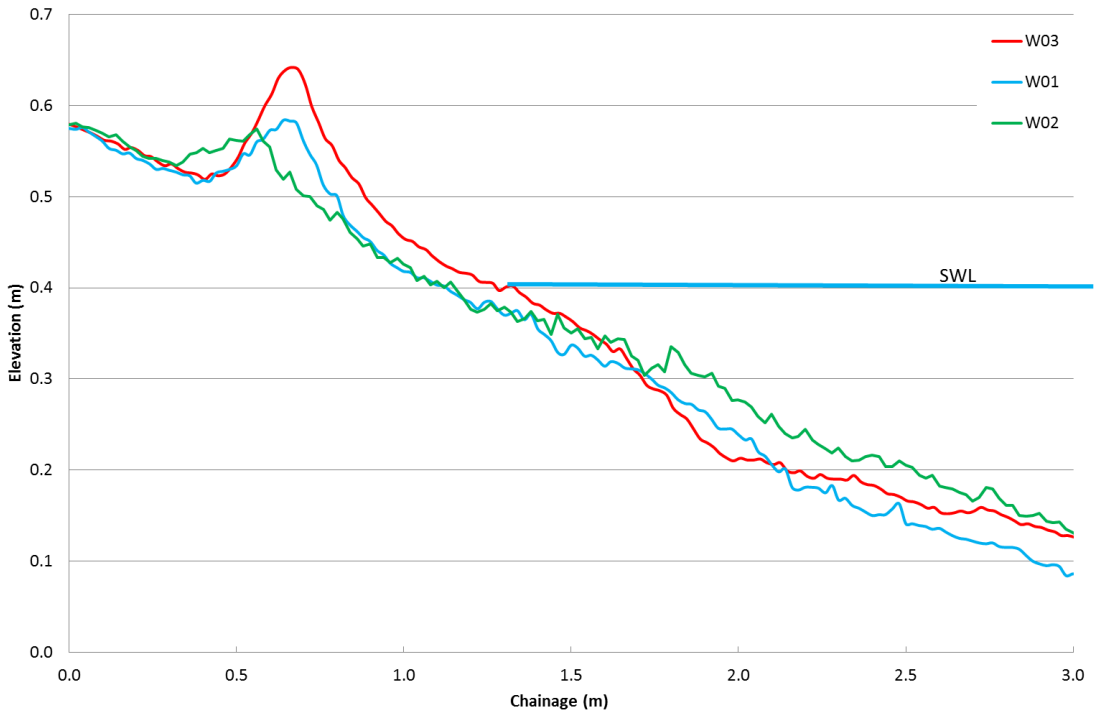

Figure 6.42: Gravel beach profiles W01, W02 and W03 tested under the same wave condition (WC03, WC03, H_{m0} = 0.14m and T_p = 1.6s). W01, W02 and W03 have the same D_{15} but different D_{50}

6.5.4. Influence of grain size distribution on the elevation of the beach crest

Examples of the beach profiles recorded at the end of each test were shown in Figure 6.39 to Figure 6.42, where each post-storm profile was parametrised in terms of the crest elevation (y_i) and distance (x_i) relative to the SWL, as schematised in Figure 6.43.

Observations made during the physical model tests show that the scatter in the data, plotted in Figure 6.44, where crest elevation is only a function of the wave parameters, is reduced as soon as the grain size parameter D_{50} is considered, as shown in Figure 6.45. The plot shown in Figure 6.44 is non-dimensional on the y-axis and dimensional on the x-axis. This was intentionally done to emphasize the scatter reduction due to the effect of D_{50} when comparing the plots in Figure 6.44 and Figure 6.45. Scatter in Figure 6.45 is likely to be triggered by the grain shape parameters and more complex swash processes that were not investigated during this study and therefore not considered in the equation. The results show that the crest elevation increases with increasing wave height and wave period and reducing the particle size D_{50}. It is interesting to observe, that the parameter (H_{m0} $L_{m-1,0}$ / D_{50}) is the parameter controlling the internal wave set-up, as shown in Eq. (6.9) (Section 6.4.5.2). These results suggest that crest elevation increases with increasing internal wave set-up. This can be explained by the fact that for higher values of internal wave set-up, the incoming waves are less likely to dissipate their momentum through percolation inside the beach (less volume of water percolates within the beach) and are therefore likely to trigger higher values of wave run-up and eventually transport larger volumes of sediment onto the crest.

The following equation, is therefore proposed to include the effect of the internal wave set-up parameter and account for different grain size diameters when predicting the beach crest elevation under unimodal wave conditions:

$$\frac{Crest\ Elevation}{H_{m0,toe}} = 0.0007 \left(\frac{L_{m-1,0}}{D_{50}}\right) + 1.136 \qquad (6.11)$$

where: $H_{m0,toe}$ is the incident spectrum wave height measured at the toe of the beach, $L_{m-1,0}$ is the wave length measured at the toe of the beach, based on the spectral period $T_{m-1,0}$ and D_{50} is the

mean size diameter of the beach grading curve, the parameter (H_{m0} $L_{m-1,0}$ / D_{50}) represents the internal wave set-up.

Measured crest elevations are compared to predictions using the suggested Equation. (6.11) in Figure 6.46, showing good agreement.

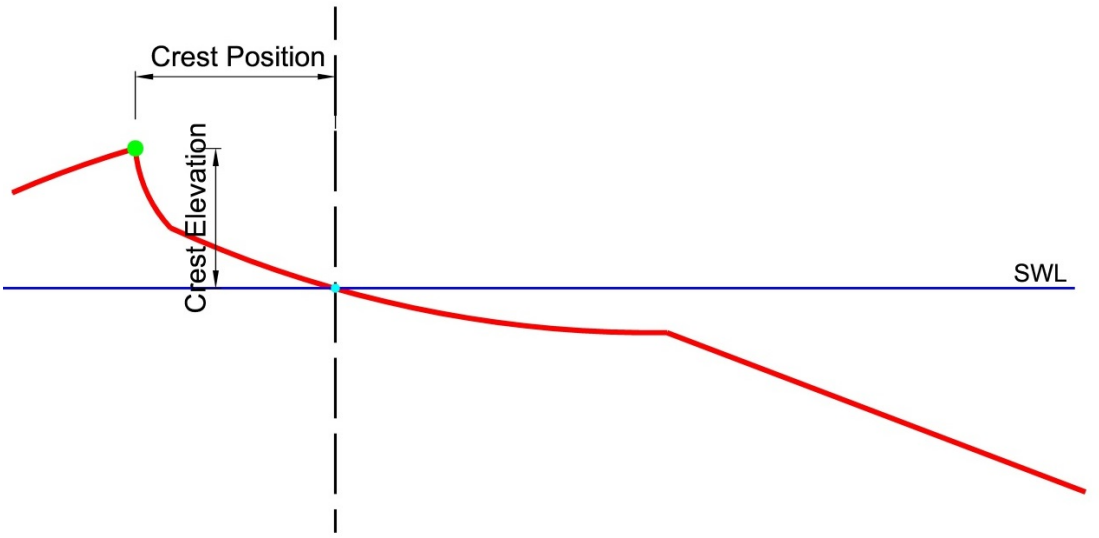

Figure 6.43: Beach crest position (x_i) and elevation (y_i), relative to SWL, extracted during tests

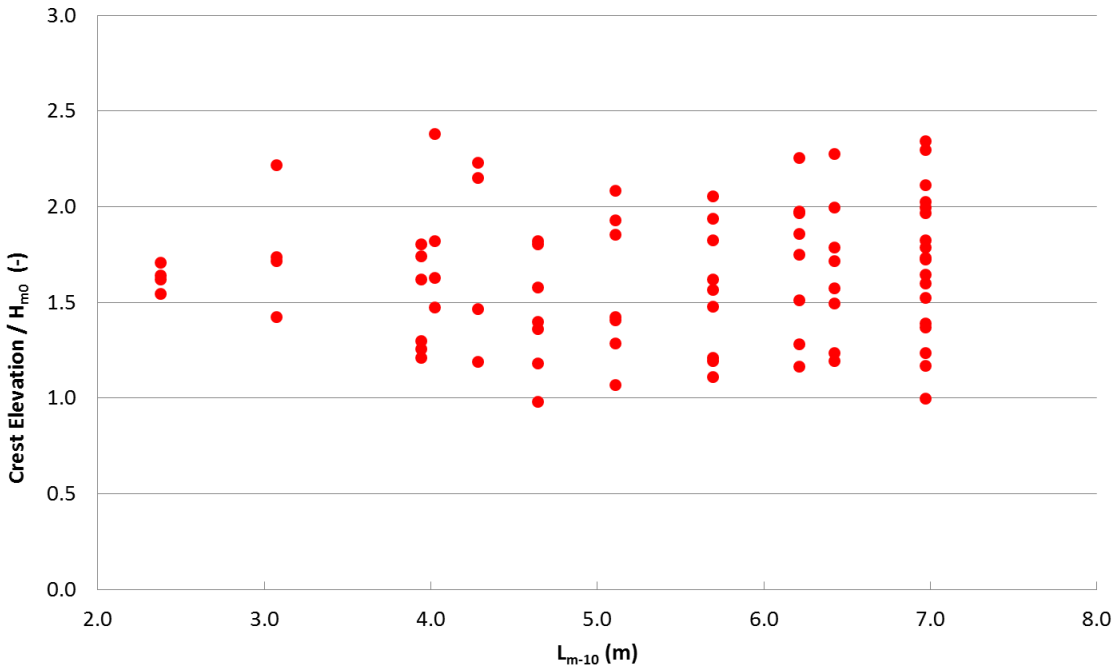

Figure 6.44: Crest elevation as a function of the wave parameter (H_{m0} and $L_{m-1,0}$)

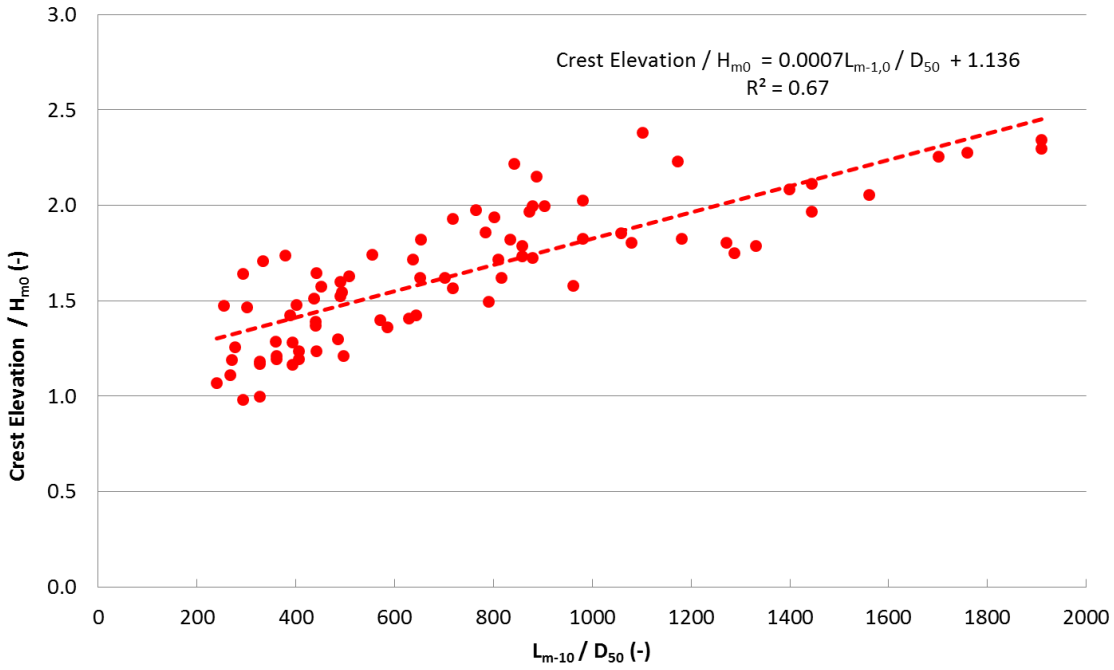

Figure 6.45: Crest elevation as a function of wave and grain size parameter D_{50}

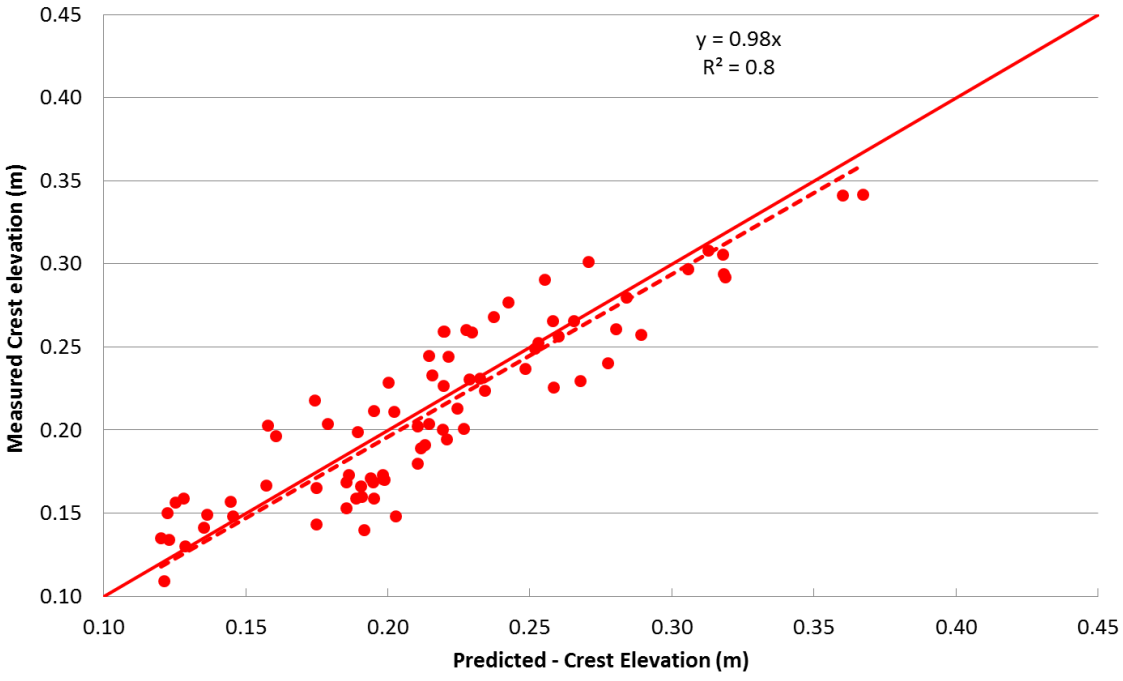

Figure 6.46: Comparison between measured crest elevation and predicted crest elevation using a proposed equation (6.11).

6.5.5. Influence of grain size distribution on beach crest position

The same approach used for the analysis on the beach crest elevation, described in the previous section, was applied to the beach crest position (see, Figure 6.43). Observations made during the physical model tests show that the scatter in the data, plotted in Figure 6.47, where crest position is only function of the wave parameters, is reduced by accounting for the effect of sediment size (D_{50}) as illustrated in Figure 6.48. Results show that the crest position increases with increasing wave height and wave period and reducing the particle size $D_{50.}$ However, an even better reduction in the scatter is obtained by using the characteristic sediment size D_{15}, as shown in Figure 6.49. This can be explained by the fact that for larger values of D_{15} (higher permeability), the incoming waves are more likely to propagate inside the beach. For this reason, the incoming waves are less likely to run up on to the top of the crest and modify its position.

The crest position can be predicted by using the best fit equation in Figure 6.49, which accounts for different grain size diameters in terms of D_{15}, and obeys the following equation:

$$\frac{Crest\ Position}{H_{m0,toe}} = 0.001\ \frac{L_{m-1,0}}{D_{15}} + 3.45 \qquad (6.12)$$

where, $H_{m0,toe}$ is the incident significant spectral wave height measured at the toe of the beach and $L_{m-1,0}$ is the wave length measured at the toe of the beach, based on the spectral period $T_{m-1,0}$ and D_{15} is the diameter of stone that exceeds the 15% value of the sieve curve.

Measured crest positions are compared to predictions using the suggested Equation (6.12) in Figure 6.50, showing good agreement.

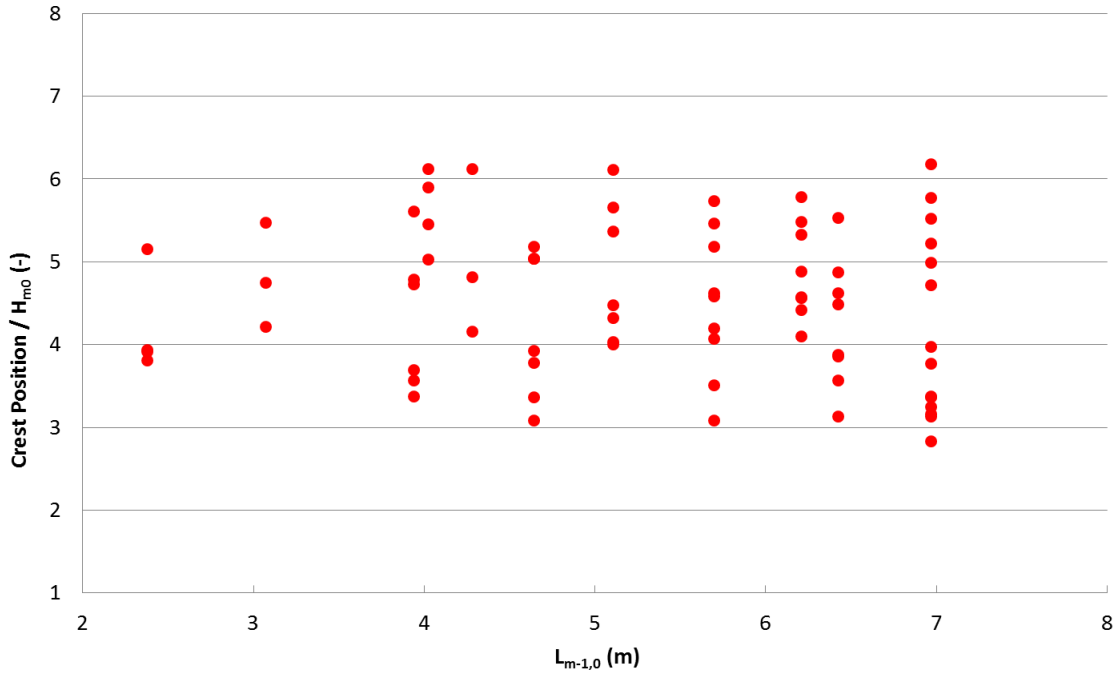

Figure 6.47: Crest position as a function of wave parameters (H_{m0} and $L_{m-1,0}$)

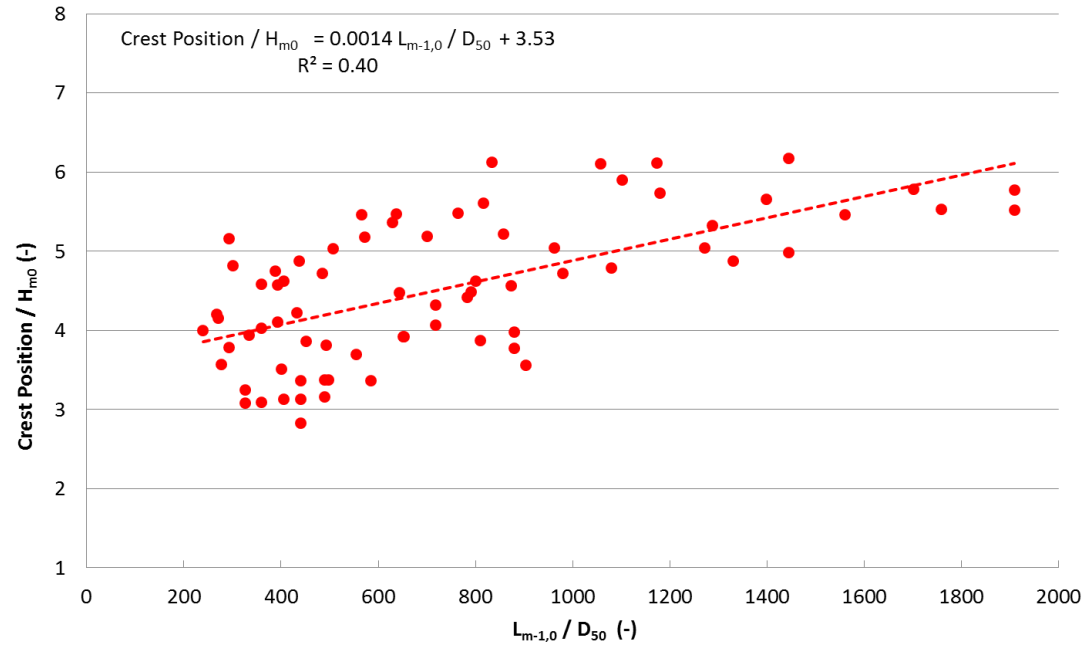

Figure 6.48: Crest position as a function of wave height, wavelength and material size characteristic D_{50}

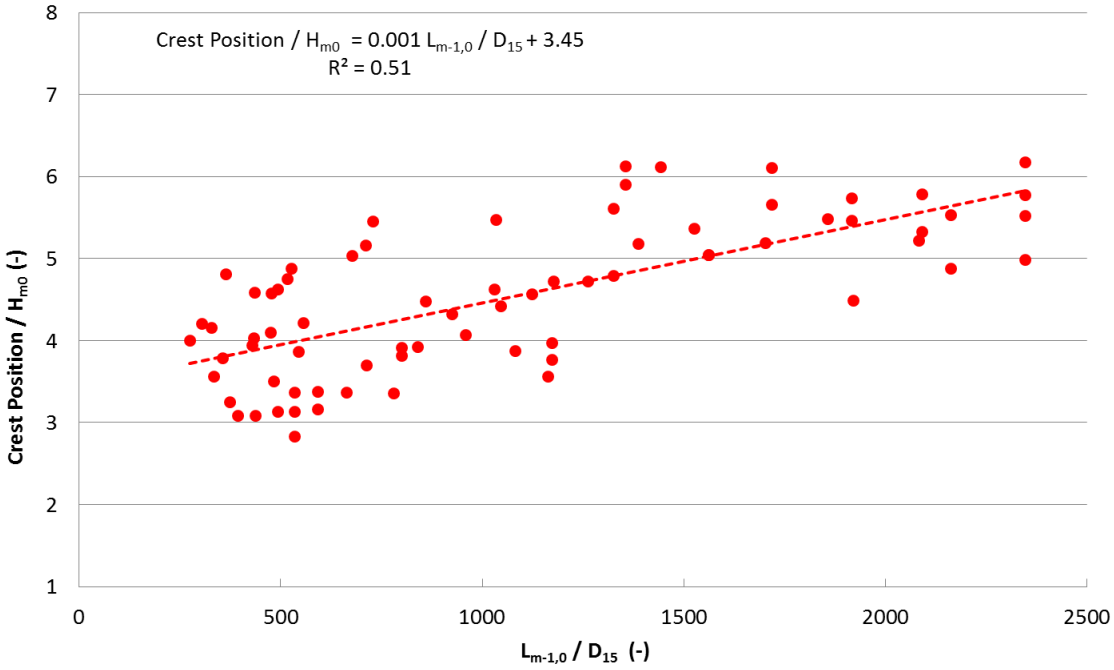

Figure 6.49: Crest position as a function of wave height, wavelength and material size characteristic D_{15}

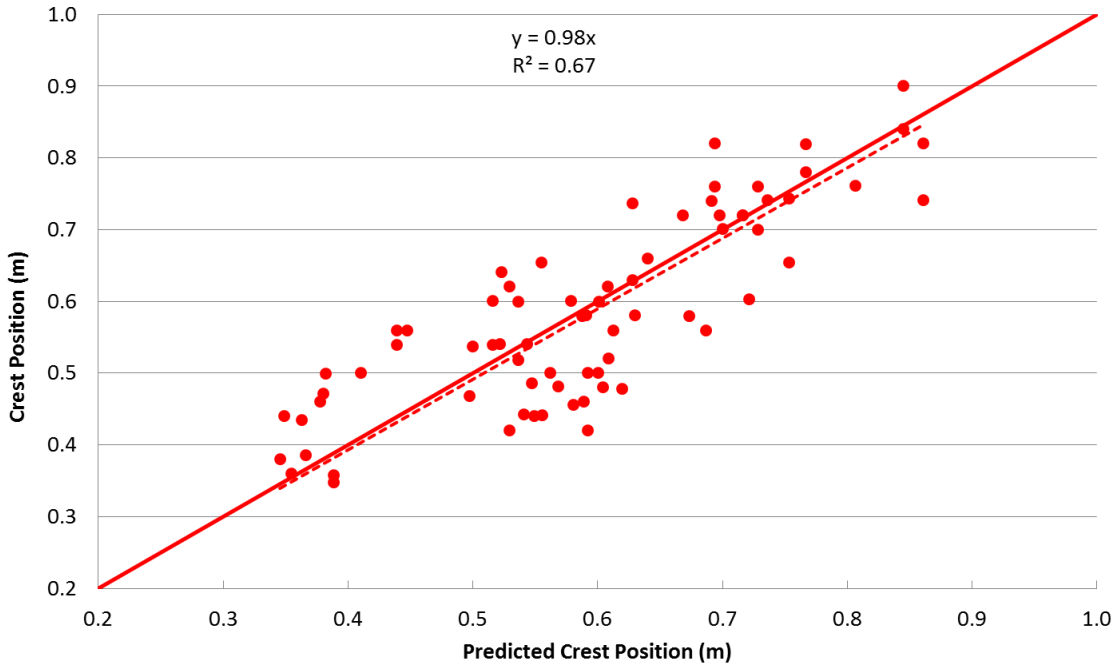

Figure 6.50: Comparison between measured crest position and predicted crest position using the newly suggested Equation (6.12).

6.6. Comparison between measured and predicted beach crest using Shingle (Powell, 1990)

Following the results discussed in the previous sections, the effect of the grain size distribution is a key parameter influencing the final response of the beach crest. The effect of the grain size has been studied and discussed in Sections 6.5.4 and 6.5.5, where post-storm beach profiles, with similar grading parameters (e.g., $D_{50,}$ D_{15} and D_{85}/ D_{15}), were compared. These comparisons have demonstrated that the crest moves upwards and shoreward as D_{50} and D_{15} decrease. In particular, the crest elevation increases with increasing internal wave set-up (a function of D_{50}), and for smaller values of D_{15} the crest moves shoreward.

To follow on from these results, a comparison between the crest elevation/position measured in the physical model and those predicted by the empirical model Shingle (Powell, 1990) was carried out and is discussed in the following sections.

The functional relationships derived by Powell (1990), for both the crest elevation (C.E.) and crest position (C.P.) are reported below:

$$C.E. = 2.86\,H_s - 62.69\left(\frac{H_s}{L_m}\right)H_s + 443.29\left(\frac{H_s}{L_m}\right)^2 H_s \tag{6.13}$$

$$C.P. = -0.23\left(\frac{H_s L_m}{D_{50}}\right)\left(\frac{H_s T_m\, g^{1/2}}{{D_{50}}^{3/2}}\right)^{-0.588} \tag{6.14}$$

where: H_s is significant wave height defined as highest one-third of wave heights, L_m is the mean wave length, T_m is the averaged wave period, D_{50} is the mean size diameter of the beach grading curve and *g* is the acceleration due to gravity. For the comparison with the model results, H_s and T_m have been replaced by H_{m0} and $T_{m0,2}$, respectively.

6.6.1. Comparison between measured and predicted crest elevation using Shingle (Powell, 1990)

Crest elevations, extracted from the physical model beach profiles, were compared with the predicted crest elevations derived by using the empirical Equation (6.13), (Powell, 1990). Results are reported in Figure 6.51, where a significant scatter in the data is observed. The scatter could be caused by the different range of input wave conditions and grain sizes used during the two

experiments, and also by the fact that in the original formulation of the crest elevation, Shingle (Powell, 1990) does not take into account the effect of the grain size diameter.

Scatter in the data shown in Figure 6.51 is reduced, as illustrated in Figure 6.52, by accounting for the effect of sediment size (D_{50}) included in the expression of the internal wave set-up parameter ($H_{m0}\ L_{m-1,0}\ /\ D_{50}$). The following modified equation, is therefore proposed to include the effect of the internal wave set-up parameter and account for different grain size diameters when predicting the beach crest elevation (C. E.) in Shingle under unimodal wave conditions:

$$C.E. = 0.8\left(2.86\,H_{m0,toe} - 62.69\frac{H_{m0,toe}}{L_{m-1,0}}H_{m0,toe} + 443.29\left(\frac{H_{m0,toe}}{L_{m-1,0}}\right)^2 H_{m0,toe}\right) + 0.00045\left(\frac{H_{m0,toe}L_{m-1,0}}{D_{50}}\right) \quad (6.15)$$

where: $H_{m0,toe}$ is the incident spectrum wave height measured at the toe of the beach, $L_{m-1,0}$ is the wave length measured at the toe of the beach, based on the spectral period $T_{m-1,0}$ and D_{50} is the mean size diameter of the beach grading curve, the parameter ($H_{m0}\ L_{m-1,0}\ /\ D_{50}$) represents the internal wave set-up.

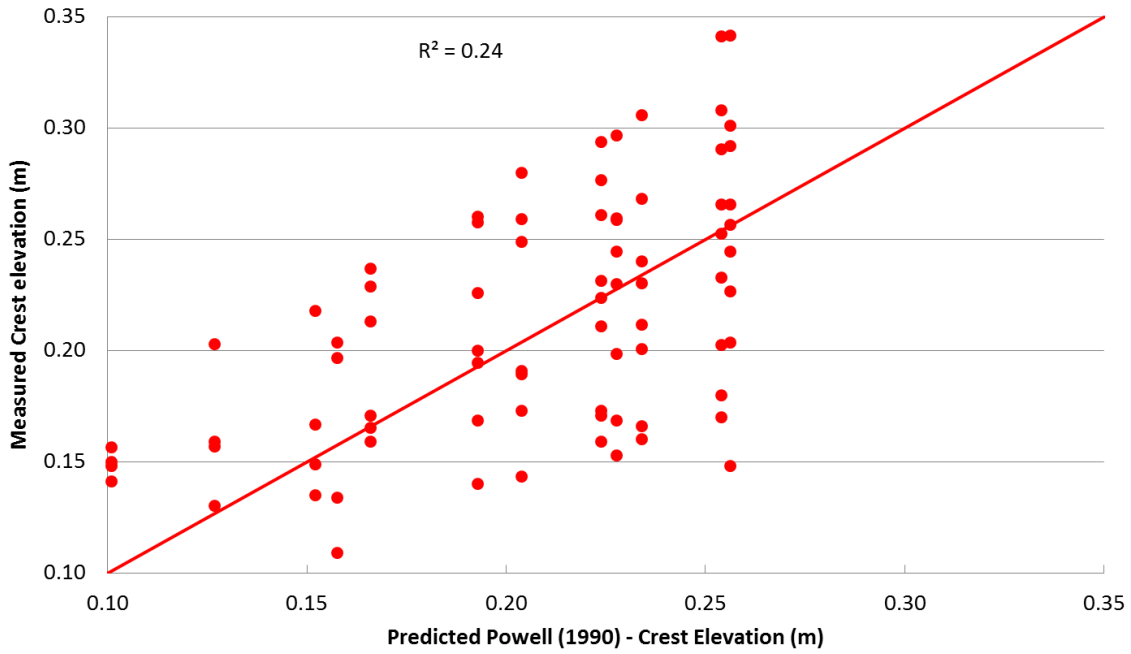

Figure 6.51: Comparison between measured and predicted crest elevation using Shingle (Powell, 1990).

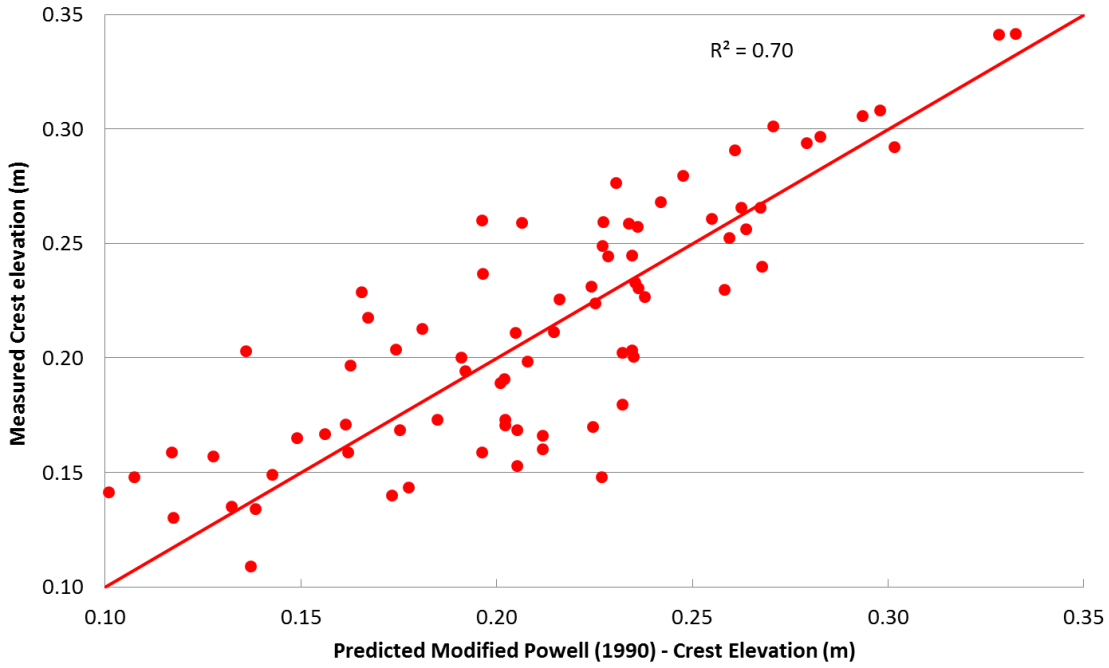

Figure 6.52: Comparison between measured and predicted crest elevations using the new modified equation of Shingle (Powell, 1990).

6.6.2. Comparison between measured and predicted crest position using Shingle (Powell, 1990)

The same approach used for the comparison on the beach crest elevation, described in the previous section, was applied to the beach crest position. Results of this comparison are shown in Figure 6.53. It can be seen that, even though the Shingle model equation to predict the position of the crest (Equation (6.14)) accounts for the effect of the internal wave set-up parameter (H_{m0} $L_{m-1,0}$ / D_{50}), the crest position is significantly underestimated. Once again this scatter could be triggered by the differences in both the wave inputs and grain sizes used during the two different studies. Also, in this case, the original Shingle model equation (Equation (6.14)) was adapted to improve the prediction of the crest position by modifying the values of the coefficients within the equation and by replacing the characteristic grain diameter D_{50} with D_{15}. The modified equation is reported as follows, and scatter in the data shown in Figure 6.53 is reduced, as illustrated in Figure 6.54:

$$C.P. = \left(\frac{H_{m0,toe} L_{m-1,0}}{D_{15}}\right) 0.135 \left(\frac{H_{m0,toe} T_{m-1,0}\, g^{1/2}}{D_{15}{}^{3/2}}\right)^{-0.45} \quad (6.16)$$

where C. P. is the crest position, $H_{m0,toe}$ is the incident significant spectral wave height measured at the toe of the beach and $L_{m-1,0}$ is the wave length measured at the toe of the beach based on the spectral period $T_{m-1,0}$, D_{15} is the diameter of stone that exceeds the 15% value of the sieve curve and *g* is the acceleration due to gravity.

In this case, rather than using the adapted equation for the prediction of the crest position (similar to what was done for the prediction of the crest elevation), we propose to predict this parameter using the best fit equation in Figure 6.50 (Equation (6.12)).

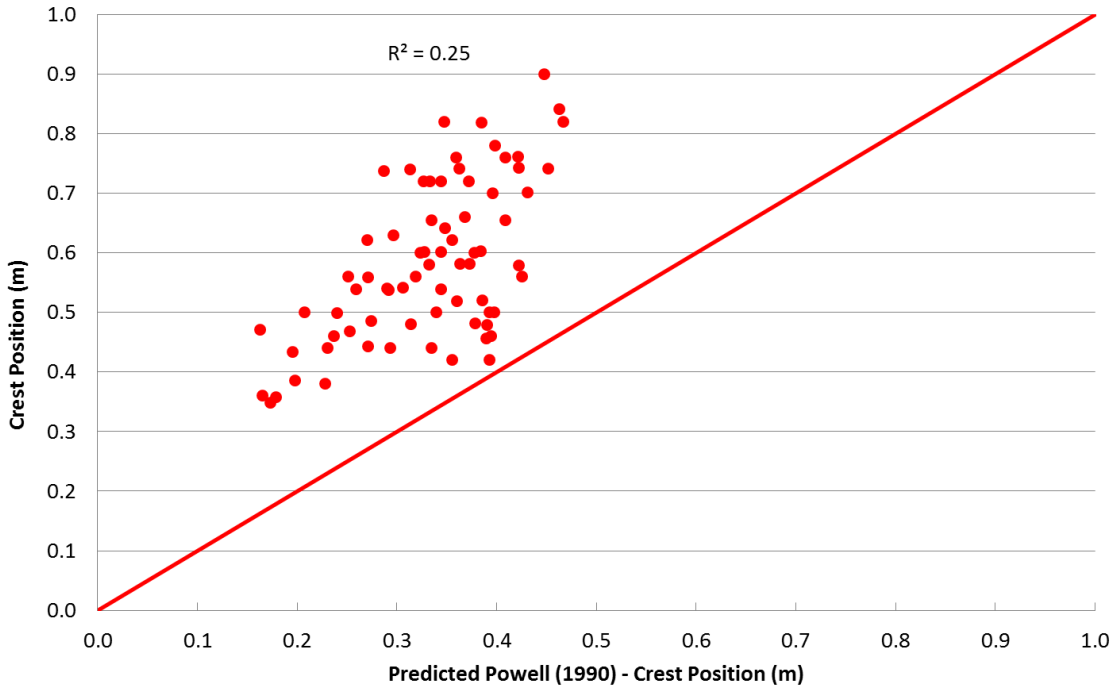

Figure 6.53: Comparison between measured and predicted crest position using Shingle (Powell, 1990) model

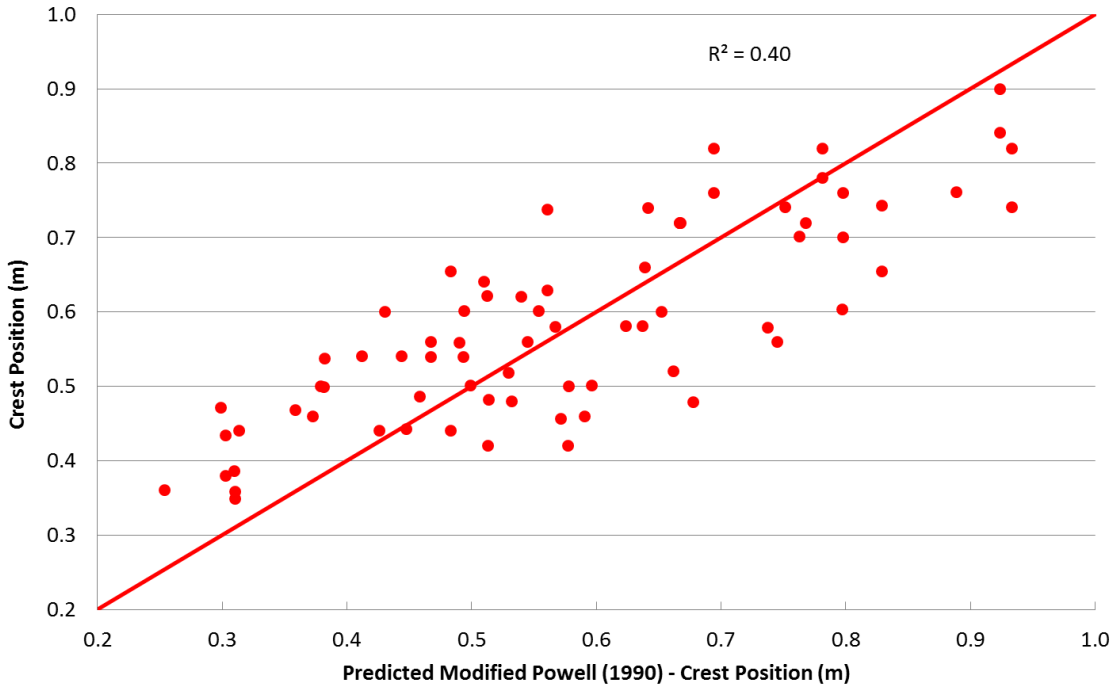

Figure 6.54: Comparison between measured and predicted crest position using a new modified equation of Shingle (Powell, 1990) model.

6.7. Comparison between measured and predicted beach profiles using a new version of the Shingle model

6.7.1. Introduction

Results from the previous sections clearly suggest that the beach crest is influenced by the grain size diameters and also indicate that the Shingle model (Powell, 1990) does not take into account the effect of grain size distribution on the beach crest response. As described in Section 6.6.1 and Section 6.6.2, new equations have been proposed to improve the prediction of both the crest elevation and position. These new expressions have been implemented in the existing Shingle (Powell, 1990) parametric model to account for different grain size diameters when predicting both the beach crest elevation and position. Hereafter the new modified version of Shingle (Powell, 1990) that accounts for different sediment sizes is referred as Shingle-S. A comparison between the measured and predicted beach profile, using Shingle-S, was carried out and is discussed in the following sections. However, before proceeding with the profile comparisons, an additional step is needed. The newly proposed equations (reported below for clarity) were derived from a 2D

physical model study (run at a scale 1 in 1) and therefore before they can be used for a prototype application a scaling correction is required. The method used to convert the model results into prototype is discussed in the next section.

$$\frac{Crest\ Position}{H_{m0,toe}} = 0.001\ \frac{L_{m-1,0}}{D_{15}} + 3.45 \tag{6.17}$$

$$C.E. = 0.8\left(2.86\,H_{m0,toe} - 62.69\frac{H_{m0,toe}}{L_{m-1,0}}H_{m0,toe} + 443.29\left(\frac{H_{m0,toe}}{L_{m-1,0}}\right)^2 H_{m0,toe}\right) + 0.00045\left(\frac{H_{m0,toe}L_{m-1,0}}{D_{50}}\right) \tag{6.18}$$

6.7.2. Scaling process

The present 2D physical model study was run at a model scale of 1 in 1, (see, Section 6.2.1) and as already extensively discussed, it investigated the effect of the interaction between wave motion and gravel beach profile evolution. A physical model study can be considered as a representation of a real-world prototype, although differences between scaled-up model and prototype measurements may results due to model and/or scale effects. In order to reproduce in prototype what was measured in the model, three main parameters needed to be scaled up: beach profile, wave condition and beach sediment sizes.

Assuming an undistorted physical model, having the same horizontal and vertical scales, the beach profiles can be scaled by using the geometric similarity between model and prototype. This means that all geometric lengths at full scale (prototype) have a constant relationship to the corresponding lengths in the model. Additionally, gravity is the predominant factor in the fluid motion, and therefore to scale-up the wave conditions, the Froude scaling law should be applied. The scaling relationships between measurements in the model and in nature can be derived from Froude's law and some important scaling relationships are:

Length = λ

Volume = λ^3

Time = $\lambda^{1/2}$

where λ is the geometric scale.

Conversely, in order to provide the most satisfactory reproduction of the prototype beach permeability, and ensure that the sediment used in the model is representative of that occurring in nature, the sediment used during the physical model can be scaled-up by using the scale criteria suggested by Yalin (1963).

In order to obtain a wide range of wave conditions and grain size particles which can be of use in prototype, the model gravel materials (Table 6.1) and wave conditions (Table 6.3) tested during this 2D physical model study were scaled up to prototype by using different scale factors (1 in 5, 1 in 10, 1 in 20 and 1 in 35). As a consequence of this scaling process, a series of different prototype wave conditions and grain size diameters was obtained. The range of wave conditions and particle sizes can be observed in Figure 6.55, where the prototype wave heights and size diameters (D_{50}) are plotted on the x-axis and y-axis, respectively.

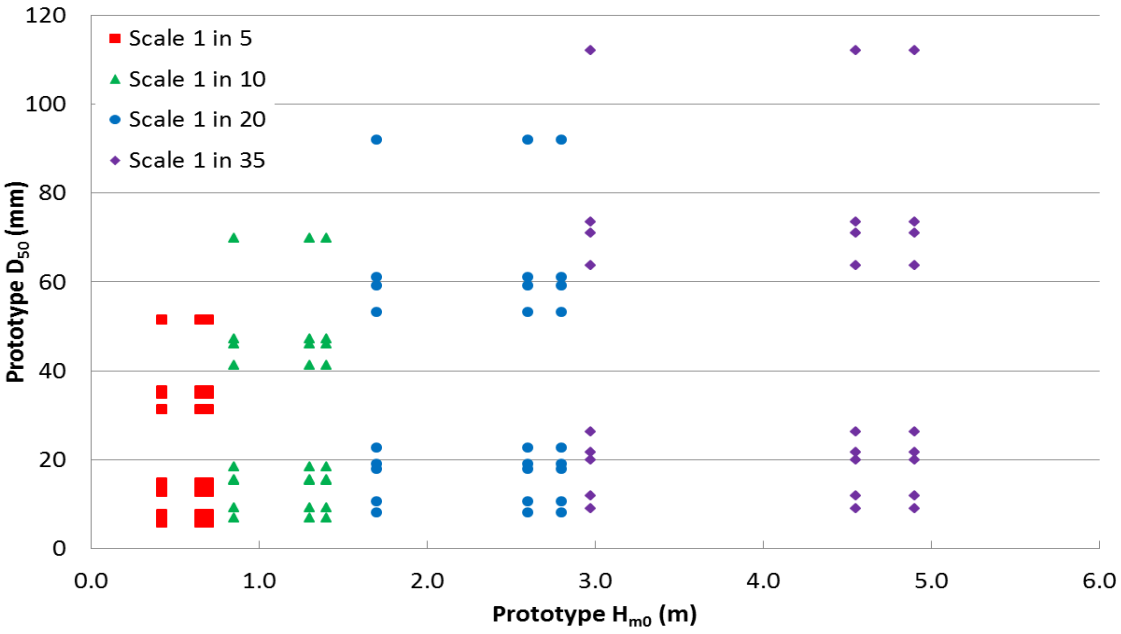

Figure 6.55: Range of the prototype wave condition and grain size diameter tested during the physical model study

The input and output model parameters (beach profiles, wave conditions and grain sizes) were scaled up to prototype using different scale factors (corresponding to geometric scales of: 1 in 5, 1 in 10, 1 in 20 and 1 in 35, but accounting for scale corrections according to Yalin (1963)). Measured (scaled up) crest elevations and positions were then fitted to the equations below, for

each geometric scale. This resulted in a range of values for coefficients C1 and C2, as a function of the geometric scale, as shown in Figure 6.56 and Figure 6.57, for C1 and C2 respectively.

$$C.E. = 0.8\left(2.86\,H_{m0,toe} - 62.69\frac{H_{m0,toe}}{L_{m-1,0}}H_{m0,toe} + 443.29\left(\frac{H_{m0,toe}}{L_{m-1,0}}\right)^2 H_{m0,toe}\right) + C1\left(\frac{H_{m0,toe}L_{m-1,0}}{D_{50}}\right) \quad (6.19)$$

$$C.P. = C2\,\frac{L_{m-1,0}}{D_{15}}H_{m0,toe} + 3.45H_{m0,toe} \quad (6.20)$$

where: *C1* and *C2* are two coefficients, which are functions of the interaction between wave action and sediment size. The values of *C1* and *C2* to be used in the equations can be extracted from the plot shown in Figure 6.58 and Figure 6.59, as described below.

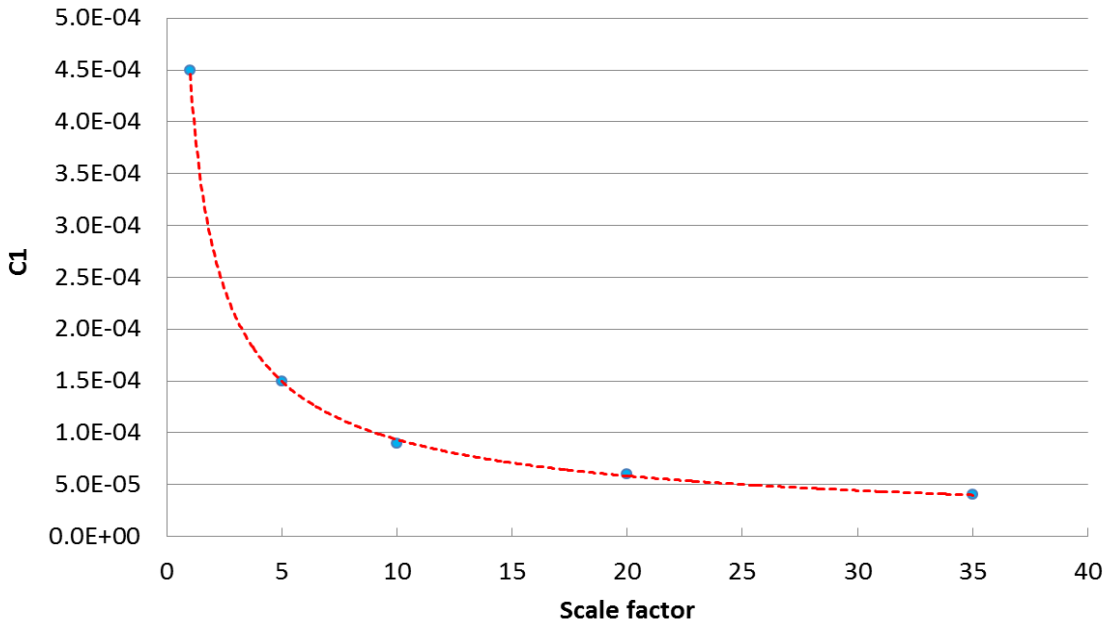

Figure 6.56: Coefficient C1 (for the crest elevation) as function of the scale factor.

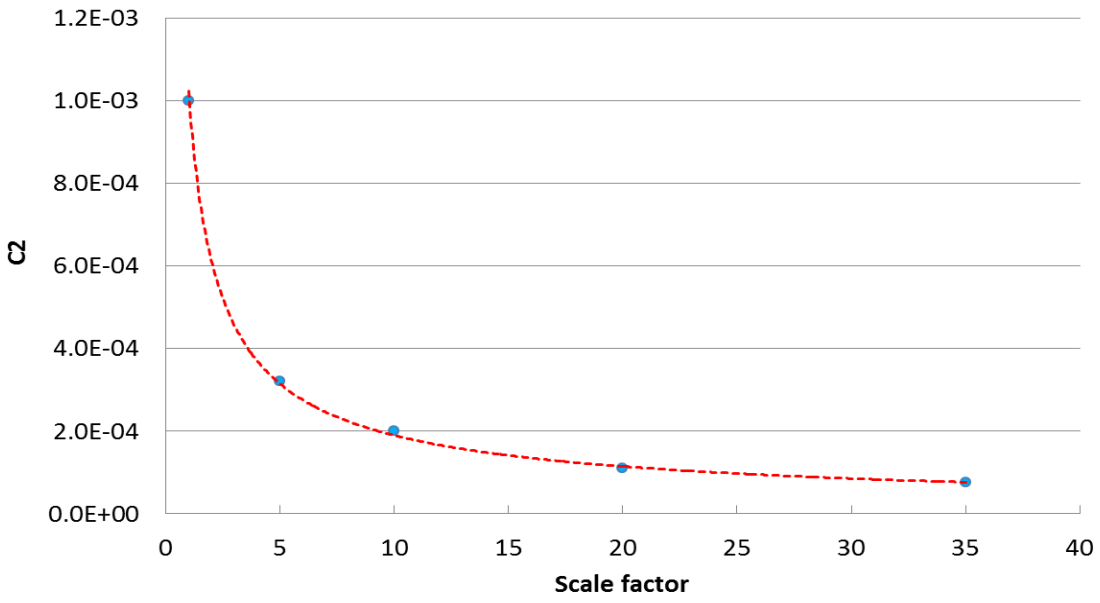

Figure 6.57: Coefficient C2 (for the crest position) as function of the scale factor.

Whilst the above provides the coefficients C1 and C2 as a function of the geometrical scale, the use of the above plots might not be straightforward for real applications where scale factor might be difficult to identify. For practical applications the user might be willing to assess coefficients C1 and C2 to match its prototype conditions in terms of both incident wave height (H_{m0}) and sediment grain size (D_{50}). To enable this, a contour map of the variation of C1 and C2 as a function of these two parameters (H_{m0} and D_{50}) was derived. This was achieved by best-fitting a surface to the sparse matrix of points in Figure 6.58 and Figure 6.59 using polynomial robust non-linear regression techniques and projecting the iso-contour onto the H_{m0} / D_{50} plane. The result of this analysis is visualised in Figure 6.58 and Figure 6.59, showing variation of C1 and C2 within the range $0m < H_{m0} < 5m$ and $5mm < D_{50} < 100mm$. These plots enable the user to estimate the best fit parameters C1 and C2 based on the values of H_{m0} and D_{50} that best match their prototype conditions/characteristics. The contours in Figure 6.58 and Figure 6.59 are derived as a 2D projection of the best fit surface having equations:

$$C1 = 0.000184 - 0.000103H_{m0} + 7.2\mathrm{E}^{-7}D_{50} + 2.14\mathrm{E}^{-5}H_{m0}^2 + 2.0\mathrm{E}^{-7}H_{m0}D_{50} - 1.45\mathrm{E}^{-8}{D_{50}}^2 - 1.4\mathrm{E}^{-6}H_{m0}^3 - 5.6\mathrm{E}^{-8}H_{m0}^2 D_{50} + 2.4\mathrm{E}^{-9}H_{m0}{D_{50}}^2 \quad (6.21)$$

$$C2 = 0.000396 - 0.000129H_{m0} + 1.76E^{-6}D_{50} + 4.37E^{-5}H_{m0}^2 + 2.5E^{-7}H_{m0}D_{50} - 3.5E^{-8}{D_{50}}^2 - 2.7E^{-6}H_{m0}^3 - 1.05E^{-7}H_{m0}^2\,D_{50} + 6.8E^{-9}H_{m0}{D_{50}}^2 \quad (6.22)$$

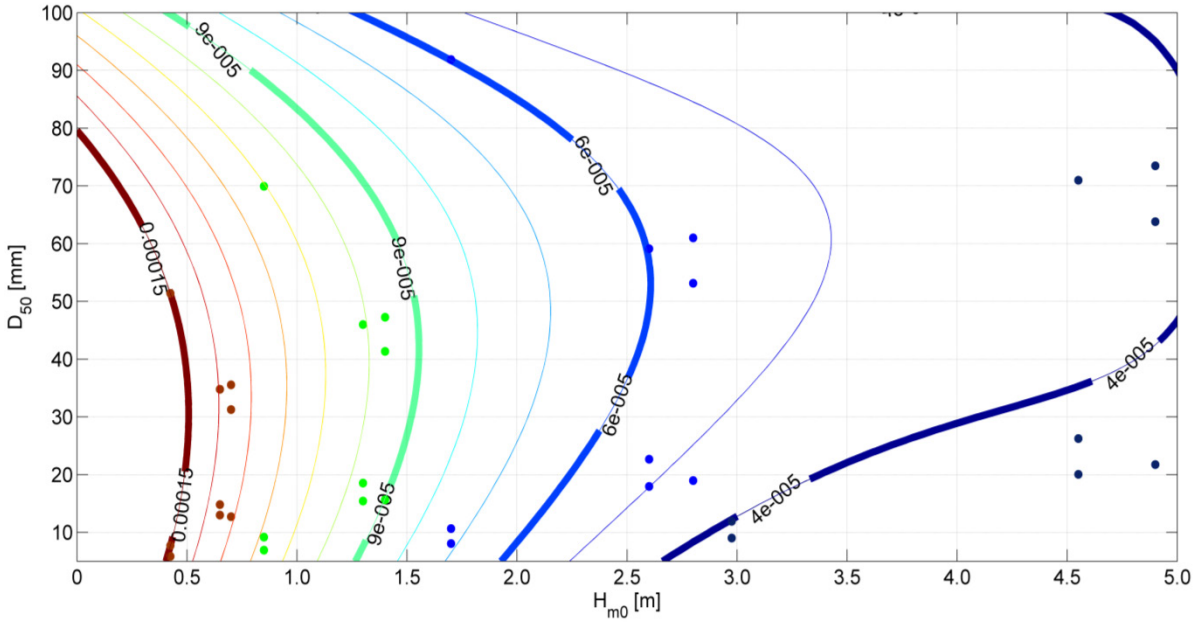

Figure 6.58: Coefficient C1 (for the crest elevation) as function of the ratio between wave height (H_{m0}) and grain size (D_{50}).

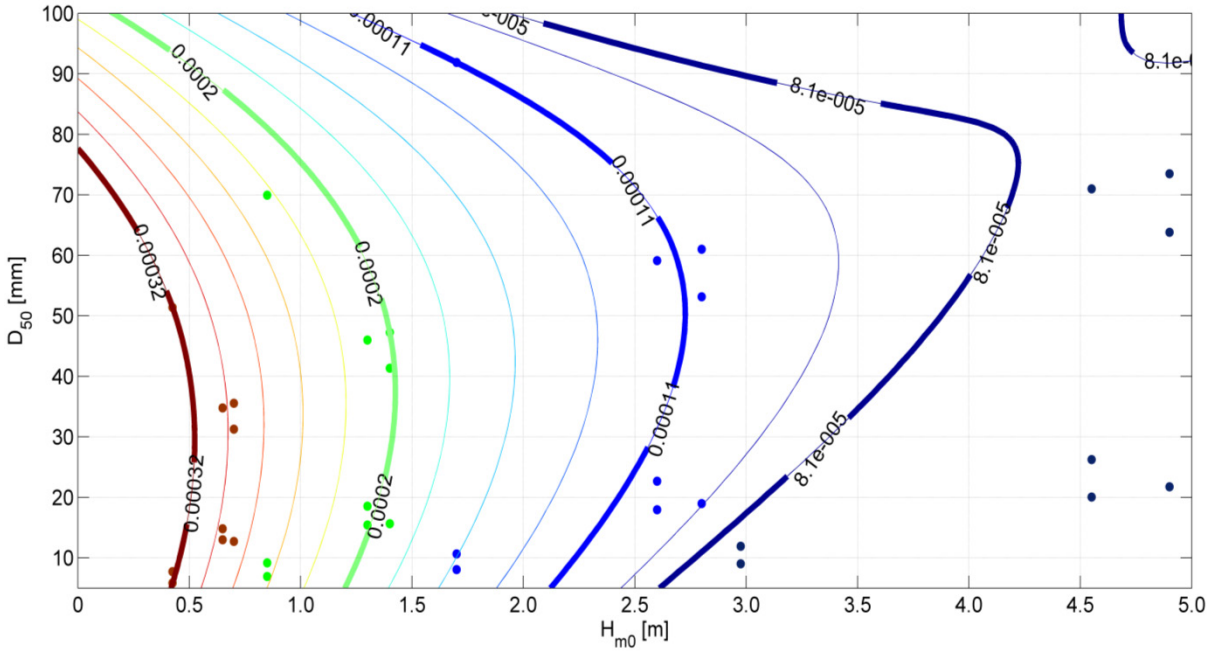

Figure 6.59: Coefficient C2 (for the crest position) as function of the ratio between wave length (H_{m0}) and grain size (D_{50})

6.7.3. Comparison between the existing Shingle (Powell, 1990) model and Shingle-S

The beach profiles measured during the 2D physical model study were scaled up to prototype and compared with the predicted profiles extracted by using both the existing Shingle model and the modified version of Shingle, Shingle-S. The latter includes the new equations (Equation (6.19) and (6.20)) for the beach crest, which account for the variation of the grain size diameters.

Some of the results of these comparisons are plotted in Figure 6.60, Figure 6.61 and Figure 6.62, where three different gravel beach materials were tested under the same prototype wave condition (H_{m0} = 5.0m and T_p = 10s) at the same constant water level (+8.0m). As expected, the influence of the different grain size diameters is observed mainly in the position and elevation of the beach crest, while the beach profile below the water level remains unaffected. The crest position and elevation increase in response to a decrease in the grain size diameter, even though they were subjected to the same wave condition. For the different gravel beach materials, the Shingle-S predicted profiles show a very good correlation with the measured results. Conversely, discrepancies are observed for the beach crest profile predicted by Shingle (Powell, 1990), where the parametric model underestimates the horizontal displacement of the beach crest. This is further confirmed in Figure 6.63, where the Shingle model significantly under predicts the elevation of the beach crest for a gravel beach material characterised by a smaller grain size and a less energetic wave condition (H_{m0} = 2.8m, T_p = 7.0s, SWL= +4.5m).

A further comparison was carried out between the gravel beach results extracted from the Large Wave Channel study (GWK, Blanco 2002) and the predicted profiles using both the Shingle and Shingle-S models. Results of these comparisons are plotted in Figure 6.64 and Figure 6.65 where the gravel beach material (D_{50} = 21mm and D_{15} = 17mm) was tested under two different wave conditions (H_{m0} = 0.9m and T_p = 4.4s; H_{m0} = 1.02m and T_p = 7.7s) at the same constant water level (+4.7m). As can be seen from these plots, both Shingle and Shingle-S show a good agreement with the large physical model measurements. Additionally, for the less energetic wave condition (Figure 6.64), the crest position is better predicted by Shingle-S model. These results suggest that the equations obtained during the present study can be used for prototype application by using the method discussed in Section 6.7.2.

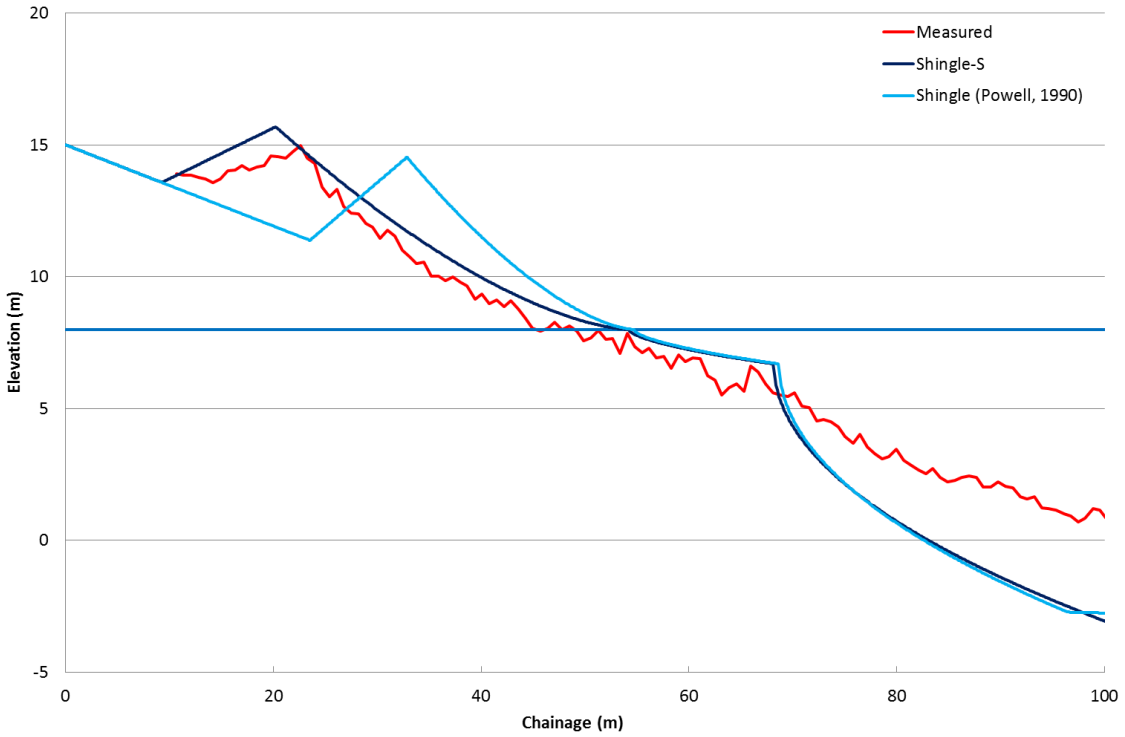

Figure 6.60: Beach profile comparison, Shingle-S, Shingle and physical model results for the wave condition (H_{m0} = 5.0m, T_p = 10s) and for the same gravel material (D_{50} = 20mm, D_{10} = 8mm)

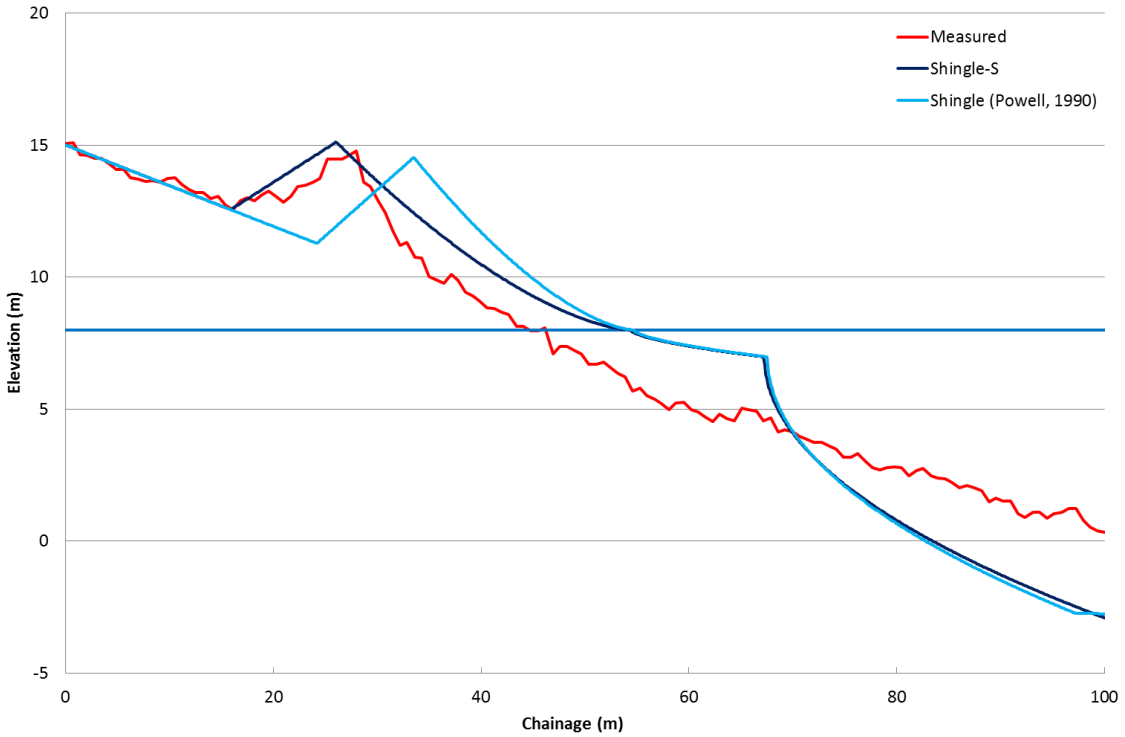

Figure 6.61: Beach profile comparison, Shingle-S, Shingle and physical model results for the wave condition (H_{m0} = 5.0m, T_p = 10s) and for the same gravel material (D_{50} = 26mm, D_{10} = 18mm)

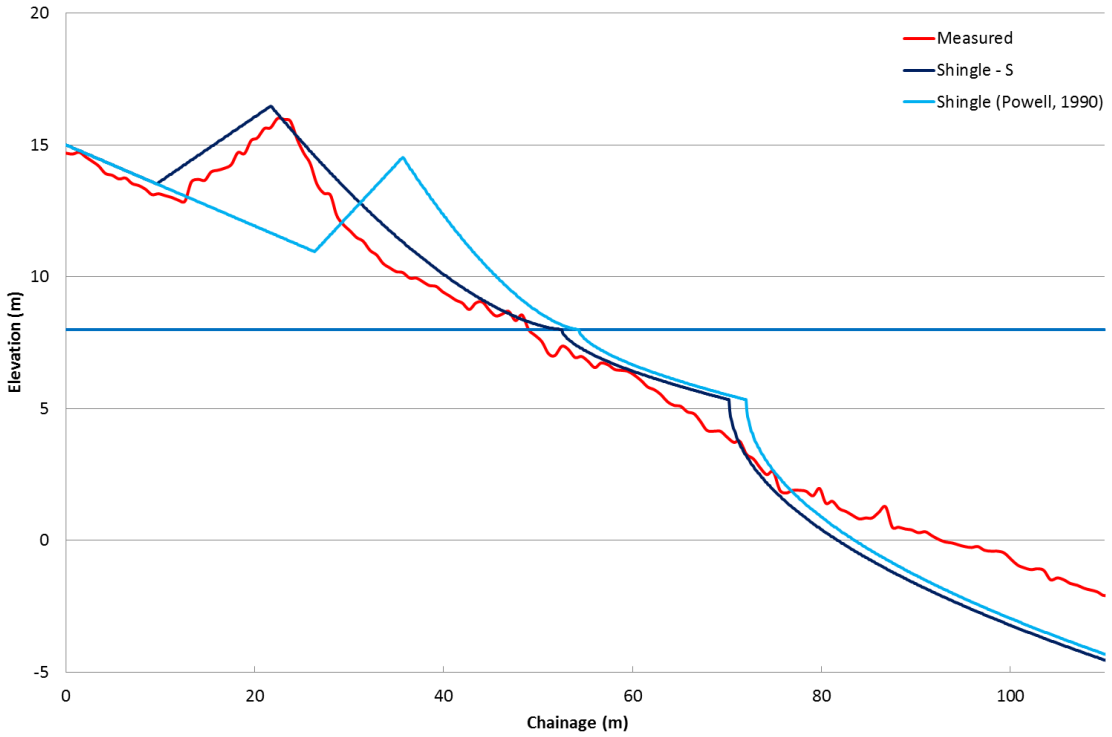

Figure 6.62: Beach profile comparison, Shingle-S, Shingle and physical model results for the wave condition (H_{m0} = 5.0m, T_p = 10s) and for the same gravel material (D_{50} = 12mm, D_{10} = 7mm)

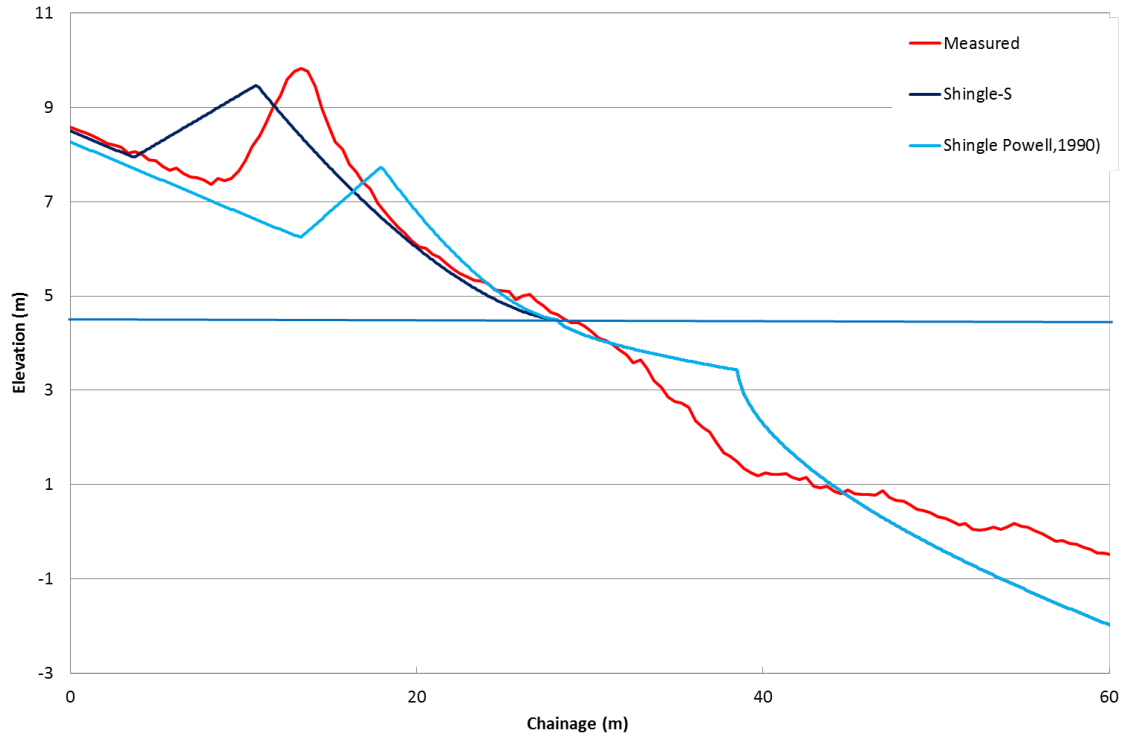

Figure 6.63: Beach profile comparison, Shingle-S, Shingle and physical model results for the wave condition (H_{m0} = 2.8m, T_p = 7.0s) and for the same gravel material (D_{50} = 9mm, D_{10} = 7mm)

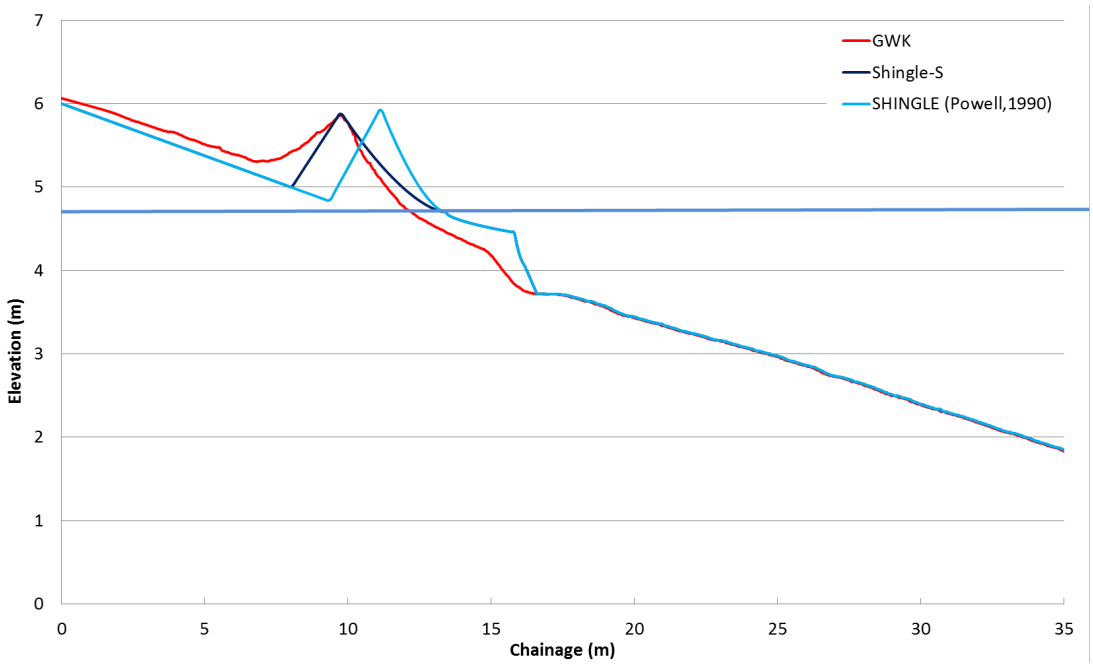

Figure 6.64: Beach profile comparison, Shingle-S, Shingle and large physical model GWK results for the wave condition (H_{m0} = 0.9m and T_p = 4.4s) and grain size characteristics (D_{50} = 21mm, D_{15} = 17mm)

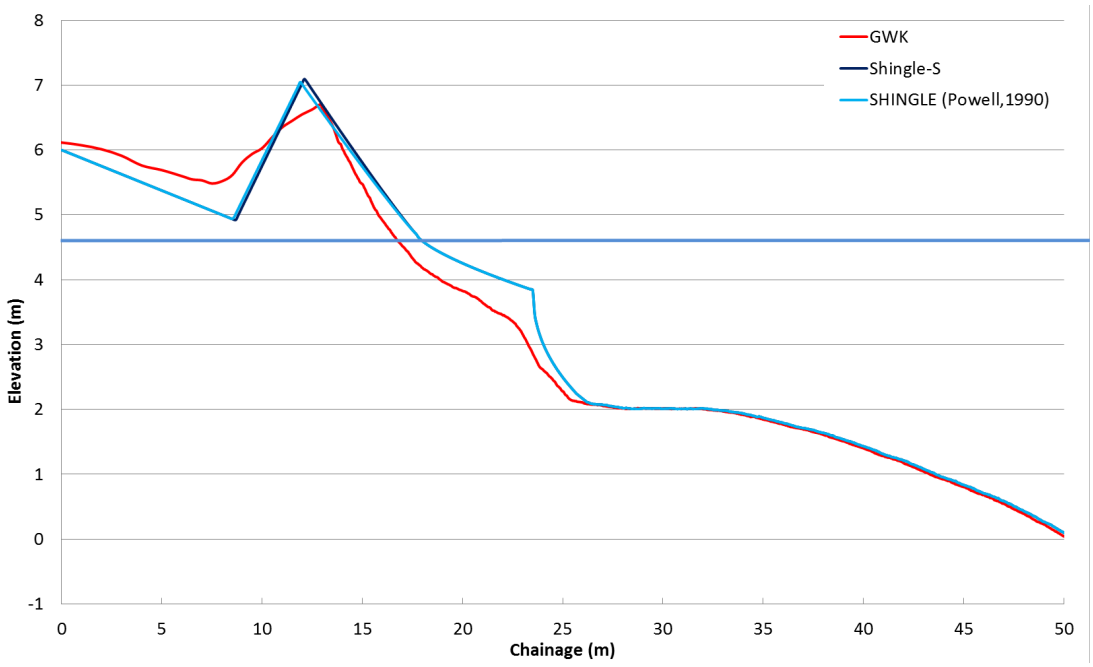

Figure 6.65: Beach profile comparison, Shingle-S, Shingle and large physical model GWK results for the wave condition (H_{m0} = 1.02m and T_p = 7.7s) and grain size characteristics (D_{50} = 21mm, D_{15} = 17mm)

6.8. Discussion

Wave transmission through a porous medium and wave damping inside a gravel material are highly complex processes and relatively little is known about their influence on gravel beaches. Results from the Large Wave Channel (GWK) (Blanco *et al.*,2006) and more recent experiments completed during the BARDEX study (Williams *et al.*, 2012) improved our understanding of the interaction between swash motion, groundwater processes and beach profile development. However, little is known about the wave–induced pore pressure and the pressure damping as a function of different sediment sizes, and how grain size distribution influences the beach profile performance.

In order to investigate how the grain size distribution influences both the wave-induced pore pressure and beach profile evolution, a 2D physical model study was carried out using ten different gravel beaches, (characterised by different grading curves, see Figure 6.5), tested under the same wave conditions (Table 6.3).

Conversely, from what was observed during the previous permeameter tests, discussed in Chapter 5, it was not only D_{15} that influenced the flow/resistance relationship but also other characteristic diameters. In particular, observations made during this study, in which more complex phenomena are involved, proved that the pore pressure attenuation was mainly influenced by the ratio D_{85}/D_{15}, which is an indication of the grading width, as discussed in Section 6.4. Specifically, for lower values of the ratio D_{85}/D_{15}, the wave-induced pore pressures decay more rapidly. Additionally, measurements on the internal wave set-up recorded during these experiments (discussed in Section 6.4.5), showed that the internal wave set-up was strongly influenced by both the incident wave conditions and the sediment characteristic D_{50}. This suggests that gravel beaches having small sediment sizes have a higher internal wave set-up (Figure 6.25) but a smaller wave-induced pore pressure than gravel beaches with higher permeability. Gravel beaches with lower permeability, therefore, are likely to be subjected to higher levels of wave run-up and internal set-up, but also to a higher energy dissipation through the porous medium. Therefore, lower permeability beaches will not be able to transmit energy through the material and result in smaller wave-induced pore pressures than beaches with high permeability. Following

these observations, new equations were suggested to predict both the damping of wave-induced pore pressure (see Equation (6.8)) and the internal wave set-up (see, Equation (6.9)), which account for the characteristic size diameters D_{15}, D_{85} and D_{50}.

The effect of pore pressure, as discussed in Chapter 2, is a key mechanism in the interaction between waves and the groundwater table, influencing the final response of the beach profile. This interaction has been widely acknowledged as a key factor in controlling the morphodynamics of coarse-grained beaches. The effect of this interaction has been studied and discussed in Section 6.5 where post-storm beach profiles, with similar grading parameters (e.g., $D_{50,}$ D_{15} and D_{85}/ D_{15}, see Table 6.2) were compared. These comparisons have demonstrated that the crest moves upwards and shoreward as D_{50} and D_{15} decrease. In particular, the crest elevation increases with increasing internal wave set-up. This can be explained by the fact that for higher values of internal wave set-up, the incoming waves are less likely to dissipate their momentum through percolation inside the beach (less volume of water percolates within the beach) and are therefore likely to trigger higher values of wave run-up and eventually transport larger volumes of sediments on the crest. Additionally, for smaller values of D_{15} the crest moves shoreward. This can be explained by the fact that, for higher values of D_{15} (higher permeability), the incoming waves are more likely to propagate inside the beach and less likely to run-up on top of the beach crest and affect its position. When plotting the measured crest elevation and position with only the wave condition parameters, a significant scatter in data was observed, suggesting that the relationship between the variables was not strong enough. This scatter has been reduced by almost 50% by accounting for the effect of the sediment size.

Based on the profile results discussed in Section 6.5, new equations were therefore derived to include the effect of the internal wave set-up parameter (H_{m0} L_{m-10}/D_{50}) and D_{15} to account for different grain size diameters when predicting both the beach crest elevation and position (see Equation (6.11) and Equation (6.12)). The measured crest positions and elevations extracted from the tested beach profiles were then compared with the values predicted by using the empirical model Shingle (Powell, 1990). Results of these comparisons are shown in Figure 6.51 and Figure 6.53, for crest elevation and crest position, respectively. Once again scatter in the data was reduced, as illustrated in Figure 6.52 and Figure 6.54, by accounting for the effect of sediment size

(D_{50} and D_{15}) and the internal wave set-up parameter (H_{m0} $L_{m-1,0}$ / D_{50}). The existing equations (Equation (6.13) and (6.14)) suggested by Powell (1990) were then modified to account for the effect of the grain size distribution. These new equations (Equation (6.19) and (6.20)) were implemented in the existing parametric Shingle model. Subsequently, the beach profiles measured during the 2D physical model study were scaled up to prototype and compared with the predicted profiles extracted by using the modified version of Shingle (Shingle-S). For different gravel beach materials the Shingle-S predicted profiles show a very good correlation with the measured results. Conversely, discrepancies are observed for the beach crest profile predicted by Shingle (Powell, 1990), where the parametric model underestimates the horizontal displacement of the beach crest.

Although these results need to be compared with prototype measurements or large scale studies, they clearly show that the beach sediment sizes exert a primary control mechanism on sediment transport processes and swash zone hydrodynamics, and that grain size parameters need to be explicitly considered in the design or assessment of shoreline management operations.

7. Beach response to bimodal sea-states

7.1. Introduction

A 2D mobile bed physical model study, using anthracite, was carried out to investigate the effect of gravel beach profile response under wave spectra characterised by swell and wind wave periods in various combinations. The results from the physical model tests have shown the significant effect of bimodal wave spectra on the beach crest erosion. The results from the physical model tests have been compared with the parametric model of Powell (1990) and numerical model, XBeach-G (McCall et al, 2014), both described in Section 2.4. Results from this comparison have shown that these models do not capture the influence of the wave spectrum shape on the beach profile response and significantly underestimate the crest erosion under bimodal wave conditions. These limitations clearly indicate that current prediction models for gravel beaches are not appropriate tools under bimodal conditions. Based on this 2D physical model study, a new parametric model, Shingle-B, for predicting gravel beach profile response has been derived and an online tool has been developed and made available on the website for the National Network of Regional Coastal Monitoring Programmes of England (http://www.channelcoast.org/shingleb/).

This chapter discusses both the design and results of the physical model and the development of the parametric model, which represents an improvement over existing models for gravel coasts, subjected to bimodal wave conditions.

7.2. Physical model study

7.2.1. Introduction

A 2D physical model study was carried out in a 100 m long, 2.0m deep and 1.8m wide wave flume at HR Wallingford. The flume is instrumented with a wave paddle that is able to generate non-repeating random sea-states to any required spectral form, including bimodal spectra. The model setup is schematised in Figure 7.1, including a 30m long flat bathymetry, leading onto two slopes of 1:30 (31m long) and 1:75 (33m long) respectively. For completeness Figure 7.1 also includes the location of the model gravel beach and the wave probes. For each wave condition, described in Section 7.2.3, an in-line array of six wave probes was used to resolve the incident wind and swell waves. These are also shown in Figure 7.1 referred to as “Offshore wave array”.

Two additional wave gauges were located at the toe of the beach and at the equivalent prototype water depth of a wave buoy (~ -13mODN).

In order to reproduce correctly the prototype beach response, the model material has to be scaled accordingly to the three main criteria described in Powell (1990). The methodology used to scale the gravel material is discussed in the following section.

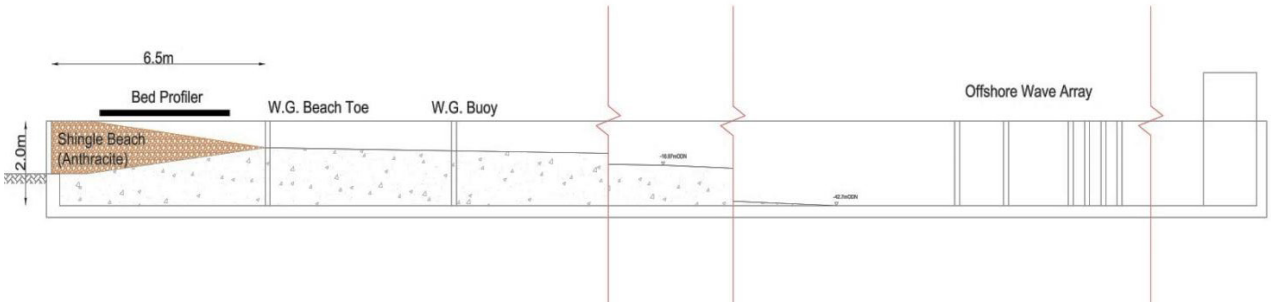

Figure 7.1: Model flume set-up. Note the flume is 100m long, 2.0m deep and 1.8m wide. A 30m long flat bathymetry, leading onto two slopes of 1:30 (31m long) and 1:75 (33m long) respectively, was built. The gravel beach extension was 6.5m long at a slope of 1 in 8. Tests were run at the same water depth of 0.43m.

7.2.2. Sediment scaling criteria

7.2.2.1 Introduction

The Froude scaling law (Fr = V/√gD, where V is a velocity, g is gravitational acceleration and L is a length, see Section 6.7.2) is usually applied to physical models where gravity is the predominant factor in the fluid motion (Hughes, 1993; HYDRALAB III, 2007). Since wave motion is essentially a gravitational phenomenon, wave models are therefore designed according to this law. In the design of a physical model of this type, the principal concern is to ensure that the main aspects of wave / beach interaction are reproduced faithfully at a scale that avoids significant scale effects. For this study, gravity waves (wind and swell) needed to be reproduced in the physical model, and so Froude scaling law was used to design the model bathymetry and model wave conditions. Conversely, for the gravel beach material a different approach was used and this is discussed here.

For the scaling of shingle beach sediment transport mechanisms, Powell (1990) stated that the model should ideally satisfy the following three main criteria:

- The permeability of the beach (Yalin, 1963), controls the beach slope.
- The relative magnitudes of the onshore and offshore motion (Dean, 1973, 1985) controls whether the beach erodes or accretes.
- The threshold of sediment motion (Komar and Miller, 1973; 1975), hence the onset of onshore-offshore transport.

A brief description of these three criteria is given below.

Yalin's (1963) study described a method for modelling gravel beaches with the correct permeability and drag forces. Since the particle-size on a shingle beach is so large, it was assumed that the direct influence of viscosity can be neglected but there remains a need to ensure similarity of the percolation through the permeable beach. Yalin (1963) stated that in an undistorted model the percolation slope must be identical to that of the prototype beach, such that the percolation slope, *J*, is given by:

$$J = \frac{k(Re_V)V^2}{gD_{10}} \qquad (7.1)$$

where k is the dimensionless permeability function of Re_v, Re_v is the voids Reynolds number (where $Re_v = V D_{10}/\nu$), V is flow velocity through the voids (m/s), g is the acceleration due to gravity (m/s^2) and D_{10} (m) is the sediment diameter at the 10% finer than percentile.

Dean (1973, 1985) suggested that sediments will move onshore or offshore depending on the parameter H_b/wT, where H_b is the wave height at breaking, T is the wave period and w is the settling velocity of the sediment particles. For $H_b/wT < 1$ then the sediment moves onshore and if $H_b/wT > 1$ then offshore movement occurs (Dean, 1973). For the correct reproduction of the relative magnitudes of onshore offshore movement, it is therefore necessary to maintain similitude of the Dean number between model and prototype (Hughes, 1993; HYDRALAB III, 2007). The particle settling velocity (w) is a function of the drag coefficient, C_D, which is a non-linear function of the sediment particle Reynolds Number, Re = wD/ν, (Soulsby, 1994).

The threshold of motion of sediments depends on the sediment characteristics. Komar and Miller's (1973, 1975) formulae may be used to define the threshold of motion for coastal mobile bed models. For oscillating flow, Komar & Miller (1973, 1975) proposed that for grain diameters greater than 0.5mm, which is usually the case for shingle beach physical models, the threshold of movement was defined with an empirical curve relating the Mobility number to the relative length, d_O/D, defined by the expression:

$$\frac{U_{max}^2}{(s-1)gD} = 0.463\pi \left(\frac{d_o}{D}\right)^{0.25} \qquad (7.2)$$

where U_{max} is the maximum orbital velocity, d_o the near bottom orbital diameter of the wave and D is the sediment diameter at the 50% finer than percentile.

Powell (1988) modified Equation (7.2), assuming a Froudian model to yield the following expression

$$\lambda^{0.75} = \lambda_{(s-1)}\lambda_D^{0.75} \qquad (7.3)$$

where λ is the geometric scale, s is the relative sediment density (ρ_s/ρ_w - 1, where ρ_s and ρ_w are the density of the sediment and water respectively) and λ_D is the ratio of model to prototype sediment

diameter. To ensure that particles in the model will begin to move under conditions similar to those that cause movement in the prototype, Powell (1988) stated that Equation (7.3) should be satisfied.

7.2.2.2 Selection of model sediment

In a coastal beach model the selection of model sediment is of primary importance. The chosen size, shape and density of the model sediment influence the sediment transport and the resulting beach profile. However, the modeller is limited by the choice of model materials, which are easily and economically available. The model sediment can be selected following two different schools of thought summarised below:

- The best model (BM), where the sediment dimensions are scaled geometrically, and the model particle density is the same of the prototype. Such a model material would be sand (specific density ~ 2650 kg/m^3).
- The light weight model (LWM), where both sediment density and sediment dimensions are different to that of the prototype. A lightweight material, such as anthracite, (density ~ 1400 kg/m^3) is an example of such a model material.

A comparison of the three scaling criteria (permeability, onshore-offshore, threshold), for a prototype material (D_{50} = 12.5mm, D_{10} = 2.8mm and density = 2650 kg/m^3), is shown in Figure 7.2. The plot shows on the x-axis a range of different geometric scales (from 1:10 to 1:40) and on the y-axis the resulting model size diameter (D_{50}). As shown in Figure 7.2, for a sand material, the scaling laws of both threshold (orange line) and onshore-offshore (blue line) laws, produce an equivalent model sediment size to the geometric scaling (dashed black line). Although, a significant difference is observed between the model sediment size obtained by using the geometric scaling and the model sediment size obtained by using Yalin's permeability criterion (green line), the latter is independent of the density of the sediment and therefore provides an equal model sediment size for both sand and anthracite (green line, Figure 7.2).

As discussed in detail in Section 2.3, the permeability is one of the most important parameters for the gravel beaches, affecting both the hydrodynamic process and the beach profile results. If the prototype material (D_{50} = 12.5mm, D_{10} = 2.8mm and density = 2650 kg/m^3) is, therefore, scaled according to the permeability criterion (green line), the resulting model particle size (y-axes) will be

larger than that given by strict Froudian scaling (geometric criterion, dashed black line). The resulting model sediment is then relatively too heavy to satisfy the remaining two criteria (onshore-offshore and threshold criteria) unless the sediment specific gravity is adjusted (anthracite, red and light-blue lines). The use of the anthracite as model material will provide a grain size larger than that indicated by geometric scaling. This will ensure that the model sediment remains inside the non-cohesive range (grain size < 0.08 mm), even at small model scales and for small sediment size within the grading curve (Ilic *et al*. 2005). Moreover the use of anthracite, i.e. lower density, will reduce the gap between the permeability criterion and the remaining two criteria (onshore-offshore and threshold). Anthracite, as lower density material, has the advantage of not being too buoyant or light, and not too dissimilar in shape to prototype sediment particles (Sharp, 1981). Anthracite is also easily available in sizes that may be used to reproduce the prototype grading curve.

During the present study, a scaling analysis was carried out to establish the model scale of the sediment size, based on the following data:

- Froude Model Scale = 25 (this was chosen to accommodate a variety of factors: the performance of the wave generator; the elevation and length of the bathymetry; the amount of material required to reproduce the beach; and, that it was deemed to be the most suitable value);
- Percolation Slope = 1:8;
- D_{50} = 12.5 mm;
- D_{10}= 2.8 mm;
- Density Fluid in prototype = 1025 kg/m^3;
- Density Fluid in model = 1000 kg/m^3;
- Density of sediment in prototype = 2650 kg/m^3 (Generic mixed beach);
- Density of sediment in model = 1400 kg/m^3 (Crushed anthracite);

Results show that, at the chosen geometric model scale of 1 in 25, for a correct reproduction of permeability, according to Yalin (1963), the sediment model scale should be equal to 1:2.25.

As discussed in Section 2.4, mobile bed modelling is very complex and it is still unclear how to scale sediments correctly (Kamphuis, 1985; Ilic *et al* 1997). The validity of the LWM approach for a mobile physical model study has been called into question from different authors (Kamphuis ,1985; 1991; Hughes, 1993; Loveless and Grant, 1995, Ilic *et al* 1997 and Ilic *et al* 2005). Ilic *et al* 1997 suggested that both the BM and the LWM do not satisfy the similitude of fall velocity, thus they do not reproduce the onshore/offshore motion correctly. Additionally, for the LWM bottom friction is distorted. The possible scale effects resulting from the use of light-weight material are the piling up of beaches due to smaller particle accelerations in the model and the relatively much higher weight of the particles in air.

Although it is known that there are scale effects in the physical modelling of sediment, it is still difficult to quantify them both for the BM and LWM models. Since Powell's parametric model is the most widely used prediction model in UK, which has been validated with both physical model and experimental data (Powell, 1993; Blanco 2003), it was decided to use the same scaling approach used by Powell (1990). As discussed in Section 2.4, the use of anthracite in reproducing correctly the behaviour of a prototype gravel beach was confirmed by the comparisons between the measured test profiles from the Großen Wellen Kanal (GWK) (Blanco, 2001) with the profile predicted by Shingle (Powell, 1990). The good agreement between predicted and measured profiles, generally indicated that the methodology previously adopted by Powell (1990) for small scale testing of shingle beaches (use of anthracite) correctly describes cross-shore profile response under normally incident wave conditions (Bradbury, 2002).

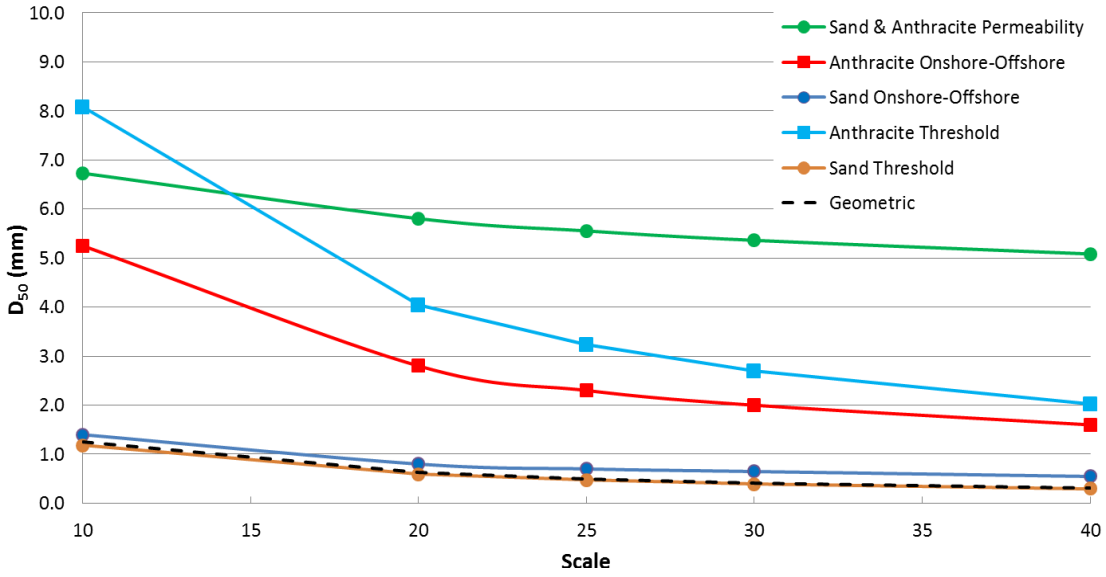

Figure 7.2: Sediment scaling criteria for both sand and anthracite, for a prototype material (D_{50}=12.5mm and D_{10}=2.8mm)

7.2.2.3 Design beach material

A study of the sediment distributions for a typical range of gravel beaches along the south coast of England, was carried out by Powell (1993). Based on Powell's work, discussed in Chapter 2, a typical grading curve (D_{50} = 12.5 mm and D_{10} = 2.8 mm) was reproduced in this study by using four distinct mixes of crushed anthracite (specific gravity of 1400 kg/m^3). The anthracite used for the beach is supplied in six different grades, which were combined to achieve the model grading curve shown in Figure 7.3 (solid line) versus the target grading curve (dashed line).

During this study, the initial beach slope, shown in Figure 7.4, was 1 in 8 (plane sloping beach) for all the test conditions. For each test, the post-storm beach profile was measured using a 2D bed profiler, which extracted the profile elevation every 20mm along the x-axis (see 6.2.1). The bed profiler was used to monitor all tests with an accuracy of ± 1.0mm vertically and horizontally (the prototype scale equivalent would be 25 mm accuracy or equivalent to one piece of large gravel).

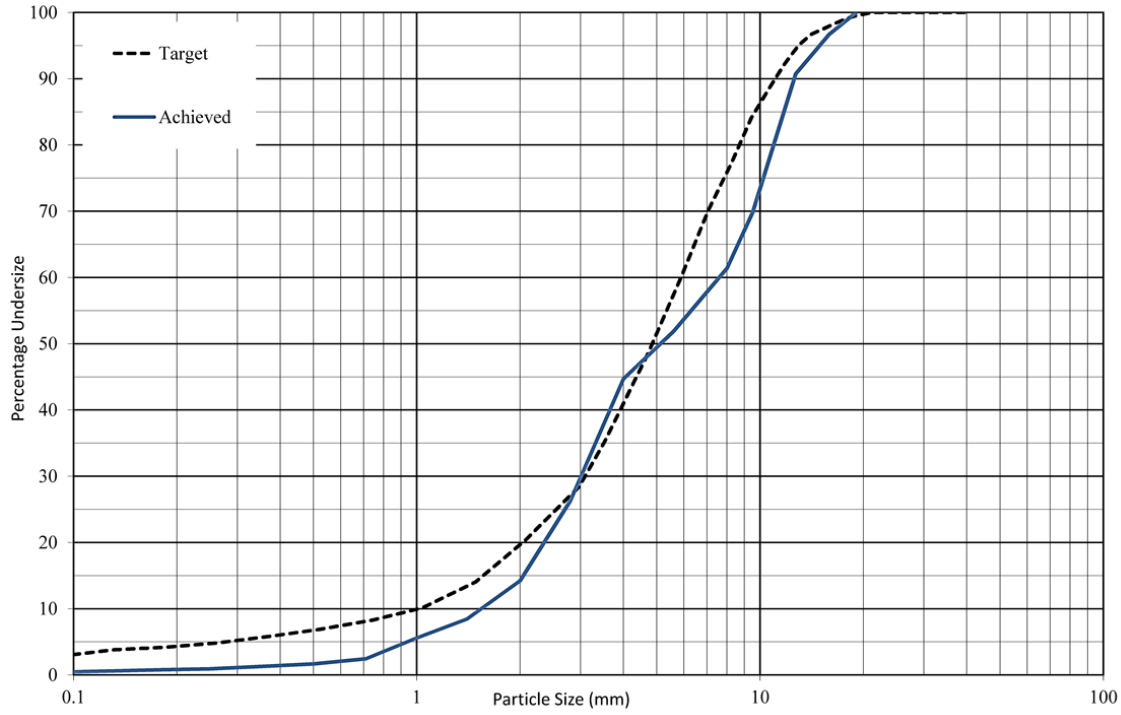

Figure 7.3: Target grading curve vs model grading curve of the anthracite used in the physical model tests

Figure 7.4: Views of the tested plain beach

7.2.3. Wave conditions during physical model study

This section summarises the wave conditions used during testing, in particular the spectral shape, the range of wave periods and how they relate to the total spectral energy (m_0). A more detailed discussion of spectral shape is given in Chapter 4. For each wave condition, an in-line array of six wave gauges was used to measure both the incident wind and swell waves. Time histories recorded by each gauge in the array were analysed spectrally to give the following parameters:

- significant incident spectral wave height, H_{m0i},
- peak wave period, T_p;
- the mean spectral wave period, $T_{m0,2}$, defined using the zeroth and 2nd moments of the frequency spectrum; and
- the spectral wave period, $T_{m-1,0}$, defined using the inverse and zeroth moments of the frequency spectrum.

The tests were carried out using a non-repeating sequence of duration equal to 3,000 times the mean spectral wind wave period, $T_{m0,2}$, of the target spectrum.

The principal purpose of this study was to cover a large range of input conditions to examine the response of shingle beaches under bimodal sea-states, where design wave attack is assumed to be normal or near normal. The wave conditions were based broadly around a framework of measured conditions (wave height, wave steepness and wave periods) derived from wave buoys at Chesil, Milford-on-Sea and Hayling Island, as described in more detail in Bradbury (2007); Bradbury and Mason (2009) and Bradbury *et al.* (2011). As discussed in Section 4.2, wave conditions were based broadly around prototype measurements covering a range of wave heights from 3.0m to 6.0m, swell periods from 15 to 25 s and wave steepness of 0.03, 0.04 and 0.05. Once the wave heights were established the wind wave periods were changed between 6 to 9 seconds to obtain the set wave steepness. Prototype wave conditions were defined at locations in 12 to15 m water depth, therefore, wave measurements in the flume were made at correspondingly equivalent depths, as shown in Figure 7.1 (wave gauge buoy).

Each test was run using both a nominal wind wave spectrum as well as its associated idealised bimodal wave spectrum. The nominal wind wave spectrum was described by wind wave spectral

shape (γ), wind wave height (H_{m0}) and wind wave period (T_p), as shown in Figure 7.5. The idealised bimodal spectrum was characterised in terms of both its wind wave and swell wave components. The bimodal wave was described by a superposition of a wind wave and a swell wave spectra, that together have the same total energy (area under the curve, [m_0]) as the nominal wind wave. The bimodal spectra is therefore predicted using the total H_{m0} (total area under the curve, [m_0]), T_{pwind}, T_{pswell} and the percentage of the swell component (Figure 7.5). The bimodal spectrum was reproduced by linearly superimposing the wind and swell spectra. For the wind spectrum a standard JONSWAP spectrum with a peak enhancement factor of γ = 3.3 was used. Conversely, for the swell spectrum, analysis of swell waves generated off New Zealand showed that the swell spectra peaks were equivalent to the JONSWAP spectra with γ = 8 ~ 9 (Goda, 1983). This is because the swell waves have a spectra confined in a narrow frequency range and thus have a peak much sharper than that of wind waves (Goda, 2010). For the swell component, even though swell waves tend to have a narrow and peaked spectrum, a JONSWAP spectrum with enhancement factor of γ = 1.5 was selected in order for the wave paddle generator to reproduce well defined wave spectra for the low frequencies, without missing information when the wave energy was shifted from high to lower frequencies. Although the peak enhancement factor (γ) is expected to have a certain degree of influence on the beach profile response, this has not been investigated in past research studies and it is outside the remit of this study.

To further investigate the effect of the spectral shape and the distribution of energy across the frequencies on the variation of beach profile response and wave run-up, each wave condition was tested with the same spectral wave energy (m_0, defined as the integral of the wave energy spectrum in the frequency domain), that is with the same spectral significant wave height H_{m0}, and subsequently subdivided to represent varying percentages of swell; including 0%, 10%, 20%, 30% and 40 %. This was obtained by starting with a nominal wind wave spectrum and then shifting part of its energy (m_0) from higher frequencies (wind waves) to lower frequencies (swell) while maintaining the value of m_0 as a constant (i.e. the total area under the wave spectrum). The resulting bimodal wave spectrum was therefore obtained by linearly superimposing the wind wave spectrum with the swell wave spectrum, the latter being a percentage (10%, 20%, 30% and 40 %) of the initial nominal wind wave spectrum.

This can be observed in Figure 7.6, where the total energy under the wave spectra is maintained, although distributed with different percentage swell components. The choice of the swell percentage was based on the work carried out by Bradbury *et al.* (2007) and the additional analysis previously discussed and summarised in Section 4.2.

Since a sea state is a stochastic process, the wave spectra resulting from the analysis of the recorded time histories showed a degree of variability from the idealised target spectra. To achieve a better correspondence between incident wave conditions and the observed beach profile response, the spectra measured during testing, rather than the target idealised ones, were used in the analysis (described in Section 7.3.7). This was achieved by fitting the idealised spectra shape, described above, to the recorded spectra obtained from each model test.

The data recorded by the array were analysed to separate the incident and reflected wave spectra, and determine the incident significant wave height, H_{m0i}. The reflection analysis is based on measuring the incident wave height at four wave gauges at known spacing and all in constant water depth. The method calculates the incident and reflected wave spectral energy and the reflection coefficient at frequencies spread over the frequency range. In order to resolve the whole range of frequency inside the bimodal wave spectrum, the reflection analysis was carried out both for wind component and swell component. Therefore an in-line array of four wave gauges was used to measure the range of frequencies for the wind component and a second in-line array of four wave gauges was used to measure the range of frequencies for the swell component. The incident wave spectra for both wind component and swell component were combined to obtain the incident bimodal wave spectrum and its relative reflection coefficient. The reflection coefficient is calculated using the following equation:

$$C_r = \sqrt{\frac{m_{0r}}{m_{0i}}} \tag{7.4}$$

where m_{0i} and m_{0r} are respectively the incident and reflected wave spectral energy.

Based on this method, four wave gauges were placed offshore for calculating the reflection coefficient and one wave gauge placed at buoy depth (13-15m) measuring the total wave height there. The total wave height (H_{Tot}) is expressed as:

$$H_{Tot} = \sqrt{H_{m0i}^2 + H_{m0r}^2} \tag{7.5}$$

and this can be expressed in terms of the incident wave height (H_{m0i}) as:

$$H_{Tot} = \sqrt{H_{m0i}^2 + C_r^2 H_{m0i}^2} \tag{7.6}$$

and so,

$$H_{m0i} = \frac{H_{Tot}}{\sqrt{1 + C_r^2}} \tag{7.7}$$

Finally, using the above equation, the incident wave height at the buoy was calculated.

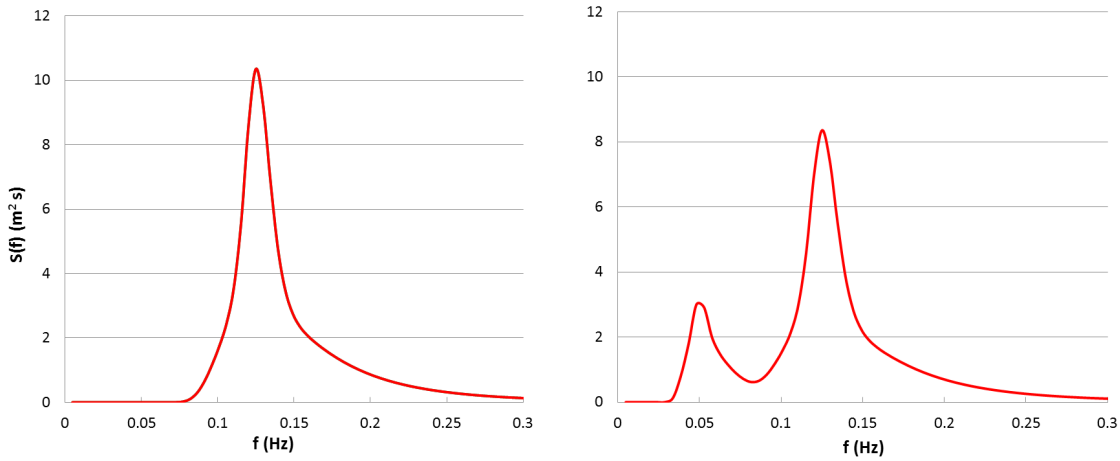

Figure 7.5: Wave spectrum: H_{m0}=4.0 m, $T_{p,wind}$=7.0 s and γ_{wind}=3.3 (left); wave spectrum: H_{m0}=4.0m, $T_{p,wind}$=7.0s, γ_{wind}=3.3, $T_{p,swell}$=15.0s, γ_{swell}=1.3, swell component=20% (right)

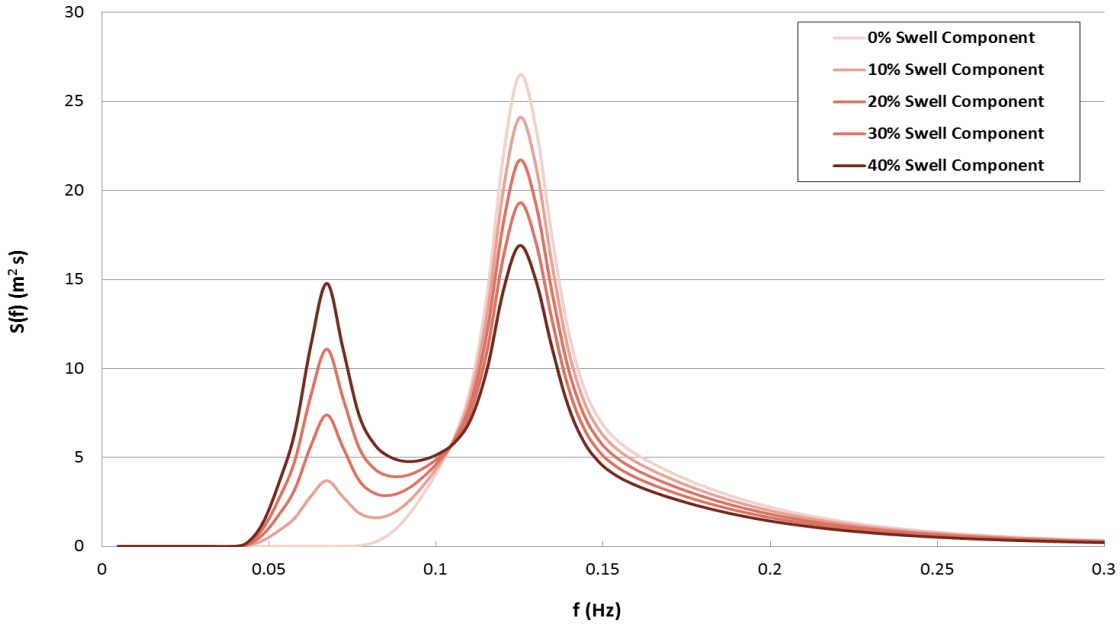

Figure 7.6: Wave spectra with different swell percentage

7.2.4. Test programme

Different combinations of wave heights and wave periods were tested at a single water depth by varying swell percentage in five steps (0-40%) on a 1 in 8 beach slope, having a difference in elevation between beach crest and beach toe of 17m (prototype). The tests were initially carried out with a single deep-water wave steepness s_{m0} = 0.05 (Test Series A) and successively extended to include reduced steepness equal to s_{m0} = 0.04 (Test Series B and D) and s_{m0} = 0.03 (Test Series C) in order to study the effect of wave steepness on the beach response. In addition, a fully developed swell sea state (unimodal wave spectra,100% swell component) was run with three different swell wave periods to investigate the profile response under these conditions (Test Series E). Table 7.1 includes information on the order in which the Test Series were run, plus brief details on: configuration of the shingle beach tested; the spectral wave heights and wave steepness; the number of waves to reach the (dynamic) equilibrium profile and the number of tests for each Test Series. All the tests were run at the same water depth of 10.75m (0.43m in model). All the test conditions run during this study are reported (in model dimensions) in Table 7.2, Table 7.3, Table 7.4, Table 7.5 and Table 7.6 for Test Series A, B, C, D and E, respectively.

Table 7.1: Test Series Programme, for each Test Series the following information is reported: configuration of the shingle beach tested; the spectral wave heights and wave steepness; the number of waves to reach the (dynamic) equilibrium profile; the number of tests for each Test Series.

Test Series	Beach Configuration	Wave Height (m)	s (-)	Number Waves	No. of Tests
A	Slope 1 in 8	3.0 - 4.5 - 5.3 - 6.0	0.053	1000 - 2000 - 3000	104
B	Slope 1 in 8	3.0	0.04	3000	20
C	Slope 1 in 8	3.0	0.03	3000	20
D	Slope 1 in 8	4.5	0.04	3000	20
E	Slope 1 in 8	3.0	0.003, 0.004 and 0.006	1000	3

Table 7.2: Wave conditions in model scale for Test Series A

Test No.	H_{m0} (m)	T_{pwind} (s)	T_{pswell} (s)	Swell (%)	No. of waves	Test Duration (s)
1	0.12	1.4	3.0	0	1000	1204
2	0.12	1.4	3.0	0	2000	2408
3	0.12	1.4	3.0	0	3000	3613
4	0.12	1.4	3.0	10	1000	1204
5	0.12	1.4	3.0	10	2000	2408
6	0.12	1.4	3.0	10	3000	3613
7	0.12	1.4	3.0	20	1000	1204
8	0.12	1.4	3.0	20	2000	2408
9	0.12	1.4	3.0	20	3000	3613
10	0.12	1.4	3.0	30	1000	1204
11	0.12	1.4	3.0	30	2000	2408
12	0.12	1.4	3.0	30	3000	3613
13	0.12	1.4	3.0	40	1000	1204
14	0.12	1.4	3.0	40	2000	2408
15	0.12	1.4	3.0	40	3000	3613
16	0.12	1.4	3.6	0	1000	1204
17	0.12	1.4	3.6	0	2000	2408
18	0.12	1.4	3.6	0	3000	3613
19	0.12	1.4	3.6	10	1000	1204
20	0.12	1.4	3.6	10	2000	2408
21	0.12	1.4	3.6	10	3000	3613
22	0.12	1.4	3.6	20	1000	1204

Test No.	H_{m0} (m)	T_{pwind} (s)	T_{pswell} (s)	Swell (%)	No. of waves	Test Duration (s)
23	0.12	1.4	3.6	20	2000	2408
24	0.12	1.4	3.6	20	3000	3613
25	0.12	1.4	3.6	30	1000	1204
26	0.12	1.4	3.6	30	2000	2408
27	0.12	1.4	3.6	30	3000	3613
28	0.12	1.4	3.6	40	1000	1204
29	0.12	1.4	3.6	40	2000	2408
30	0.12	1.4	3.6	40	3000	3613
31	0.12	1.4	4.2	0	1000	1204
32	0.12	1.4	4.2	0	2000	2408
33	0.12	1.4	4.2	0	3000	3613
34	0.12	1.4	4.2	10	1000	1204
35	0.12	1.4	4.2	10	2000	2408
36	0.12	1.4	4.2	10	3000	3613
37	0.12	1.4	4.2	20	1000	1204
38	0.12	1.4	4.2	20	2000	2408
39	0.12	1.4	4.2	20	3000	3613
40	0.12	1.4	4.2	30	1000	1204
41	0.12	1.4	4.2	30	2000	2408
42	0.12	1.4	4.2	30	3000	3613
43	0.12	1.4	4.2	40	1000	1204
44	0.12	1.4	4.2	40	2000	2408
45	0.12	1.4	4.2	40	3000	3613
46	0.12	1.4	5.0	0	1000	1204
47	0.12	1.4	5.0	0	2000	2408
48	0.12	1.4	5.0	0	3000	3613
49	0.12	1.4	5.0	10	1000	1204
50	0.12	1.4	5.0	10	2000	2408
51	0.12	1.4	5.0	10	3000	3613
52	0.12	1.4	5.0	20	1000	1204
53	0.12	1.4	5.0	20	2000	2408
54	0.12	1.4	5.0	20	3000	3613
55	0.12	1.4	5.0	30	1000	1204
56	0.12	1.4	5.0	30	2000	2408
57	0.12	1.4	5.0	30	3000	3613
58	0.12	1.4	5.0	40	1000	1204
59	0.12	1.4	5.0	40	2000	2408
60	0.12	1.4	5.0	40	3000	3613

Test No.	H_{m0} (m)	T_{pwind} (s)	T_{pswell} (s)	Swell (%)	No. of waves	Test Duration (s)
61	0.18	1.8	3.0	0	3000	4425
62	0.18	1.8	3.0	10	3000	4425
63	0.18	1.8	3.0	20	3000	4425
64	0.18	1.8	3.0	30	3000	4425
65	0.18	1.8	3.0	40	3000	4425
66	0.18	1.8	3.6	0	3000	4425
67	0.18	1.8	3.6	10	3000	4425
68	0.18	1.8	3.6	20	3000	4425
69	0.18	1.8	3.6	30	3000	4425
70	0.18	1.8	3.6	40	3000	4425
71	0.18	1.8	4.2	0	3000	4425
72	0.18	1.8	4.2	10	3000	4425
73	0.18	1.8	4.2	20	3000	4425
74	0.18	1.8	4.2	30	3000	4425
75	0.18	1.8	4.2	40	3000	4425
76	0.18	1.8	5.0	0	3000	4425
77	0.18	1.8	5.0	10	3000	4425
78	0.18	1.8	5.0	20	3000	4425
79	0.18	1.8	5.0	30	3000	4425
80	0.18	1.8	5.0	40	3000	4425
81	0.24	2.0	3.0	0	3000	5109
82	0.24	2.0	3.0	10	3000	5109
83	0.24	2.0	3.0	20	3000	5109
84	0.24	2.0	3.0	30	3000	5109
85	0.24	2.0	3.0	40	3000	5109
86	0.24	2.0	3.6	0	3000	5109
87	0.24	2.0	3.6	10	3000	5109
88	0.24	2.0	3.6	20	3000	5109
89	0.24	2.0	3.6	30	3000	5109
90	0.24	2.0	3.6	40	3000	5109
91	0.24	2.0	4.2	0	3000	5109
92	0.24	2.0	4.2	10	3000	5109
93	0.24	2.0	4.2	20	3000	5109
94	0.24	2.0	4.2	30	3000	5109
95	0.24	2.0	4.2	40	3000	5109
96	0.24	2.0	5.0	0	3000	5109
97	0.24	2.0	5.0	10	3000	5109
98	0.24	2.0	5.0	20	3000	5109

Test No.	H_{m0} (m)	T_{pwind} (s)	T_{pswell} (s)	Swell (%)	No. of waves	Test Duration (s)
99	0.24	2.0	5.0	30	3000	5109
100	0.24	2.0	5.0	40	3000	5109
101	0.21	1.9	3.6	0	3000	4779
102	0.21	1.9	3.6	10	3000	4779
103	0.21	1.9	3.6	20	3000	4779
104	0.21	1.9	3.6	30	3000	4779

Table 7.3: Wave conditions in model scale for Test Series B

Test No.	H_{m0} (m)	T_{pwind} (s)	T_{pswell} (s)	Swell (%)	No. of waves	Test Duration (s)
1	0.12	1.7	3.0	0	3000	4159
2	0.12	1.7	3.0	10	3000	4159
3	0.12	1.7	3.0	20	3000	4159
4	0.12	1.7	3.0	30	3000	4159
5	0.12	1.7	3.0	40	3000	4159
6	0.12	1.7	3.6	0	3000	4159
7	0.12	1.7	3.6	10	3000	4159
8	0.12	1.7	3.6	20	3000	4159
9	0.12	1.7	3.6	30	3000	4159
10	0.12	1.7	3.6	40	3000	4159
11	0.12	1.7	4.2	0	3000	4159
12	0.12	1.7	4.2	10	3000	4159
13	0.12	1.7	4.2	20	3000	4159
14	0.12	1.7	4.2	30	3000	4159
15	0.12	1.7	4.2	40	3000	4159
16	0.12	1.7	5.0	0	3000	4159
17	0.12	1.7	5.0	10	3000	4159
18	0.12	1.7	5.0	20	3000	4159
19	0.12	1.7	5.0	30	3000	4159
20	0.12	1.7	5.0	40	3000	4159

Table 7.4: Wave conditions in model scale for Test Series C

Test No.	H_{m0} (m)	T_{pwind} (s)	T_{pswell} (s)	Swell (%)	No. of waves	Test Duration (s)
1	0.12	1.9	3.0	0	3000	4802
2	0.12	1.9	3.0	10	3000	4802
3	0.12	1.9	3.0	20	3000	4802
4	0.12	1.9	3.0	30	3000	4802
5	0.12	1.9	3.0	40	3000	4802
6	0.12	1.9	3.6	0	3000	4802

Test No.	H_{m0} (m)	T_{pwind} (s)	T_{pswell} (s)	Swell (%)	No. of waves	Test Duration (s)
7	0.12	1.9	3.6	10	3000	4802
8	0.12	1.9	3.6	20	3000	4802
9	0.12	1.9	3.6	30	3000	4802
10	0.12	1.9	3.6	40	3000	4802
11	0.12	1.9	4.2	0	3000	4802
12	0.12	1.9	4.2	10	3000	4802
13	0.12	1.9	4.2	20	3000	4802
14	0.12	1.9	4.2	30	3000	4802
15	0.12	1.9	4.2	40	3000	4802
16	0.12	1.9	5.0	0	3000	4802
17	0.12	1.9	5.0	10	3000	4802
18	0.12	1.9	5.0	20	3000	4802
19	0.12	1.9	5.0	30	3000	4802
20	0.12	1.9	5.0	40	3000	4802

Table 7.5: Wave conditions in model scale for Test Series D

Test No.	H_{m0} (m)	T_{pwind} (s)	T_{pswell} (s)	Swell (%)	No. of waves	Test Duration (s)
1	0.18	2.0	3.0	0	3000	5093
2	0.18	2.0	3.0	10	3000	5093
3	0.18	2.0	3.0	20	3000	5093
4	0.18	2.0	3.0	30	3000	5093
5	0.18	2.0	3.0	40	3000	5093
6	0.18	2.0	3.6	0	3000	5093
7	0.18	2.0	3.6	10	3000	5093
8	0.18	2.0	3.6	20	3000	5093
9	0.18	2.0	3.6	30	3000	5093
10	0.18	2.0	3.6	40	3000	5093
11	0.18	2.0	4.2	0	3000	5093
12	0.18	2.0	4.2	10	3000	5093
13	0.18	2.0	4.2	20	3000	5093
14	0.18	2.0	4.2	30	3000	5093
15	0.18	2.0	4.2	40	3000	5093
16	0.18	2.0	5.0	0	3000	5093
17	0.18	2.0	5.0	10	3000	5093
18	0.18	2.0	5.0	20	3000	5093
19	0.18	2.0	5.0	30	3000	5093
20	0.18	2.0	5.0	40	3000	5093

Table 7.6: Wave conditions in model scale for Test Series E

Test No.	H_{m0} (m)	T_{pwind} (s)	T_{pswell} (s)	Swell (%)	No. of waves	Test Duration (s)
1	0.12	-	3.6	100	1000	3020
2	0.12	-	4.2	100	1000	3524
3	0.12	-	5.0	100	1000	4195

7.2.5. Physical model results

7.2.5.1 Introduction

At the start of the testing programme, for each wave condition, the wave generation used non repeating wave sequences, with durations equal to 1000, 2000 and 3000 times the wind mean wave period, $T_{m0,2,wind}$, of the target spectrum. Beach profiles were measured following each sequence of 1000 waves, with the intention to continue each test until dynamic equilibrium had been reached. Results of the first set of tests showed that after 2000 waves the profile did not change significantly (see Figure 7.7) and that continuing the tests until 3000 waves lead to no discernible difference. To be also consistent with the study described in Chapter 6, it was decided therefore, to run for 3000 waves for the remaining tests, and only profile them once at the end of testing. This is in agreement with the results obtained by Powell (1990), where it was observed that approximately 80% of the total volumetric change occurred during the first 500 waves.

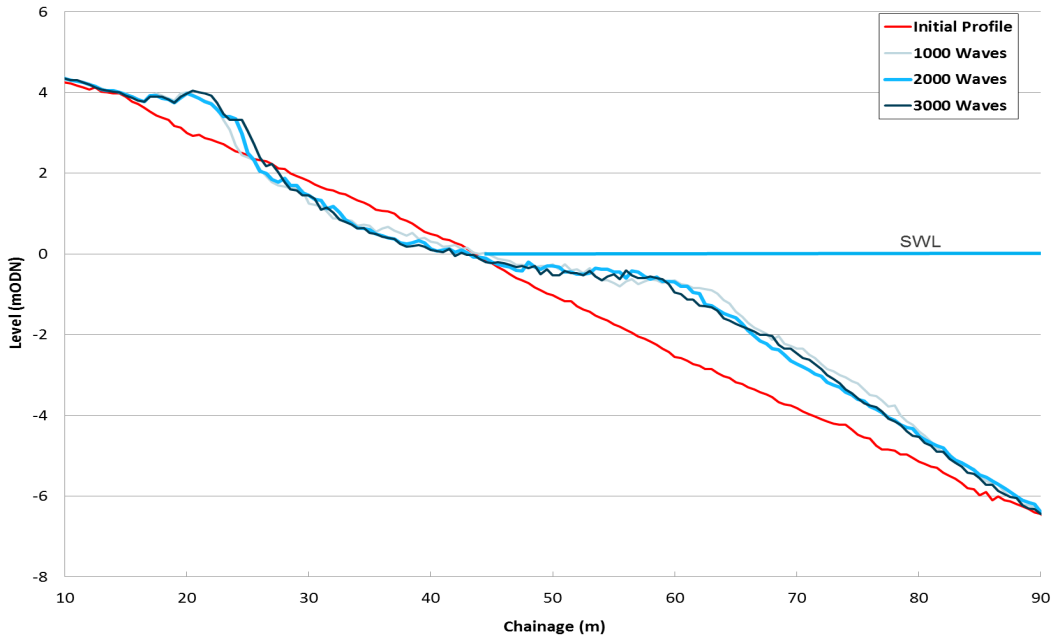

Figure 7.7: Profile development for a wave condition run for a duration of 1000, 2000 and 3000 waves (based on $T_{m0,2}$) in the physical model tests

A random sea state can be considered as a stochastic process varying randomly with time (Goda, 2010). A given sea-state, defined in terms of its wave spectrum, corresponds to an infinite number of time series having the same spectral energy (Goda, 2010). In order to investigate the effect of the time series sequence on the final beach profile response, four different random time series (with the same wave spectrum) were generated using different phase shift between different wave component frequencies. Example results of this procedure is shown in Figure 7.8 comparing the beach profiles obtained using four energy-equivalent random time series. Analysis of the final beach profiles showed that the crest position and the lower limit of the profile developments are relatively insensitive to the sequence of the time series. However, the beach profile within the surf-zone is, as expected, slightly more sensitive to the sequence of the wave trains. This can be explained because within the surf-zone waves break, and therefore non-linear effects can significantly influence the sediment transport. This part of the beach profile is very dynamic, changing almost wave by wave so that even the last sequence of waves affects the final profile. As a consequence, the final beach profile shows a small variability within the surf-zone, possibly due to the effect of the final sequence of waves. Based on these observations, throughout this study it was decided to run different time series for each test condition. The ability to generate long non-repeating time series is of great importance when testing models have a non-linear response, as in this case.

During the model study, the run-up was measured using a laser line and a bed profiler (Figure 7.9). More details on the measurements and results can be found in Polidoro *et al*, 2013 and 2014. The proposed formula (Polidoro *et al*, 2013) discussed in Section 2.3.6, is function of the spectral wave period parameters and also included the effect of wave set-up. Physical model results showed a good agreement between predicted and measured wave run-up for field and laboratory measurements (Polidoro *et al*, 2013 and 2014). This result further confirmed the use of anthracite in reproducing correctly the behaviour of a prototype gravel beach.

Overall, almost 200 profiles were recorded, and it is therefore not possible to present all of them in this section. Instead, results are presented where they assist understanding of the main outcomes or where it is necessary to illustrate trends or specific aspects of interest.

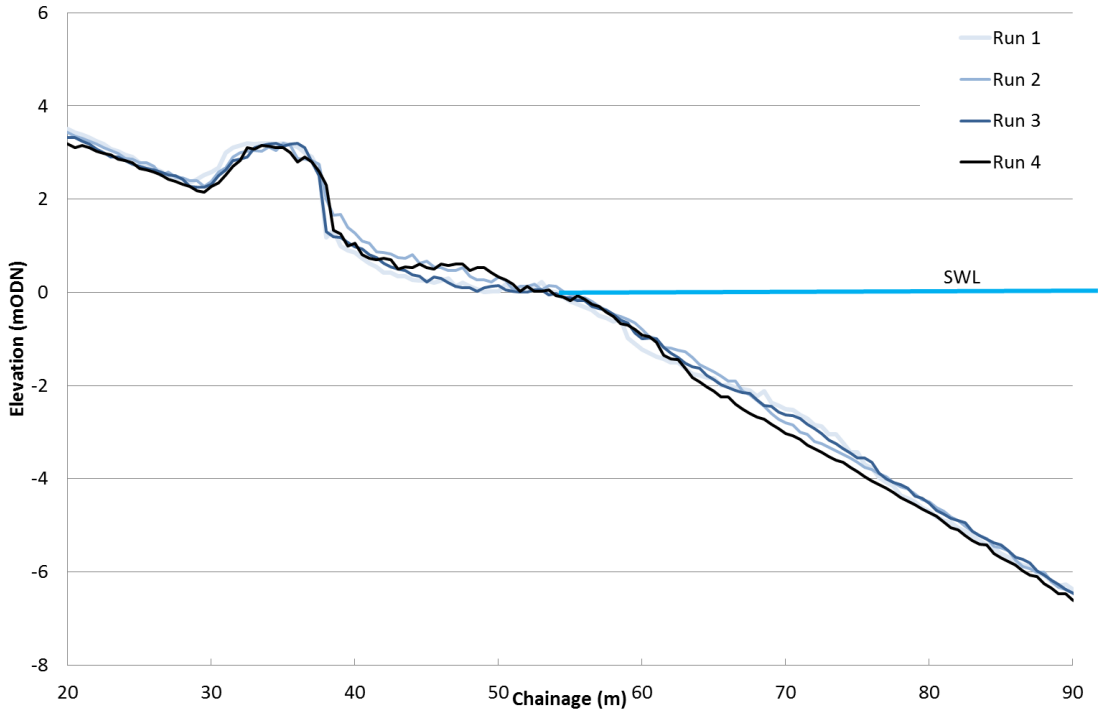

Figure 7.8: Effect of varying time series sequence on beach profile response in the physical model tests

Figure 7.9: Laser line (right) and bed profiler (left) used to measure wave run up

7.2.5.2 Swell component effect on beach profile response

The effect of the swell percentage on the beach profile is plotted in Figure 7.11, showing profiles corresponding to wave conditions having the same swell wave period ($T_{p,swell}$ =18s), and same wave height (H_{m0} = 3.0m), but different swell components. The influence of the swell component was observed mainly in the upper portion of the profile; in particular, the width of the surf-zone increased significantly in response to an increase in swell percentage. This can be explained when considering the interaction of wind and swell waves on the final beach profile evolution. During the wave motion, long swell waves run up the beach and a significant volume of water infiltrates into the beach. The amount of the water that infiltrates and it is retained by the beach, is also a function of the beach permeability i.e., the beach grain size distribution (which was outside the remit of this study). This will raise the groundwater elevation, which is a function of both wave conditions and sediment sizes and obviously the tidal level, which was not considered within these experiments. If the beach is almost saturated with water, during the backwash a thick layer of water within the swash zone will be present (see Figure 7.10). The next incoming wave will surf on top of this water layer and, as the beach is now saturated, part of its energy cannot be dissipated within the beach (see swash-swash interaction phenomenon in Section 2.3.1). Most of the wave energy is, therefore, used to run up to the top of the crest and push the beach crest landward. This phenomenon can be observed in Figure 7.10, where a breaking wave can be seen running on a beach already saturated with water. Additionally, as described in Section 2.3, the transport of sediment within the swash zone is not only influenced by wave, beach slope, and sediment characteristics, but also by the secondary influence of swash infiltration / exfiltration (i.e., the vertical flow of water into and out of a permeable beachface (Turner and Masselink, 1998). Over an uprush-backwash cycle, seepage forces change the effective weight of the uppermost sediments and the resulting shear stresses at the bed are altered. It is the combined effect of these two (opposing) mechanisms that further influence the net sediment transport rates across the beachface. The results observed during this study are consistent with the general conclusion of Turner and Masselink, 1998, in which the net upslope transport of sediment is significantly enhanced by swash infiltration-exfiltration across a saturated beachface. Moreover, accordingly to Erikson *et al*. (2005) and Blenkinsopp *et al*. (2011), a swash-swash interaction phenomenon (see

Section 2.3.1) enhances the turbulence in the swash motion and influences the maximum run-up length and the swash duration, inducing larger onshore transport rates.

The beach profile results (Figure 7.11) showed that the beach crest experienced a horizontal displacement in response to a shift of energy from high to low frequency. Interestingly, results demonstrated that an increase of swell component to more than 20% (e.g. 30-40%) had a more significant impact on the vertical displacement of the beach crest rather than in its horizontal displacement. This suggests that an increased swell percentage (> 20%), will trigger an increase in crest elevation, rather than a horizontal displacement of the beach crest. It also suggests that there is an ultimate limit to the landward extension of the beach profile. Similar trends were also observed for the other swell-wave periods tested (15s, 21s and 25s). This can be also explained by assuming, that for the same wave height and swell wave period, an increase of swell component to more than 20% does not correspond to an increment of the degree of saturation within the beach. Therefore the influence of swash infiltration / exfiltration is not significant to further contribute to a landward displacement of the crest.

Figure 7.10: Beach saturated by the swell waves and wind waves surfing on top of the sheet of water created by the previous swell wave

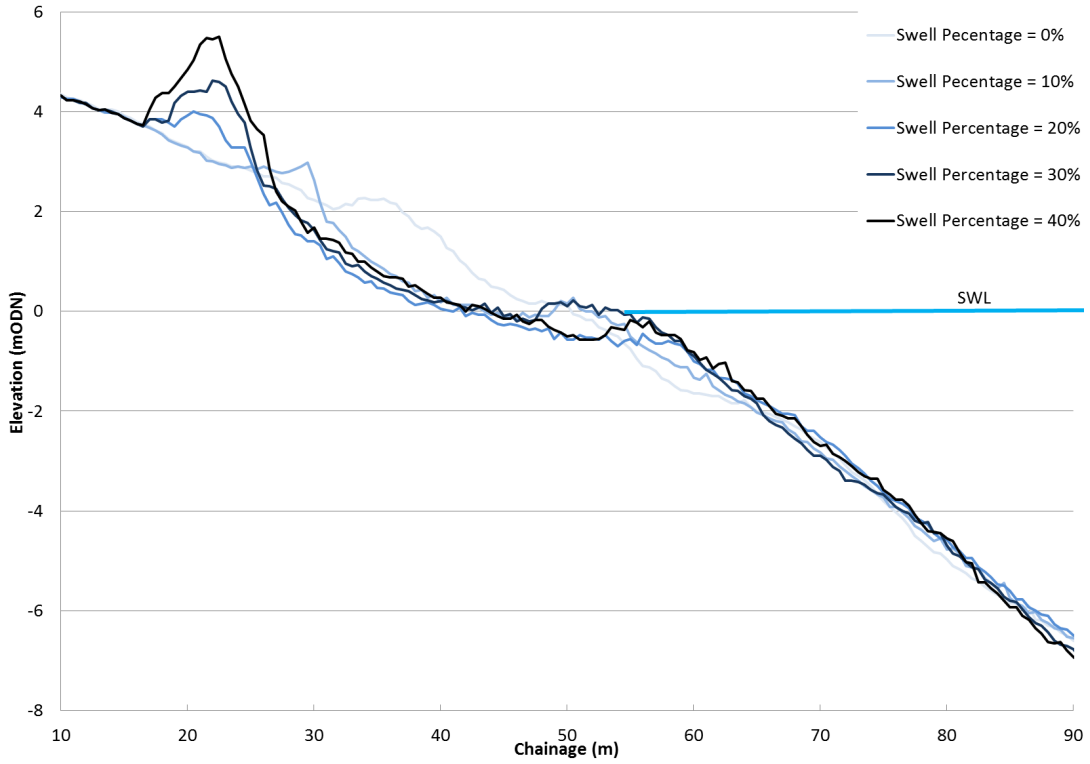

Figure 7.11: Effect of swell component percentage on shingle beach profiles (H_{m0}=3.0m, $T_{p,wind}$=7.18s, $T_{p,swell}$=18s) in the physical model tests

7.2.5.3 Swell wave period effect on beach profile response

The test performed using different swell component demonstrated that the crest elevation was also affected by the wave period of the swell component. In particular, the effect of the swell wave period ($T_{p,swell}$) on the beach profile was investigated by comparing profiles obtained using sea-states characterised by the same wave height (H_{m0} = 3.0m), same wind wave period ($T_{p,wind}$ = 7.18s), same swell percentage (10%, 20%, 30% and 40), but different swell periods (15s, 18s, 21s, 25s). An example of the effect of the swell period on the beach profile is shown in Figure 7.12 (H_{m0} = 3.0m, $T_{p,wind}$ = 7.18s and Swell% = 30), demonstrating that variations of swell wave period has a substantial effect on the final beach profiles. The influence of the swell wave period manifested itself mainly on the beach crest, with the crest position moving backwards and the crest elevation moving vertically in response to an increasing swell wave period. This is because longer waves saturate the beach quicker, since more water per wave is dumped on the beach so wave run up is enhanced. Similarly there is an increase in the crest elevation in response to an increasing swell wave period as the swell percentage is increased. For the same

swell wave period, the higher the swell percentage the higher the increase of the crest elevation. Although both the swell wave height and swell wave period have an effect on the beach crest, the swell wave period seemed to have much more influence on the beach crest displacement than the swell wave height. This is due to the volume of water that penetrates within the beach under longer wave periods compared to bigger wave heights.

It was also observed that the width of the breaker-zone was increased with increasing swell wave period and swell percentage. The increase in the width of the breaker-zone is a necessary response of the beach to dissipate increased incident wave energy but, during these wave conditions, the energy spectrum was kept constant (H_{m0} = 3.0m). This beach response may be attributed to the interaction within the surf zone between wind and swell waves which significantly affects the up-rush, backwash and groundwater elevation (see Section 2.3), triggering a horizontal displacement (landward) of the beach crest. The effect of the groundwater elevation on the final beach profile is a phenomenon extremely important for the beach evolution, and it was investigated and discussed in Chapter 6.

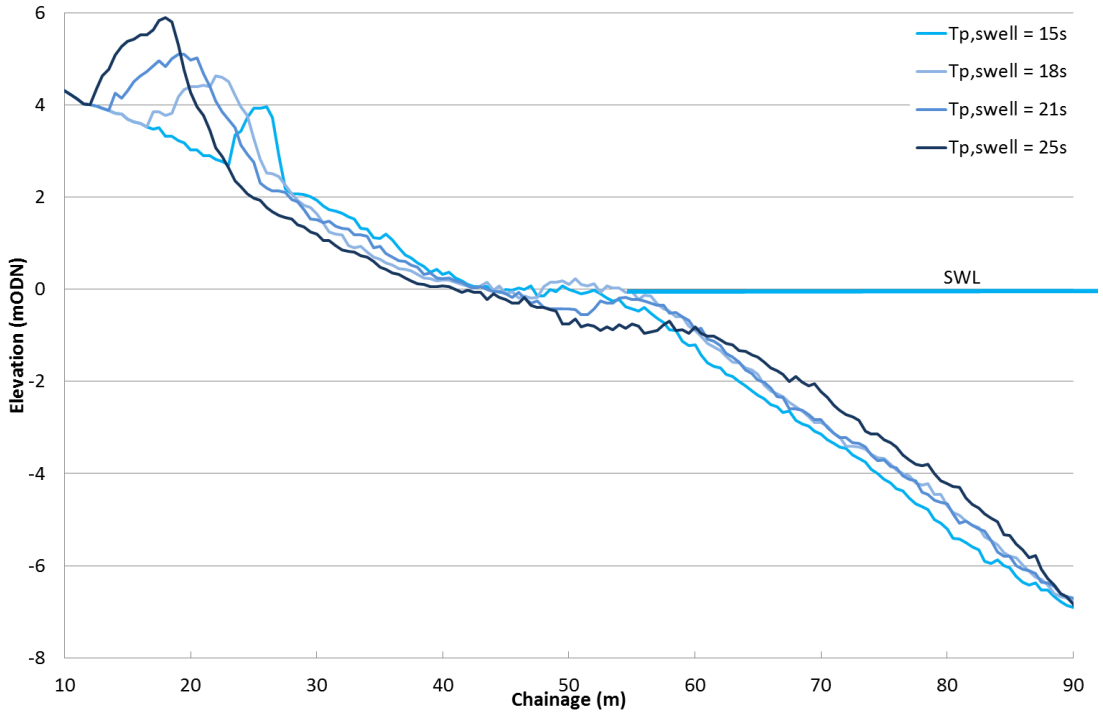

Figure 7.12: Effect of swell wave period on the shingle beach profile (H_{m0}=3.0m, $T_{p,wind}$= 7.18s; Swell percentage = 30%)

7.2.5.4 Effect of wind wave period on beach profile response

The effect of the wind wave period ($T_{p,wind}$) on the beach profile was investigated for both unimodal and bimodal spectra. The beach profiles, shown in Figure 7.13, were obtained testing the same initial beach profile using the same unimodal wave energy, that is, having the same wave height of H_{m0} = 3.0m, but different wind wave periods ($T_{p,wind}$ = 7.18s, 8.26s and 9.54s). The effect of variations in the wind wave period was observed more in the vertical than in the horizontal displacement of the profile. Thus, as the wind wave period increases, so does the beach crest elevation. This behaviour is in agreement with the results observed in Powell (1990), where only unimodal spectra were tested. This is because the wind wave periods are not long enough to completely saturated the beach (as under swell periods), therefore more wave energy is dissipated within the beach and less energetic wave run-up occurs. This triggers a building up of sediment on top of the crest but not a landward displacement.

Interestingly, under bimodal wave conditions, the increase of the crest elevation in response to an increasing wind wave period is less significant than an increase of the wind wave period under unimodal wave conditions, as shown in Figure 7.14. This plot shows four beach profiles subject to the same wave height, but under two different wind wave periods. The profile response to unimodal wave conditions is represented with solid lines, while the profile response to bimodal wave conditions (20% swell component) is plotted with dashed lines. Clearly, the increment of the wind wave period has a more significant impact on the unimodal condition than the bimodal one. This can be explained because under the bimodal wave conditions, the swell component and swell wave period have a more significant impact than the wind wave period on the amount of water infiltrating into the beach (groundwater elevation) and therefore affecting the final profile. Therefore, the effect of the wind wave period is mainly observed under unimodal wave conditions, as under bimodal wave conditions it is the swell wave period that has a more significant effect on the beach crest elevation.

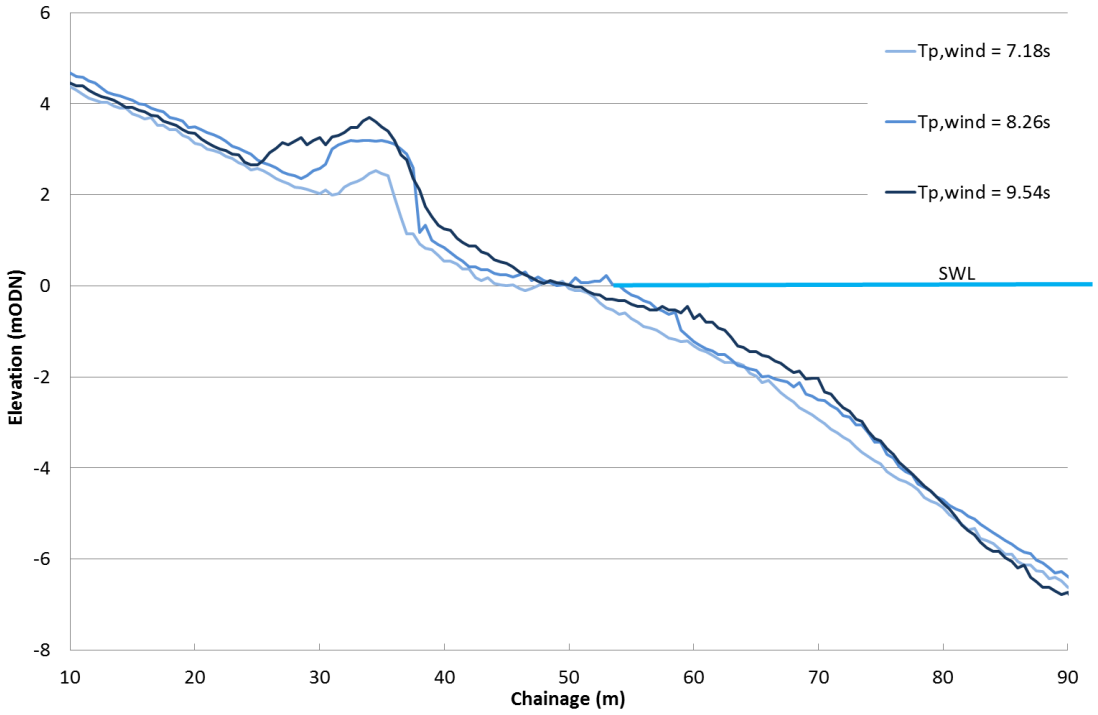

Figure 7.13: Effect of wind wave period on the shingle beach profile under unimodal wave spectra with H_{m0}=3.0m in the physical model tests

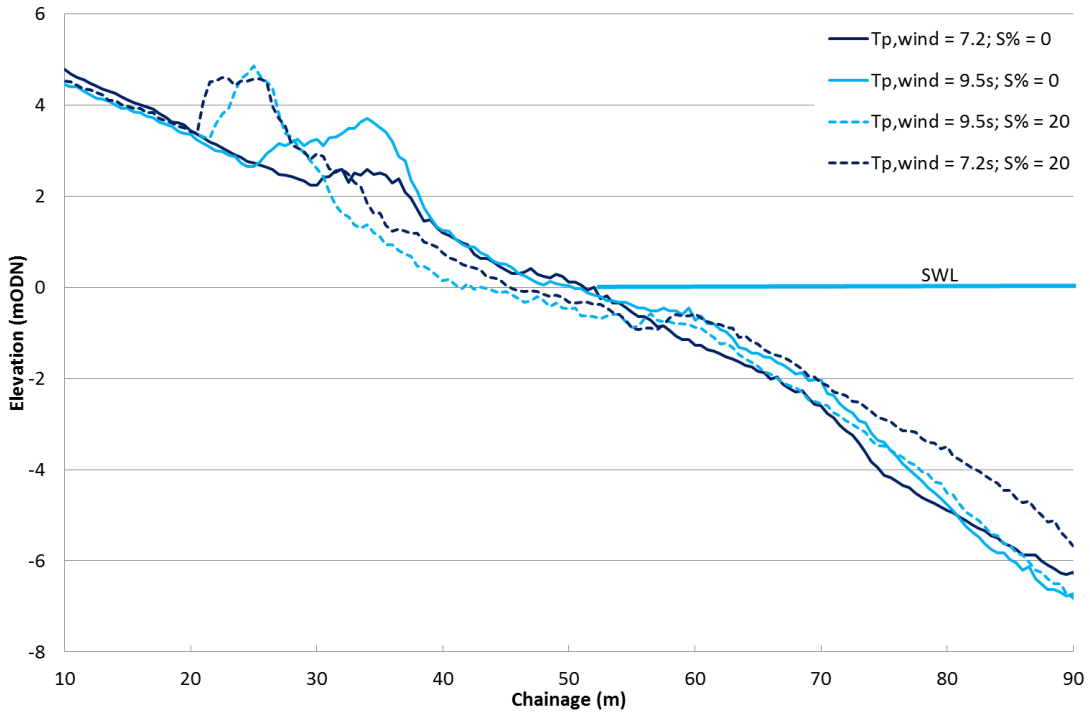

Figure 7.14: Effect of swell component on the influence of wind wave period on the shingle beach profile in the physical model tests

7.2.5.5 Wave height effect on beach profile response

The influence of the wave height on the beach profile is shown in Figure 7.15 comparing the post storm beach profiles corresponding to two different incident wave heights (H_{m0} = 3.0m, dark blue line and H_{m0} = 4.5m, light blue line) but same wind and swell wave periods. As can be seen, the effect of the variation in the wave height triggers a different horizontal displacement. The surf-zone width increases significantly in response to an increasing wave height. This behaviour is in agreement with the results observed in Powell (1990). The increase in the width of the surf zone is necessary to dissipate increased incident wave energy, and this is realised by a lengthening of the surf zone rather than a change of the profile. This behaviour was also observed for all the different tested wave heights.

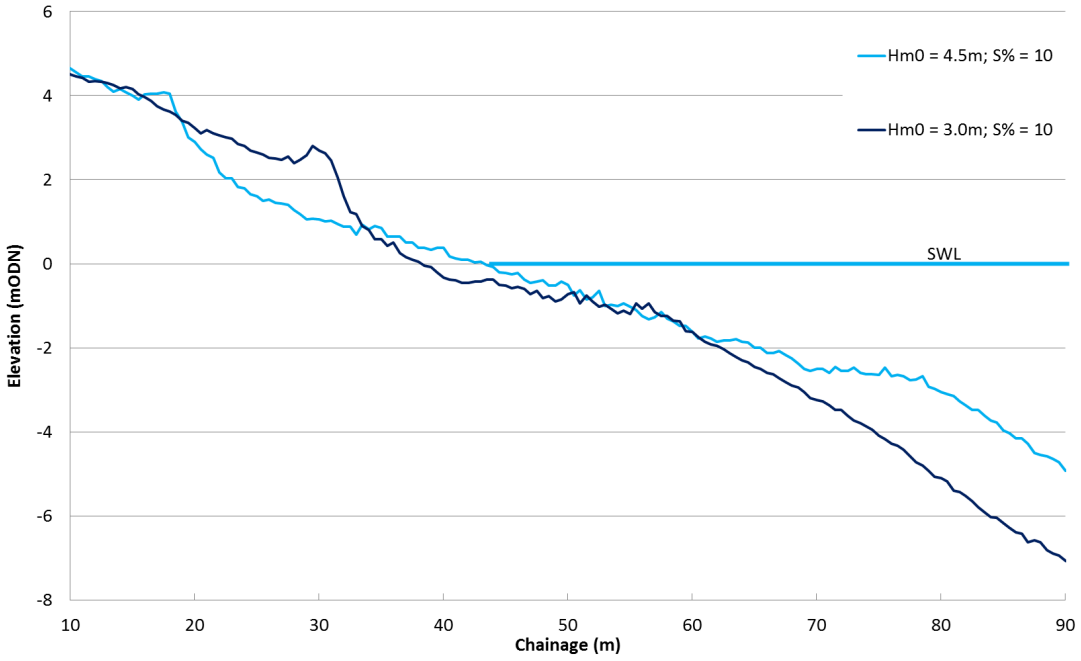

Figure 7.15: Effect of wave height on the shingle beach profile for bimodal (10% swell component) wave conditions (H_{m0} = 3.0m, dark blue line and H_{m0} = 4.5m, light blue line)

7.3. Comparison with the existing predictive methods and development of Shingle-B

7.3.1. Introduction

The first part of this section compares the beach behaviour observed in the physical model study with prediction from the most established models available to predict gravel beach response under wave attack. The second part describes the development of the new parametric tool Shingle-B to predict beach profile response under bimodal wave conditions.

7.3.2. Comparison with the existing predictive methods

The Shingle (Powell 1990) and XBeach-G (McCall *et al.*, 2014) prediction models, discussed in more detail in Section 2.4, were used to predict beach profile responses for both a typical unimodal JONSWAP wave spectrum (shown in Figure 7.16) and bimodal wave spectra (shown in Figure 7.17 and Figure 7.18). For a typical unimodal JONSWAP wave spectrum (H_{m0} = 3.0m, $T_{p,wind}$ = 7.18s), Shingle predicts profiles in very good agreement with the physical model results. The parametric model correctly predicts not only the location of the crest beach, which tends to be the area of most interest to coastal engineers, but also the location of the step (see Figure 7.16). Conversely, significant discrepancies were observed between observations in the physical model and the beach profiles predicted by XBeach-G, with the numerical model underestimating the horizontal displacement of the beach crest and predicting erosion where accretion was observed. It is worth mentioning that for the prediction of the beach profiles, the recently developed XBeach-G GUI was used. The default wave parameters (e.g. calibration factor time averaged flows due to wave skewness and wave asymmetry) were therefore used. It is likely that by varying/calibrating these parameters a better prediction would be obtained. However, the investigation/calibration of these parameters was out of the scope of this study, which aimed to use the available models without prior validation. Only the effect of the hydraulic conductivity on the beach profile response was investigated, and better profile predictions were obtained using a *k* value of 1.0 m/s.

As previously described, in order to investigate the effect of the spectral shape on the variation of the beach profile, the same spectral wave height H_{m0}, (i.e. the same area under the spectrum) was tested at the same water level but using four different swell percentage (10-40%). The same

experiment was performed using both Shingle and XBeach-G. Predictions of beach profile responses obtained from each model were compared with those observed in the physical model test, for different bimodal wave spectra. Predicted beach profiles corresponding to bimodal wave conditions having respectively 10% and 40% of swell component are compared to the post physical model test results in Figure 7.17 and Figure 7.18.

It is worth mentioning that the Shingle model allows the user to input the wave height and the mean wave period ($T_{m0,2}$), but does not take into account the bimodality of the wave spectrum. During these tests, when varying the swell percentage (10-40%) the wave height remained constant and the spectral period ($T_{m-1,0}$) increased. Therefore, when increasing the swell percentage during the tests, the input mean wave period ($T_{m0,2}$) in the Shingle model was replaced by the spectral period ($T_{m-1,0}$). In Shingle the effect of variations in the wave period triggers the vertical displacement at the beach crest neglecting its horizontal displacement. This simplification, results in a significant discrepancy between the measured and predicted profiles for bimodal wave spectra, as demonstrated in Figure 7.17 and Figure 7.18.

In contrast, the XBeach-G model allows the user to input a double-peaked wave spectrum, by specifying the wave height and wave period for both the wind and the swell components. A significant discrepancy was nevertheless observed when comparing the measured and the predicted profiles. In particular, the model does not predict the variation of the surf-zone width as a function of the variation of swell percentage, resulting in a significant under-estimation of the crest erosion (of the order of 10 - 20m). The higher the swell percentage within the incident wave condition, the higher the discrepancy observed (see Figure 7.17 and Figure 7.18).

The laboratory experiments clearly demonstrated the effect of the double-peaked wave spectrum on the beach profile response whereby a slight increase of low-frequency energy, within the incident wave spectrum, triggered a significant erosion of the beach crest. The comparison between predicted and measured beach profiles has shown that the available prediction models (Shingle and XBeach-G) do not encompass the effect of the bimodality of the incident wave spectrum and, consequently, they significantly under-estimate the crest erosion. XBeach-G allows bimodal spectra to be input, although results were not in agreement with the test results.

Moreover, these prediction models fail to predict correctly the position of the beach crest, which, as discussed in Chapter 2, is an important feature for coastal management. These limitations clearly indicate that the current prediction models are not appropriate tools under bimodal sea-states. Based on this 2D physical model study a new parametric model, for predicting beach profile response under bimodal sea-states, Shingle-B, was derived, which is explained within the next section.

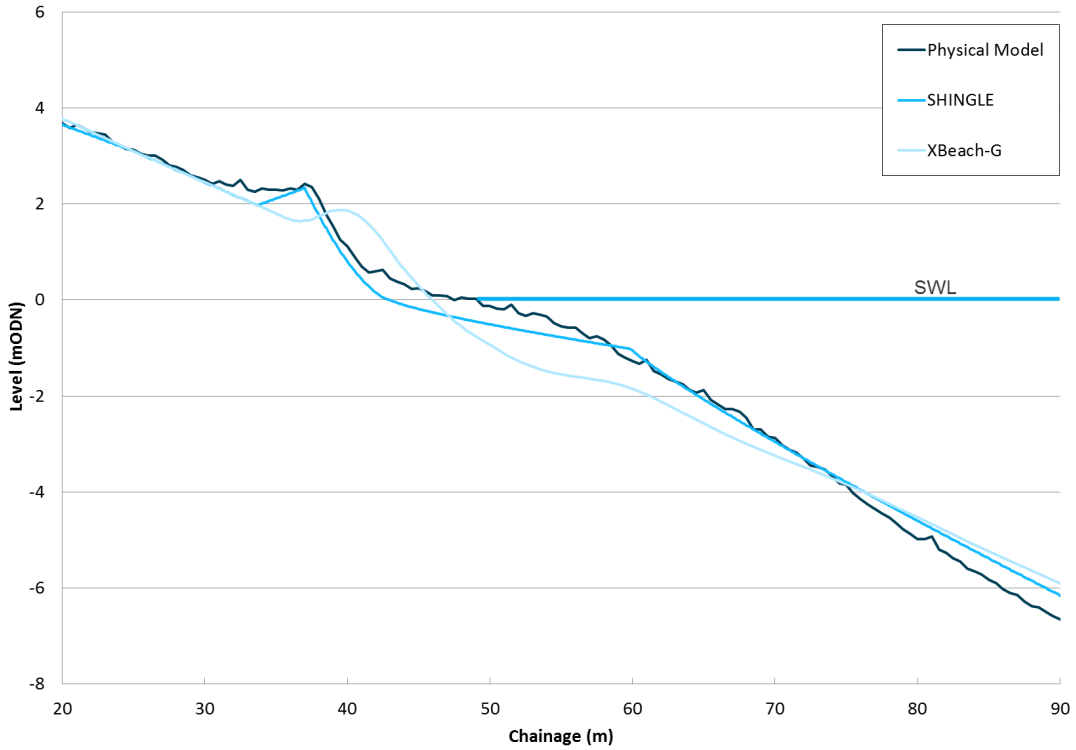

Figure 7.16: Beach profile comparison, XBeach-G, Shingle and physical model results for a unimodal wave spectra (H_{m0} = 3.0m, $T_{p,wind}$ = 7.18s, $T_{p,swell}$ = 15s, Swell percentage = 0%)

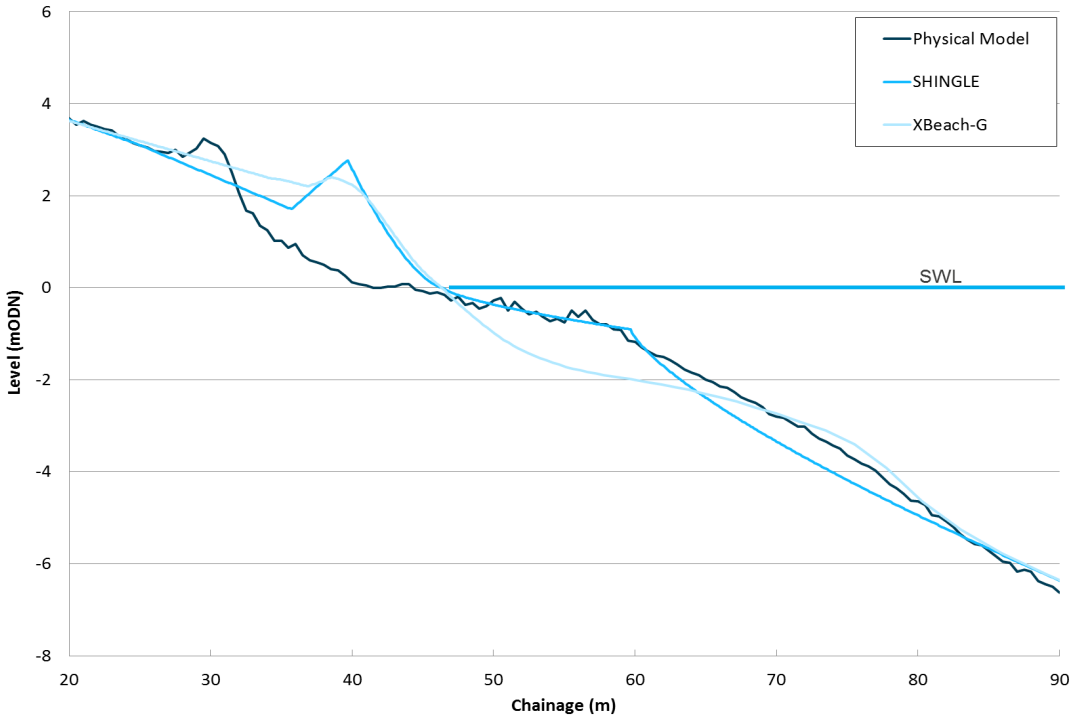

Figure 7.17: Beach profile comparison, XBeach-G, Shingle and physical model results for a bimodal wave spectra (H_{m0} = 3.0m, $T_{p,wind}$ = 7.18s, $T_{p,swell}$ = 15s and Swell percentage = 10%)

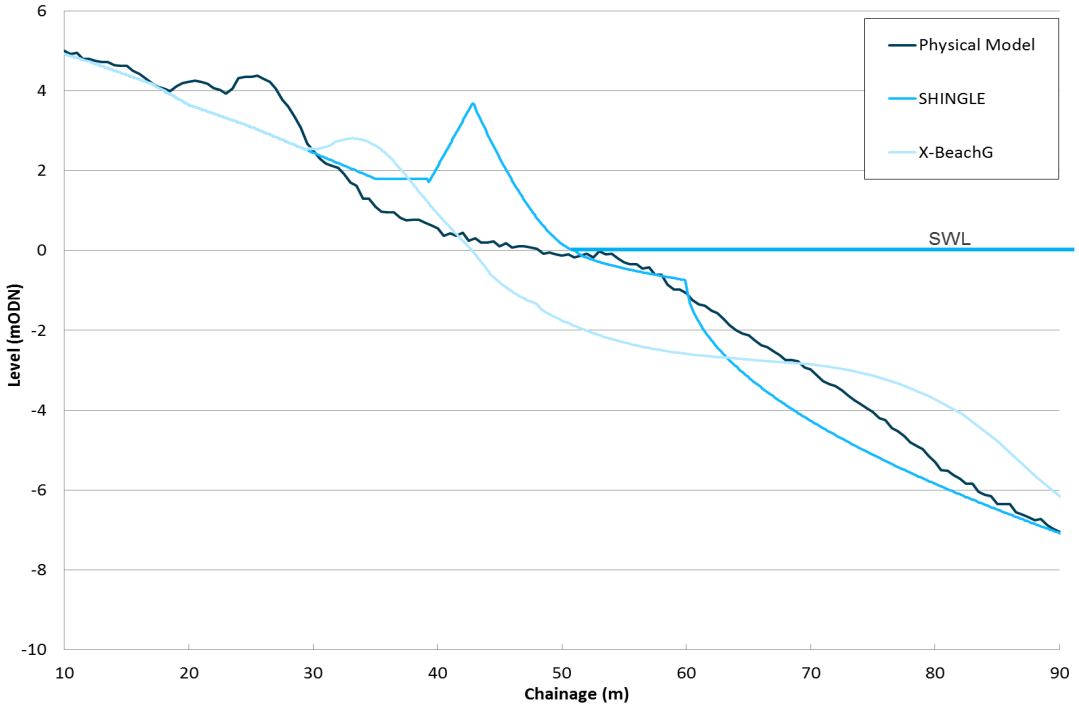

Figure 7.18: Beach profile comparison, XBeach-G, Shingle and physical model result for a bimodal wave spectra (H_{m0} = 3.0m, $T_{p,wind}$ = 7.18s, $T_{p,swell}$ = 15s and Swell percentage = 40%)

7.3.3. Shingle-B model

7.3.4. Introduction

This section presents the Shingle-B model, in particular, it first describes the way in which the new model schematises the beach profile and the relationships between profile parameters and the bimodal wave variables and then provides a validation against field data.

7.3.5. Profile schematisation

Results observed during the physical model study highlighted the criticality of bimodal sea-states for the erosion of the beach crest. This critical aspect of the evolution of the beach profile was also observed along the south coast of England over the course of the storm sequences during the winters of 2013 - 2014 as discussed in Section 4.2. Considerations in Sections 7.3, suggested that the Shingle model provides a valid tool for the prediction of the beach profile response under the action of unimodal sea-states, and was therefore taken as a starting point to develop a new model. The profile schematisation adopted for the present model has therefore been based on the profile employed by Powell (1990).

Powell's (1990) model defines a shingle beach profile using three power-law curves, as shown in Figure 7.19: 1) Beach crest and still water level shoreline; 2) Still water level shoreline and top edge of step; 3) Top edge of step and lower limit of profile deformation.

Since the width of the crest is an important parameter for the evolution of the beach profile under bimodal sea-states, it has been necessary to allow the present model to predict the landward displacement of sediment and the resulting final crest width. This has been obtained by extending the Shingle model, by employing four curves to schematise the beach profile: 1) Landward displacement and beach crest; 2) Beach crest and start beach-face point; 3) Beach-face point and top edge of step; 4) Top edge of step and lower limit of profile deformation. The resulting schematisation is shown in Figure 7.20. Except for the crest width, the parameters were measured relative to the still water level and shoreline axes, as shown in Figure 7.21. The coordinates for the vertices of the curves are denoted by x_1, y_1 to x_5, y_5 as shown in Figure 7.20.

Many authors (see among others Keulegan and Krumbein, 1949; Bruun, 1954; Dean, 1977; Hughes and Chiu, 1981; Van Hijum and Pilarzyk, 1982; Powell, 1990) have suggested that a power

expression of the form $y = A\,x^n$ provides the best description for a profile of a natural beach, where the coefficients *A* and *n* are functions of the beach characteristics and incident wave conditions, and *y* and *x* are the vertical and horizontal displacements. The proposed model therefore assumes the same power relationship to describe the profile between these vertices. Once the beach profile had been schematised, the functional relationship for each of the parameters listed above was to be determined. The relationship between the beach profile parameters and incident wave parameters is described in the following section.

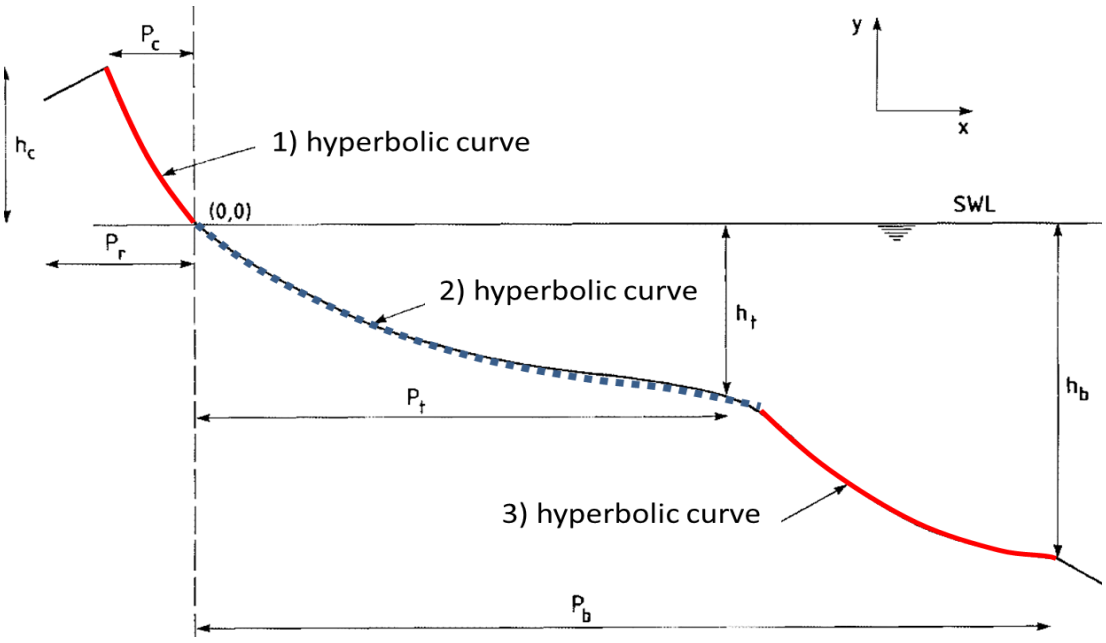

Figure 7.19: Schematised beach profile (Powell, 1990)

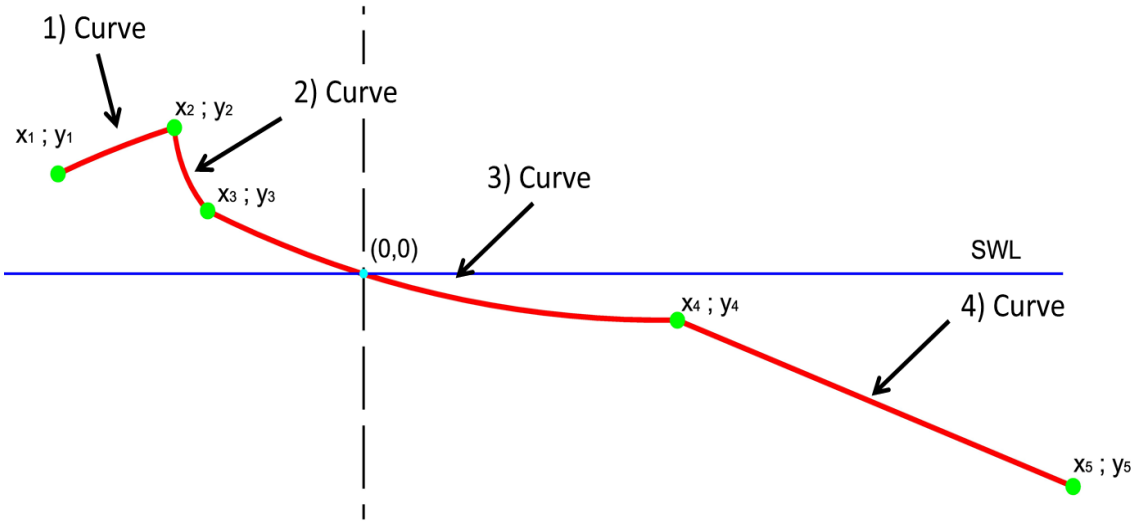

Figure 7.20: Schematised beach profile using four curves

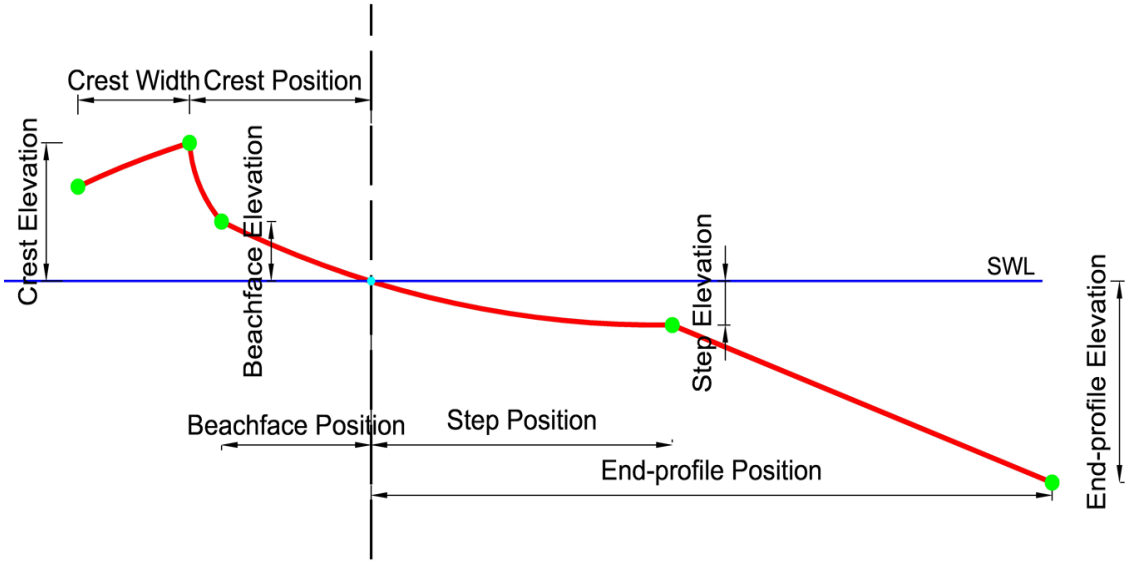

Figure 7.21: Schematised beach profile: parameters were characterised relative to the still water level and shoreline axes

7.3.6. Identification of beach profile parameters

The model beach profiles were derived during the physical model tests using a bed profiler (discussed in Section 7.2.2.3). This instrument is capable of logging levels along the chainage of the beach to derive the profile of the beach itself. In order to derive functional relationships between beach profile and bimodal wave variables, the beach profile (co-ordinates x_i and y_i) had to be parameterised into simplified parametric curves (see Figure 7.22). This was done by a combination of expert judgement and a least squares optimisation.

The crest position (Point 2) and still water level intersection (circle, Figure 7.22) were manually selected for each of the observed profiles; as well as the seaward (Point 5) and landward (Point 0) ends of the profile (see Figure 7.22).

A genetic algorithm (GA) (Deb, *et al.* 2002) was used to best fit observations to the parameterised curves defined above. A GA is a method for solving both constrained and unconstrained non-linear optimisation problems by mirroring the natural selection process of biological evolution. GAs can generate a vast number of possible model solutions and use these to evolve towards an approximation of the best solution of the model. They mimic evolution by evolving solutions able to predict correctly and dismissing those that diverge from the results. The algorithm is initialised with a population of multiple randomly generated potential solutions, each of which provides the x and y co-ordinates of the remaining beach parameters (i.e. for Points 1, 3 and 4) in addition to a power n_i for each of the four curves. This population is 'evolved' over a number of 'generations' using selection, crossover and mutation processes that mirror natural selection. At each generation, the algorithm uses the 'fitness' of each solution to determine which 'parents' to use to create the 'children' of the next generation. Given a potential solution of beach parameter co-ordinates and curve powers, the fitness is determined as the sum of the squared errors between the resulting fitted curves and the observed beach profile at every observed chainage, with lower errors preferred.

The resulting algorithm uses least squares optimisation to find the best fitting set of analytical curves (as defined above) for each observed profile. This dataset of beach parameter co-ordinates and hyperbolic curve powers then forms the training data for the subsequent regression analysis.

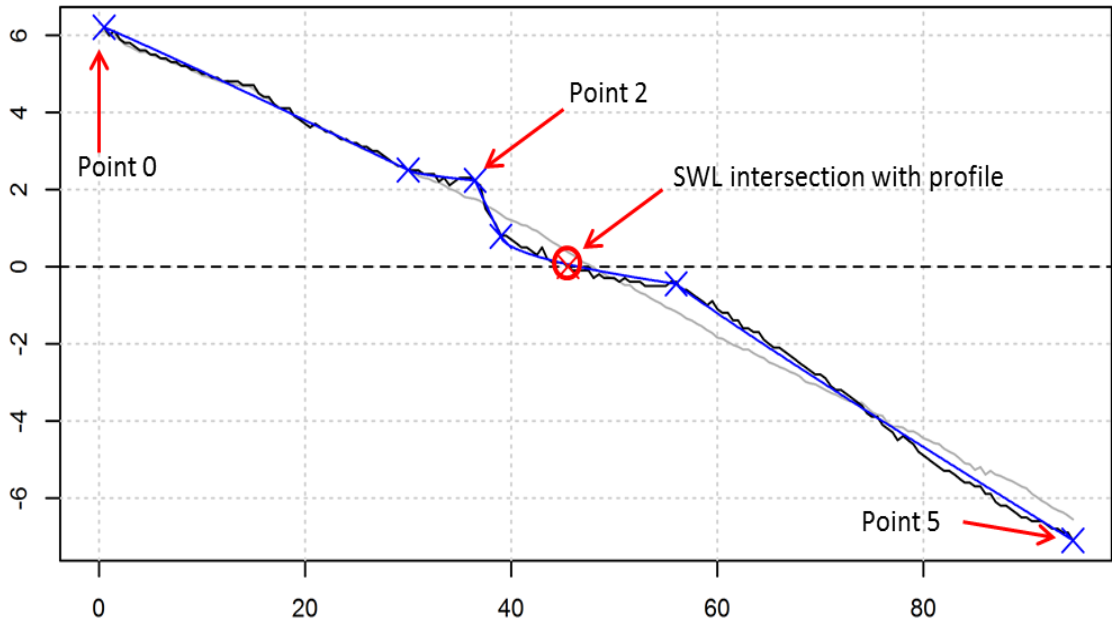

Figure 7.22: Beach parameter coordinates extracted from the physical model observed profile

7.3.7. Functional relationships between beach profile and bimodal wave variables

Functional relationships between the observed beach profile parameters (defined in Figure 7.21) and the bimodal sea state variables, were subsequently derived by means of multiple linear regression. This gives prediction equations of the general form:

$$y = \beta_0 + \beta_1 x_1 + \beta_2 x_2 \cdots$$

where y is the parameter prediction, x_i are covariates and β_i are corresponding best fit regression coefficients. The covariates may potentially be any bimodal wave variable or transformations of them. Test Series A to D, described in Table 7.1 (plane beach profile), were used to fit the model, ignoring the profiles at 1000 and 2000 waves, as discussed in Section 7.2.5.1.

For each profile parameter (e.g.: crest elevation, crest position, etc.), a model building exercise was undertaken to determine the exact form of the final regression equation by selecting which wave parameter to be included. Finding this subset of parameters involves two opposing criteria: firstly, the regression model has to be as complete and realistic as possible, i.e., including every parameter that is related to the dependent variable; and secondly, including as few parameters as possible. This is because including any irrelevant parameter in the model decreases the precision

of the model estimated coefficients as well as that of its predictions. Moreover, the presence of extra parameter unnecessarily increases the complexity of the prediction model. The goal of the parameter selection exercise is therefore a balance between simplicity (i.e. identify as few key parameters as possible) and complexity (i.e. include all the relevant parameters).

The process was therefore initiated by selecting a range of relevant wave parameters, and applying a stepwise procedure. This procedure initially defines the simplest model with no parameters, to which new terms are sequentially added or removed to assess their relevance. The selection of the relevant parameter occurs by means of selecting the term that minimises the Akaike Information Criterion (AIC) value (Akaike, 1974; Burnham and Anderson, 2002). AIC can be used to compare the performance of prediction models for a given dataset, and therefore the AIC provides a means for model selection. At each step this process systematically adds the most significant parameters and/or removes the least significant of them. This approach measures the goodness-of-fit of the equation while penalising the number of parameters used in the model. This is done to discourage the use of irrelevant parameters whose use would likely lead to poorer model estimates, particularly outside the fitted range (Burnham and Anderson, 2002). For each profile parameter, a set of equations were derived using the AIC method, the final one was manually selected to balance the goodness-of-fit with the model complexity while also ensuring the equation was physically meaningful (i.e. guaranteeing the physical phenomena observed and described in Section 7.2.5).

The preliminary parametric analysis described in Section 7.2.5, concluded that the most influential wave variables for the beach profile evolution are the spectral wave height (H_{m0}), wind wave peak period ($T_{p,wind}$), swell wave peak period ($T_{p,swell}$) and swell percentage (S). During the regression analysis, in addition to these main four variables, the following wave variables were also considered as key parameters: spectral significant wave period ($T_{m-1,0}$), mean wave period ($T_{m0,2}$), mean wave length (L_{0m}), breaker parameter (ξ_0), wave steepness (s_0) together with three parameters related to the wave spectrum, namely: broadness (ε), narrowness (ν) and peakedness (Q_p).

As a result of the stepwise regression analysis, the following four wave parameters were considered for inclusion in the regression model: H_{m0}, S, (1-S) $T_{p,wind}$ and S $T_{p,swell}$, where S is the

swell percentage as a decimal between 0 and 1. The wind and swell peak periods were multiplied by factors involving the proportion of swell to ensure that the parameter had a meaningful value in all cases, including when the swell is 0% or 100% for which one of these periods is undefined.

The model selection process was conducted using 90% of the selected tests with a randomly selected 10% used for independent validation of the fitted models. The results of the analysis for each beach profile parameter (fitted vs observed values plots) are shown in Figure 7.23. Ultimately, the selected regression equations were refitted using all of the selected tests. The final equations describing each parameter, and hence the profile curve, as a function of bimodal wave variables are reported from Equation (7.8) to (7.15). These equations are the basis of the online beach prediction tool Shingle-B.

As can be seen in Equation (7.8), there is a wide scatter between the predicted and observed values for the crest width. This is mainly due to the complexity of the phenomena involved during the formation of the crest width. The latter is a function of the type of wave breaking along the surf zone, which influences the amount of particles that are mobilised. Once a certain number of particles have been mobilised, a proportion of these are pushed by the wave run-up to the top of the crest, and this proportion is generally a function of the wave energy and particle size. As a result of these interconnected and complex phenomena, a prediction of the crest width is not well correlated.

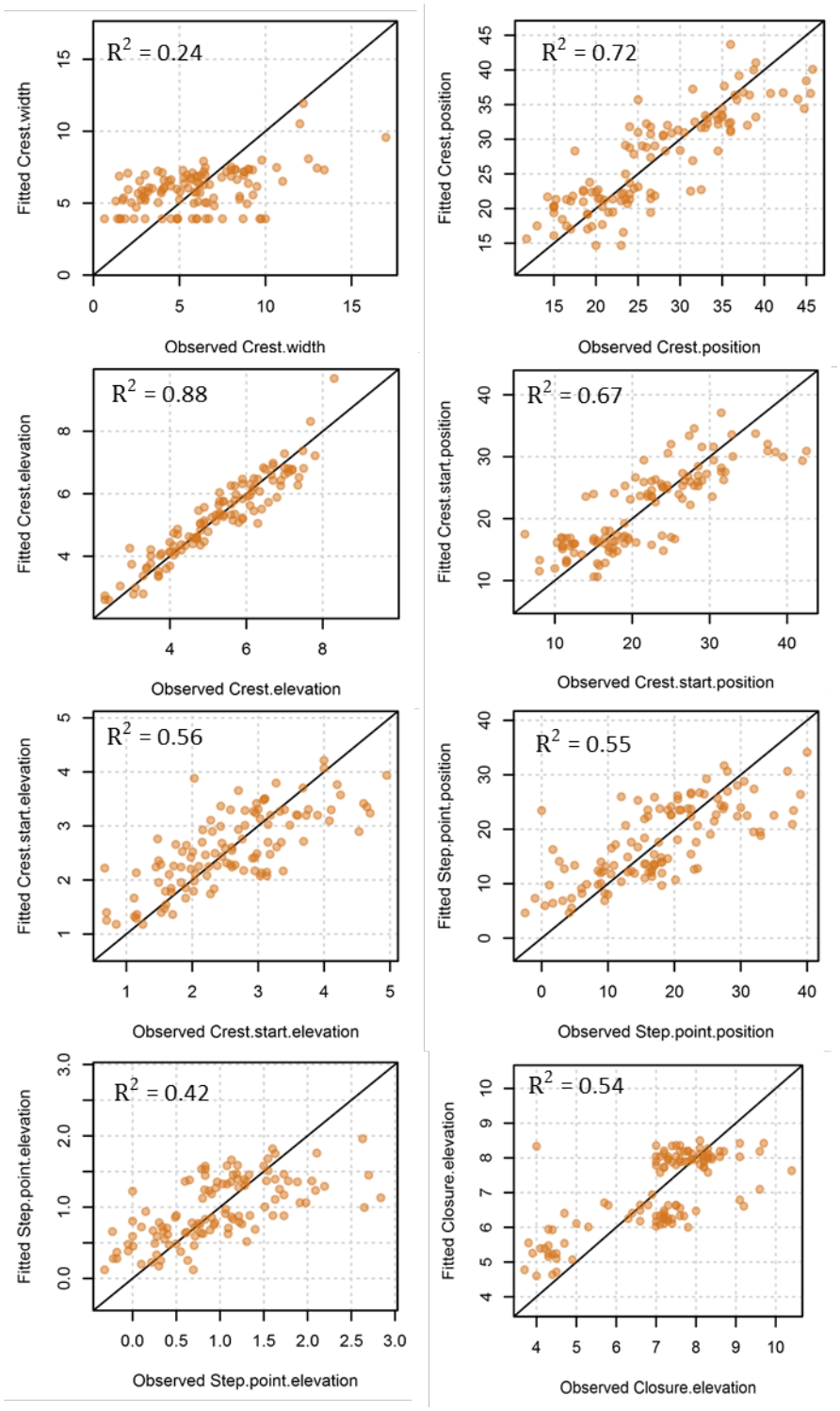

Figure 7.23: Fitted vs observed values for validation for the beach profile parameters.

$$\text{Crest width} = 3.92 + 0.31\ ST_{p,swell} \quad (7.8)$$

R^2 = 0.24

$$\text{Crest position} = -8.80 + 9.10\ H_{m_0} + 0.66\ ST_{p,swell} \quad (7.9)$$

R^2 = 0.72

$$\text{Crest elevation.} = -1.88 + 0.81\ H_{m_0} + 0.31\ (1 - S)T_{p,wind} + 0.37\ ST_{p,swell} \quad (7.10)$$

R^2 = 0.88

$$\text{Beachface position.} = -11.66 + 8.63\ H_{m_0} + 0.52\ ST_{p,swell} \quad (7.11)$$

R^2 = 0.67

$$\text{Beachface elevation} = -0.65 + 0.71\ H_{m_0} + 0.12\ ST_{p,swell} \quad (7.12)$$

R^2 = 0.56

$$\text{Step point position} = -17.76 + 8.67\ H_{m_0} + 0.83\ ST_{p,swell} \quad (7.13)$$

R^2 = 0.55

$$\text{Step point elevation.} = -1.19 + 0.51\ H_{m_0} + 0.06\ ST_{p,swell} \quad (7.14)$$

R^2 = 0.42

$$\text{End profile elevation} = 12.23 - 1.50\ H_{m_0} \quad (7.15)$$

R^2 = 0.54

7.3.8. Model validation

An important stage of this research has seen the validation of the Shingle-B model against field data. This confirms the correctness of the theory behind the beach physical modelling and strengthens confidence in the application of the prediction models to real world situations. The following section focuses on some of the English south coast sites and provides comparison of profile response under known storm events. At each site, data from the nearshore directional Datawell Waveriders®, owned and maintained by the Regional Coastal Monitoring Programmes, were used to derive wave conditions throughout the survey period. The wave buoys are part of a national network of nearshore wave measurements and are moored in ~12 m water depths providing wave statistics in real-time on a half hourly basis.

West Bay

West Bay, near Bridport in Dorset, comprises East and West beach. The East beach consists of a very fine shingle ridged beach with sand at the water's edge (see Figure 7.24). The West beach consists of a fine, smooth, pebbly beach, with shingle and sand at the water's edge.

A comparison between model results and post-storm beach profiles extracted at East beach, was carried out. Data provided by CCO's website included simultaneous wave measurements and beach profiles (the pre-storm profile was used as input for Shingle-B). A single storm with a unimodal wave spectrum was recorded during January 2011 (H_{m0} = 4.6m ; $T_{p,wind}$ = 10s; Swell % = 0) and it was reproduced by using Shingle-B, XBeach-G and Shingle (Powell, 1990). The prototype and model post-storm profile are plotted in Figure 7.25, where a reasonable agreement between measured prototype profile and Shingle-B predicted profile is observed. As expected, under unimodal wave conditions, the Shingle (Powell, 1990) model also shows a reasonable agreement with the prototype position of the beach crest and the rate of the crest erosion. Conversely XBeach-G significantly underestimates the crest erosion.

Figure 7.24: West Bay (East beach)

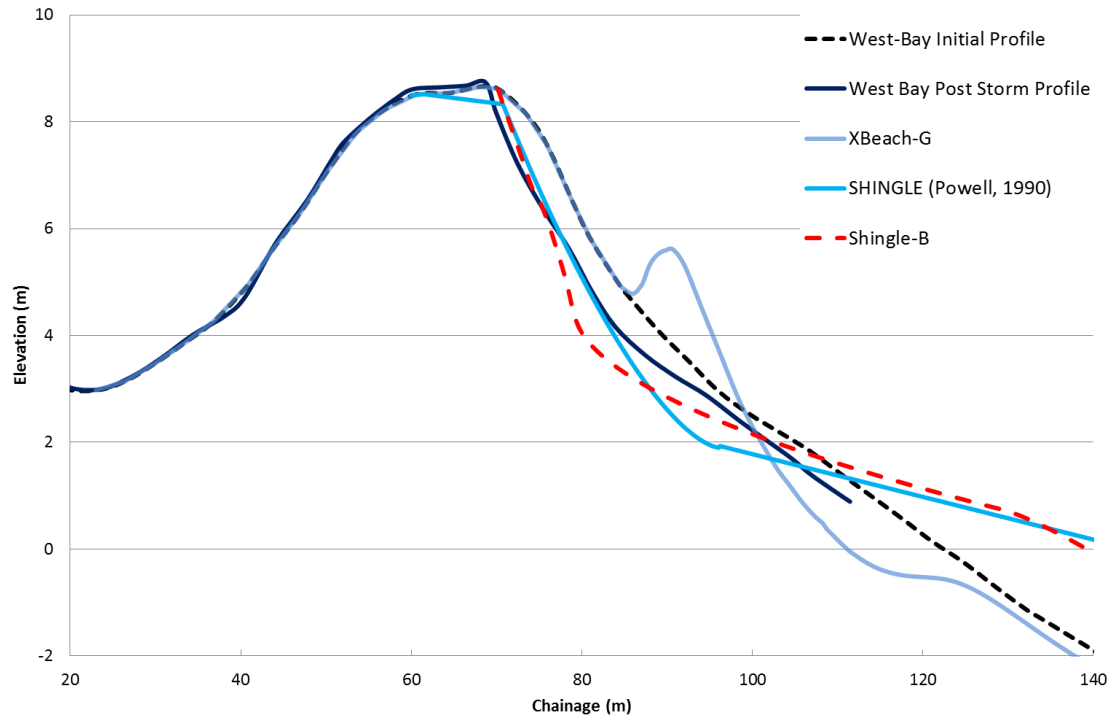

Figure 7.25: West-Bay: Post-storm profile against XBeach-G, Shingle (Powell, 1990) and Shingle-B predictions

Rustington

Rustington beach, in West Sussex, is a shingle beach with compacted sand at low tide. A comparison between model results and post-storm beach profiles extracted at Rustington, was carried out. Data provided by CCO's website included simultaneous wave measurements and beach profiles (the pre-storm profile was used as input for Shingle-B). A single storm with a bimodal wave spectrum was recorded during November 2005 (H_{m0} = 3.5m ; $T_{p,wind}$ = 7.0s ; $T_{p,swell}$ = 12s ; Swell % = 10) and it was reproduced by using Shingle-B. The prototype and model post-storm profiles are plotted in Figure 7.26 where the Shingle-B model shows a reasonable agreement with the prototype position of the beach crest and the rate of the crest erosion. Conversely, as expected under bimodal wave conditions, both Shingle (Powell, 1990) and XBeach-G significantly underestimate the horizontal displacement of the crest. These discrepancies between measured and modelled beach profiles are due to the fact the Shingle does not allow the user to input bimodal wave spectra, and therefore underestimate the crest erosion. Similarly for XBeach-G, the prediction can potentially be improved if the input parameters are calibrated before the prediction. However the model provides a very nice and intuitive GUI for the user, which then requires a proper calibration/validation exercise to be undertaken.

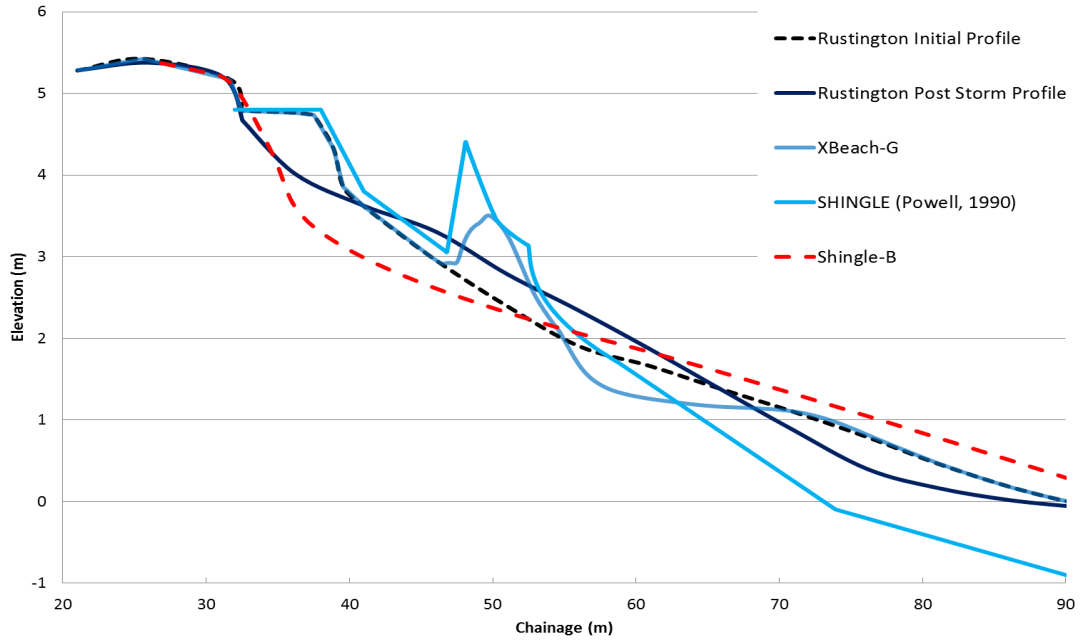

Figure 7.26: Rustington: Post-storm profile against XBeach-G, Shingle (Powell, 1990) and Shingle-B predictions

7.3.9. Limitations

In this section the combined effects of wave height (H_{m0}), wind wave period ($T_{p,wind}$), swell wave period ($T_{p,swell}$), swell percentage (S%) and the distribution of the spectral energy on the morphology of shingle beaches as a response to a storm condition has been investigated and an empirical method derived.

As with all empirical methods it is important to consider the range of applicability of the model, particularly in terms of the input parameters for which the model is capable to provide reliable predictions. Using the fitted functions beyond the range of the data used to generate them, has little theoretical basis and is therefore discouraged. Although the range of the input data used to train the model could be tabulated for each of the specific input parameters, it is worth emphasising that the practice of using the maximum and minimum values of each input parameter to define the range of applicability is questionable, particularly when parameters are correlated. There can be significant areas of unpopulated input parameter space within which model predictions are generated by extrapolation rather than interpolation. This is illustrated in concept and for two variables only in Figure 7.27, where the parameter space covered by the maximum and minimum of two variables is given by the dashed rectangle; the orange area inside, although within the range of the variables, has no data to support the underlying predictions. This effect is significantly exacerbated when more dimensions are included in the parameter space; in our case four parameters (wave height (H_{m0}), wind wave period ($T_{p,wind}$), swell wave period ($T_{p,swell}$) and swell percentage (S%)).

The desire to extend the range of applicability of the model outside the range of the training data is perhaps understandable given the preponderance of existing similar structure types and the additional expense associated with constructing site-specific physical models or more sophisticated numerical models. It is however, appropriate to explicitly recognise and acknowledge that predictions resulting from extrapolation should be treated with particular care and validated by other means whenever possible. Within the approach described here, specific attention has been paid towards the provision of guidance with respect to the area of applicability of the model. The Mahalonobis Distance (MD - Mahalonobis, 1930) is a measure of a point from a multivariate distribution and provides a quantifiable measure that can guide users on regions of valid

application. Unlike Euclidean Distance (ED), the MD accounts for correlated parameters, an important factor in the development of profile of gravel beaches. In the online tool Shingle-B, the MD has been used as a measure to come up with a range of applicability. This has been represented in the tool as a coloured thumb which is provided as part of the model output and indicates if the input wave conditions are within the limits of the training dataset (green thumb), within input range but far from the training data (orange thumb) or outside the data range against which the model was trained (red thumb). This is also illustrated in Figure 7.27.

It is worth mentioning that the model Shingle-B is not a breaching model nor does it deal with solid structures. Similarly, Shingle-B only deals with the cross-shore profile; the longshore transport not being considered. Formulations such as van Wellen *et al,* (2000) should be used in order to deal with the longshore transport of coarse grained beaches. Future physical modelling tests should explore the effect of oblique wave attack and the effect of longshore sediment transport.

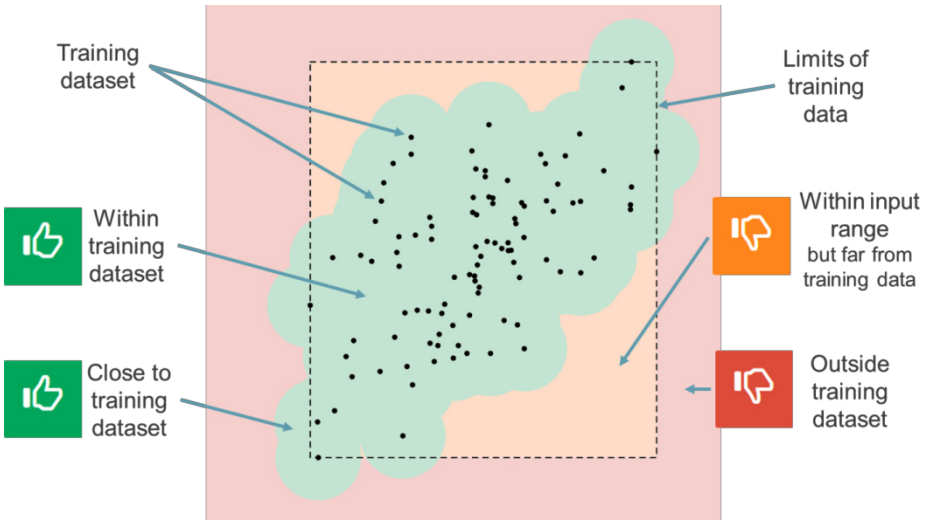

Figure 7.27: Input wave condition validation

Bathymetry

While a fixed bathymetry seawards of the toe of the beach, typical of south coast beaches, was used, sites with extensive shallow foreshores will require some transformation of the wave conditions to determine more realistic input conditions. Also, for other sites around the world, where more complicated bathymetry off the beach might be present, the user will be required to adjust the Shingle-B input wave conditions to account for the difference in wave transformation over the site specific bathymetry.

Diameter and grading of the beach material

Sediment characteristics such as D_{50} and grading width (D_{85}/D_{15}) may affect the beach profile response. During this study only one grading curve was used (D_{50} = 12.5 mm, D_{10} = 2.8 mm and D_{85}/D_{15} = 5.0) for the physical model tests, this was representative of typical shingle beaches along the south coast of England, as discussed in Section 7.2.2.3. The sediment used within the physical modelling was scaled following Yalin (1963) in order to provide the most satisfactory reproduction of the prototype beach permeability (Powell, 1990). The scaling process results showed that the sediment model scale (anthracite), with a geometric scale of 1 in 25, should be 1 in 2.25. The grading of the beach material, which affects its permeability, may influence crest elevation and crest regression, however this effect was not explored during this study. The effect of the grading of the beach on the crest elevation was studied by Powell (1990), who observed decreasing crest levels for narrower grading curve, although insufficient data were available to confirm this trend.

Beach slope

During this study the initial beach slope in the physical model tests was fixed at 1 in 8 for each of the tests. Although the effect of the initial slope was not investigated, different wave conditions were repeated without reshaping the beach to the initial plane profile. Results of non-reshaped and reshaped profiles showed a very good agreement suggesting that the initial profile does not affect significantly the final profile.

Similar results were also discussed in Powell (1990) where it was concluded that whilst the initial beach slope does not necessarily affect the form of the active length of beach profile it does affect its development.

Underlying impermeable structure

Physical model tests were run with a full thickness of beach material and the effect of impermeable internal layers or sea walls was not considered during this study. The presence of an underlying impermeable layer within a shingle beach was investigated by Powell (1990). During this study (Powell, 1990) it was observed that if the ratio of effective beach thickness to median material size (D_{50}) was less than 30, the thickness of the beach was usually insufficient to retain material over the profile, and the beach structure was not stable.

7.4. Discussion

An extensive series of physical model tests was undertaken to explore the behaviour and performance of the gravel beaches under bimodal wave conditions. The tests considered the effect of the wave height, wind wave period, swell wave period and swell component percentage on the resultant beach profiles. Results from this study clearly demonstrated the effect of bimodal spectral, i.e., the distribution of the spectral energy of a sea-state, on the evolution of the beach profile. Test results have shown the critical effect of the bimodal sea-state on both the vertical / horizontal displacement of the beach crest and the dynamics of the surf-zone. The tested wave conditions were based broadly around prototype measurements covering a range of wave heights from 3.0m to 6.0m, swell periods from 15 to 25 s and wave steepness of 0.03, 0.04 and 0.05. As discussed in Section 2.4 and Section 7.2.2.3, mobile bed modelling is very complex and it is still not clear how to correctly scale sediments (Kamphuis, 1985; Ilic *et al* 1997). Scale effects due to the sediment scaling process could affect the results of the recorded beach profiles, possibly by overestimating the build-up of sediment at the crest, due to the lighter material used during the experiment. However, as previously discussed, it is still very difficult to quantify these scale effects unless a large scale physical model study is carried out. The use of anthracite in reproducing correctly the behaviour of a prototype gravel beach was however confirmed by the comparisons between the measured test profiles from the Großen Wellen Kanal (GWK) (Blanco, 2001) with the profile predicted by Shingle (Powell, 1990). As discussed in 7.2.5.1, the main beach parameters showed strong statistical repitibility during testing, showing that the evolution of the beach response is modelled consistently in the physical model and is not significantly affected by the stocahastic nature of the wave forcing.

The parametric model of Powell (1990) and the numerical model XBeach-G (McCall et al, 2014) were found not to account for the influence of the spectral shape on the beach profile response and significantly underestimated the crest erosion under the bimodal wave conditions. As previously mentioned in Section 7.3.2, comparison with XBeach-G was carried out using the default setting wave parameters in the newly available GUI. Only the effect of the hydraulic conductivity on the beach profile response was investigated, and a better profile prediction was obtained using a k value of 1.0 m/s. It is likely that by varying/calibrating these parameters a better prediction could

be obtained. The physical model results have allowed the development of a new parametric model, Shingle B, for predicting beach profile response on gravel beaches under bimodal sea-states. Using the new parametric model, an online tool was developed and made available on the website for the National Network of Regional Coastal Monitoring Programmes of England (http://www.channelcoast.org/ccoresources/shingleb/). The new model, Shingle-B, aims to provide an engineering tool to increase confidence in beach cross-section design under wave conditions characterised by double peaked spectrum.

Initial validation of the model predictions against field data yielded encouraging results, suggesting that the parametric model provides a good representation of natural beaches, and therefore represents an improvement over existing models for gravel coasts, subjected to bimodal wave conditions. Nevertheless the present model would benefit from some additional comparisons and verification with field data. As a typical parametric model, the new tool Shingle-B, must be used within the range of the tested wave conditions used to develop it. As previously discussed (Section 2.3), swash zone processes are influenced by the permeability of the gravel beach material. During this study only one gravel beach material was tested, and therefore it is recommended to use the parametric model only for pure gravel beaches having a D_{50} similar to 13mm.

Another important phenomenon which is influenced by the grain size distribution and that takes place within the swash zone is the internal wave set-up. As discussed in Section 6.4, wave action affects the elevation of the water table, by increasing the mean water surface through infiltration. As observed during the previous study (see Chapter 6), also during this experiments the volume of water that filters and is retained by the beach, affected the profile response. More precisely, the incident wave conditions triggered the raising of the groundwater elevation, which is a function of both wave condition and sediment size, causing saturation of part of the beach. As the beach was saturated, part of the energy of the incoming wave could not be dissipated within the beach. Most of the wave energy was, therefore, used to run up to the top of the crest and pushed it landward. The groundwater elevation, as discussed in Section 6.4, acted as a key factor in the process of crest erosion.

8. Conclusion and future work

This research was intended to improve the current understanding of gravel beach profile response for various grain size distributions and under bimodal sea-states. The findings suggest that the grain size distribution has a significant influence on the wave-induced pore pressure and consequently on the internal wave set-up and beach profile response and bimodal seas states significantly affect the beach profile behaviour.

The study concluded that:

- Under stationary flow conditions the D_{15} is the grain size parameter that dominates the flow/resistance behaviour within porous media. A new set of parametric equations has been derived to improve Forchheimer coefficients for granular material.
- D_{15}, D_{50} and D_{85}, in this order, are the most informative parameters for wave-induced flow resistance within porous media as well as the hydraulic performance and the profile evolution of shingle beaches. A new set of parametric equations has been derived to assess the relative importance of these parameters on the evolution of the profile of shingle beaches and their hydraulic performance.
- Bimodal sea-states affect the response of shingle beaches more than their energetically equivalent unimodal sea-states. A new parametric tool has been developed to assess the effect of bimodal sea-states on cross-shore beach profile response.

The rest of this chapter summarises the main conclusions derived from the findings arising from the present research and introduced in Section 1.2 of this thesis. Finally, some recommendations for future work arising from the research are suggested.

8.1. Verification of the Forchheimer coefficients for coarse grained materials

As discussed in Chapter 2, wave interaction with structures involves several processes, such as: wave run-up, wave overtopping, wave reflection and wave transmission. These are influenced by the incident wave conditions, the properties of the material and the wave-induced porous flow inside the structure (Van Gent, 1992; Burcharth, 1991; Horn, 2006). Ground water elevation combined with wave induced pore water pressure fluctuations influence the beach profile response.

These groundwater elevations and wave induced pore water pressures are controlled by the physical property of permeability which is related to the grain size distribution. As stated in Chapter 2, the importance of porous flow was highlighted and in Chapter 5 the Forchheimer equation was examined to investigate both the influence of the grading of the sediment samples and the dependence of the Forchheimer coefficient values on the flow regimes. A new set of experimental data using a permeameter under statistically stationary flow conditions was collected. Six samples with narrow graded materials and six samples with wide graded materials were tested. The flow resistance measurements for each test sample have been presented and compared with the formulae proposed by previous studies. As the samples tested by various authors were produced under a range of different conditions, a comparison is rather difficult, and so the creation of a consistent tested dataset which includes the effect of the grading of the material and flow regime, was necessary.

The results, discussed in Section 5.4, clearly demonstrated that the D_{15} parameter dominates the flow/resistance behaviour for all the samples, this is due to the relationship between the D_{15} and the size of the voids within the sample. The other parameters: D_{50} or D_{85}/D_{15}, have only second order effects on the flow/resistance relationship. A new formulation for the Forchheimer coefficients was therefore derived in terms of the D_{15} parameter.

These equations can be applied to improve the modelling (both physical and numerical) of a number of coastal processes. Particularly in all those cases in which the driving factor is the behaviour of the groundwater flow and the percolation throughout the porous media (even if characterised by different grain size distributions). It is nevertheless recommended, that the dependency of parameters like shape and aspect ratio of gravel materials is investigated further to obtain a more generalised description of porous media flow.

8.2. Effect of grain size distribution on gravel beach response

A 2D physical model study, discussed in Chapter 6, was designed and completed to improve our understanding of wave-induced pore pressures within gravel material, for a range of sediment sizes and to investigate its influence on beach profile dynamics. During the previously completed permeameter tests, the particle parameter D_{15} was established as the main characteristic diameter

influencing the flow/resistance relationship for both narrow and wide graded sediment distribution curves under steady flow conditions. Throughout this study, the flow/resistance relationship was observed to also be influenced by different characteristic size diameters, i.e. D_{85}/D_{15}, as reported in Section 6.4. In particular, observations made during this study, in which more complex phenomena are involved, showed that the pore pressure attenuation was mainly influenced by both D_{15} and the ratio D_{85}/D_{15}, which is an indication of the grading width. The findings can be summarised as follows:

- Most of the incident wave energy is dissipated within the gravel beach material. The steeper the waves the more pronounced is this dissipation;
- The pore pressure amplitudes inside the gravel beach decrease rapidly in the direction of wave propagation;
- The maximum pore pressure amplitudes decay exponentially in the direction of wave propagation;
- The wave-induced pore pressure increases almost linearly with the incident wave height for constant wave period;
- The wave-induced pore pressure increases almost linearly with the wave period for constant wave height;
- For lower values of the ratio D_{85}/D_{15}, the wave-induced pore pressure decays more rapidly;
- Gravel beaches with lower permeability are likely to be subjected to a higher level of wave run-up and internal set-up, but also to a higher energy dissipation through the porous medium;
- Lower permeability beaches will not be able to transmit energy through the beach material and result in smaller wave-induced pore pressures than beaches with higher values of permeability.

Following the above observations, a new equation was derived to predict the damping of wave-induced pore pressure (Equation (6.8)), which incorporates the characteristic size diameters D_{15}, D_{85} and D_{50}. The present results may be used to estimate the rate of attenuation of a wave as

it propagates into a gravel beach material and better describes the processes within the swash zone.

During this physical model study the effect of the interaction between waves and the groundwater table was also analysed and discussed in Section 6.5, where post-storm beach profiles, with similar grading parameters (e.g., $D_{50,}$ D_{15} and D_{85}/ D_{15}) were compared. For the internal wave set-up it was observed that:

- The internal wave set-up was strongly influenced by both the incident wave condition and the sediment characteristic D_{50};
- The smaller the D_{50} the higher is the internal set-up;
- The elevation of the beach water table increases as the permeability of the beach material decreases;
- Gravel beaches with small sediment sizes showed a higher internal wave set-up but a smaller wave-induced pore pressure than gravel beaches with higher permeability.

Moreover, the current investigations undertaken to improve present levels of understanding on the effect of beach sediment sizes on beach profile response are summarised as follows:

- The profile response of shingle beaches is a function both of the incident wave conditions, described by the spectral wave height and peak wave period, and the beach sediment characteristics, in particular the median size D_{50} and D_{15};
- Beach profiles showed the coarsest material occurring in the wave breaker zone and at the beach crest, with finer material located at the shoreline;
- The beach crest moves upwards as D_{50} decreases, i.e., increases with increasing internal wave set-up. For higher values of internal wave set-up, the incoming waves are less likely to dissipate their momentum through percolation inside the beach (less volume of water percolates within the beach) and are therefore likely to trigger higher values of wave run-up and eventually transport larger volumes of sediments onto the crest.
- The beach crest moves shoreward as D_{15} decreases. For higher values of D_{15}, the wave induced pore pressure decays less rapidly and therefore the incoming waves are more

likely to propagate inside the beach than to run up, and are therefore less likely to modify the position of the beach crest.

Following the above observations, new equations were proposed to include the effect of the internal wave set-up parameter (H_{m0} L_{m-10}/D_{50}) and D_{15} to account for different grain size diameters when predicting both the beach crest elevation and position. These equations are an improvement over the existing parametric equations in the Shingle model (Powell, 1990). Therefore, a modified version of Shingle (Shingle-S) was created to improve the prediction of the beach position and elevation as a function of the grain size characteristics. This new modified version of Shingle, "Shingle-S", can be used to optimise the design profile for beach replenishment which involves different grain sizes.

This study has demonstrated that, for beach protection schemes, coastal engineers must take into account the grain size distribution, which has been shown to influence the profile response and the hydraulic behaviour of the beach. Since the effect of tide has not been investigated in this study, the results presented here are strictly applicable to those cases in which the effect of tide on the response of the beach can be neglected.

Since a reliable method for quantifying and correcting for scale effects in modelling wave-induced internal flow is still missing, large-scale model tests are needed to investigate and quantify any relevant scale effects.

8.3. Beach response to bimodal sea-states

An extensive series of physical model tests was completed to explore the behaviour and performance of gravel beaches under bimodal wave conditions, which were reported in Chapter 7. The tests considered the effect of the wave height, wind wave period, swell wave period and swell component percentage on the resultant beach profiles. Results from this study clearly demonstrated the effect of bimodal wave conditions on the evolution of the beach profile. In particular they have demonstrated the critical effect of the bimodal sea-state on both the vertical and horizontal displacement of the beach crest and the dynamics of the surf-zone. The findings can be summarised as follows:

- The influence of the swell component is observed mainly in the upper portion of the profile; the width of the surf zone increases significantly in response to an increase in swell percentage;
- The beach crest experiences a horizontal displacement in response to a shift of wave spectral energy from high to low frequency;
- The influence of the swell wave period manifests itself mainly on the beach crest, with the crest position moving backwards and the crest elevation moving vertically in response to an increasing swell wave period;
- The effect of variations in the wind wave period is observed more in the vertical than in the horizontal displacement of the profile. Thus, as the wind wave period increases, so does the beach crest elevation. However, the effect of the wind wave period is mainly observed under unimodal wave conditions, as under bimodal wave conditions it is the swell wave period that has much more significant effect on the beach crest elevation;
- The crest position moves backwards in response to an increasing spectral wave height.

Analysis with the parametric model Shingle (Powell, 1990) and the numerical model XBeach-G (McCall et al, 2014) showed they could not account for the influence of bimodal sea-states on the beach profile response and thus significantly underestimated the crest development under bimodal wave conditions.

The physical model results informed the development of the new parametric model described in Chapter 7, 'Shingle B', for predicting the beach profile response of gravel beaches under bimodal sea-states. This model has been made available on the website for the National Network of Regional Coastal Monitoring Programmes of England (http://www.channelcoast.org/ccoresources/shingleb/). Validation of the model predictions against field data yielded positive results, as shown in Section 7.3.8, suggesting that the parametric model provides a good representation of natural beaches, and therefore represents an improvement over existing models for gravel coasts subjected to bimodal sea-states. This model can be easily used by coastal designers and managers to improve their predictions of the beach profile response under bimodal sea-states, and therefore attain cost savings and improved beach stability.

8.4. Further work

Based on the conclusions of the research it is apparent that further physical model studies need to be carried out to investigate the effect of grain size distribution on the beach profile evolution using a large physical model scale. This future research will improve our understanding on the scale effects involved during the process of scaling different model gravel beaches characterised by different permeability.

More physical model tests or field measurements should be carried out to investigate the effect of the grain size distribution on the beach profile response under bimodal wave conditions. The results of this research could be used to merge the parametric model Shingle-B with the modified version Shingle-S. Although this research would require a large number of tests, it will definitely give a significant improvement of gravel beach profile prediction.

Future research into the effect of the shape of the wave spectrum, in terms of the peak enhancement factor (γ) on the beach profile response should be carried out. Swell wave conditions are characterised by having a wide range of the peak enhancement factor (γ), however, how this parameter might influence the beach profile response is not yet clear.

During this research, the results also underlined the importance of grain size distribution on the hydrodynamics and the morphodynamic response of gravel beaches. More field / laboratory data should be collected to better understand the effect of grain size distribution on beach profile response under bimodal wave conditions. In order to eliminate uncertainties related to scale effects, large scale physical model studies are required to further investigate the interaction between groundwater elevation and the morphodynamic response of gravel beaches. Results of these studies could be very beneficial in optimising the investments for beach replenishment and beach management.

List of references

Almeida, L.P., Masselink, G., Russell, P., Davidson, M., Poate, T., McCall, R., Blenkinsopp, C.,Turner, I.L., 2013. Observations of the swash zone on a gravel beach during a storm using a laser-scanner (Lidar). J. Coastal Res. 65, 636–641.

Almeida, L.P., Masselink, G., McCall, R. and Russell, P., 2017. Storm overwash of a gravel barrier: field measurements and XBeach-G modelling. Coastal Engineering, 120, 22-35

Akaike, H., 1974. A new look at the statistical model identification. IEEE Transactions on Automatic Control 19: 716–723.

Austin, M., Masselink, G., 2005. Infiltration and exfiltration on a steep gravel beach: Implications for sediment transport. In: Coastal Dynamics. No. 101.

Bagnold, R., 1940. Beach formation by waves; some model-experiments in a wave tank. Journal of the ICE 15, 27–52.

Baldock, T.E., Holmes, P., Horn, D.P., 1997. Low frequency swash motion induced by wave grouping. Coastal Engineering 32, 197–222.

Baird, A.J., Horn, D.P., 1996. Monitoring and modelling ground water behaviour in sandy beaches. Journal of Coastal Research 12 (3), 630–640.

Baird, A.J., Mason, T.E., Horn, D.P., Baldock, T.E., 1997. Monitoring and modelling groundwater behaviour in sandy beaches as a basis for improved models of swash zone sediment transport. In: Thornton, E.B. (Ed.), Coastal Dynamics ’97. American Society of Civil Engineers, New York, pp. 774– 783.

Baird, A.J., Horn, D.P., Mason, T.E., 1998. Validation of a Boussinesq model of beach ground water behaviour. Marine Geology 148, 55– 69.

BARDEX: a large-scale laboratory study of gravel barrier dynamics. Special Edition - Coastal Engineering Volume 63, May 2012.

Barnes, M. P., & Baldock, T. E., 2010. A Lagrangian model for boundary layer growth and bed shear stress in the swash zone. Coastal Engineering, 57(4), 385-396

Bascom, W.H., 1951. The relationship between sand size and beach face slope. Transactions, American Geophysical Union 32, 866–874.

Bakhtyar, R., Barry, D. A., Li, L., Jeng, D. S., & Yeganeh-Bakhtiary, A. (2009). Modeling sediment transport in the swash zone: A review. Ocean Engineering, 36(9-10), 767-783.

Bear, J. 1972. Dynamics of fluids in porous media, American Elsevier, New York.

Birkemeier, W.A., Miller, H.C., Wilhelm, S.D., DeWall, A.E., Gorbics, C.S. 1985. A user's guide to the Coastal Engineering Research Center's (CERC's) Field Research Facility. Instruction Report CERC-85-1 Coastal Engineering Research Center, U.S. Army Engineer Waterways Experiment Station, Vicksburg, MS.

Blenkinsopp, C. E., Turner, I. L., Masselink, G., & Russell, P. E. (2011). Swash zone sediment fluxes: Field observations. Coastal Engineering, 58(1), 28-44.

Bluck, B., 1967. Sedimentation of beach gravels: examples from SouthWales. J. Sediment. Petrol. 37 (1), 128–156

BGS, 1987. Sea Bed Sediments around the United Kingdom, 1:1,000,000 map (North sheet and South sheet). British Geological Survey, Natural Environment Research Council.

Bowen, A. J., Inman, D. L., Simmons, V. P. 1968. Wave ‘set-down’ and set-up. J. Geophys. Res., 73(8), 2569–2577.

Bowen, A.J. and Inman, D.L., 1969. Rip currents, 2. Laboratory and field observations. J. Geophys. Res., 74(23): 5479--5490.

Bradbury, A., 1998. Response of shingle barrier beaches to extreme hydrodynamic conditions. Ph.D. thesis, University of Southampton

Bradbury, A.P, 2000 Predicting Breaching of Shingle Barrier Beaches-Recent Advances to Aid Beach Management. Proc. 35th. Annual MAFF Conference of River and Coastal Engineers.

Bradbury A.P., McFarland S., Horne J and Eastick C, 2002 Development of a strategic coastal monitoring programme for southeast England (*International Coastal Engineering Conf, Cardiff, ASCE*

Bradbury A.P., Mason T.E., Holt M.W., 2004. Comparison of the Performance of the Met Office UK-Waters Wave Model with a Network of Shallow Water Moored Buoy Data, 2004 - Proc. 8th International Workshop on Wave Hindcasting and Forecasting, Hawaii

Bradbury, A.P., Cope, S.N., and Prouty, D.B., 2005. Predicting the response of shingle barrier beaches under extreme wave and water level conditions in southern England Proc. Coastal Dynamics 2005 ASCE

Bradbury A.P., Mason T.E., Holt M, 2006. Design and management implications for the use of modelled wave data in the southeast - a comparison between modelled and measured conditions. Proc DEFRA Conference of river and coastal engineers

Bradbury, A.P., Mason, T.E., Poate, T., 2007. Implications of the spectral shape of wave conditions for engineering design and coastal hazard assessment - evidence from the English Channel. Presented at the 10th International Workshop on Wave Hindcasting and Forecasting, 11-16 Nov. 2007, Oahu, Hawaii.

Bradbury A.P., Mason T.E., Picksley, 2009. A performance based assessment of design tools and design conditions for a beach management scheme. Proceedings of the International Conference on Breakwaters, Structures and Coastlines ICE; Edinburgh in press

Bradbury, A.P., Stratton, M., Mason, T.E., 2011. Impacts of wave climate with bi-modal wave period on the profile response of gravel beaches. DOI: 10.1142/9789814355537_0151. Conference: The Proceedings of the Coastal Sediments 2011

Bradbury, A.P., Mason, T.E., 2014. Review of south coast beach response to wave conditions in the winter of 2013-2014. Channel Coastal Observatory, SR01.

Bray, M. J., 1997. Episodic Shingle Supply and the Modified Development of Chesil Beach, England, Journal of Coastal Research, 13(4), 1035-1049.

Bray, M.J., Duane, W.J., 2001. Porlock Bay: geomorphological investigation and monitoring. Environment Agency Report, STCG024

Bretschneider, C. L , 1959. Wave Variability and Wave Spectra for Wind Generated Gravity Waves. Beach Erosion Board, U, S. Arm y Corps of Engineers, Tech. Memo No. 118, 192 pp

Bruun, P., 1954. Coast erosion and the development of beach profiles. US Army Corps of Engrs, BEB, TM-44.

Burcharth, H.F., Christensen, C, 1991. On stationary and non-stationary porous flow in coarse granular materials. MAST G6-S report, Dept. of Civil Engineering, Aalborg University, Denmark.

Burcharth, H.F., Liu, Z., Troch, P., 1999. Scaling of core material in rubble mound breakwater model tests. Proceedings of the 5th International Conference on Coastal and Port Engineering in Developing Countries (COPEDEC), Cape Town (South Africa), 1518-1528.

Burnham KP, Anderson DR, 2002 Model selection and multimodel inference: a practical information-theoretic approach, 2nd edn. Springer, New York

Bürger, W. , Oumeraci, H. , Partenscky, H.W. 1988. “Geohydraulic invesigations of rubble mound breakwaters”, Proc. 21th International Conference on Coastal Engineering, ASCE, 2242-2256.

Buscombe, D., Masselink, G., 2006. Concepts in gravel beach dynamics. Earth-Science Reviews 79, 33–52.

Butt, T., P. Russell, 2000. Hydrodynamics and cross-shore sediment transport in the swash-zone of natural beaches: A review, J. Coastal Res., 16, 255–268

Butt, T., Russell, P., Turner, I., 2001. The influence of swash infiltration-exfiltration on beach face sediment transport: onshore or offshore? Coastal Engineering 42 (1), 35 – 52.

Butt, T., Russell, P., Puleo, J.A., Masselink, G., 2005. The application of Bagnold-type sediment transport models in the swash zone. Journal of Coastal Research 21, 887–895.

Calliari, L. J., 1994. Cross-Shore and Longshore Sediment Size Distribution on Southern Currituck Spit, North Carolina: Implications for Beach Differentiation. Journal of Coastal Research, 10(2), 360-373

Carmen, P.C., 1937. Fluid flow through a granular bed: Transaction of the Institution of Chemical Engineers, Vol. 15, pp. 150-156

Cartwright, D.E., Longuet-Higgins, M.S., 1956. The statistical distribution of the maxima of a random function. Proceedings of the Royal Society of London. Series A, Mathematical and Physical 237, 212–232.

Carter, R.W.G., Johnston, T.W., Mckenna, J., J.D Orford, 1987. Sea-Level, Sediment Supply and Coastal Changes: Examples from the Coast of Ireland. Prog. Oceanog, 18, 79-101.

Carter, R., Orford, J., 1993. The morphodynamics of coarse clastic beaches and barriers: a short-and long-term perspective. Journal of Coastal Research, 158–179.

Carrier, W.D., 2003. Goodbye, Hazen; hello, Kozeny-Carman: Journal of Geotechnical and Geo environmental Engineering

Chakrabarti, S. K. (ed) 1987. Fluid Structure Interaction in Offshore Engineering, Southampton: Computational Mechanics Publications.

CCO, 2008. Channel Coastal Observatory [WWW Document]. URL http://www.channelcoast.org/ (accessed 2.16.11).

CIRIA, CUR, CETMEF, 2010. The Rock Manual. The use of rock in hydraulic engineering (2nd edition). C683, CIRIA, London.

Coates,T.T., Bona, P.F.D., 1997. Recharged beach development, a field study at Highcliffe Beach, Dorset. Report SR438, HR Wallingford.

Cope, S.N., 2004. Breaching of UK Coarse-clastic Barrier Beach Systems: Methods developed for predicting breach occurrence, stability and flooded hinterland evolution. Ph.D thesis, Department of Geography, University of Portsmouth

Craig, R.F., 2004. Craig's Soil Mechanics. CRC Press

Dalrymple, R.A., Thompson, W.W., 1976. Study of equilibrium profiles. Proceedings 15th International Conference on Coastal Engineering, ASCE, pp. 1277–1296.

Deb, K., Pratap, A., Agarwal, S.. A, 2002. Fast and Elitist Multiobjective Genetic Algorithm: NSGA-II. IEEE Transactions on Evolutionary Computation, 6 (8), 182-197.

Deb K, Agrawal S, Pratap A, T Meyarivan, 2000. A fast elitist non-dominated sorting genetic algorithm for multi-objective optimization: NSGA-II. Proceedings of the 6th International Conference on Parallel Problem Solving from Nature.; 849-858

Deb, K., Pratap, A., Agarwal, S., and Meyarivan, T. 2002. A fast and elitist multiobjective genetic algorithm: NSGA-II. IEEE Transactions on Evolutionary Computation, 6(2), 182-197.

DEFRA, 2001. Shoreline Management Plans. A Guide for Coastal Defence Authorities.

DEFRA, 2008. Understanding Barrier Beaches. TR FD1924.

DEFRA, 2016. The Costs and Impacts of the Winter 2013 to 2014 Floods; UK Government: London, UK, February 2016.

Dean, R.G., 1973. Heuristic models of sand transport in the surf zone. Proceedings of the 1st Australian Conference on Engineering dynamics in the surf zone, 208 – 214.

Dean, R.G., 1985. Physical modelling of littoral processes. In: Physical modelling in coastal engineering, R.A.Dalrymple, Edited by A.A.Balkema, Rotterdam, The Netherlands, 119 – 139.

Dean, R.G., 1977. Equilibrium beach profiles: US Atlantic and Gulf coasts. Univ delaware, Dept of Civil Engrg. Report No 12.

Den Adel, H., 1987. Re-analysis of permeability measurements using Forchheimers equation. Report CO 272550/56, Delft Geotechnics, Delft.

Domenico P. A., Schwartz F. W, 1997. Physical and chemical hydrology, 2nd Edition.

Dudgeon C R., 1967. Wall effects in permeameters.. Proc. ASCE Journal Hyd. Div, HY5 : 137-148. Paper No 5433.

Duncan, J. R. J., 1964. The effects of water table and tide cycle on swash-backwash sediment distribution and beach profile development. Marine Geology 2 (3), 186–197. URL

Dybbs, A., Edwards, R.V., 1982. A New Look at Porous Media Fluid Mechanics - Darcy to Turbulent, in: Fundamentals of Transport Phenomenon in Porous Media. Bear, J. and Corapcioglu, M.Y. (Eds.), NATO ASI, Series E: Applied Sciences, No. 82, pp. 199-256.

Emery, K.O., Foster, J.F. 1948. Water tables in marine beaches. Journal of Marine Research 7: 644-654

Engelund, F., 1953. On the laminar and turbulent flows of groundwater through homogeneous sand. Technical Report.Danish Academy of Technical Sciences.

Elfrink, B., Baldock, T., 2002. Hydrodynamics and sediment transport in the swash zone:a review and perspectives. Coastal Engineering, 45(3-4), pp. 149-167.

Erikson, L., Larson, M., & Hanson, H., 2005. Prediction of swash motion and run-up including the effects of swash interaction. Coastal Engineering, 52(3), 285-302.

Ergun, S., 1952. Fluid flow through packed columns, Chem. Eng. Prog. (48) 89–94.

EurOtop, 2007. European Manual for the Assessment of Wave Overtopping. Pullen, T, Allsop, N.W.H. Bruce, T. Kortenhaus, A. Schüttrumpf, H., Van der Meer, J.W. At: www.overtoppingmanual.com.

Ewans, K. Bitner-Gregersen E., Soares C. G., 2006 .Estimation of Wind-Sea and Swell Components in a Bimodal Sea State. November 2006 Journal of Offshore Mechanics and Arctic Engineering 128(4)

Fairchild, J. C., 1958. Model study of wave set-up induced by hurricane waves at Narragansett Pier, Rhode Island. Bulletin of the Beach Erosion Board, U.S. Army Corps of Engineers, Washington, DC.

Foote, M., Horn, D.P., 2002. Using video and GIS to measure two-dimensional water surface elevation in the swash zone.

Forbes, D.L., Taylor, R.B., Orford, J.D., Carter, R.W.G. and Shaw, J., 1991. Gravel-barrier migration and overstepping. Marine Geology, Vol.97, 305-313.

Freeze, R.A., J.A. Cherry, 1979. Groundwater. Prentice Hall: Englewood Cliffs, New Jersey.

Fredsøe J, Deigaard R., 1992. Mechanics of Coastal sediment transport. World Scientific Publishing, Advance Series on Ocean Engineering – Vol.3, ISBN 981-02-0840-5.

Galvin, C.J., 1972. Wave breaking in shallow water. In: R.E. Meyer (Editor), Waves on Beaches and Resulting Sediment Transport. Academic Press, New York, N.Y., pp.413--456.

Garcia-Gabin, W. 2015. Wave Bimodal Spectrum based on Swell and Wind-sea Components IFAC-PapersOnLine Volume 48, Issue 16, 2015, Pages 223-228

Goldberg, D., 1989. Genetic algorithms. Addison-Wesley, Reading, MA.

Grant, U., 1948. Influence of the water table on beach aggradation and degradation. Journal of Marine Research 7, 655–660

Grasso, F., Michallet, H., & Barthélemy, E., 2011. Sediment transport associated with morphological beach changes forced by irregular asymmetric,skewed waves. Journal of Geophysical Research, 116(C03020).

Goda, Y., 1976. On wave groups. Proc. BOSS' 76 (Trondheim, 1976), pp. 115-128.

Goda, Y., 1985. Random seas and design of maritime structures. University of Tokyo Press, Tokyo.

Goda, Y., 2010. Random seas and design of maritime structures, 3rd ed, Advanced Series on Ocean Engineering. World Scientific, Vol 33.

Gourlay, M.R., 1968. Beach and dune erosion tests. Delft Hydraul. Lab., Rep. M935/M936

Gu, Z., Wang, H., 1991. Gravity waves over porous bottoms. Coastal Engineering 15, 497 – 524.

Guza, R.T. and Bowen, A.J., 1975. The resonant instabilities of long waves obliquely incident on a beach. J. Geophys. Res., 80: 4529--4534.

Guza R T., Thorton E B., 1981. Wave set-up on a natural beach. Journal of Geophysical Research, 86, C5;4133-4137

Gourlay, M.R., 1992. Wave set-up, wave run-up and beach water table: interaction between surf zone hydraulics and groundwater hydraulics. Coastal Engineering 17, 93– 144

Guedes Soares, C., 1984. Representation of double-peaked sea wave spectra. Ocean Eng. 11, 185–207

Guo, Q. N., H. Li, M. C. Boufadel, Y. Xia, G. Li, 2007. Tide-induced groundwater head fluctuation in coastal multi-layered aquifer systems with a submarine outlet-capping, Adv. Water Resour., 30, 1746–1755, doi:10.1016/j.advwatres.2007.01.003.

Hall, K.R., 1991. Trends in phreatic surface motion in rubble-mound breakwaters. ASCE; Journal of Waterway, Port, Coastal, and Ocean Engineering; Vol. 117, No. 2, pp. 179–187; New York;

Hall, K.R., 1994. Hydrodynamic pressure changes in rubblemound breakwater armour layers. IAHR; Proceedings International Symposium: Waves – Physical and Numerical Modelling; pp. 1394–1403; Vancouver, Canada.

Hanslow D J, Nielsen P., 1993. Shoreline set-up on natural beaches. Journal of Coastal Research, 15; 1-10.

Hanafin, J.A., Quilfen, Y., Ardhuin, F., Sienkiewics, J., Queffeulou, P., Obrenski, M., Chapron, B., Reul, N., Collard, F., Corman, D., De Azevedo, E.B., Vandemark, D., and Stutzmann, E. 2012. Phenomenal Sea States and Swell from a North Atlantic Storm in February 2011: a comprehensive analysis. Bulletin of the American Meteorological Society, 93, 1825–1832, doi: 10.1175/BAMS-D-11-00128.1.

Hayes, M. O., J. Michel, D. V. Betenbaugh, 2009. The intermittently exposed, coarse-grained gravel beaches of Prince William Sound, Alaska: Comparison with open-ocean gravel beaches, J. Coastal Res., 26, 4–30

Hawkes P.J., Coates T.T., Jones R.J., 1998. Impact of Bi-modal seas on Beaches and Control Structures. Report SR507, Hydraulics Research, Wallingford, copy available on request.

Harleman, D.R.F., P.F. Melhorn, 1963, Dispersion-permeability correlation in porous media. Amer. Soc. Civil Eng., 89, 67-85.

Hasselmann, K., R.P. Barnett, E. Bouws, H. Carlsen, D.E. Cartwright, K.Enke, J.A.Ewing, H.Gienapp, D.E. Hasselmann, P. Kruseman, A. Meerburg, P. Mueller, D.J. Olbers, K. Richter, W. Sell, H. Walden, 1973. Measurements of wind-wave growth and swell decay during the Joint North Sea Wave Project (JONSWAP), Dtsch. Hydrogr. Z., A8, No. 12.

Hazen, Allen, 1930. Flood Flows: A Study of Frequencies and Magnitudes. New York:Wiley.

Herbers, T.H.C., Elgar, S., and Guza, R.T. (1995a) Generation and propagation of infragravity waves. Journal of Geophysical Research, 100 (C12), 24863–24872. doi: 10.1029/95JC02680 HYDRALAB III, 2007, Guidelines for wave modelling in flumes and basins: Hydraulic model testing in waves, Deliverable NA3.1-1, EC contract no. 022441 (RII3)

Hogben, N., Lamb, F.E., 1967. Ocean Wave Statistics. London H.M, Stationary Office

Holmes, R. R., Jr., 1996. Floods in the upper Mississippi River Basin. Sediment transport in the Lower Missouri and the central Missippi rivers, June 26 through September 14, 1993: U. S. Geological Circular 1120-I.

Horn, D.P., Mason T., 1994. Swash zone sediment transport modes. Marine Geology 120 (1994) 309-325

Horn, D.P., 2002. Beach groundwater dynamics. Geomorphology 48 (1-3), 121-146

Horn, D., Li, L., 2006. Measurement and modelling of gravel beach groundwater response to wave run-up: Effects on beach profile changes. Journal of Coastal Research, 1241– 1249.

Horn, D. P., S. M. Walton, 2007. Spatial and temporal variations of sediment size on a mixed sand and gravel beach, Sediment. Geol., 202(3), 509–528

Horn, D.P., Baldock, T.E., Li, L., 2007. The influence of groundwater on profile evolution of fine and coarse sand beaches. Proceedings of Coastal Sediments '07, New Orleans, ASCE, pp. 506–519.

Holtz, R.D., Kovacks, W. D., Sheahan, T. C., 2011. An introduction to Geotechnical Engineering: Prentice-Hall, Upper Saddle River, NJ, 853 p

Holthuijsen, L.H. 2007. Waves in Oceanic and Costal Waters, Cambridge University Press, Cambridge.

Hughes, S.A., Chiu, T., S., 1981. Beach and dune erosion during severe storms. Univ. of Florida. Coastal and Oceanographic Engrg. Dept. Report No. TR/043.

Hughes, M.G., 1992. Application of a non-linear shallow water theory to swash following bore collapse on a sandy beach. J. Coastal Res., 8: 562-578

Hughes, S.A., 1993. Physical models and laboratory techniques in coastal engineering. Advanced series on Ocean Engineering – Volume 7, World Scientific, 237-332.

Hughes, S.A., 2003. Estimating irregular wave runup on smooth, impermeable slopes (No. ERDC/CHL CHETN-III-68). U.S. Army Engineer Research and Development Center, Vicksburg, MS.

Hughes, S.A., 2005. Estimating Irregular Wave Runup on Rough, Impermeable Slopes (No. ERDC/CHL CHETN-III-70). US Army Corps of Engineers.

IAHR 1989. List of sea-state parameters Journal of Waterway, Port, Coastal, and Ocean Engineering Vol 115, No 6. pp 793-808.

Ilic, S., Chadwick, A., Li, B. and Fleming, C., 1997, June. Composite modeling of an offshore breakwater scheme in the UKCRF. In Coastal Dynamics' 97 (pp. 684-693). ASCE.

Ilic, S., Chadwick, A.J. and Fleming, C., 2005, December. Investigation of detached breakwaters. Part 2—morphodynamics. In Proceedings of the Institution of Civil Engineers-Maritime Engineering (Vol. 158, No. 4, pp. 163-172). Thomas Telford Ltd.

Inman, D. L., Bagnold, R. A., 1963. Beach and nearshore processes. Part II. Littoral processes, p. 529-553 in Hill, M. N., gen. ed., The Sea--ideas and observations on progress in the study of the seas: New York and London: Wiley-Interscience, v. 3, The Earth beneath the sea, 963 p.

Jamal, M.H., 2011. Modelling coarse-grained beach profile evolution. PhD Thesis, University of Plymouth, UK

Jamal, M.H., Simmonds, D.J., Magar, V., Pan, S., 2010. Modelling infiltration on gravel beaches with an XBeach variant. Proceedings of 32nd International Conference on Coastal Engineering, No. 32(2010), Shanghai, China, paper no. 156, 1-11

Jamal, M.H., Simmonds, D.J., Magar, V., 2012. Gravel beach profile evolution in wave and tidal environment. Proceedings of 33rdInternational Conference on Coastal Engineering, Santander, Spain, Paper No. 491, pp. 1–10

Jennings, R., Shulmeister, J., 2002. A field based classification scheme for gravel beaches. Marine Geology 186, 211–228.

Kamphuis, J.W. 1985. On understanding scale effect in coastal mobile bed models. In Dalrymple, R.A. (ed.) Physical modelling in coastal engineering, Rotterdam: A.A. Balkema, 141–162.

Kamphuis, J.W. 1991. Alongshore sediment transport rate. Journal of Waterway, Port, Coastal and Ocean Engineering, Vol. 117, 624-640

Kang H-Y, Aseervatham A M., Nielsen P., 1994. Field Measurements of Wave Runup and the Beach Watertable. Research report N CE148. Department of Civil Engineering, University of Queensland, 43pp.

Kang, H.-Y., Nielsen, P., 1996. Watertable dynamics in coastal areas. Proceedings of the 25th International Conference on Coastal Engineering. American Society of Civil Engineers, New York, pp. 4601–4612.

Kemp, P., 1960. The relationship between wave action and beach profile characteristics. In: Proceedings of 7th International Conference on Coastal Engineering, The Hague, The Netherlands

Kenney, T.C., Lau, D., 1984. Stability of Particle Grading of Compacted Granular Filters. University of Toronto, Toronto

Kerbiriou, M.A., Prevosto, M., Maisondieu, C., 2007. Influence of an improved seastate description on a wave energy converter production. In: Proceedings of the 26th International Conference on Offshore Mech. and Arct. Eng., San Diego, California, USA, June 07

Keulegan, G. H., Krumbein, W.C., 1949. Stable configuration of bottom slope in shallow water and its bearing on geological processes. Trans Amer geophys Union, 30, No 6.

King, C.A.M., 1972. Beaches and Coasts, 2rid ed. St. Martin's Press, New York, N.Y.

Kikkert, G. A., D. Pokrajac, T. O'Donoghue, and K. Steenhauer, 2013. Experimental study of bore-driven swash hydrodynamics on permeable rough slopes, Coastal Eng., 79, 42–56, doi:10.1016/j.coastaleng.2013.04.008.

Kobayashi, N., Wurjanto, A. 1992. Irregular wave interaction with permeable slopes. Proceedings of the 23rd International Conference on Coastal Engineering, 1299-1312.

Kobayashi N., 1988. Review of wave transformation and cross-shore sediment transport processes in surf zones. J. Coastal Res., 4: 435-445.

Koenders, M.A., 1985. Hydraulic criteria for filters. Delft Geotechnics, Unnumbered Report; Estuary Filters.

Komar, P. D., 1998. Beach Processes and Sedimentation. Prentice-Hall, Englewood Cliffs, New Jersey.

Komar, P.D., Miller, M.C., 1973. The threshold of sediment movement under oscillatory water waves. Journal of Sedimentary Petrology, 43, 4, 1101 – 1110.

Komar, P.D., Miller, M.C., 1975. On the comparison between the threshold of sediment motion under waves and unidirectional currents with a discussion of the practical evaluation of the threshold. Journal of Sedimentary Petrology, 45, 362 – 367.

Kozeny J., 1927. Uber kapillare Leitung des Wassers in Boden. S. B. Akad. Wiss. Wien Math. Naturwiss 136; 271-306.

Krumbein, W. C., G. D. Monk, 1943. Permeability as a function of the size parameters of sedimentary particles: Am. Inst. Min. and Met. Eng. Tech. Pub. 1492, p. 153-163.

Lamb, H. 1994. Hydrodynamics, 6th edn, Cambridge University Press, Cambridge.

Lara, I.J. Losada, P.L.- Liu, 2006. Breaking waves over a mild gravel slope: experimental and numerical analysis Journal of Geophysical Research C: Oceans, 111

Lee, E.M. & Clark, A.R., 2002. Investigation and Management of Soft Rock Cliffs. Thomas Telford, London

Le Méhauté, B., 1958. Perméabilité des digues en enrochements aux ondes de gravité periodiques. La Houille Blanche No. 6, 1957 et No. 2, 3, 1958.

Le Méhauté, B., 1958. An Introduction to Hydrodynamics and Water Waves. By B. Le Méhauté, B.,. Springer, 1976. 323 pp. Volume 91 Issue 4 - D. H. Peregrine

Li, L., Barry, D.A., Pattiaratchi, C.B., 1996. Modelling coastal groundwater response to beach dewatering. Journal of Waterway, Port, Coastal and Ocean Engineering 122, 273– 280.

Li, L., Barry, D.A., Pattiaratchi, C.B., 1997. Numerical modelling of tide-induced beach water table fluctuations. Coastal Engineering 30 (1– 2), 105– 123.

Li, L., Barry, D., 2000. Wave-induced beach groundwater flow. Advances in Water Resources 23, 325–337.

Longuet-Higgins, M., Stewart, R., 1962. Radiation stress and mass transport in gravity waves, with application to 'surf beats'. Journal of Fluid Mechanics 13, 481–504.

Longuet-Higgins, M.S. and Stewart, R.W., 1964. Radiation stress in water waves; a physical discussion with applications. Deep-Sea Res., 11 : 529--562.

Longuet-Higgins M. S., 1983. On the Joint Distribution of Wave Periods and Amplitudes in a Random Wave Field. DOI: 10.1098/rspa.1983.0107.

Lopez de San Román-Blanco, B.L. de, 2001. Morphodynamics of Mixed Beaches (Unpublished transfer MPhil/PhD Report). Civil and Environmental Engineering Department, Imperial College, London.

López de San Román-Blanco, B., Coates, T., Holmes, P., Chadwick, A. J., Bradbury, A., Baldock, T., Pedrozo-Acuña, A., Grüne, J., 2006. Large scale experiments on gravel and mixed beaches: experimental procedure, data documentation and initial results. Coastal Engineering 53 (4), 349-363.

Loveless, J. H., Grant, G. T., 1995. Physical modelling of scour at coastal structures. Hydra 2000, Proceedings of the 26th Congress of the International Association for Hydraulic Research, London, 293-298.

Mackay, E., 2016. A unified model for unimodal and bimodal ocean wave spectra. International Journal of Marine Energy Volume 15, September 2016, Pages 17-40

Mahalanobis, 1930. P C. On tests and measures of group divergence, Joumal of the Asiatic Society of Bengal, 26, 541-588.

Mason T., 1997. Hydrodynamics and sediment transport on a macro-tidal, mixed (sand and shingle) beach. Unpublished PhD Thesis University of Southampton

Mason, T., Coates, T. T., 2001. Sediment transport processes on mixed beaches: A review for shoreline management. Journal of Coastal Research 17 (3), 645–657.

Mason T., Bradbury A., Poate T., Newman R., 2008. Nearshore wave climate of the English Channel – evidence for bi-modal seas. Proceedings of 31st International Conference on Coastal Engineering, American Society of Civil Engineers; 605-616

Masselink, G., Hughes, M.G., 1998. Field investigation of sediment transport in the swash zone. Cont. Shelf Res. 18, 1179– 1199.

Masselink, G., Li, L., 2001. The role of swash infiltration in determining the beachface gradient: a numerical study. Marine Geology 176, 139 – 156.

Masselink, G., Puleo, J, A. 2006. Swash-zone morphodynamics. Continental Shelf Research, 2006, Vol.26(5), pp.661-680

Masselink, G., Russell, P., Blenkinsopp, C., Turner, I., 2010. Swash zone sediment transport, step dynamics and morphological response on a gravel beach. Marine Geology 274, 50–68.

Masselink, G., Turner, I., 2012. Large-scale laboratory investigation into the effect of varying back-barrier lagoon water levels on gravel beach morphology and swash zone sediment transport. Coastal Engineering 63, 23–38, BARDEX: a large-scale laboratory study of gravel barrier dynamics

Masselink, G., Castelle, B., Scott, T., Dodet, G., Suanez, S., Jackson, D., Floc'h, F., 2016. Extreme wave activity during 2013/2014 winter and morphological impacts along the Atlantic coast of Europe. Geophys. Res. Lett. 43.

McCall, R.T.,Masselink, G., Poate, T., Roelvink, J.A., Almeida, L.P., Davidson,M., Russell, P.E., 2014. Modelling storm hydrodynamics on gravel beaches with XBeach-G. Coast. Eng. 91, 231–250.

McCall, R.T., Masselink, G., Poate, T.G., Roelvink, J.A., Almeida, L.P., 2015. Modelling the morphodynamics of gravel beaches during storms with XBeach-G. Coast. Eng. 103, 52–66.

McLean, R.F., Kirk, R.M., 1969. Relationships between grain size, sorting and foreshore slope on mixed sand-shingle beaches. New Zealand Journal of Geology and Geophysics 12: 138-155.

McLean R. F. & Kirk . M. R., 1969. Relationships between grain size, size sorting, and foreshore slope on mixed sand - shingle beaches, New Zealand Journal of Geology and Geophysics, 12:1, 138-155

McLachlan, A., 1989. Water filtration by dissipative beaches. Limnology and Oceanography 34, 774– 78

McLean, R. F., 1970. Variations in grain-size and sorting on two Kaikoura beaches. New Z

Moskowitz, L., 1963.: Estimates of the power spectra for fully developed seas for wind speeds of 20 to 40 knots. Tech. Rept. for the U. S. Naval Oceanographic Office, New York University, School of Engineering and Science, Research Division

Moses, C. A., Williams, R. B., 2008. Artificial beach recharge: the south east England experience. Zeitschrift für Geomorphologie, Supplementary Issues 52 (3), 107–124.

Muttray, M.; Oumeraci, H.; Zimmermann, C.; Partenscky, H.–W., 1992. Wave energy dissipation on and in rubble mound breakwaters. ASCE; Proceedings International Conference Coastal Engineering (ICCE); Vol. 23, pp. 1434–1447; Venice, Italy.

Muttray, M.; Oumeraci, H.; Zimmermann, C., 1995. Wave-induced flow in a rubble mound breakwater. Proceedings of Coastal and Port Engineering in Developing Countries; Vol. 4, pp. 1219–1231; Rio de Janeiro, Brazi

Nelson, C.L., Miller, R.L., 1974. The Interaction of Fluid and Sediment on the Foreshore. Univ. Chicago, Dep. Geophys. Sci., Fluid Dynamics and Sediment Transport Labor. Tech. Rep., 15, 175 pp.

Nicholls, R., 1990. Managing erosion problems on shingle beaches: examples from Britain. In: Moutzouris, C. (Ed.), Proc. 3rd European Workshop on Coastal Zones, Paralimni, Cyprus

Nielsen, P., 1984. Field measurements of time-averaged suspended concentrations under waves. Coastal Eng., 8: 51-72.

Nielsen P (1989) Wave setup and runup: An integrated approach. Coastal Engineering. Vol. 13, pp 1-9.

Nielsen, P. (1992), Coastal Bottom Boundary Layers and Sediment Transport, Adv. Ser. Ocean Eng., vol. 4, World Scientific, Singapore.

Nielsen, P., 1997. Coastal groundwater dynamics. In: Proceedings of Coastal Dynamics, Plymouth, UK. pp. 546–555.

Nielsen, P., 1999. Groundwater dynamics and salinity in coastal barriers. Journal of Coastal Research 15 (3), 732– 740.

Nielsen, P., Kang, H.Y., 1995. Ground water dynamics in beaches and coastal barriers. In: Dally, W.R., Zeidler, R.B. (Eds.), Coastal Dynamics ’95. American Society of Civil Engineers, New York, pp. 521– 532.

Nielsen, P., Voisey, C.J., 1998. Watertable heights and salinity in coastal barriers: field measurements. Research report no. CH49/ 98, Department of Civil Engineering, The University of Queensland, October 1998.

Obhrai, C., Powell, K., Bradbury, A., 2008. A laboratory study of overtopping and breaching of shingle barrier beaches. In: Proceedings of 31st International Conference on Coastal Engineering, Hamburg, Germany.

Ochi, MK, Hubble, EN., 1976. Six Parameter Wave Spectra. Proc 5th Coastal Eng. Conf., ASCE, Honolulu, pp.301-328.

Oumeraci, H., Partenscky, H.W., 1990. Wave-induced pore pressures in rubble mound breakwaters. Proceedings of 22th International Conference on Coastal Engineering, ASCE, 1334-1347.

Orford, J.D., 1975. Discrimination of particle zonation on a pebble beach. Sedimentology 22, 441-463

Orford, J.D., Carter, R.W.G., 1991. The sedimentary organisation and behaviour of drift-aligned gravel barriers. Coastal Sediments '91, A.S.C.E, 934-948.

Orford, J.D., Carter, R.W. G., Mckenna, J., Jennings, S.C., 1995. The relationship between the rate of mesoscale sea-level rise and the rate of retreat of swash-aligned gravel-dominated barriers. Marine Geology, 124; 177-186.

Orford, J., Carter, R.W.G., 1982. Geomorphological Changes on the Barrier Coasts of South Wexford., Irish Geographer, 15, 70-84.

Orford, J.D., Forbes, D.L., Jennings, S.C., 2002. Organisationalcontrols, typologies and time scales of paraglacial gravel-dominated coastal systems. Geomorphology 48, 51–8

Ortega-Sánchez, M., Bergillos, R.J., López-Ruiz, A., Losada, M.A., 2017. Morphodynamics of Mediterranean Mixed Sand and Gravel Coasts.

Packwood, A., 1983. The influence of beach porosity on wave uprush and backwash. Coastal Engineering 7 (1), 29 – 40.

Pedrozo-Acuña, A., Simmonds, D., Otta, A., Chadwick, A., 2006. On the cross-shore profile change of gravel beaches. Coastal Engineering 53 (4), 335–347.

Pedrozo-Acuña, A., Simmonds, D. J., Chadwick, A. J., Silva, R., 2007. A numericalempirical approach for evaluating morphodynamic processes on gravel and mixed sand-gravel beaches. Marine Geology 241, 1 – 18.

Peregrine, D.H. 1983. Breaking waves on beaches. Ann.Rev.Fluid Mech. 15, 149-178

Pierson, W. J. , Jr. , G. Neumann, R. W. James, 1955. Observing and Forecasting Ocean Waves by Means of Wave Spectra and Statistics. Hydrographic Office Publication No. 603, U. S. Department of the Navy, 284 pp.

Pintado-Pati , J C , Torres-Freyermuth , A , Puleo , J A & Pokrajac , D, 2015. On the role of infiltration and exfiltration in swash zone boundary layer dynamics. Journal of Geophysical Research: Oceans , vol. 120 , no. 9 , pp. 6329-6350 . https://doi.org/10.1002/2015JC010806

Poate, T., McCall, R., Masselink, G., Russell, P., Davidson, M., 2012. Contrasting storm impacts on gravel beaches - examples from South England. In: Proceedings of the 33rd International Conference on Coastal Engineering

Poate, T., McCall, R., Masselink, G., 2016. A new parameterisation for runup on gravel beaches, Coastal Engineering, Volume 117, 2016, Pages 176-190, ISSN 0378-3839,

Polidoro, A., Dornbusch, U., Pullen, T., 2013. Improved maximum run-up formula for mixed beaches based on field data. ICE Coasts, Marine Structures and Breakwaters Conference, Edinburgh, pp. 389–398.

Polidoro, A.and Pullen, T.A. and Dornbusch, U, 2014. Comparison of field and laboratory measurements of wave run-up and validation of a new prediction method. In: Coastlab14 (5th International Conference on the Application of Physical Modelling in Coastal and Port Engineering and Science), 29 September – 2 October 2014, Varna, Bulgaria.

Polidoro, A., Pullen, T., Powell, K., 2015. Modelling Shingle Beaches in bimodal Seas, Test methodologies & Test programme. HR Wallingford report CAS1217-RT001-R03-00, UK.

Polidoro, A., Pullen, T., Eade, J., Mason, T., Blanco, B., Wyncoll, D., 2018. Gravel beach profile response allowing for bimodal sea-states. Maritime Engineering. 10.1680/jmaen.2018.11

Polubarinova Kochina, P.Ya., 1962. Theory of Ground Water Movement. Princeton University Press, New York.

Powell, K.A., 1990. Predicting Short TermProfile Response for Shingle Beaches. Hydraulics Research Limited, Wallingford, Oxfordshire. Report SR 219.

Powell, K.A., 1993. Dissimilar sediments: Model tests of replenished beaches using widely graded sediments. HR Wallingford report SR 350, UK.

Puleo, J.A., Beach, R.A., Holman, R.A., Allen, J.S., 2000. Swash zone sediment suspension and transport and the importance of bore-generated turbulence. Journal of Geophysical Research 105, 17021–17044.

Puleo, J. A., 2000. Swash zone sediment suspension and transport and the importance of bore-generated turbulence, J. Geophys. Res., 105, 17,021 – 17,044

Puleo, J. A., and K. T. Holland, 2001. Estimating swash zone friction coefficients on a sandy beach, Coastal Eng., 43, 25–40.

Puleo, J. A., T. Butt, 2006. The 1st international workshop on swashzone processes, Cont. Shelf Res., 26, 556 – 560.

Quick, M.C., 1991. Onshore–offshore sediment transport on beaches. Coastal Engineering 15, 313–332

Raubenheimer, B., Guza, R.T., Elgar, S., 1998. Watertable fluctuations in a sandy ocean beach. Proceedings of the 26th International Conference on Coastal Engineering. American Society of Civil Engineers, New York, pp. 3588–3600

Raubenheimer, B., Guza, R.T., Elgar, S., 1999. Tidal watertable fluctuations in a sandy ocean beach. Water Resources Research 35, 2313– 2320.

Roelvink, D., Reniers, A., van Dongeren, A., van Thiel de Vries, J., McCall, R., Lescinski, J., 2009. Modelling storm impacts on beaches, dunes and barrier islands. Coast. Eng. 56 (11-12), 1133–1152.

Savage, R. P., 1957. Model tests for hurricane protection project. Bulletin of the Beach Erosion Board, U.S. Army Corps of Engineers, Washington, DC.

Saville, T. J., 1961. Experimental determination of wave set-up. Proc., 2nd Technical Conf. on Hurricanes, U.S. Department. of Commerce, Washington, DC, 242–252.

Saulnier J.B., A. Clement a , A. F. de O. Falcao , T. Pontes, M. Prevosto, P. Ricci, 2011. Wave groupiness and spectral bandwidth as relevant parameters for the performance assessment of wave energy converters. Ocean Engineering 38 130–147.

Scheidegger, 1961. Physics of Flow in Porous Media. University of Toronto Press, Toronto.

Schneebeli, G., 1955. Expériences sur la limite de validité de la loi de darcy et l'apparition de la turbulence dans un écoulement de filtration. La Houille Blanche, (2), 141-149.

Sharp, J.J., 1981. Hydraulic modelling. Butterworth & Co. (Publishers) Ltd., 57 – 61, 96 – 126.

Shepard, F.P., Lafohd, E.C., 1940. Sand Movement Along the Scripps Institution Pier, Amer. J. of Science, v. 238, pp. 272-285,

Shepard, F., 1963. Submarine geology. Harper & Row, New York.

Shields, A. 1936. Application of similarity principles and turbulence research to bed load movement. California Institute of Technology, Pasadena (translated from German).

Shih, R.W.K.1990. Permeability characteristics of rubble material – New formulae. Proc. 22nd ICCE, Delft. Available as HR Published paper No. 38, HR Wallingford, the U.K.

Silveira, A, Peixoto Jr. T. d. L., Nogueira J. 1975: On Void Size Distribution of Granular Materials. In 5th panamerican conference on soil mechanics and foundation engineering, Buenos Aires, Argentina, volume 3.

Smit, P., Zijlema, M. Stelling, G., 2013.Depth-induced wave breaking in a non-hydrostatic, near shore wave model. Coast. Engng., 76, 1-16.

Smit, P., Stelling, G., Roelvink, J., Van Thiel de Vries, J., McCall, R., Van Dongeren, A., Zwinkels, C., Jacobs, R., 2010. XBeach: Nonhydrostatic model: Validation, verification and model description. Tech. rep., Delft University of Technology.

Smith, G., 1991. Comparison of stationary and oscillatory flow through porous media. Thesis TU Delft

Soares CG., 1984. Representation of double-peaked sea wave spectra. Ocean Engineering 11 (2), 185-207.

Steenhauer, K., D. Pokrajac, T. O'Donoghue, and G. A. Kikkert, 2011. Subsurface processes generated by bore-driven swash on coarse-grained beaches, J. Geophys. Res., 116, C04013, doi:10.1029/2010JC006789.

Strekalov, S.S., Tsyploukhin, V.P., Massel, S.T., 1972. Structure of Sea Wave Frequency Spectrum, Proc. 13th Coastal Eng. Conference, Volume 1,.

Stoker, J. J., 1957. Water waves: The mathematical theory with applications, Wiley-Interscience, New York.

Stockdon, H.F., Holman, R.A., Howd, P.A., Sallenger Jr., A.H., 2006. Empirical parameterization of setup, swash, and runup. Coastal Engineering 53, 573–588.

Toffoli, A., Bitner-Gregersen, E. M., 2017. Types of Ocean Surface Waves, Wave Classification. DOI: 10.1002/9781118476406.emoe077. In book: Encyclopedia of Maritime and Offshore Engineering

Torsethaugen, K. Haver, S., 2004. Simplified double peak spectral model for ocean waves. In: Proceedings of the International Symposium on Offshore and Polar Engineering '04, Toulon, France.

Trim L., 2003. Physical modelling of shingle beaches, Unpublished PhD thesis, University of Brighton.

Troch P., De Somer M., De Rouck J., Van Damme L., Vermeir D., Martens J.P., Van Hove C., 1996. Wave attenuation inside a rubble mound breakwater based on full scale measurements. Proc. 25th Int. Conference on Coastal Engineering, Orlando, USA.

Troch P., De Rouck J., Van Damme L., 1998. Instrumentation and prototype measurements at the Zeebrugge rubble mound breakwater. Coastal Engineering, Vol. 35 (1-2), pp. 141-166.

Troch, P. , De Rouck, J., Burcharth, H.F., 2002. Experimental study and numerical modeling of wave induced pore pressure attenuation inside a rubble mound breakwater. Proc. 28th International Conference on Coastal Engineering, ASCE, 1607-1619

Tucker, M.J. (1950) Surf beats: sea waves of 1 to 5 minute period. Proceedings of the Royal Society of London A, 202, 565–573. doi: 10.1098/rspa.1950.0120

Turner, I.L., 1995. Simulating the influence of groundwater seepage sediment on sediment transported by the sweep of the swash zone across macro-tidal beaches. Marine Geology, 125(1-2): 153-174.

Turner, I.L., Masselink, G., 1998. Swash infiltration-exfiltration and sediment transport. Journal of Geophysical Research, 103(C13): 30813-30824.

Turner, I.L., Nielsen, P., 1997. Rapid water table fluctuations within the beach face: Implications for swash zone sediment mobility?, Coastal Engineering, 32, pp. 45-59

Turner, I. L., Masselink, G., 2012. Coastal gravel barrier hydrology - observations from a prototype-scale laboratory experiment (BARDEX). Coastal Engineering 63, 13 – 22.

Thompson, D. A., H. Karunarathna, D. E. Reeve, 2017. Modelling Extreme Wave Overtopping at Aberystwyth Promenade" by Water 2017, 9(9), 663

Van der Meer, J. W., 1988. Rock slopes and gravel beaches under wave attack. Ph.D. thesis, Delft University of Technology

Van der Meer, J.W., Janssen, J.P.F.M., 1994. Wave run-up and wave overtopping at dikes (No. 485), Delft Hydraulics Publication. Delft Hydraulics.

van Gent, M.R.A., 1995. Wave interaction with permeable coastal structures, PhD Thesis, TU Delft, The Netherlands.

van Gent, M.R.A., 1992. Formulae to describe porous flow. Communications on Hydraulic and Geotechnical Engineering, Delft University of Technology.

van Gent, M.R.A., 1993. Stationary And Oscillatory Flow Through Coarse Porous Media. Communications on Hydraulic and Geotechnical Engineering, Report No. 93-9. Delft University of Technology, Delft.

Van Hijum, E., Pilarczyk, K., W., 1982. Equilibrium profile and longshore transport of coarse material under regular and irregular wave attack. Delft Hyd. Lab. Pub No 274.

Van Rijn, L.C., Walstra, D.J.R., Grasmeijer, B., Sutherland, J., Pan, S., Sierra, J.P., 2003. The predictability of cross-shore bed evolution of sandy beaches at the time scale of storms and seasons using process-based profile models. Coastal Engineering, Vol. 47, p. 295-327.

Van Rijn, L.C., 2006. Principles of sedimentation and erosion engineering in rivers, estuaries and coastal seas. Aqua Publications, The Netherlands (www.aquapublications.nl.

Van Rijn, L.C., 2007. Unified view of sediment transport by currents and waves, IV: Application of morphodynamic model. Journal of Hydraulic Engineering, ASCE, Vol. 133, No. 7, p. 776-793.

Van Wellen, E, Chadwick, Mason, T., 2000. A review and assessment of longshore sediment transport equations for coarse grained beaches. Coastal Engineering, 40, 3, 243-275.

Williams, J., Buscombe, D., Masselink, G., Turner, I., Swinkels, C., 2012. Barrier dynamics experiment (BARDEX): Aims, design and procedures. Coastal Engineering 63 (0), 3 – 12.

Whitehouse, R.J.S (1998). Scour at coastal structures: A manual for practical applications. Thomas Telford. London, 198 p.

Wright, D.E., 1968. Non-Linear How through Granular Media. j . Hydraulics Div., ASCE, v. 94, No. HY4, pp. 851-872

Wright, L.D ; Chappell, J ; Thom, B.G ; Bradshaw, M.P ; Cowell, P, 1979. Morphodynamics of reflective and dissipative beach and inshore systems: Southeastern Australia. Marine Geology, 1979, Vol.32(1), pp.105-140.

Wright, D. 1998. Hurst Spit: the local authority perspective. Pp. 256-266

Yalin, M.S., Franke, L., 1961. Experimental Investigations of the Laws of Filter Flow. Proc. IAHR 9th Congress, Dubrovnic, pp. 324-331.

Yalin, M.S., 1963. A model shingle beach with permeability and drag forces reproduced. Proceedings of the 10th IAHR congress, 1, 169 – 175

Yalin, M.S., 1971. Theory of Hydraulic Models, The MacMillan Press Ltd., London.

Zijlema, M., Stelling, G. Smit, P., 2011. Swash: an operational public domain code for simulating wave fields and rapidly varied flows in coastal waters. Coastal Engineering, 58 (10), 992–1012.

Appendices

Appendix A – Gravel Beach Profile Response Allowing for Bimodal Seastate

Cite this article
Polidoro A, Pullen T, Eade J *et al.*
Gravel beach profile response allowing for bimodal sea states.
Proceedings of the Institution of Civil Engineers – Maritime Engineering,
https://doi.org/10.1680/jmaen.2018.11

Research Article
Paper 201811
Received 13/02/2018;
Accepted 17/09/2018

Keywords: coastal engineering/
granular materials/maritime engineering

Maritime Engineering

ice publishing

Gravel beach profile response allowing for bimodal sea states

Andrea Polidoro BEng (Hons), MEng
Engineer, Coastal Structures, HR Wallingford Ltd, Wallingford, UK
(corresponding author: a.polidoro@hrwallingford.com)
(Orcid:0000-0002-3044-0360)

Tim Pullen BEng (Hons), MEng, PhD
Principal Engineer, Coastal Structures, HR Wallingford Ltd, Wallingford, UK

Jack Eade BEng, MEng
Coastal Process Scientist, Channel Coastal Observatory,
National Oceanography Centre, Southampton, UK

Travis Mason PhD
Director, Channel Coastal Observatory, National Oceanography Centre,
Southampton, UK

Belen Blanco PhD
Principal Scientist, Coasts & Estuaries, HR Wallingford Ltd, Wallingford, UK

David Wyncoll PhD
Senior Scientist, Flood Management, HR Wallingford Ltd, Wallingford, UK

The south coast of the UK is identified as a location where significant wave swell components are present within the regional wave climate. During the winters of 2006 and 2014, several sites along the south coast of the UK were subject to significant damages where flood events were recorded. These sea states were characterised by having a double-peaked wave spectra, observing a connection between wave spectrum shape and beach response. A two-dimensional (2D) physical model study was carried out to investigate the effect of gravel beach profile response under wave spectra characterised by swell-wave and wind-wave periods in various combinations. The physical model results showed the effect of bimodal wave spectrum on beach crest erosion and were compared with the parametric model Shingle and the numerical model XBeach-G. Based on this 2D physical model study, a new parametric model, Shingle-B, was derived and an online tool developed and made available on the website for the National Network of Regional Coastal Monitoring Programmes of England. This new tool has been validated at two sites in the south of England where field data of both waves and profiles were available.

Notation

$D_{x\%}$	grain size that exceeds by size x% of the sediment distribution
D_{50}	median grain size
H_{m0}	wind wave height
H_{m0i}	significant incident spectral wave height
L_{m0}	mean wavelength
$L_{m-1,0}$	deep water wave length
m_0	total spectral energy
Q_p	peakedness parameter
$S(f)$	incident spectral density
S%	swell percentage
s, s_0, s_{m0}	wave steepness
$T_{m0,2}$	mean spectral wave period defined using the zeroth and second moments of the frequency spectrum
$T_{m-1,0}$	spectral wave period defined using the inverse and zeroth moments of the frequency spectrum
T_p	peak wave period
y	wind wave spectral shape
β_i	corresponding regression coefficients to be estimated when fitting
ε	broadness parameter
v	narrowness parameter
ξ_0	breaker parameter

1. Introduction

Gravel beaches are a particular type of beach in which the sediments are solely composed of gravel sediment (2–64 mm, according to the Wentworth scale, Folk scheme (BGS, 1987)) according to López de San Román-Blanco *et al.* (2006). It is also common to find coarse-grained beaches that include both gravel and mixed (sand and gravel) sediments.

These beaches are common in mid- to high-latitude coasts (Carter and Orford, 1993; Hayes *et al.*, 2009; Horn and Walton, 2007) but are also present on the shores of many parts of the world. Gravel beaches assume particular importance as defence systems along stretches of the heavily populated south coast of England where they are known as shingle beaches (Moses and Williams, 2008; Nicholls, 1990). Approximately one-third of the beaches in England and Wales are classified as coarse grained, especially along the south coast of England (López de San Román-Blanco, 2001). A gravel beach can be seen as a sum of different zones where the interaction of hydrodynamic processes and beach characteristics influence the final response of the beach. These zones are schematised in Figure 1. The most important zones for these beaches are the surf and swash zone. The surf zone is the zone of wave action extending from the water line out to the most seaward point of the zone where waves start breaking (breaker zone). In the surf zone, the sediments will be subject to a complex set of forces that are

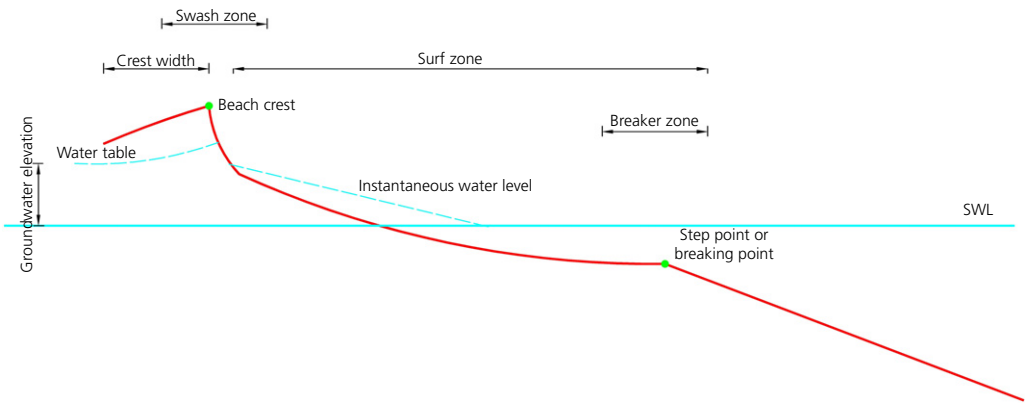

Figure 1. Schematisation of a general beach profile

produced due to bed friction and the impact of the breakers, which generates significant turbulence and sediment sorting. The surf zone is a very dynamic zone and the response of the beach profile is strongly linked to a change of the incident wave energy. The swash zone is the zone of wave action on the beach, extending from the limit of run-up to the limit of run-down. As discussed in more detail by Horn (2002), the interaction between wave motion and the beach groundwater table (see Figure 1) provides an important control on swash zone sediment transport.

Gravel beaches are an important form of natural coastal defence, protecting significant urban settlements as well as agricultural, recreational and environmental land areas against flooding and erosion (Powell, 1990; van Wellen *et al.*, 2000). Their functions as coastal defences and natural habitats therefore compel coastal engineers to understand the processes occurring across the gravel beachface (Buscombe and Masselink, 2006). Beach behaviour is coupled with the incident wave conditions, hence the need for coastal engineers to study the approaching wave climate in order to have a reliable prediction of the beach response. In the south coast of England, it is common to have Atlantic swell waves penetrating into the English Channel (up to about Beachy Head), often leading to wave conditions with a broad, bimodal (combination of wind-wave and swell-wave components) or multi-modal spectrum (Bradbury *et al.*, 2007). Along the south coast of England, a significant presence of bimodal sea states is recorded. The typical sites affected by bimodal conditions are Milford-on-Sea, Hayling Island, Rustington, Boscombe, Chesil, West Bay and Penzance (Bradbury *et al.*, 2007).

The impact of wind waves on the coast in terms of overtopping, beach erosion, armour damage and so on are relatively well understood for many simple configurations (EurOtop, 2007; Powell, 1990; van der Meer, 1988). Conversely, swell waves, having longer periods than wind waves (Goda, 2010), are not generally considered in coastal structures design. However, it is possible that a combination of wind sea and swell waves represent a worst-case sea state for some aspects of beach design (Bradbury *et al.*, 2006). Indeed, recent work carried out by Thompson *et al.* (2017) noted that bimodal sea states lead to greater overtopping and that the formulae available in the literature underestimate wave overtopping under bimodal wave conditions. An example of the effect of the bimodal sea states on coastlines was observed during the winters of 2006 and 2014, where several sites along the south coast of England were subjected to significant damage due to flooding events. The total economic damage for England during the winter period was estimated to be between £1000 million and £1500 million, including damage due to fluvial and groundwater flooding (Defra, 2016). A programme of near-shore wave measurement, wave hindcasting and beach response to extreme storm events in the English Channel found that bimodal (double-peaked) wave conditions produced more damage to the beaches than suggested by empirical models (based on statistical wave parameters) (Bradbury *et al.*, 2002, 2004, 2007). In particular, the beach responses related to the measured wave data during these events suggested that the unexpected beach behaviour and breaching phenomena were linked to the spectral characteristics of the storm events (Bradbury *et al.*, 2007). Interestingly, these sea states were characterised by having moderate rather than storm wave conditions, and their wave spectra presented a notable energy within low frequencies (Mason *et al.*, 2008). Subsequent to these storm events, a correlation between bimodal wave spectra, beach response and breaching events was identified.

A two-dimensional (2D) physical model study carried out by Hawkes *et al.* (1998) confirmed the critical impact of long-period energy influencing the beach response; however, in that study a predictive method was not developed. Hawkes *et al.* (1998) stated that, following the results of the study, the existing method of predicting beach response could be inadequate when bimodal conditions are present.

Similar conclusions were confirmed by Bradbury *et al.* (2007), who observed that bimodal conditions significantly affect the beach profile performance, influencing the impact of wave run-up, erosion and overwashing. They also emphasised the need to consider bimodal wave conditions as a design variable for some areas of the English Channel coast.

Unfortunately, little is still known about the effect of bimodal sea conditions on sea defences and beaches (Bradbury, 1998; Bradbury *et al.*, 2007; Coates and Bona, 1997) and swell is rarely considered explicitly in the design or assessment of shoreline management operations. Indeed, as will be described in more detail in the following sections, the use of the existing prediction model for gravel beach profiles (Powell, 1990), known as Shingle, and the process-based XBeach-G (McCall *et al.*, 2014) are not appropriate tools for bimodal conditions. This is because these prediction models are based on experiments carried out with simple unimodal sea states, neglecting the possibility of having the complex wave conditions that combine wind wave and swell, forming a bimodal spectrum. There was therefore an urgent need to better understand the effect of the interaction between wind waves and swell waves on the beach response and to developing understanding of the prediction of beach response under bimodal storm conditions.

The objective of this study was to develop a new parametric model for predicting beach profile response of shingle beaches under bimodal wave conditions in order to increase confidence in beach cross-section design. An empirical framework, based on extensive 2D physical model data and field work, was developed to examine the profile response of gravel beaches to bimodal wave spectra, characterised by swell-wave and wind-wave periods in various combinations. Based on this 2D physical model study, a new parametric model for predicting gravel beach profile response was derived. This model, called Shingle-B, is available online on the website for the National Network of Regional Coastal Monitoring Programmes of England (CCO, 2018a).

This paper discusses both the results of the physical model and the development of a parametric model, which represents an improvement over existing models for gravel coasts, subjected to bimodal wave conditions. Section 2 provides a more detailed description of bimodal sea states. The 2D physical model study and its results are discussed in Sections 3 and 4, respectively. The existing predictive methods for shingle beach morphological response are reviewed in Section 5 and applied to some of the physical model experiment results. The new parametric model, Shingle-B, is described in Section 6.

2. Occurrence of bimodal sea states

The presence of bimodal (double-peaked) wave spectra has been observed along several coasts of the globe – for example Atlantic and Pacific Oceans (Garcia-Gabin, 2015), the west coast of New Zealand (Ewans *et al.*, 2006) and the Gulf of Mexico and southern California (Mackay, 2016). In particular, on the south coast of England, Atlantic swell waves penetrate into the English Channel, often leading to wave conditions with a broad, bimodal or multi-modal (having several maxima) spectrum (Bradbury *et al.*, 2007). The swell propagates up the English Channel reaching the coastline east of the Isle of Wight and can, occasionally extend the full length of the English Channel (Mason *et al.*, 2008). Analysis of wave spectra from the National Network of Regional Coastal Monitoring Programmes' coastal wave network has identified that bimodal sea conditions occur on a regular basis (Mason *et al.*, 2008). Typically, the highest presence of bimodal seas is associated with sites exposed to Atlantic swell – for example Porthleven in Cornwall. The occurrence of bimodal seas is seasonal, being more common during the winter months (December, January and February) and less common in the summer (June, July and August), as shown in Figure 2, where the average seasonal percentage of bimodal wave conditions recorded during the period from July 2003 to July 2016 is reported.

The effect of long-period waves on gravel beaches in the south coast of England was observed in the past. A typical example is Hurst Spit, which was breached several times during its life, and the spit was indeed breached several times between 1983 and 1984. The most severe damage, however, occurred on 16 and 17 December 1989, when southwesterly storms combined with a surge in excess of 1 m flattened an 800 m length of Hurst Spit (Bray and Hooke, 1998), as shown in Figure 3.

More recently, during the winter of 2013–2014, the south coast of England was exposed to an unusual and prolonged combination of severe storms. Many sites in central southern England experienced between five and seven storms during this period (October 2013 to February 2014). A number of storms exceeded the extreme wave conditions of one in ten years, or one in 50 year return periods, as shown in Figure 4, where the geographical occurrence/location of recorded return period exceedance between October 2013 and February 2014 is shown. Analysis of a 60-year hindcast wave model record (validated by offshore wave buoy measurements) by Masselink *et al.* (2016) suggests that the 2013–2014 winter was the most energetic since 1948. The storm sequences during the winter of 2013–2014 along the south coast of England had a considerable impact on many of the beaches. During these storms, Hurst Spit was subject to an unpredicted breaching (see Figure 5) and flooding and overwash events were observed in many other parts of the south coast of England.

The driving force behind this new research, however, has its roots in less stormy bimodal conditions. A sequence of

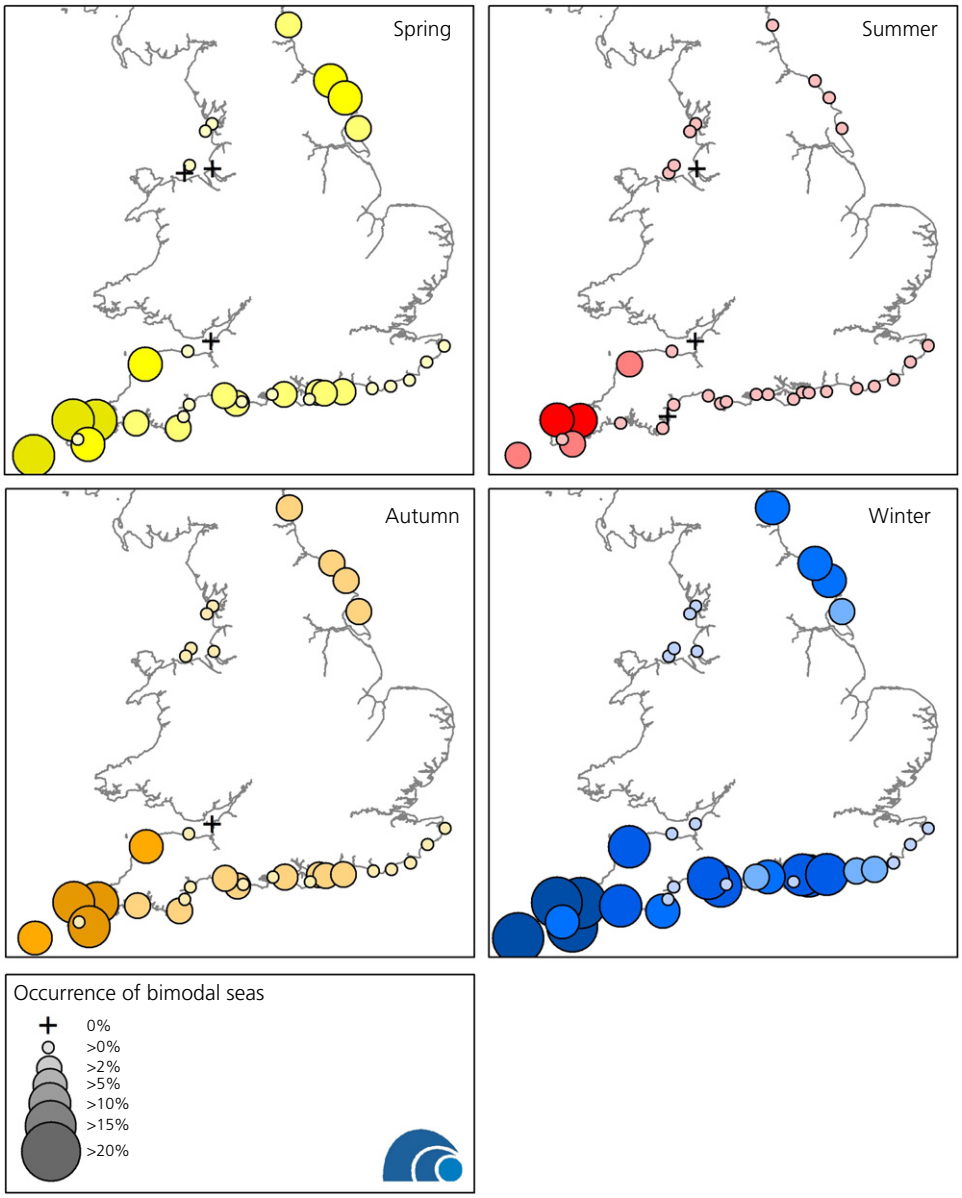

Figure 2. Seasonal occurrence of bimodal seas (extracted from CCO (2018b))

unexpected (not forecasted) coastal flooding events was observed at Seaton, Cornwall, in October 2006 and at Hayling Island on 3 November 2005. All these instances were recorded during periods of moderately, rather than stormy wind-wave conditions, but notable for the underlying presence of long-period swell waves (Mason *et al*., 2008). Figure 6 shows Seaton during one of these unpredicted flooding events in October 2006. As it can be seen in the figure, the flood gate had remained open during the flooding event, highlighting the fact that the wind-wave forecast alone was unable to predict the potential for flooding.

In this study, the bimodal half-hourly spectra recorded at Chesil, Milford, Rustington and Hayling Island, from January 2005 to September 2015, were used to extract the occurrence of the swell percentage (S%) on the total wave energy spectrum. The spectra were obtained from the National Network of Regional Coastal Monitoring Programmes, and the results are shown in Figure 7, where it can be seen that for a bimodal wave spectrum, the swell component percentage ranged between 10 and 70%. Most of the bimodal wave spectra present a swell component between 10 and 20%, but cases of swell between 30 and 50% are common. In some cases,

Figure 3. Hurst Spit, breached in 1989, at New Forest District Council (NFDC)

bimodal spectra with 70% of swell component have also been recorded. As discussed in more detail in the following section, the wave conditions tested in the 2D physical model consisted of S% ranging between 10 and 40%, as these represent the vast majority of all the sea states analysed.

3. Physical model study

3.1 Introduction

A 2D physical model study was carried out using a 100 m long wave flume at HR Wallingford, with a wave paddle able to generate non-repeating random sea states to any required spectral form, including bimodal spectra. The model set-up is schematised in Figure 8 (model scale 1 in 25), where the location of the tested gravel beach and wave probes is shown. In order to reproduce the prototype beach response correctly, the model material had to be scaled according to the three main criteria described by Powell (1990). The methodology used to scale the gravel material is outlined here, with further detail given by Polidoro *et al.* (2015).

The three criteria defined by Powell (1990) needed to produce the correct beach response in a mobile bed physical model study are the permeability of the beach (Yalin, 1963) (controls the beach slope) the relative magnitudes of the onshore and offshore motion (Dean, 1973, 1985) (controls whether the beach erodes or accretes) and the threshold of sediment motion (Komar and Miller, 1973, 1975) (hence the onset of onshore–offshore transport).

A study of the sediment distributions for a typical range of gravel beaches along the south coast of England was carried out by Powell (1993). Based on Powell's work, a typical grading curve ($D_{50} = 12{\cdot}5$ mm and $D_{10} = 2{\cdot}8$ mm) was reproduced in this study by using four distinct mixes of crushed anthracite (specific gravity of 1400 kg/m^3). The anthracite used for the beach is supplied in six different grades, which were combined to achieve the model grading curve shown in Figure 9 (solid curve) plotted against the target grading curve (dashed curve). The use of anthracite to reproduce correctly the behaviour of a prototype gravel beach was confirmed by comparisons between the measured test profiles from the Großen Wellen Kanal (López de San Román-Blanco *et al.*, 2006) with the profile predicted by Shingle (Powell, 1990). The good agreement between predicted and measured profiles generally indicated that the methodology previously adopted by Powell (1990) for small-scale testing of shingle beaches (use of anthracite) correctly describes the cross-shore profile response under normally incident wave conditions (Bradbury *et al.*, 2002).

During this study, the initial beach slope was 1 in 8 (plane sloping beach) for all the test conditions, as shown in Figure 10. For each test, the post-storm beach profile was measured using a 2D bed profiler, which extracted the profile elevation every 20 mm along the x-axis. The bed profiler was mounted above the central section of the beach, enabling coverage of a 4 m (model) long profile across the mobile sediment. The touch-sensitive probe had a proximity switch that allowed it to detect the bed with the minimum of contact pressure. The probe was stepped forward and lowered down on the bed; the encoder in the profiler then determined the bed height. This probe is particularly suitable for profiling both below and above the water surface. The bed profiler was used to monitor all tests with an accuracy of ±1·0 mm vertically and horizontally (the prototype scale equivalent would be 25 mm accuracy or equivalent to one piece of large gravel).

For each wave condition, described in the following section, an in-line array of six wave gauges was used to measure both the incident wind and swell waves. Time histories recorded by each gauge in the array were analysed spectrally to give the following parameters: significant incident spectral wave height, H_{m0i}; peak wave period, T_p; mean spectral wave period, $T_{m0,2}$, defined using the zeroth and second moments of the frequency spectrum; the spectral wave period, $T_{m-1,0}$, defined using the inverse and zeroth moments of the frequency spectrum. The tests were carried out using a non-repeating sequence of duration equal to 3000 times the mean wind-wave period, $T_{m0,2}$, of the target spectrum.

3.2 Design wave conditions

This section briefly outlines the waves used during testing, the shape of the spectrum, range of wave periods and how these are all related to the total spectral energy (m_0). A more detailed discussion of the spectral shape is given in Polidoro *et al.* (2015).

The principal purpose of this study was to cover a large range of input conditions to examine the response of shingle beaches

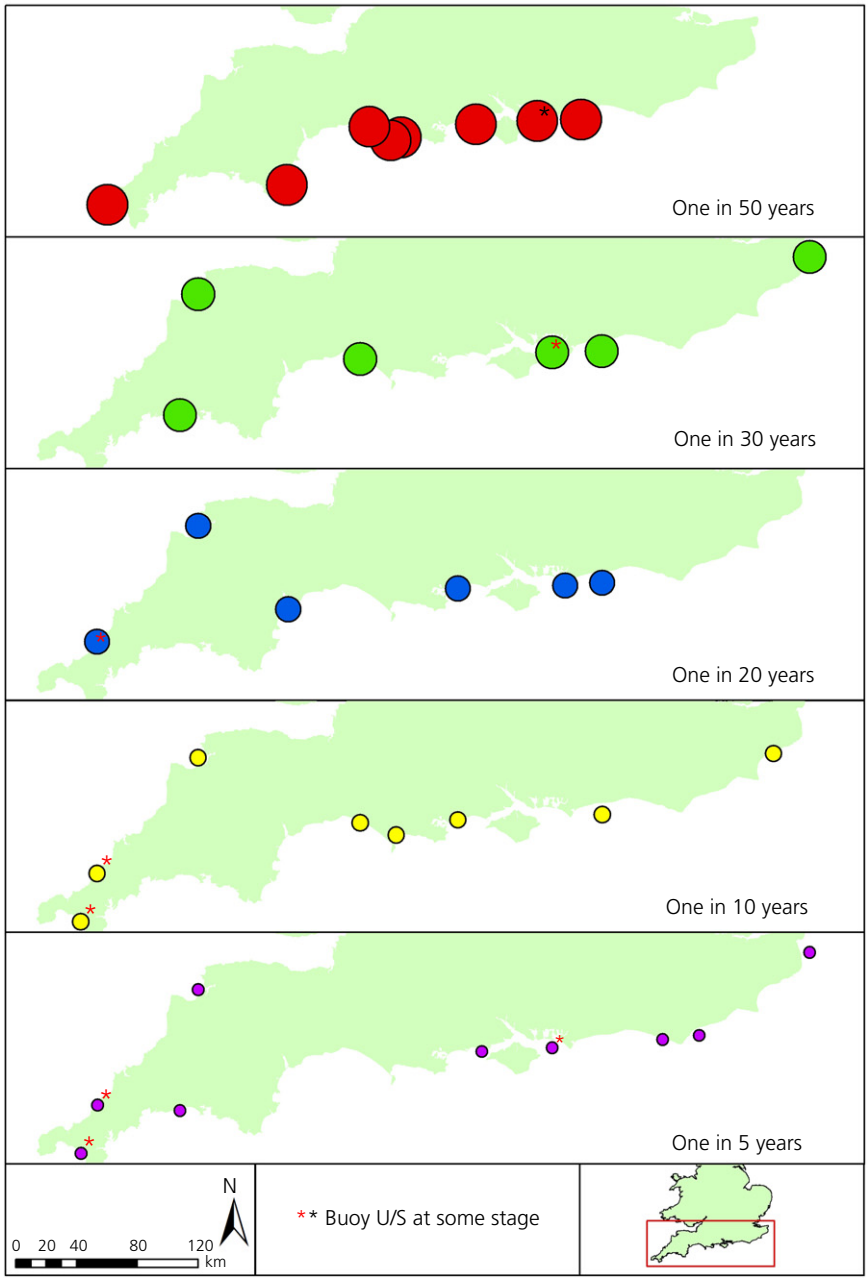

Figure 4. Distribution of storms exceeding the one in 5 year return period between October 2013 and February 2014 (adapted from Bradbury and Mason (2014))

under bimodal sea states, where design wave attack is assumed to be normal or near normal. The wave conditions were based broadly around a framework of measured conditions (wave height, wave steepness and wave periods) derived from wave buoys at Chesil, Milford-on-Sea and Hayling Island, as described in more detail by Bradbury *et al*. (2007) and Bradbury *et al.* (2009). Wave conditions were based broadly around prototype measurements covering a range of wave heights from 3·0 to 6·0 m, swell periods from 15 to 25 s and wave steepness of 0·03, 0·04 and 0·05. Once the wave heights were established, the wind-wave periods were changed to between 6 and 9 s to obtain the set wave steepness. Prototype wave conditions were defined at locations in 12–15 m water depth, therefore, wave measurements in the flume were made at correspondingly equivalent depths, as shown in Figure 8 (wave gauge buoy).

Figure 5. Hurst Spit, unpredictably breached in 2014 (courtesy Peter Ferguson at NFDC)

Figure 6. Seaton beach, Cornwall, 2006, the flood gate remained open during the flooding event (NFDC)

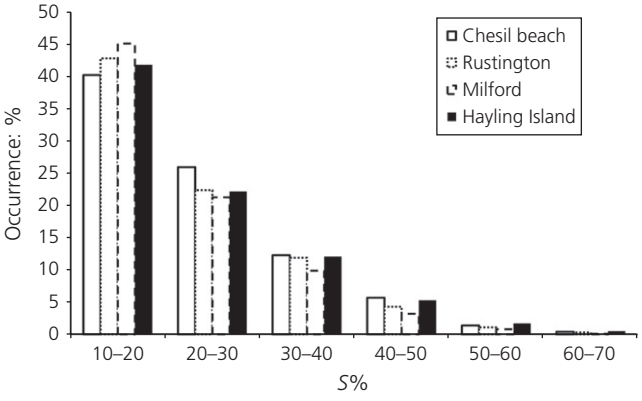

Figure 7. *S*% occurrence for the bimodal wave spectra recorded during the period from 2005 to 2015

Each test was run with both a nominal wind wave and the associated idealised bimodal wave. The nominal wind wave was described by wind-wave spectral shape (γ), wind-wave height (H_{m0}) and wind-wave period (T_p), as shown in Figure 11. The bimodal wave was described by a superposition of a wind wave and a swell wave, that together have the same total energy (area under the curve, m_0) as the nominal wind wave. The bimodal spectra is therefore predicted using the total H_{m0} (the sum of the energy in the spectrum), T_{pwind}, T_{pswell} and the percentage of the swell component (Figure 11). The bimodal spectrum was modelled using a standard Jonswap spectrum with a peak enhancement factor of $\gamma = 3{\cdot}3$ for the wind component. Analysis of swell waves generated off New Zealand showed that the swell spectra peaks were equivalent to the Jonswap spectra with $\gamma = 8$–9 (Goda, 1985). This is because the swell waves have spectra confined in a narrow frequency range and thus have a peak much sharper than that of wind waves (Goda, 2010). For the swell component, even though swell waves tend to have a narrow and peaked spectrum, a Jonswap spectrum with enhancement factor of $\gamma = 1{\cdot}5$ was selected in order for the wave paddle generator to reproduce well-defined wave spectra for the low frequencies, without missing information when the wave energy was shifted from high to lower frequencies. Although the peak enhancement factor (γ) is expected to have a certain degree of influence on the beach profile response, this has not been investigated in past research studies and it is outside the remit of this study.

To further investigate the variation of beach profile response and wave run-up with the spectral shape and the distribution of energy across the frequencies, each wave condition was run with the same spectral wave height H_{m0} (i.e. the same area under the spectrum) and successively subdivided to represent varying percentages of swell (0, 10, 20, 30 and 40%). This can be observed in Figure 12, where the total energy under the wave spectra is maintained, although distributed with different percentage swell components. The choice of *S*% was based on work carried out by Bradbury *et al.* (2007) and the additional analysis previously discussed and summarised in Figure 7.

3.3 Test programme

During these tests, different combinations of wave heights and wave periods were used in four steps of varying *S*% (10–40%) at a single water level on a 1 in 8 beach slope, with a difference in elevation between beach crest and beach toe of 17 m. The tests were initially carried out with a single deep-water wave steepness $s_{m0} = 0{\cdot}05$ and successively reduced to $s_{m0} = 0{\cdot}04$ and $s_{m0} = 0{\cdot}03$ in order to study the effect of wave steepness on the beach response. In addition, a fully developed swell sea state (unimodal wave spectra, 100% swell component) was run with three different swell-wave periods to investigate the profile

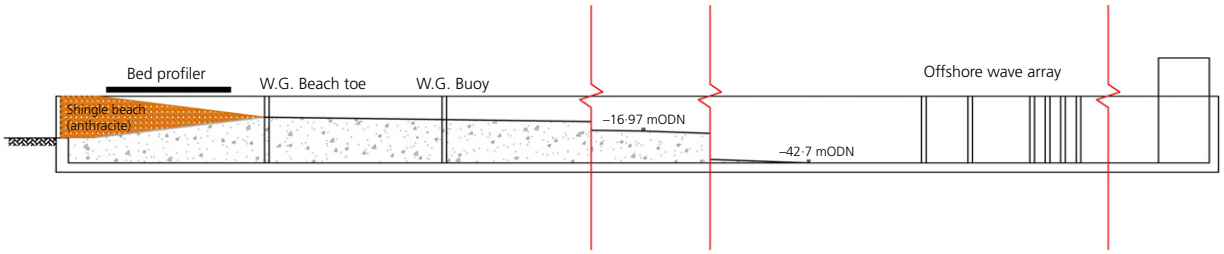

Figure 8. Model flume set-up. Note the flume is 100 m long. ODN, Ordnance Datum Newlyn; W.G., wave gauges

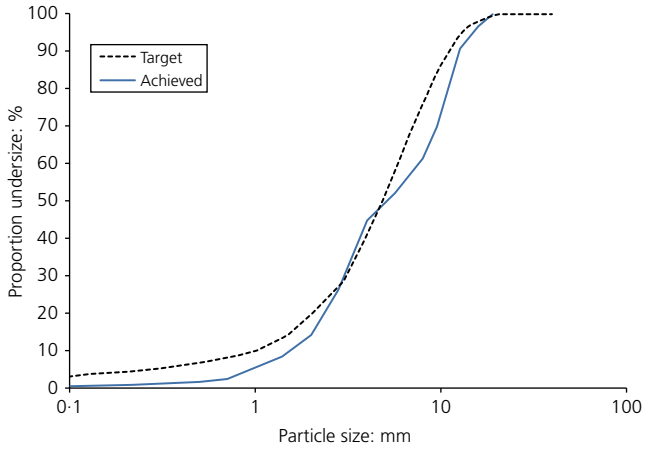

Figure 9. Target grading curve plotted against model grading curve of the anthracite used in the physical model tests

response under these conditions. A detailed description of each test series is given by Polidoro *et al.* (2015). Table 1 includes information on the order in which the test series were run plus brief details on the configuration of the shingle beach tested, the spectral wave heights and wave steepness that were run, the number of waves to reach the (dynamic) equilibrium profile and the number of tests.

4. Physical model results

4.1 Introduction

Each test was run initially for a duration of 1000, 2000 and 3000 waves; the duration being defined by the mean wave period $T_{m0,2\text{wind}}$. Beach profiles were measured following each sequence of 1000 waves. Although the initial intention was to continue each test until dynamic equilibrium was reached, the first test results showed that after 2000 waves the profile did not change significantly (see Figure 13) and that there was no discernible difference after 3000 waves. It was decided, therefore, to run for 3000 waves for the remaining tests, and only profile them once at the end of testing. This is in agreement with the results obtained by Powell (1990), who observed that approximately 80% of the total volumetric change occurred during the first 500 waves.

The representation of random sea waves can be considered as a stochastic process where the whole varies randomly with time (Goda, 2010). A given sea state, characterised by spectral energy, can be reproduced by an infinite number of time series having the same spectral energy (Goda, 2010). In order to investigate the effect of the time-series sequence on the final beach profile response, four different random time series (with the same wave spectrum and different random sequences) were generated. Results of the beach profiles under these four random time series are plotted in Figure 14. The final profiles showed that the crest position and the lower limit of the profile developments are relatively insensitive to the sequence of the time series. However, the beach profile within the surf zone is, as expected, slightly more sensitive to the sequence of the train of waves. This can be explained because within the surf zone waves start breaking and therefore non-linear responses influence the sediment transport. This part of the beach profile is very dynamic, changing almost wave by wave so that even the last sequence of waves affects the final profile. As a consequence, the final beach profile shows a small variability within the surf zone, possibly due to the effect of the final sequence of waves. Based on these observations, throughout this study it was decided to run different time series for each test condition. The ability to generate long non-repeating time series is of great importance when testing models that have a non-linear response, as in this case.

Almost 200 profiles were recorded and it is therefore not possible to present all of them in this section. Instead, results are presented where they assist understanding of the main outcomes or where it is necessary to illustrate trends or specific aspects of interest.

4.2 Swell component effect on beach profile response

An example of the effect of S% on the beach profile is plotted in Figure 15, where wave conditions with the same swell-wave

Figure 10. View of the tested plain beach

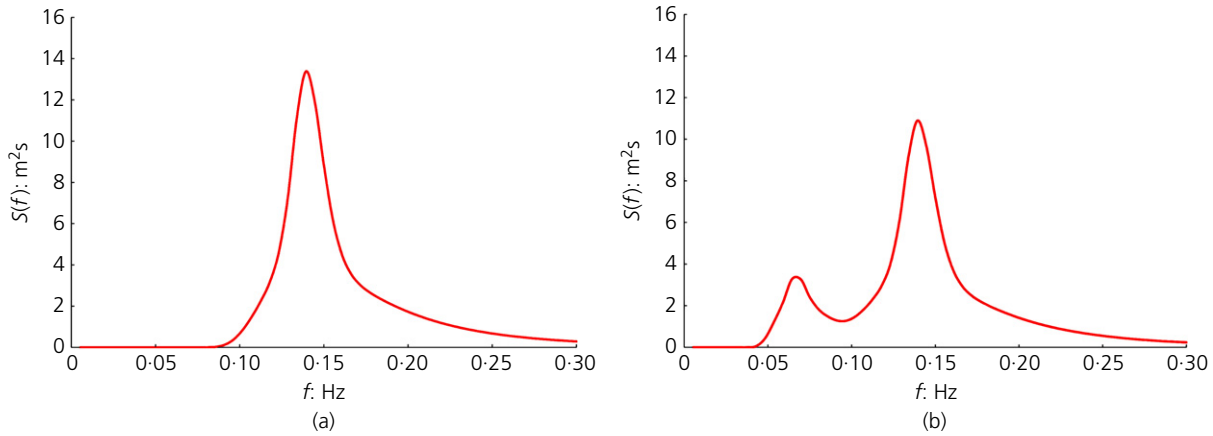

Figure 11. Wave spectra: (a) $H_{m0} = 4{\cdot}0$ m, $T_{p,wind} = 7{\cdot}0$ s and $\gamma_{wind} = 3{\cdot}3$; (b) $H_{m0} = 4{\cdot}0$ m, $T_{p,wind} = 7{\cdot}0$ s, $\gamma_{wind} = 3{\cdot}3$, $T_{p,swell} = 15{\cdot}0$ s, $\gamma_{swell} = 1{\cdot}3$, swell component = 20%

period of $T_{p,swell} = 18$ s, same wave height of $H_{m0} = 3{\cdot}0$ m, but different swell components are plotted. The influence of the swell component was observed mainly in the upper portion of the profile. The surf zone width increased significantly in response to an increase of S%. This can be explained by the interaction of wind and swell waves on the final beach profile evolution. During the wave motion, long swell waves run up the beach and a significant volume of water infiltrates the beach. The amount of water that penetrates and is retained by the beach is also a function of the beach permeability – that is, the beach grain-size distribution (which was outside the remit of this study). This will raise the groundwater elevation, which is a function of both wave conditions and sediment sizes, and obviously the tidal level, which was not considered within these experiments. If the beach is almost saturated with water, during the backwash a thick layer of water within the surf zone

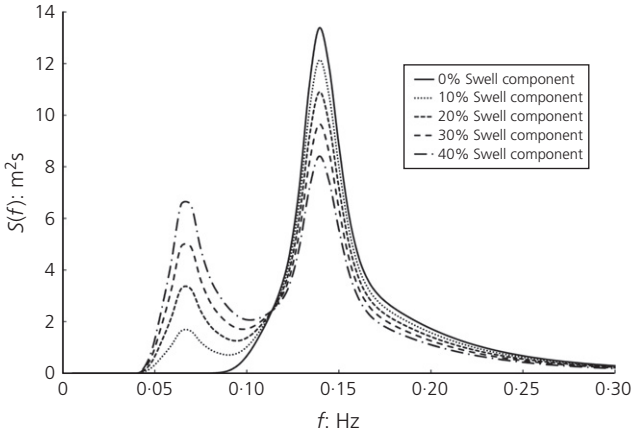

Figure 12. Wave spectra with different S%

Table 1. Test series programme

Test series	Beach configuration	Wave height: m	*s*: dimensionless	Number of waves	Purpose	Number of tests
A	Slope 1 in 8	3·0–4·5–5·3–6·0	0·053	1000, 2000, 3000	Profile response to bimodal sea state	104
B	Slope 1 in 8	3·0	0·04	3000	Profile response to bimodal sea state	20
C	Slope 1 in 8	3·0	0·03	3000	Profile response to bimodal sea state	20
D	Slope 1 in 8	4·5	0·04	3000	Profile response to bimodal sea state	20
E	Slope 1 in 8	3·0	0·003–0·004–0·006	1000	Profile response to bimodal sea state	3

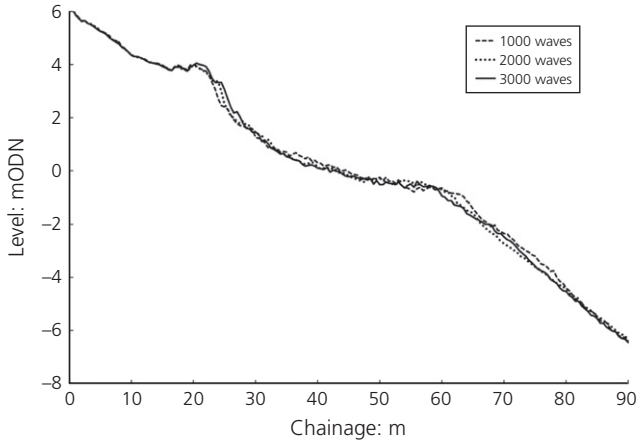

Figure 13. Profile development for a wave condition run for a duration of 1000, 2000 and 3000 waves (based on $T_{m0,2}$) in the physical model tests

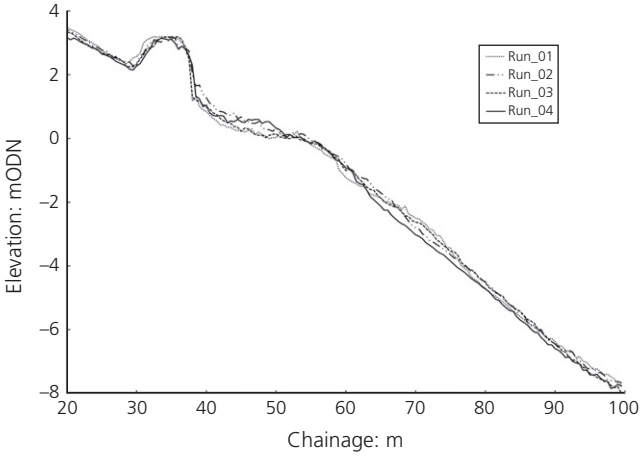

Figure 14. Effect of varying time-series sequence on beach profile response in the physical model tests

will be present (see Figure 16). The next incoming wave will surf on top of this water layer and, as the beach is now saturated, part of its energy cannot be dissipated within the beach. Most of the wave energy is, therefore, used to run on top of

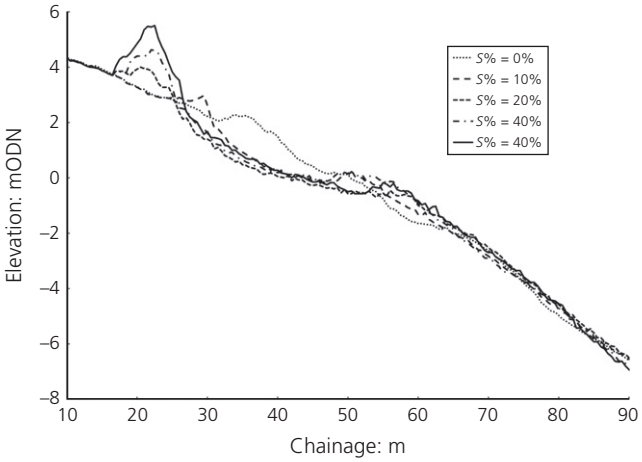

Figure 15. Effect of swell component percentage on shingle beach profiles ($H_{m0} = 3{\cdot}0$ m, $T_{p,wind} = 7{\cdot}18$ s, $T_{p,swell} = 18$ s) in the physical model tests

the crest and push the beach crest landward. This phenomenon can be observed in Figure 16, where a breaking wave can be seen running on a beach already saturated with water.

Beach profile results (Figure 15) showed that the beach crest experienced a horizontal displacement in response to a shift of energy from high to low frequency. Interestingly, the results demonstrated that an increase of swell component higher than 20% (e.g. 30–40%) had a more significant impact on the vertical displacement of the beach crest rather than the horizontal displacement. This suggests that an increased *S*% (>20%) will trigger an increase in crest elevation, rather than a horizontal displacement of the beach crest. Similar trends were also observed for the other swell-wave periods tested (15, 21 and 25 s).

4.3 Swell-wave period effect on beach profile response

The swell component tests demonstrated that the crest elevation was also affected by the swell-wave period. Accordingly, the effect of the swell-wave period ($T_{p,swell}$) on the beach profile was investigated by comparing profiles subject to the same wave height ($H_{m0} = 3{\cdot}0$ m), same wind-wave period

Figure 16. Beach saturated by swell waves and wind waves surfing on top of the sheet of water created by the previous swell wave

($T_{p,wind} = 7{\cdot}18$ s), same S% (10, 20, 30 and 40) but different swell periods (15, 18, 21 and 25 s). An example of the effect of the swell periods on the beach profile is plotted in Figure 17 ($H_{m0} = 3{\cdot}0$ m, $T_{p,wind} = 7{\cdot}18$ s and $S\% = 30$). Figure 17 shows that variations of swell-wave period had a substantial effect on the resulting profiles. The influence of the swell-wave period manifested itself mainly on the beach crest, with the crest position moving backwards and the crest elevation moving vertically in response to an increasing swell-wave period. Similarly, there is an increase in the crest elevation in response to an increasing swell-wave period as S% is increased. For the same swell-wave period, the higher the S% the higher the increase of the crest elevation.

It was also observed that the breaker zone increased in width in response to an increase in both the swell-wave period and S%. The increase in the width of the breaker zone is a necessary response of the beach to dissipate increased incident wave energy but, during these wave conditions, the energy spectrum was kept constant ($H_{m0} = 3{\cdot}0$ m). This beach response may be attributed to the interaction within the surf zone between wind and swell waves, which significantly affects the run-up, run-down and groundwater elevation (see Figure 1), triggering a horizontal displacement (landward) of the beach crest. The effect of the groundwater elevation on the final beach profile was also discussed by Horn (2002) and Horn *et al.* (2006); it is a phenomenon extremely important for the beach evolution of coarse-grained beaches in particular, although it was not investigated during this study.

4.4 Effect of wind-wave period on beach profile response

The effect of the wind-wave period ($T_{p,wind}$) on the beach profile was investigated for both unimodal and bimodal spectra. The beach profiles, shown in Figure 18, were tested under the same unimodal wave spectra, with an equivalent wave height of $H_{m0} = 3{\cdot}0$ m and different wind-wave periods ($T_{p,wind} = 7{\cdot}18$, $8{\cdot}26$ and $9{\cdot}54$ s). The effect of variations in the wave period was observed more in the vertical dimension of the profile than in the horizontal displacements. Thus, as the wind-wave period increases, so does the beach crest elevation. This behaviour is in agreement with the results observed by Powell (1990), where only unimodal spectra were tested.

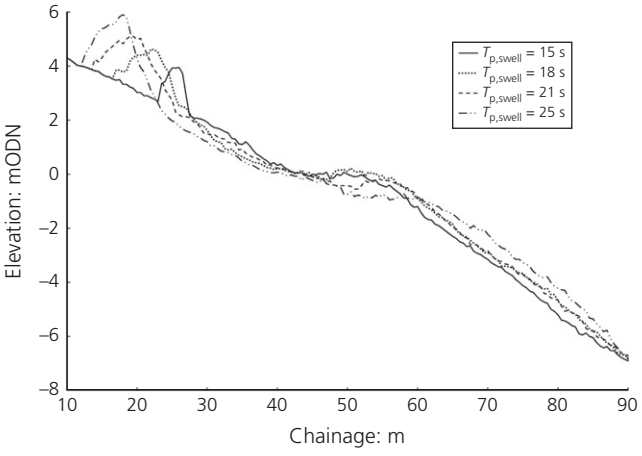

Figure 17. Effect of swell-wave period on the shingle beach profile ($H_{m0} = 3{\cdot}0$ m, $T_{p,wind} = 7{\cdot}18$ s; $S\% = 30\%$)

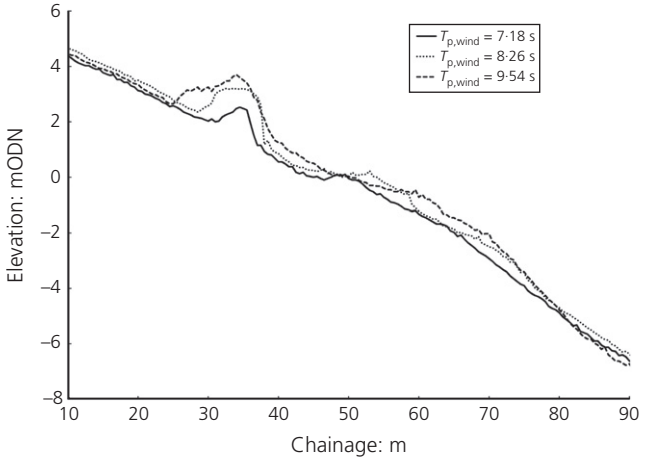

Figure 18. Effect of wind-wave period on the shingle beach profile under unimodal wave spectra with $H_{m0} = 3{\cdot}0$ m in the physical model tests

Interestingly, under bimodal wave conditions, the increase of the crest elevation in response to an increasing wind-wave period is less significant than an increase of the wind-wave period under unimodal wave conditions, as shown in Figure 19. This plot shows four beach profiles subject to the same wave height, but under two different wind-wave periods. The profile response to unimodal wave conditions is represented with solid curves, while the profile response to bimodal wave conditions (20% swell component) are plotted with dashed curves. Clearly, the increment of the wind-wave period has a more significant impact on the unimodal condition than the bimodal one. This can be explained because, under bimodal wave conditions, the swell component and swell-wave period have a more significant impact than the wind-wave period on the amount of water infiltrating the beach (groundwater elevation) and therefore affecting the final profile.

4.5 Wave height effect on beach profile response

The influence of the wave height on the beach profile is shown in Figure 20. This figure shows the post-storm beach profiles exposed to two different incident wave heights ($H_{m0} = 3{\cdot}0$ m, dashed curve and $H_{m0} = 4{\cdot}5$ m, solid curve) having the same wind-wave and swell-wave periods. As can be seen, the effect of the variation in the wave height triggers a horizontal displacement. The surf zone width increases significantly in response to an increasing wave height. This behaviour is in agreement with the results observed by Powell (1990). The increase in the width of the surf zone is necessary to dissipate increased incident wave energy, and this is realised by a lengthening of the surf zone rather than a change of the profile. This behaviour was observed for all the different tested wave heights.

5. Comparison with existing predictive methods

This section examines the main available methods used to predict gravel beach response under wave attack. The Shingle (Powell, 1990) and XBeach-G (McCall *et al*., 2014) prediction models are examined by comparing the predicted beach profile responses with the physical model test results for both a typical unimodal Jonswap wave spectrum (shown in Figure 21) and a bimodal wave spectrum (shown in Figures 22 and 23).

For a typical unimodal Jonswap wave spectrum ($H_{m0} = 3{\cdot}0$ m, $T_{p,wind} = 7{\cdot}18$ s), Shingle predicted profiles showing a very good correlation with the physical model results. The parametric

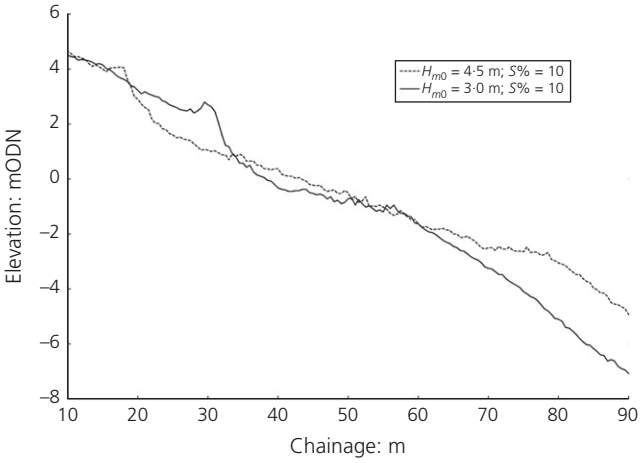

Figure 20. Effect of wave height on the shingle beach profile for bimodal (10% swell component) wave conditions ($H_{m0} = 3{\cdot}0$ m, dashed curve; $H_{m0} = 4{\cdot}5$ m, solid curve)

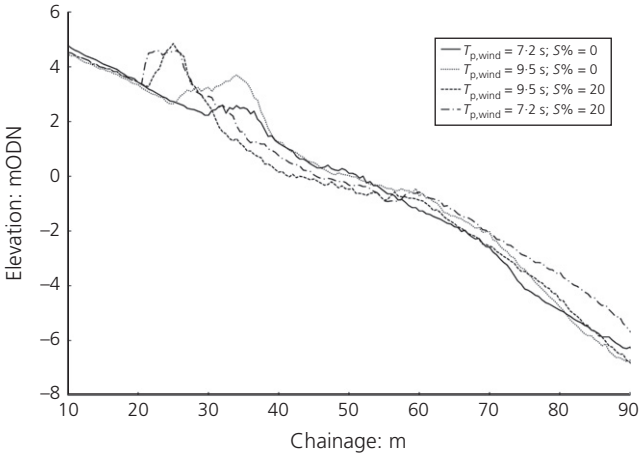

Figure 19. Effect of swell component on the influence of wind-wave period on the shingle beach profile in the physical model tests

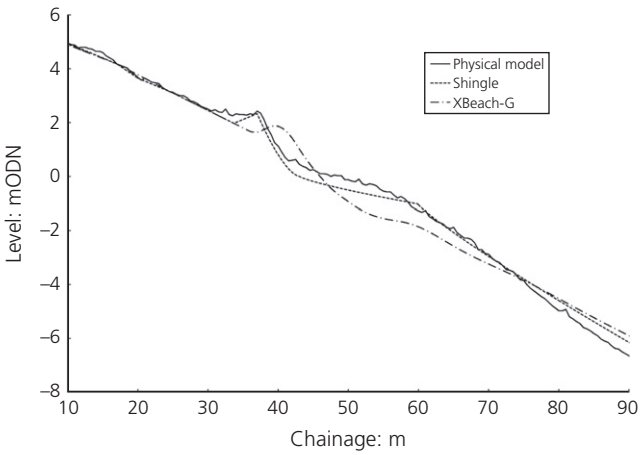

Figure 21. Beach profile comparison: XBeach-G, Shingle and physical model results for a unimodal wave spectra ($H_{m0} = 3{\cdot}0$ m, $T_{p,wind} = 7{\cdot}18$ s, $T_{p,swell} = 15$ s, $S\% = 0\%$)

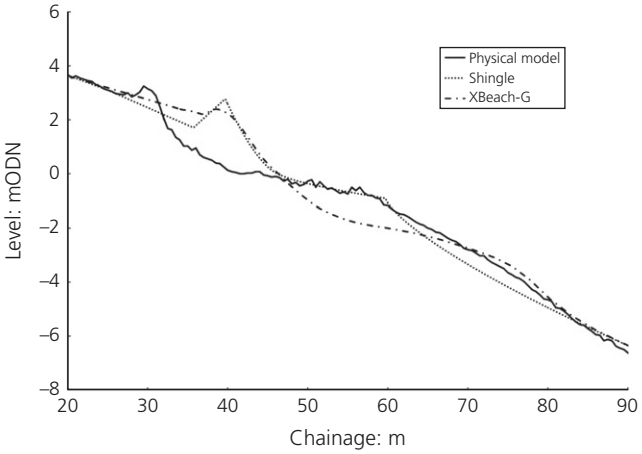

Figure 22. Beach profile comparison: XBeach-G, Shingle and physical model results for a bimodal wave spectra ($H_{m0} = 3{\cdot}0$ m, $T_{p,wind} = 7{\cdot}18$ s, $T_{p,swell} = 15$ s and $S\% = 10\%$)

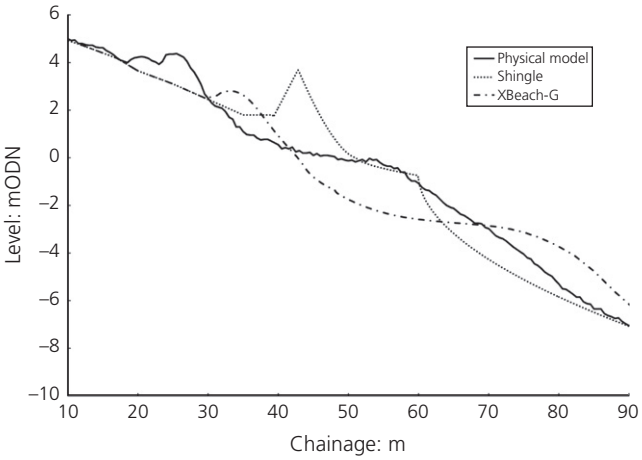

Figure 23. Beach profile comparison: XBeach-G, Shingle and physical model result for a bimodal wave spectra ($H_{m0} = 3{\cdot}0$ m, $T_{p,wind} = 7{\cdot}18$ s, $T_{p,swell} = 15$ s and $S\% = 40\%$)

model correctly predicted both the location of the beach crest, which tends to be the area of most interest to coastal engineers, and the location of the step (see Figure 21). Conversely, significant discrepancies were observed for the beach profiles predicted by XBeach-G, where the numerical model underestimated the horizontal displacement of the beach crest and predicted erosion where accretion was observed.

As previously described, in order to investigate the variation of beach profile with the spectral shape and the distribution of energy, the same spectral wave height H_{m0} (i.e. the same area under the spectrum) was run in four additional steps of varying $S\%$ (10–40%) at the same water level. Similarly, Shingle and XBeach-G models were examined by comparing the predicted beach profile responses with the physical model test for different bimodal wave spectra. Figures 22 and 23 show a comparisons of the predicted beach profiles and the post-physical model test results for bimodal wave conditions having, respectively, 10% and 40% of swell component.

It is worth mentioning that the Shingle model allows the user to input the wave height and the mean wave period ($T_{m0,2}$), but does not take into account the bimodality of the wave spectrum. During these tests, when varying $S\%$ (10–40%), the wave height remained constant and the spectral period ($T_{m-1,0}$) increased. Therefore, when increasing $S\%$ during the tests, the input mean wave period ($T_{m0,2}$) in the Shingle model was replaced by the spectral period ($T_{m-1,0}$). In Shingle, the effect of variations in the wave period triggers only the vertical displacement of the beach crest, neglecting its horizontal displacement. As a consequence of this deficiency, a significant discrepancy between the measured and predicted profiles for bimodal wave spectra was observed, as shown in Figures 22 and 23.

In contrast, in the XBeach-G model, the user is allowed to input a double-peaked wave spectrum, specifying the wave height and wave period for both wind and swell components. By comparing the measured and predicted profiles, a significant discrepancy was observed. The model does not predict the variation of the surf zone width in response to an increase of $S\%$ and, as a consequence, significantly underestimates the crest erosion (of the order of 10–20 m). The higher the $S\%$ within the incident wave condition, the higher the discrepancy observed (see Figures 22 and 23).

The laboratory experiments clearly demonstrated the effect of the double-peaked wave spectrum on the beach profile response, whereby a slight increase of low-frequency energy within the incident wave spectrum triggered a significant erosion of the beach crest. The comparison between predicted and measured beach profiles showed that the available prediction models (Shingle and XBeach-G) do not encompass the effect of the bimodality of the incident wave spectrum and, consequently, they significantly underestimate the crest erosion. Moreover, these models fail to predict the width of the beach crest correctly (see Figure 1), which, as discussed in Section 2, is an important feature for beach coastal management. These limitations clearly indicate that the current prediction models are not appropriate tools under bimodal sea states. Based on this 2D physical model study, a new parametric model for predicting beach profile response under bimodal sea states, Shingle-B, was derived, which is explained in the next section.

6. Shingle-B

6.1 Introduction

The first part of this section describes how the new model schematises the beach profile and the relationship between profile parameters and bimodal wave variables. In the second part of this section, a validation against field data is presented.

6.2 Profile schematisation

The results observed during the physical model study showed how critical the crest erosion is during bimodal sea states. This critical aspect of the beach profile was also observed, as discussed in Section 2, over the course of the storm sequences during the winters of 2013–2014 along the south coast of England. For these reasons, the profile schematisation adopted for the present model is essentially a combination of the profile employed by Powell (1990) and the necessity to predict the post-storm crest width.

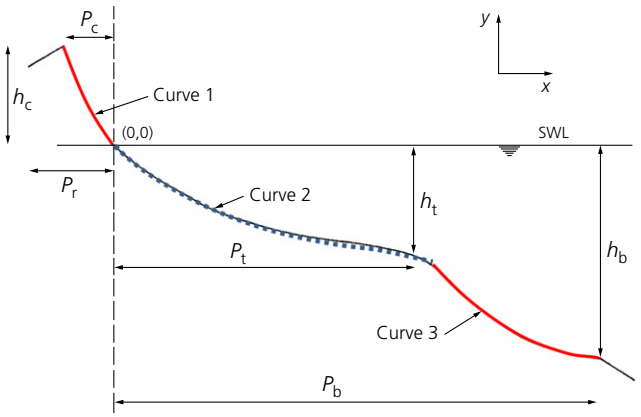

Figure 24. Schematised beach profile (Powell, 1990). h_b, elevation of the beach base; h_c, elevation of the beach crest; h_t, elevation of the beach step; P_b, position of the beach base; P_c, position of the beach crest; P_r, position of the maximum run-up; P_t, position of the beach step

The model proposed by Powell (1990) employs three power-law curves to define the shingle beach profile, as shown in Figure 24: curve 1, beach crest and still water level (SWL) shoreline; curve 2, SWL shoreline and top edge of step; curve 3, top edge of step and lower limit of profile deformation.

As discussed in Section 1, for the present model there was the necessity to predict the landward displacement of sediment and the final crest width. In contrast to Shingle, the suggested beach profile schematisation adopts four curves, defined by their vertices as: curve 1, landward displacement and beach crest; curve 2, beach crest and start beachface point; curve 3, beachface point and top edge of step; curve 4, top edge of step and lower limit of profile deformation. The resulting schematisation is shown in Figure 25. Except for the crest width, the parameters were measured relative to the SWL and shoreline axes, as shown in Figure 26. The coordinates for the vertices of the curves are denoted by x_1, y_1 to x_5, y_5, as shown in Figure 25.

Many authors (Bruun, 1954; Dean, 1977; Hughes and Chiu, 1981; Keulegan and Krumbein, 1949; Powell, 1990; Van Hijum and Pilarczyk, 1982) have suggested that a hyperbolic curve of the form $y = Ax^n$ provides the best description for a profile of a natural beach, where the coefficients A and n are functions of the beach characteristics and incident wave conditions, and y and x are the vertical and horizontal displacement.

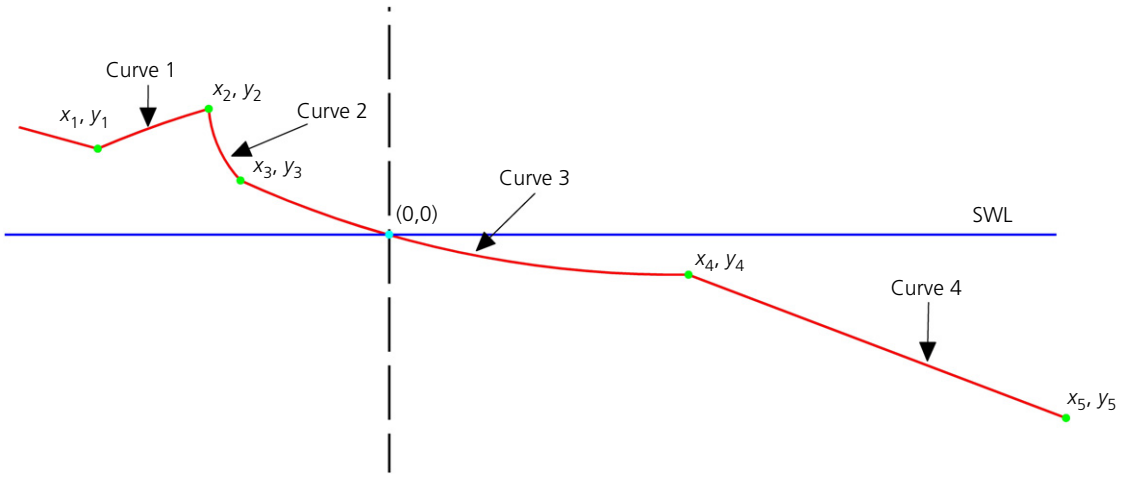

Figure 25. Schematised beach profile using four curves for Shingle-B model

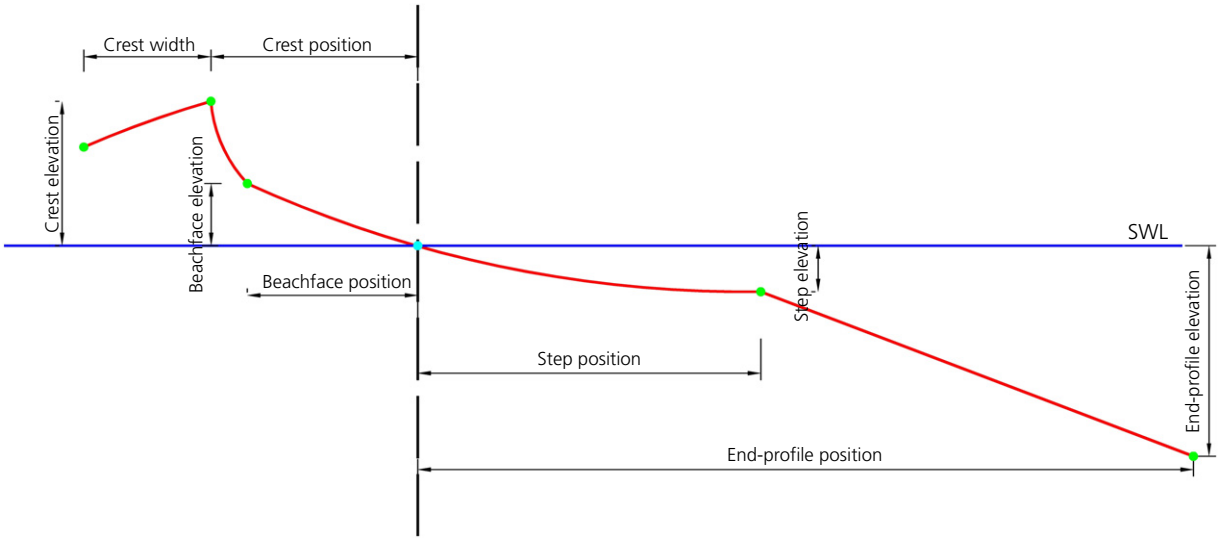

Figure 26. Schematised beach profile: parameters were characterised relative to the SWL and shoreline axes

During this analysis, the profile curves between the vertices assumed the same hyperbolic relationship. Once the beach profile was schematised, the functional relationship for each of the parameters listed above had to be determined. The relationship between the beach profile parameters and incident wave parameters is described in the following section.

6.3 Beach profile parameter identification

The physical model beach profiles were extracted using a bed profiler (see Section 3.1) that recorded chainage and level at any location along the beach. In order for functional relationships between beach profile and bimodal wave variables to be extrapolated, values (coordinates x_i and y_i) of each of the beach parameters described above were extracted from the beach profiles recorded during the tests (see Figure 27). This was done by a combination of expert judgement and a least-squares optimisation.

First, the crest position (point 2) and SWL intersection (bold cross, Figure 27) were manually selected for each of the observed profiles. The end profile location (point 5) was set to the end of the observed profile and an additional point (point 0) was temporarily assigned beyond the landward limit to the opposite end to cover the whole observed profile (see Figure 27).

A genetic algorithm is a method for solving both constrained and unconstrained non-linear optimisation problems by mirroring the natural selection process of biological evolution.

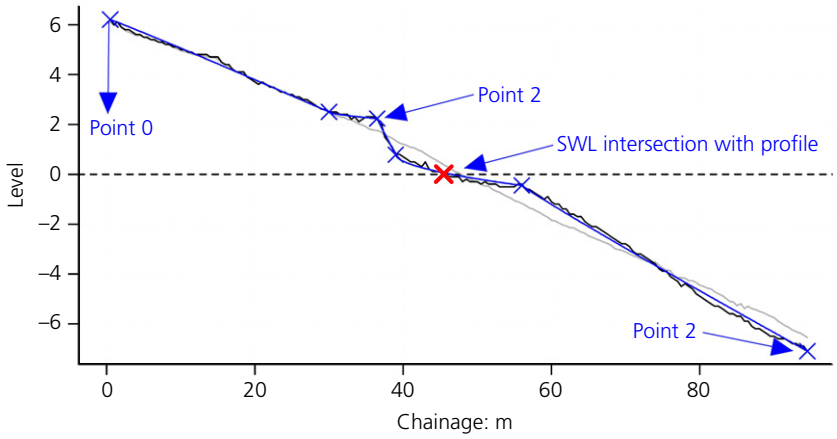

Figure 27. Beach parameter coordinates extracted from the physical model observed profile

The algorithm is initialised with a population of multiple randomly generated potential solutions, each of which provides the x and y coordinates of the remaining beach parameters (i.e. for points 1, 3 and 4) in addition to a power n_i for each of the six curves. This population is 'evolved' over a number of 'generations' using selection, cross-over and mutation processes that mirror natural selection. At each generation, the algorithm uses the 'fitness' of each solution to determine which 'parents' are used to create the 'children' of the next generation. Given a potential solution of beach parameter coordinates and power curves, the fitness is determined as the sum of the squared errors between the resulting fitted curves and the observed beach profile at every observed chainage, with lower errors preferred.

The resulting algorithm uses least-squares optimisation to find the best fitting set of hyperbolic curves for each observed profile.

This data set of beach parameter coordinates and hyperbolic curves then forms the training data for the subsequent regression analysis.

6.4 Functional relationships between beach profile and bimodal wave variables

The data set of the observed beach parameter values, shown in Figure 26, with the corresponding bimodal wave variables, was used to fit the equations for predicting each parameter, and hence the profile curve, as a function of bimodal wave variables. Multiple linear regression was used to describe each profile parameter by a parametric function of potentially multiple wave variables. This gives prediction equations of the general form

$$y = \beta_0 + \beta_1 x_1 + \beta_2 x_2$$

where y is the parameter prediction, x_i are covariates and β_i are corresponding regression coefficients to be estimated when fitting. The covariates may potentially be any bimodal wave variable or transformations of them. Test series A–D, described in Table 1 (plane beach profile), were used to fit the model, ignoring the profiles at 1000 and 2000 waves, as discussed in Section 4.1.

For each profile parameter (e.g. crest elevation, crest position etc.), a model building exercise was undertaken to determine the exact form of the final regression equation by selecting which wave covariates to include. Finding this subset of covariates involves two opposing criteria: first, the regression model has to be as complete and realistic as possible – that is, including every covariate that is even remotely related to the dependent variable; and second, including as few variables as possible. This is because each irrelevant covariate decreases the precision of the estimated coefficients and predicted values. Moreover, the presence of extra variables increases the complexity of the final model. The goal of variable selection becomes a balance between simplicity (as fewer covariates as possible) and fit (as many covariates as needed).

On the basis of the discussion above, from a selection of potential covariates, a stepwise procedure was applied whereby the simplest model with no covariates was initially chosen then new terms were added or removed sequentially by selecting the term that minimises the Akaike information criterion (AIC) (Akaike, 1974; Burnham and Anderson, 2002). The AIC can be used to perform model comparisons, given a collection of models for the data. The AIC is an estimator of the relative quality of statistical models for a given set of data. Thus, it provides a means for model selection. The process systematically adds the most significant variable or removes the least significant variable during each step. This approach measures the goodness of fit of the equation but penalises the number of covariates to discourage overfitting, which would likely lead to poor estimates outside the fitted range (Burnham and Anderson, 2002). For each profile parameter, a set of equations was derived by the AIC method; the final one was manually selected to balance the goodness of fit with the model complexity, while also ensuring that the equation was physically meaningful (i.e. guaranteeing the physical phenomena observed and described in Section 4).

In Section 4, it was concluded that the most influential wave variables for the beach profile evolution were the spectral wave height (H_{m0}), wind-wave peak period ($T_{\mathrm{p,wind}}$), swell-wave peak period ($T_{\mathrm{p,swell}}$) and S%. During the regression analysis, in addition to the main four variables, the following wave variables were also considered as covariates: spectral significant wave period ($T_{m-1,0}$); mean wave period ($T_{m0,2}$); mean wavelength (L_{m0}); breaker parameter (ξ_0); wave steepness (s_0); and also three parameters related to the wave spectrum: broadness (ε); narrowness (ν); peakedness (Q_{p}).

Ultimately, as a result of the stepwise regression analysis, the following four covariates were considered for inclusion in the regression equations: H_{m0}, S, $(1–S)T_{\mathrm{p,wind}}$ and $ST_{\mathrm{p,swell}}$, where S is S% as a decimal between 0 and 1. The wind and swell peak periods were multiplied by factors involving the proportion of swell to ensure that the covariate has a valid value in all cases, including when the swell is 0% or 100% for which one of these periods is undefined.

The model selection process was conducted using 90% of the selected tests with a randomly selected 10% used for independent validation of the fitted models. An example of the analysis shows the results for the crest position and crest elevation in Figure 28. Ultimately, the selected regression equations were

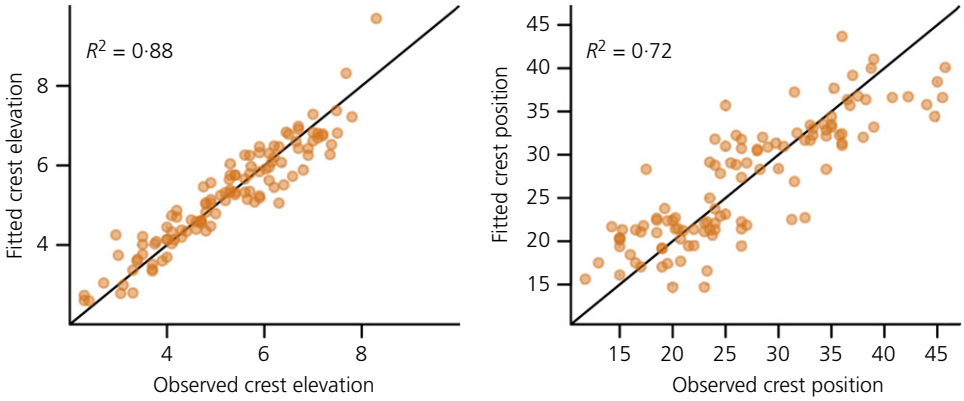

Figure 28. Fitted against observed values for validation of crest elevation and crest position

refitted using all of the selected tests. The final equations describing each parameter, and hence the profile curve, as a function of bimodal wave variables are reported in the Appendix. These equations are the basis of the online beach prediction tool Shingle-B.

6.5 Model validation

The final and perhaps most important stage was the validation of the Shingle-B model against field data. This, if successful, would confirm the correctness of the theory behind the beach physical modelling and generate confidence in the application of results from those models to natural situations. The following section focuses on some sites along the south coast of England and provides comparisons of profile response under known storm events. At each site, near-shore directional Datawell Waveriders, owned and maintained by the Regional Coastal Monitoring Programmes, were used to measure wave conditions throughout the survey period. The wave buoys form a national network of near-shore wave measurements and are moored in ~12 m water depths, providing wave statistics on a half hourly basis.

6.5.1 West Bay

West Bay comprises East and West Beach. East Beach consists of a very fine shingle ridged beach with sand at the water's edge (see Figure 29). West Beach consists of a fine, smooth, pebbly beach, with shingle and sand at the water's edge.

A comparison of model results and post-storm beach profiles extracted at East Beach was carried out. Data obtained from the Channel Coastal Observatory website (CCO, 2018b) included simultaneous wave measurements and beach profiles. A single storm with a unimodal wave spectrum was recorded during January 2011 ($H_{m0} = 4{\cdot}6$ m, $T_{p,wind} = 10$ s, $S\% = 0$) and it was reproduced using Shingle-B, XBeach-G and Shingle (Powell, 1990). The prototype post-storm profile together with

Figure 29. West Bay (East Beach)

the three predicted model profiles are plotted in Figure 30, where a reasonable agreement between measured prototype profile and Shingle-B predicted profile can be observed. As expected, under unimodal wave conditions, the Shingle (Powell, 1990) model also shows reasonable agreement with the prototype position of the beach crest and the rate of the crest erosion. Conversely, XBeach-G significantly underestimates the crest erosion.

6.5.2 Rustington

Rustington beach is a shingle beach with compact sand at low tide.

A comparison between model results and post-storm beach profiles extracted at Rustington was carried out. The data obtained from the CCO website (CCO, 2018b) included simultaneous wave measurements and beach profiles. A single storm with a bimodal wave spectrum was recorded during November

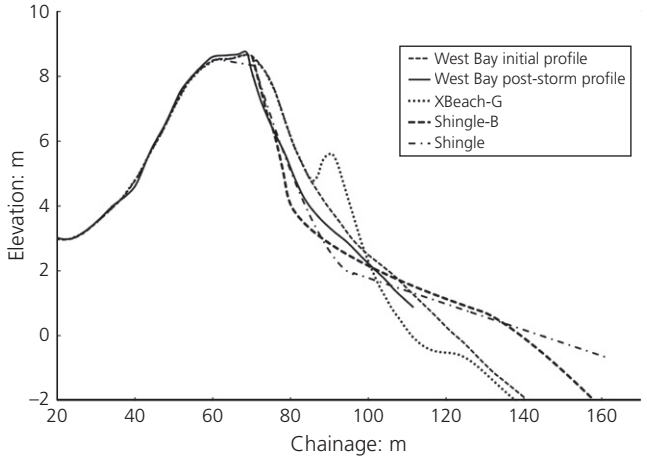

Figure 30. West Bay: post-storm profile against XBeach-G, Shingle (Powell, 1990) and Shingle-B predictions

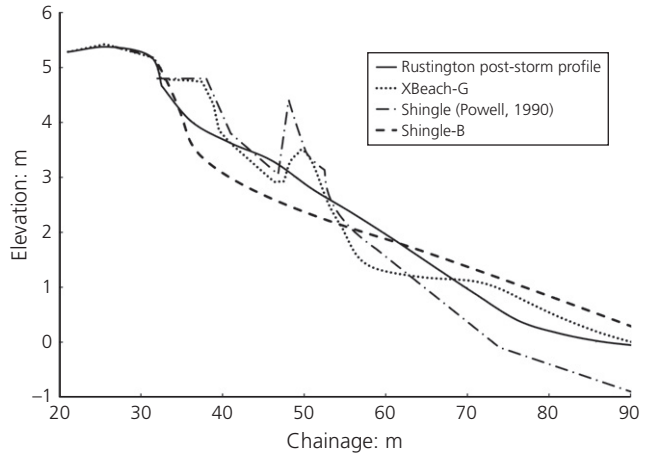

Figure 31. Rustington: post-storm profile against XBeach-G, Shingle (Powell, 1990) and Shingle-B predictions

2005 ($H_{m0} = 3{\cdot}5$ m, $T_{p,wind} = 7{\cdot}0$ s, $T_{p,swell} = 12$ s, $S\% = 10$) and it was reproduced by using Shingle-B, XBeach-G and Shingle (Powell, 1990). The prototype post-storm profile together with the three predicted model profiles are plotted in Figure 31, where Shingle-B model shows reasonable agreement with the prototype position of the beach crest and the rate of the crest erosion. Conversely, as expected under bimodal wave conditions, both Shingle (Powell, 1990) and XBeach-G significantly underestimated the horizontal displacement of the crest.

7. Limitations of Shingle-B

The study considered the effect of wave height (H_{m0}), wind-wave period ($T_{p,wind}$), swell-wave period ($T_{p,swell}$), $S\%$ and the distribution of the spectral energy on the morphology of shingle beaches as a response to a storm condition.

As with all empirical methods, it is important to consider the range of applicability of the model in terms of the input parameters used for predictions. Whilst the fitted functions can provide estimates beyond the range of the data, there is little theoretical basis for their use in this regard. Although the range of the input data used to train the model could be tabulated for each of the specific input parameters, the practice of using the maximum and minimum values of each input parameter to define the range of applicability is questionable, particularly when parameters are correlated. There can be significant areas of the input parameter space unpopulated and hence predictions in these areas are generated by extrapolation not interpolation. This is illustrated in concept and for two variables only in Figure 32, where the parameter space covered by the maximum and minimum of two variables is given by the dashed rectangle; the area inside the dashed rectangle, although within the range of the variables, has no data to support the underlying predictions. This effect is significantly exacerbated the more dimensions are in the parameter space; in the current case four parameters (wave height (H_{m0}), wind-wave period ($T_{p,wind}$), swell-wave period ($T_{p,swell}$) and $S\%$).

The desire to extend the range of applicability of the model outside the range of the training data is perhaps understandable given the preponderance of existing similar structure types and the additional expense associated with constructing site-specific physical models or more sophisticated numerical models. It is, however, appropriate to explicitly recognise and acknowledge that predictions resulting from extrapolation should be treated accordingly. Within the approach described here, specific attention has been directed towards the provision of guidance relating to the area of applicability of the model. The Mahalanobis distance (MD) (Mahalanobis, 1930) provides a quantifiable measure that can guide users on regions of valid application. The MD is a measure of a point from a multivariate distribution. Unlike the Euclidean distance, the MD accounts for correlated parameters, an important factor in the development of gravel beach profiles. In the online tool Shingle-B, the MD was used as a measure to come up with a range of applicability. This is represented in the tool as a coloured thumb, which is shown to indicate if the input wave conditions are within the limits of the training data set (green thumb), within input range but far from the training data (orange thumb) or outside the data range against which the model was trained (red thumb). This is also illustrated in Figure 32.

It is worth mentioning that the model Shingle-B is neither a breaching model nor does it deal with structures. Shingle-B only deals with the cross-shore profile; the longshore transport

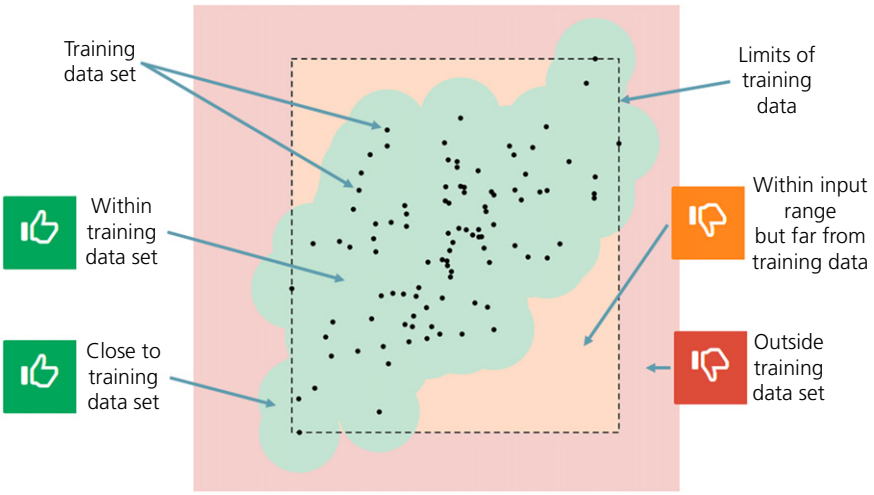

Figure 32. Input wave condition validation

not being considered. Formulations such as that proposed by van Wellen *et al.* (2000) should be used in order to deal with the longshore transport of coarse-grained beaches. Future physical modelling tests should include oblique wave attack and the inclusion of longshore sediment transport.

7.1 Bathymetry

While a fixed bathymetry seawards of the toe of the beach (typical of south coast beaches) was used, sites with extensive shallow foreshores will require some transformation of the wave conditions to determine more realistic input conditions. Such sites will likely have higher wave heights at the toe of the beach. Also, for other sites around the world, where more complicated bathymetry of the beach might be present, the user will be therefore required to adjust the Shingle-B input wave conditions to account for the difference in bathymetry.

7.2 Diameter and grading of the beach material

Sediment characteristics such as D_{50} and grading width (D_{85}/D_{15}) may affect the beach profile response. During this study, only one grading curve was used ($D_{50} = 12{\cdot}5$ mm, $D_{10} = 2{\cdot}8$ mm and $D_{85}/D_{15} = 5{\cdot}0$) for the physical model tests; this was representative of south coast beaches, as discussed in Section 3. The sediment used within the physical modelling was scaled following Yalin (1963) in order to provide the most satisfactory reproduction of the prototype beach permeability, sediment mobility threshold and onshore–offshore transport characteristics (Powell, 1990). The scaling process results showed that the sediment model scale (anthracite), with a geometric scale of 1 in 25, should be 1 in 2·25. The grading of the beach material, which affects its permeability, may influence crest elevation and crest regression; however, this effect was not explored during this study. The effect of the grading of the beach on the crest elevation was studied by Powell (1990), who observed decreasing crest levels for a narrower grading curve, although insufficient data were available to confirm this trend.

7.3 Beach slope

During this study, the initial beach slope in the physical model tests was fixed at 1 in 8 for each of the tests. Although the effect of the slope was not investigated, different wave conditions were repeated without reshaping the beach to the initial plane profile. The results of non-reshaped and reshaped profiles showed very good agreement, suggesting that the initial profile does not significantly affect the final profile.

Similar results were also discussed by Powell (1990) who concluded that whilst the initial beach slope does not necessarily affect the form of the active length of beach profile, it does affect its development.

7.4 Underlying impermeable structure

Physical model tests were run with a full thickness of beach material and the effect of impermeable membrane or sea walls was not considered during this study. The presence of an underlying impermeable layer within a shingle beach was investigated by Powell (1990). During that study (Powell, 1990) it was observed that if the ratio of effective beach thickness to median material size (D_{50}) was less than 30, the thickness of the beach was usually insufficient to retain material over the profile, and the beach structure was not stable.

8. Conclusions

An extensive series of physical model tests was undertaken to explore the behaviour and performance of gravel beaches under bimodal wave conditions. The tests considered the effect

of the wave height, wind-wave period, swell-wave period and swell component percentage on the resultant beach profiles. The results from this study clearly demonstrated the effect of bimodal spectra on the evolution of a beach profile. The test results showed the critical effect of the bimodal sea state on both the vertical/horizontal displacement of the beach crest and the dynamic of the surf zone.

The model Shingle (Powell, 1990) and the numerical model XBeach-G (McCall *et al*., 2014) were found not to account for the influence of the spectral shape on the beach profile response and significantly underestimated the crest erosion under the bimodal wave conditions.

The physical model results allowed the development of a new parametric model, Shingle B, for predicting beach profile response on gravel beaches under bimodal sea states. Using the new parametric model, an online tool was developed and made available on the website for the National Network of Regional Coastal Monitoring Programmes of England (CCO, 2018a). The aim of Shingle-B is to offer an engineering tool to increase confidence in beach cross-section design under wave conditions characterised by double-peaked spectrum.

Initial validation of the model predictions against field data yielded encouraging results, suggesting that the parametric model provides a good representation of natural beaches and therefore represents an improvement over existing models for gravel coasts subjected to bimodal wave conditions. However, the present model would benefit from some additional comparisons and verification with field data.

Acknowledgements

This project was the brainchild of Professor Andy Bradbury, whose untimely death in August 2014, in the middle of the experiments, deprived the coastal engineering community of one of its foremost experts on gravel beaches. The authors are grateful to Keith Powell for guidance and supervision. The authors also wish to acknowledge support provided by the HR Wallingford Froude Modelling Hall staff. Shingle-B was funded by the Environment Agency as a flood and coastal erosion risk management grant-in-aid project, grant number LDW 4123.

Appendix

1. $\text{Crest width} = 3{\cdot}92 + 0{\cdot}31\ ST_{\text{p,swell}}$

$R^2 = 0{\cdot}24$

2. $\text{Crest position} = -8{\cdot}80 + 9{\cdot}10\ H_{m0} + 0{\cdot}66\ ST_{\text{p,swell}}$

$R^2 = 0{\cdot}72$

3. $\text{Crest elevation} = -1{\cdot}88 + 0{\cdot}81\ H_{m0} + 0{\cdot}31\ (1 - S)\,T_{\text{p,wind}} + 0{\cdot}37\ ST_{\text{p,swell}}$

$R^2 = 0{\cdot}88$

4. $\text{Beachface position} = -11{\cdot}66 + 8{\cdot}63\ H_{m0} + 0{\cdot}52\ ST_{\text{p,swell}}$

$R^2 = 0{\cdot}67$

5. $\text{Beachface elevation} = -0{\cdot}65 + 0{\cdot}71\ H_{m0} + 0{\cdot}12\ ST_{\text{p,swell}}$

$R^2 = 0{\cdot}56$

6. $\text{Step point position} = -17{\cdot}76 + 8{\cdot}67\ H_{m0} + 0{\cdot}83\ ST_{\text{p,swell}}$

$R^2 = 0{\cdot}55$

7. $\text{Step point elevation} = -1{\cdot}19 + 0{\cdot}51\ H_{m0} + 0{\cdot}06\ ST_{\text{p,swell}}$

$R^2 = 0{\cdot}42$

8. $\text{End profile elevation} = 12{\cdot}23 \pm 1{\cdot}50\ H_{m0}$

$R^2 = 0{\cdot}54$

REFERENCES

Akaike H (1974) A new look at the statistical model identification. *IEEE Transactions on Automatic Control* **19(6)**: 716–723.

BGS (British Geological Survey) (1987) *Sea Bed Sediments around the United Kingdom, 1:1,000,000 Map (North Sheet and South Sheet)*. BGS, Natural Environment Research Council, Nottingham, UK.

Bradbury A (1998) *Response of Shingle Barrier Beaches to Extreme Hydrodynamic Conditions*. PhD thesis, University of Southampton, Southampton, UK.

Bradbury AP and Mason TE (2014) *Review of South Coast Beach Response to Wave Conditions in the Winter of 2013–2014*. Channel Coastal Observatory, Southampton, UK, Technical Report SR01.

Bradbury AP, Mason TE and Holt M (2006) Design and management implications for the use of modelled wave data in the southeast – a comparison between modelled and measured conditions. *Proceedings of the DEFRA Conference of River and Coastal Engineers*.

Bradbury AP, Mason TE and Holt MW (2004) Comparison of the performance of the Met Office UK – waters wave model with a network of shallow water moored buoy data, 2004. *Proceedings of the 8th International Workshop on Wave Hindcasting and Forecasting, Hawaii*.

Bradbury AP, Mason TE and Poate T (2007) Implications of the spectral shape of wave conditions for engineering design and coastal hazard assessment – evidence from the English Channel. *Presented at the 10th International Workshop on Wave Hindcasting and Forecasting, Oahu, Hawaii*.

Bradbury AP, Mason TE and Picksley D (2009) A performance based assessment of design tools and design conditions for a beach management scheme. *Proceedings of the International Conference on Breakwaters, Structures and Coastlines, Edinburgh, UK*. Thomas Telford, London, UK, pp. 338–351.

Bradbury AP, McFarland S, Horne J and Eastick C (2002) Development of a strategic coastal monitoring programme for southeast England. *Proceeding of the International Coastal Engineering Conference, Cardiff, UK*. ASCE, Reston, VA, USA.

Bray M and Hooke J (1998) Geomorphology and management of sites in Poole and Christchurch bays. In *Coastal Defence and Earth Science Conservation* (Hooke J (ed.)). The Geological Society, Bath, UK, pp. 233–266.

Bruun P (1954) *Coast Erosion and the Development of Beach Profiles*. U.S. Army Engineer Waterways Experiment Station, Vicksburg, MS, USA, Beach Erosion Board Technical Memorandum no. 44.

Burnham KP and Anderson DR (2002) *Model Selection and Multimodel Inference: A Practical Information-Theoretic Approach*, 2nd edn. Springer, New York, NY, USA.

Buscombe D and Masselink G (2006) Concepts in gravel beach dynamics. *Earth-Science Reviews* **79(1–2)**: 33–52.

Carter R and Orford J (1993) The morphodynamics of coarse clastic beaches and barriers: a short and long-term perspective. *Journal of Coastal Research* **15**: 158–179.

CCO (Channel Coastal Observatory) (2018a) *Shingle-B*. CCO, Southampton, UK. See http://www.channelcoast.org/ccoresources/shingleb/ (accessed 10/10/2018).

CCO (2018b) http://www.channelcoast.org/ (accessed 16/02/2011).

Coates TT and Bona PFD (1997) *Recharged Beach Development, a Field Study at Highcliffe Beach, Dorset*. HR Wallingford, Wallingford, UK, Technical Report SR438.

Dean RG (1973) Heuristic models of sand transport in the surf zone. *Proceedings of the 1st Australian Conference on Engineering Dynamics in the Surf Zone*, pp. 208–214.

Dean RG (1977) *Equilibrium Beach Profiles: US Atlantic and Gulf Coasts*. University of Delaware, Newark, DE, USA, Technical Report No 12.

Dean RG (1985) Physical modelling of littoral processes. In *Physical Modelling in Coastal Engineering* (Dalrymple RA (ed.)). Balkema, Rotterdam, the Netherlands, pp. 119–139.

Defra (Department for Environment, Food and Rural Affairs) (2016) *The Costs and Impacts of the Winter 2013 to 2014 Floods*. Defra, London, UK.

EurOtop (2007) *European Manual for the Assessment of Wave Overtopping* (Pullen T, Allsop NWH, Bruce T, Kortenhaus A, Schüttrumpf H and Van der Meer JW (eds)). EurOtop, Wallingford, UK. See http://www.overtoppingmanual.com (accessed 13/10/2018).

Ewans K, Bitner-Gregersen E and Soares CG (2006) Estimation of wind-sea and swell components in a bimodal sea state. *Journal of Offshore Mechanics and Arctic Engineering* **128(4)**: 265–270.

Garcia-Gabin W (2015) Wave bimodal spectrum based on swell and wind-sea components. *IFAC-PapersOnLine* **48(16)**: 223–228.

Goda Y (1985) *Random Seas and Design of Maritime Structures*, 2nd edn. World Scientific, Singapore.

Goda Y (2010) *Random Seas and Design of Maritime Structures*, 3rd edn. Advanced Series on Ocean Engineering. World Scientific, Singapore.

Hawkes PJ, Coates TT and Jones RJ (1998) *Impact of Bi-Modal Seas on Beaches and Control Structures*. Hydraulics Research, Wallingford, UK, Technical Report SR507.

Hayes MO, Michel J and Betenbaugh DV (2009) The intermittently exposed, coarse-grained gravel beaches of Prince William Sound, Alaska: comparison with open-ocean gravel beaches. *Journal of Coastal Research* **26(1)**: 4–30.

Horn D and Li L (2006) Measurement and modelling of gravel beach groundwater response to wave run-up: effects on beach profile changes. *Journal of Coastal Research* **22(5)**: 1241–1249.

Horn DP (2002) Beach groundwater dynamics. *Geomorphology* **48(1–3)**: 121–146.

Horn DP and Walton SM (2007) Spatial and temporal variations of sediment size on a mixed sand and gravel beach. *Sedimentary Geology* **202(3)**: 509–528.

Hughes SA and Chiu TS (1981) *Beach and Dune Erosion during Severe Storms*. Coastal and Oceanographic Engineering Department, University of Florida, Gainesville, FL, USA, Technical Report No. TR/043.

Keulegan GH and Krumbein WC (1949) Stable configuration of bottom slope in shallow water and its bearing on geological processes. *Transactions of the American Geophysical Union* **30(6)**: 855–861.

Komar PD and Miller MC (1973) The threshold of sediment movement under oscillatory water waves. *Journal of Sedimentary Petrology* **43(4)**: 1101–1110.

Komar PD and Miller MC (1975) On the comparison between the threshold of sediment motion under waves and unidirectional currents with a discussion of the practical evaluation of the threshold. *Journal of Sedimentary Petrology* **45(1)**: 362–367.

López de San Román-Blanco BL (2001) *Morphodynamics of Mixed Beaches*. Unpublished transfer MPhil/PhD Report, Civil and Environmental Engineering Department, Imperial College, London, UK.

López de San Román-Blanco B, Coates T, Holmes P *et al.* (2006) Large scale experiments on gravel and mixed beaches: experimental procedure, data documentation and initial results. *Coastal Engineering* **53(4)**: 349–363.

Mackay E (2016) A unified model for unimodal and bimodal ocean wave spectra. *International Journal of Marine Energy* **15**: 17–40.

Mahalanobis PC (1930) On tests and measures of group divergence. *Journal of the Asiatic Society of Bengal* **26**: 541–588.

Mason T, Bradbury A, Poate T and Newman R (2008) Nearshore wave climate of the English Channel – evidence for bi-modal

seas. *Proceedings of 31st International Conference on Coastal Engineering*. World Scientific, Singapore, pp. 605–616.

Masselink G, Castelle B, Scott T *et al.* (2016) Extreme wave activity during 2013/2014 winter and morphological impacts along the Atlantic coast of Europe. *Geophysical Research Letters* **43(5)**: 2135–2143.

McCall RT, Masselink G, Poate T *et al.* (2014) Modelling storm hydrodynamics on gravel beaches with XBeach-G. *Coastal Engineering* **91**: 231–250.

Moses CA and Williams RB (2008) Artificial beach recharge: the south east England experience. *Zeitschrift für Geomorphologie* **52(3)**: 107–124.

Nicholls R (1990) Managing erosion problems on shingle beaches: examples from Britain. *Proceeding of the 3rd European Workshop on Coastal Zones, Paralimni, Cyprus* (Moutzouris C (ed.)).

Polidoro A, Pullen T and Powell K (2015) *Modelling Shingle Beaches in Bimodal Seas, Test Methodologies & Test Programme.* HR Wallingford, Wallingford, UK, Technical Report CAS1217-RT001-R03-00.

Powell KA (1990) *Predicting Short Term Profile Response for Shingle Beaches.* Hydraulics Research Limited, Wallingford, UK, Technical Report SR 219.

Powell KA (1993) *Dissimilar Sediments: Model Tests of Replenished Beaches Using Widely Graded Sediments.* HR Wallingford, UK, report SR 350.

Smit P, Zijlema M and Stelling G (2013) Depth-induced wave breaking in a non-hydrostatic, near shore wave model. *Coastal Engineering* **76**: 1–16.

Thompson DA, Karunarathna H and Reeve DE (2017) Modelling extreme wave overtopping at Aberystwyth Promenade. *Water* **9(9)**: 663.

van der Meer JW (1988) *Rock Slopes and Gravel Beaches under Wave Attack*. PhD thesis, Delft University of Technology, Delft, the Netherlands.

Van Hijum E and Pilarczyk KW (1982) *Equilibrium Profile and Longshore Transport of Coarse Material Under Regular and Irregular Wave Attack*. Delft Hydraulics Laboratory, Delft, the Netherlands, Pub no. 274.

Van Wellen E, Chadwick AJ and Mason T (2000) A review and assessment of longshore sediment transport equations for coarse grained beaches. *Coastal Engineering* **40(3)**: 243–275.

Yalin MS (1963) A model shingle beach with permeability and drag forces reproduced. *Proceedings of the 10th IAHR congress*, vol. 1, pp. 169–175.